RAIN STORMS INDUCED HAZARDS ASSESSMENT: SUSCEPTIBILITY ASSESSMENT OF SHALLOW LANDSLIDES USING SINMAP AND DEBRIS FLOW SIMULATION USING DEBRIS2D

TRIBHUVAN UNIVERSITY

INSTITUTE OF ENGINEERING

PULCHOWK CAMPUS

DEPARTMENT OF CIVIL ENGINEERING

M.Sc. PROGRAM IN WATER RESOURCES ENGINEERING

(A Thesis Submitted for the partial fulfillment of the requirement for the degree of Master of Science in Water Resources Engineering)

 By

Er. Tejaswi Sharma (Author)

er.tejaswisharma@gmail.com

Supervisor

Prof. Dr. Narendra Man Shakya

COPYRIGHT

TRIBHUVAN UNIVERSITY

INSTITUTE OF ENGINEERING

PULCHOWK CAMPUS

DEPARTMENT OF CIVIL ENGINEERING

The undersigned certify that they have read, and recommended to the Institute of Engineering for acceptance, a thesis entitled **"Rain Storms Induced Hazards Assessment: Susceptibility Assessment of Shallow Landslides Using SINMAP and Debris Flow Simulation Using DEBRIS2D"** submitted by Tejaswi Sharma in partial fulfillment of the requirements for the degree of Masters of Science in Water Resources Engineering

Supervisor: Dr. Narendra Man Shakya

Professor

Department of Civil Engineering

M.Sc. Water Resources Engineering

External Examiner: Dr. K. N. Dulal

Committee Chairperson: Dr. Narendra Man Shakya

Professor

Department of Civil Engineering

M.Sc. Water Resources Engineering

NOVEMBER, 2014

ACKNOWLEDGEMENT

Above all I want to panegyrize, the Supreme God, most compassionate, the redeemer. I bow down with my greatest regards to the almighty God, the creator of this grandiose planet we dwell on enjoying its intriguing landscapes.

I would like to start off by thanking my parents for their persuasion and continuous support throughout my academic perseverance. They were always there cheering me up and stood by me through the good times and bad.

I most heartily thank my supervisor, Prof. Dr. Narendra Man Shakya, for his exceptional guidance, advice, patience, knowledge, support, and willingness in allowing me to conduct a study on landslides and debris flows. I fully express my gratitude for his heroic endeavor to ensure scientific integrity for completing this thesis. The blessing, help and guidance given by him time to time shall carry me a long way in the journey of life ahead.

I am in great debt to Dr. Ranjan Kumar Dahal and Dr. Manita Timilsina of Himalayan Conservation Group for their precious suggestions that helped me to create a solid framework for this Thesis.

I am particularly grateful and offer my sincere appreciation to David Tarbatoon of Uttah State University, USA and Ying-Hsin Wu of Shimane University, Japan for their consistent response throughout the thesis period of the confusions I faced via email.

I would like to express a deep sense of gratitude to my friends Mr. Prasiddha Kharel and Mr. RamSundar Shrestha for their cordial support, suggestions with kindness, enthusiasm and dynamism which helped me in completing this task through various stages.

I owe a deep sense of honour to Mr. Shree Kamal Dwibedi and Mr.Shad Mukesh Amatya of DWIDP for providing me with the reports being required and I am gratified to them for sharing the illuminative views on a number of issues related to this thesis work.

My sincere thanks is also reserved for my friends, classmates and my seniors. Benediction to Mr. Ved B. Khadka for providing all kinds of departmental assistance.

Thank you all.

ABSTRACT

Landslides and debris flows are geomorphologic calamitous events that endanger human life and property. The higher intensity rainfall for longer duration during the monsoon season is one of the major prompting and stimulating factor for landslides and debris flows in Nepal. In this study, the deterministic Stability Index Mapping (SINMAP), which is the integration of a mechanistic infinite slope stability model and hydrological model, was applied for the susceptibility assessment of shallow landslides along Narayanghat-Mugling (N-M) Highway.Similarly,DEBRIS2D numerical model, which uses the generalized Julien and Lan (1991) visco-plastic collision concept along with x,y mass and momentum conservation form as governing equations with time step holding Courant-Friedrichs-Lewy(CFL) condition for stable computation, was used for debris flow simulation in Kamere Khola Watershed(24+740) along N-M Highway.

Inputs to the SINMAP model were a 5m interpolated Digital Elevation Model(DEM) , an inventory of storm induced landslides and listings of geotechnical and hydrological parameters including transmissivity, steady state recharge, angle of internal friction and dimensionless cohesion index. For hazard assessment random partition approach was applied in which 197 debris slides were used for modeling calibration and 142 landslide zones were used for validation. Outputs of the SINMAP Model were saturation index map, slope-stability index distribution maps, slope versus specific catchment area charts and statistical summaries for the calibrated values.

The predicted result was that out of the total study area 0.097% was in the defended zone, 35.216% in the upper threshold zone and the remaining in lower threshold, quasi stable, moderately stable and stable zones. This result can aid in making emergency decisions and ultimately mitigating future landslide risks. Rainfall and dimensionless cohesion index 'C' was seen to be the most sensitive parameter in landslides modeling. whereas angle of internal friction showed only a slight change.

The validation of the modeling output was done in three ways. First the validating landslide polygon theme was overlaid on the obtained map which showed a very good matching. Second, the Receiver Operating Characteristics (ROC) curve was plotted and the Area Under Curve (AOC) was calculated as 0.601(higher than classification by

chance).Third, efficiency (also the proportion of the correctly classified observations) was calculated as 72.68% considering 0.5 as threshold (Youden's Index(J) being maximum for safety factor 0.5).

Inputs to the DEBRIS2D model were a 5m interpolated DEM, mass parameter as yield stress which was set at 700Pa from the field measurement, mass source with it's distribution, simulation range and time interval. Outputs of the model were depth averaged X and Y direction velocities, final maximum depth, debris flow path and the affected area.

The result revealed that the process of transport of debris flow was about 1 hour with the maximum runout distance as 640.22 m and the debris covering the portion of N-M Highway at about 7.6 minute from it's initiation .In this study, the sensitivity factor considered on the debris flow spreading was the amount of debris flow initial volume. It was revealed that a 33.33% and 66.67% variation in estimating the volume resulted in 13.33% and 23.33% variation respectively on the final depositional front, 18.33% and 54.66% variation respectively on the final depositional lateral spread and 21.64% and 60.06% variation respectively on the final depositional depth.

The validation of the model output was done in three ways. First the estimated volume from the model when it invaded the section of N-M Highway was compared with the recorded real event scenario of 2003 disaster. It was seen that about 12% of the variation occurred which was quite acceptable. Second, the different parameters obtained were compared with different empirical equations which again produced a good result besides a few. Third, the debris flow depth path obtained from the model was overlaid on the google earth image which depicted the consistency with the actual debris flow path .

The model used in this study can be an advantageous and utile tool for disaster prevention and other land resources development. Similarly the sensitivity analysis carried out in this study is anticipated to administer souped up perspicacity and sapience for disaster and geohazard managers. Hence, in the end, it is assessed that the model presented in this study can be further used for pragmatic engineering concerns in Nepalese context.

Keywords: landslide, debris flow, rainfall, SINMAP, DEBRIS2D

Available online at http://www.ijart.info/

Table of Contents

Available online at http://www.ijart.info/

LIST OF FIGURES

Available online at http://www.ijart.info/

LIST OF TABLES

LIST OF ABBREVIATIONS

AUC   : Area Under Curve

CDF   : Cumulative Distribution Function

CFL   : Courant Friedrichs Lewy

CHASM   : Combined Hydrology and Slope Stability Model

CM   : Central Meridian

CRED   : Centre for Research on Epidemiology of Disasters

DEM   : Digital Elevation Model

DOR   : Department Of Roads

DOS   : Department Of Survey

DTM   : Digital Terrain Model

DWIDP   : Department of Water Induced Disaster Prevention

EIA   : Environmental Impact Assessment

ESRI   : Environmental System Research Institute

GIS   : Geographical Information System

GUI   : Graphical User Interface

ICL   : International Consortium on Landslides

IfSAR   : Interferometric Synthetic Aperture Radar

JICA   : Japanese International Cooperation Agency

LAPSUS   : LandscApe ProcesS modeling at mUlti dimensions and Scales

LIDAR   : LIght Detection And Ranging

LISA   : Level I Stability Analysis

MOHA   : Ministry Of Home Affairs

MOPPW   : Ministry of Physical Planning and Works

MUTM   : Modified Universal Transverse Mercator

NEOC   : National Emergency Operation Centre

N-M   : Narayanghat - Mugling

PDF   : Probability Density Function

RAMMS   : Rapid Mass Movement Simulation

ROC   : Receiver Operating Characteristics

SF   : Safety Factor

SHALSTAB   : SHAlow Landsliding STABility model

SI   : Stability Index

SINMAP   : Stability Index MAPping

SPH   : Smoothed Particle Hydrodynamics

TRIGRS   : Transient Rainfall Infiltration and Grid based Regional Slope stability

               analysis

TWI   : Topographic Wetness Index

UNESCO   : United Nations Educational, Scientific and Cultural Organization

USDA   : United Stated Department of Agriculture

USGS   : United States Geological Survey

1D   : One dimensional

2D   : Two dimensional

1. INTRODUCTION

1.1 Background and Problem Statement

Landslides and debris flows are geomorphologic events that may threaten different entities of mountainous societies. This risk is not only the risk of the processes as such, but of the interaction with human systems, infrastructures and their associated vulnerabilities. Understanding the mechanism, simulating, forecasting and mitigating the hazard associated to this type of slope movements is still an empirical task which requires a mixture of qualitative and quantitative analyses. When both hazard and vulnerability have the same coordinates in space and time, natural disasters can occur (Alcantara-Ayala,2002). Mass movements which are commonly triggered in mountainous area represents one of the most destructive natural hazards in terms of economic losses and the amount of human casualties, and are often underestimated (Petley,2012).

Between 2004 and 2010, 2,620 fatal landslides killed a total of 32,322 people. That figure excludes landslides triggered by earthquakes, and comes in at a little more than half the total number of people killed by floods, which claimed more than 7600 lives annually between 1990 and 2006. Landslides and debris tend to occur during the Northern hemisphere summer and autumn, when monsoons strike eastern and southern Asia and hurricanes and typhoons slam Central America , Islands of the Caribbean and land bordering the North Western Pacific Ocean (Petley,2012).
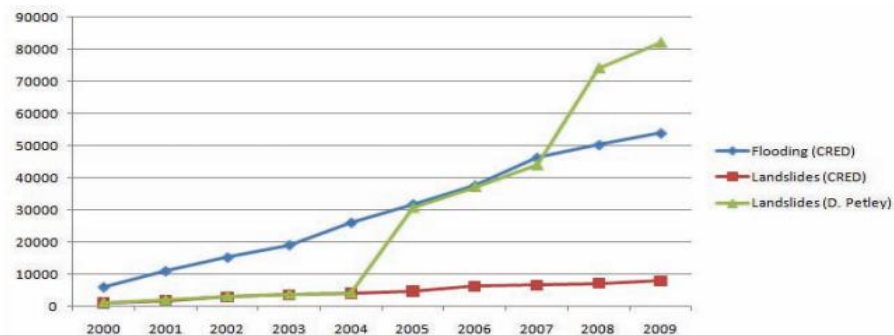
Figure 1.1 Representation of landslide fatalities during 2000 to 2009 around the world
(Source: Luna ,2012)

Landslide is defined as the movement of a mass of rock, debris or earth down a slope (Cruden, 1991). Landslides are natural phenomena related to mass wasting processes that model the earth surface. Conversely to other movements, like soil creep, some landslides occur suddenly and move fast, and sometimes cause great damage. The identification of areas where landslides are likely to occur is important for the reduction of potential damage. Occurrence of shallow landslides depends on local terrain conditions, such as slope-forming materials, topography, groundwater, and land cover; in addition to triggering events, like intense rainfall or earthquakes, that modify those characteristics and produce changes that cause slope instability (Soeters and van Westen,1996). Assessment of landslide hazard is difficult due to the lack of historical data of triggering events; instead, landslide susceptibility assessments are common. Landslide susceptibility maps express the likelihood of occurrence of landslides (spatial probability), estimated from local terrain conditions.

One of the most fascinating and destructive type of landslides are debris flows. Debris flow is a type of slope failure where by the material made up of debris ranging from unconsolidated soil particles to large boulders descends down the slope in a saturated flow like movement. They can move as granular rocky flows, muddy cement like flows, or as gradual change to floods with increasing water content such as hyperconcentrated flows (Jakob and Hungr,2005).The debris flow phenomena is specially challenging for researchers not only due to the wide ranging types of debris incorporated within the flow, but also due to the behavior of the debris flow runout which can range from flowing on an open slope to being confined to a completely channelized environment.

Landslides, that means downward movements of rocks and/or soils occur as a consequence of slope instabilities. Since landslides pose a major threat to human lives, private property and infrastructure in mountain regions all over the world, they need to be investigated quite intensely. Therefore, and since the understanding about the way how landslides occur is essential for the prediction of debris flows as well.

Though it is seen that the particular occurrence of landslides is chaotic, they do not happen randomly over time and space. Fig: 1.2 illustrates the conditioning and triggering factors for landslides.
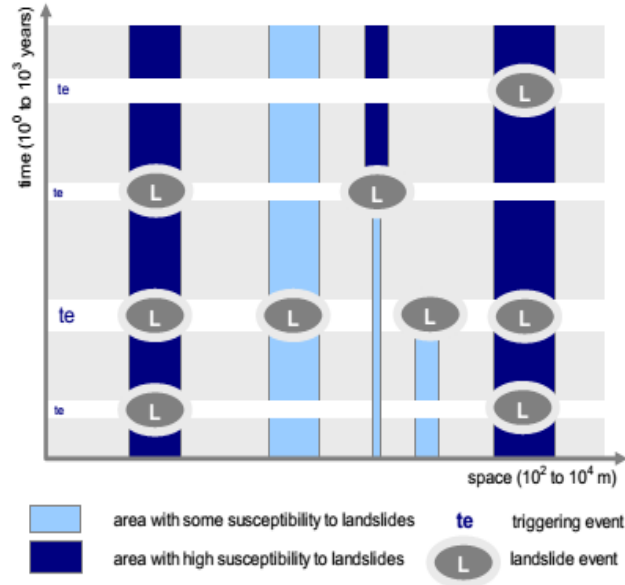
Figure 1.2 Conditioning factors (determining susceptibility) and triggering factors for landslides. (Source: Mergili, 2008).

Their occurrence is coupled to conditioning and to triggering factors. While conditioning factors rather determine the spatial distribution of landslide occurrence (the landslide susceptibility of an area), triggering factors determine the time at which landslides occur. Not every triggering event necessarily leads to landslides in all susceptible areas, and landslide events may alter the susceptibility of an area, e.g. by removing or, reverse, by exposing unstable material. Furthermore, conditioning factors may have a different importance under different regimes of triggering factors.

Three fundamental principles for landslide susceptibility modeling are (Varnes,1978) -

- The past and present are keys to the future i.e. the occurrence of landslides in future will be in similar geologic, geomorphic and hydrologic conditions as that of present and past landslides (estimation based on historical data).
- The major conditions leading to landslides such as surficial material conditions, topography, effect of ground water, and triggering mechanisms can be identified (prediction in larger areas based on site observations).
- Degree of hazard can be determined from the relative contribution of the conditions that cause landslides and can be expressed qualitatively or quantitatively as a map.

Table 1.1 Loss of Lives and Properties from landslides and debris during 2014 Monsoon
(Source: NEOC, MOHA Data Assessed: 22nd Oct, 2014)

Districts	Date of Occurrence	Death	Missing	Injured	Houses Destroyed	Estimated loss Rs.
Ilam	22-Apr-14	1		2		
Dadeldhura	27-May-14	1				
Pyuthan	19-Jun-14	5		1	3	12407979
Gulmi	19-Jun-14	9			1	
Gulmi	19-Jun-14				1	170000
Gulmi	19-Jun-14				1	
Gulmi	19-Jun-14				1	218000
Gulmi	19-Jun-14					140000
Gulmi	19-Jun-14					150000
Gulmi	19-Jun-14					70000
Gulmi	19-Jun-14				1	195000
Pyuthan	20-Jun-14				1	
Lalitpur	22-Jun-14	1		6		
Taplejung	24-Jun-14				1	467000
Sankhuw asabha	29-Jun-14					700000
Tanahu	30-Jun-14	1				
Kapilbastu	9-Jul-14	1				
Nuw akot	12-Jul-14				1	
Lalitpur	13-Jul-14	4		3		
Sindhupalchow k	13-Jul-14	3		4	1	1000000
Sindhupalchow k	13-Jul-14	1			1	600000
Sindhupalchow k	13-Jul-14	2			1	500000
Kalikot	20-Jul-14	1				
Gorkha	22-Jul-14					
Kalikot	28-Jul-14	1		1		
Bajhang	29-Jul-14		1			
Taplejung	29-Jul-14				1	
Okhaldhunga	29-Jul-14				1	1500000
Rolpa	31-Jul-14				1	500000
Sindhupalchow k	2-Aug-14	33	123	47	97	
Kalikot	2-Aug-14	1				
Sankhuw asabha	4-Aug-14	8	2		3	
Kavrepalanchow k	4-Aug-14				10	2000000
Bajura	5-Aug-14			1		
Sindhupalchow k	8-Aug-14	2			1	
Mugu	8-Aug-14					700000
Dolakha	9-Aug-14	4		8		
Jajarkot	13-Aug-14	2		3	1	
Jajarkot	13-Aug-14		2	4		
Jajarkot	14-Aug-14				1	
Jajarkot	14-Aug-14				2	
Jajarkot	14-Aug-14				1	
Lalitpur	14-Aug-14	2				
Khotang	14-Aug-14			1	1	286000
Rukum	14-Aug-14	2		2	1	
Humla	15-Aug-14					
Gorkha	15-Aug-14	3		8		
Dang	15-Aug-14	2				
Rolpa	15-Aug-14	2			1	
Salyan	15-Aug-14	3			1	
Nuw akot	16-Aug-14					152000
Nuw akot	16-Aug-14					150000
Baglung	23-Aug-14	1				
Sindhupalchow k	23-Aug-14	1			1	
Baglung	24-Aug-14	1			1	
Rasuw a	26-Aug-14			3		150000
Nuw akot	28-Aug-14	3			1	
Nuw akot	28-Aug-14				1	200000

Table 1.2 Total Death from different disasters during Monsoon Days of 2014(Source: National Emergency Operation Centre, Ministry Of Home Affairs, Data Assessed: 22nd Oct, 2014)

S.No.	Type of Disaster	Total Death
1	Avalanche	13
2	Boat Capsize	2
3	Cold Wave	0
4	Drowning	6
5	Earthquake	0
6	Epidemic	12
7	Fire	23
8	Flood	27
9	Landslide and Debris	105
10	Heavy Rainfall	5
11	Wind Storm	3
12	Thunderbolt	68
Total		**264**

From the above table 1.2, it is clear that the death of people due to landslides and debris is more than due to other disasters during the monsoon of 2014 in Nepal. Hence, it is a matter of great concern to properly mitigate the effects due to landslides and debris even more during the monsoon season.

Rainfall may be considered as the most triggering factor for the landslides and debris flow in Nepal, since most of the landslides and debris flow were reported to occur during

the monsoon season (as in Table: 1. 1 and 1.2 above).Prolonged rainfall will increase the infiltration and create a saturated soil which decreases the shear strength and thus leads to slope failure. Besides it, the presence of water in the soil or rock supplements the overall weight of the slope ,which increases the shear forces, causing the slopes less stable(Smith,K.,Petley D.N,2008)

Similarly, if we consider the social vulnerability index , then Li (2012) defines Social vulnerability as the degree of damage and resistance of a community against slope-land hazard event.
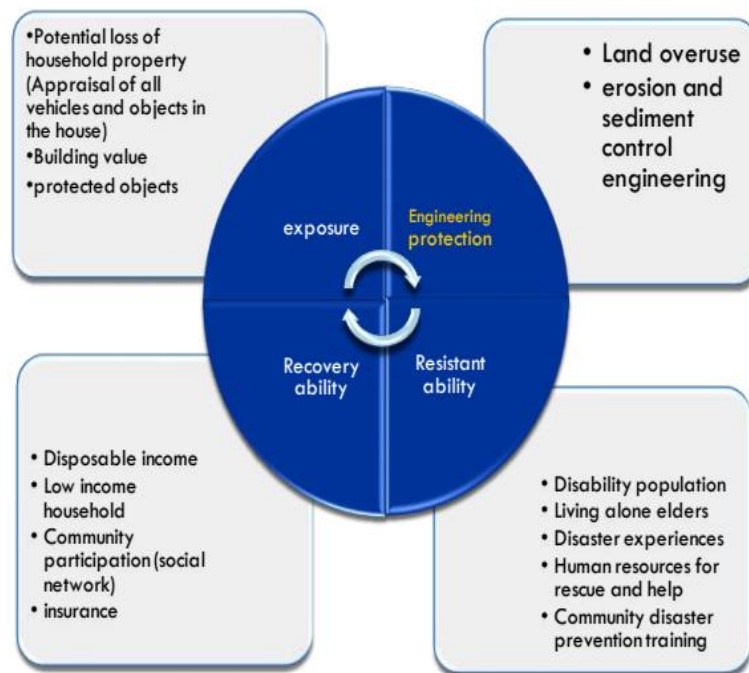
Figure 1.3 Social Vulnerability Index of slope land Disaster (Source: Liu et.al, 2012)

1.2 Objectives of the Study

The master goal of the present thesis is to contribute to the reduction of the risk posed to human lives and economic values by landslides and debris flows. For being operationalized, this objective has to be split up into smaller and more specific objectives, in order to achieve the master goal. The specific objectives of the present thesis are-

a. To determine the susceptibility assessment(mapping) of shallow landslides across Narayanghat-Mugling Highway

b. To assess the sensitive parameters for landslide triggering and more specifically determine the sensitivity of SINMAP Model with respect to various input parameters

c. To evaluate the accuracy of SINMAP terrain stability mapping proposed by Pack et.al,2005 for it's further use in context of Nepal

d. To identify the flow depth, X and Y direction velocities and affected area of debris flow, thus evaluating various scenarios and damages, in the Kamere Khola Watershed across N-M Highway

e. To analyze the sensitivity of initiation volume in the debris flow runout and more specifically, present the sensitivity of debris flow initial volume in case of DEBRIS2D Model regarding the affected area

f. To assess the applicability of DEBRIS2D Model, in modeling debris flow runouts in the Nepalese environment

1.3 Limitations of the Study

The limitations of the study are as follows-

a. This study on landslide susceptibility is based on the assumption that the subsurface hydrologic boundary is parallel to the surface and that soil thickness and hydraulic conductivity are uniform. Soil thickness is interpreted perpendicular to the slope. It assumes the steady shallow subsurface flow and the absence of deep drainage and flow in the substratum.

b. In this thesis work, single calibration region was used across N-M highway for SINMAP modeling because of lack of detailed comprehensive geologic, geomorphologic and soil mapping.

c. SINMAP model cannot be used to predict the failure size, mobility or consequences.

d. The temporal probability of occurrence of landslides is not considered.

e. In this study, rainfall was considered as the main triggering factor for landslide in the study area. The other triggering factors such as earthquake, excessive wind velocity etc was not taken into account.

f. Bed or lateral bank erosion was not incorporated in the modeling of debris flow simulation

g. The entrainment process has not been taken into account for debris flow simulation

1.4 Organization of the Chapters

The chapters in this document have been organized as follows:

1. Chapter 1 introduces the reader with the overall topic of the study.

2. Chapter 2 presents a brief overview of the literature review consulted during the course of this thesis work.

3. Chapter 3 explains the methodology and tools adopted for landslides susceptibility mapping and debris flow simulation during the study in detail.

4. Chapter 4 describes the brief introduction of the study area .

5. Chapter 5 deals with the model preprocessing (preliminary model setup) i.e. model parameterization and calibration

6. Chapter 6 provides a detailed result of SINMAP and DEBRIS-2D Model along with the discussion and interpretation of the model results.

7. Chapter 7 deals with the validation of SINMAP and DEBRIS2D along with sensitivity analysis of their parameters.

8. Chapter 7 deals with the concluding remarks and recommendations made.

2. LITERATURE REVIEW

2.1 Introduction to landslides

Landslide is a general term for a wide variety of movements of slope materials due to gravity. Landslides not only occur in mountainous regions, but also occur in gentle slope terrain. Landslide type and occurrence depend on local geomorphology, hydrology, geology, vegetation, land use, and the characteristics of triggering events (Soeters and van Westen, 1996).The trigger is an external stimulus that modifies the slope stability conditions, increasing the material stress or reducing its strength, and causes the landslide. Intense rainfall, earthquakes, volcanic eruptions, storm waves and rapid erosion are natural triggers; activities, such as excavation or irrigation can be human triggers (Wieczorek, 1996). The term landslide is generally used to denote a downslope movement of mass of earth,debris or rock down a slope due to the action of external forces such as rainfall, snowmelt, volcanic eruption, earthquakes, anthropogenic activities etc. (Varnes,1978).

The movement of mass of rocks, debris, or earth down the slope resulting in geomorphic alteration of earth's surface which contributes to landscape evolution is often referred as a landslide. Landslides could be due to the temporal conjunction of several quasi-static and dynamic factors (Dai et. al,2002). Quasi-static factors, such as geology, slope characteristics (gradient, slope aspect, elevation, etc.), geotechnical properties, long-term drainage paterns, etc. contribute to landslide susceptibility, while dynamic variables, such as rainfall, earthquakes, etc.tend to trigger landslides.

Any landslide is generally classified and described by two nouns: the first describes the materials (e.g. earth, debris or rock); and the second, the type of movement (e.g. falls, topples, slides, flows, spread etc.).

Table 2.1 Classification of Landslides (Varnes,1978)

Type of movement		Type of material		
		Bedrock	Soil	
		Coarse	Fine	
Fall		Rock fall	Debris fall	Earth fall
Topple		Rock topple	Debris topple	Earth topple
Slide	Rotational	Rock Slide	Debris slide	Earth Slide
	Translational			
Spread		Rock spread	Debris spread	Earth spread
Flow		Rock flow	Debris flow	Earth flow
Complex		Combination of two or more		

Table 2.2 Classification of Landslides (Smith,1996)

Mass wasting Type	Character of Movement	Subdivision	Speed and Type of Movement
Falls	Particles fall from cliff and accumulate at base	Rockfall and Topples	Extremely rapid; develops in rocks
		Soilfall	Extremely rapid; develops in sediments
Slides	Masses of rock or sediment slide down slope along planar surface	Rockslides (Translational)	Rapid to very rapid sliding of rock mass along a rectilinear/ inclined surface
		Slump (Rotational)	Extremely slow to moderate sliding of sediment or rock mass along a curved surface
Flows	Displaced mass flows as plastic or viscous liquid	Solifluction	Very slow to slow movement of saturated regolith as lobate grows
		Mudflow	Very slow to rapid movement of fine grained particles with 30% water
		Debris flow	Very rapid flow of debris; commonly starts as a slump in the upslope area
		Debris avalanche	Extremely rapid flow;fall and sliding of rock debris
Creeping	Regolith soil and rock		Extremely slow superficial deposits and the influence of gravity. Predominantly seasonal.
Complex	Combination of two or more principle types of movements		

Table 2.3 Cause of Landslides (Source:MCall,1992)

External Causes	Internal Causes
1. Geometrical change • Height • Gradient • Slope length	**1. Progressive Failure (internal response to unloading)** • Expansion and swelling • Fissuring • Straining, softening • Stress concentration
2. Loading • Natural • Man-induced	**2. Weathering** • Physical property changes • Chemical changes
3. Unloading • Natural • Man-induced	**3. Seepage erosion** • Removal of cements • Removal of fine particles
4. Shocks and Vibrations • Single • Multiple/continuous	**4. Water regime change** • Saturation • Rise in water table • Excess pressures • Draw down
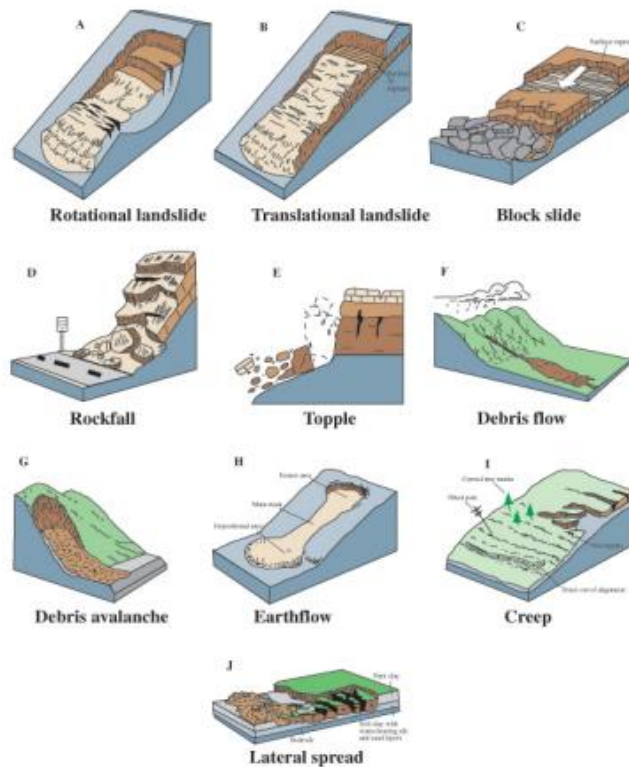
Figure 2.1 Schematic Representation of landslides (Source: United States Geological Survey, 2014)

2.2 Rainfall induced shallow landslides

Shallow landslide, also known as slope failure, is a movement that involves earth or debris from supercial deposits (mainly soil and colluvium) and does not affect the bed rock.Shallow refers to the depth of displaced mass. Shallow landslides occur frequently in mountainous terrain worldwide triggered by earthquakes, or intense rainfall. Their occurrence greatly depends on slope topography and the presence of weathered rock mass or superficial deposits. They occur suddenly and usually move fast; and can cause great damage.

Landslides in which the sliding surface is located within the soil mantle or weathered bedrock (typically to a depth from a few decimeters to several meters) are categorized as shallow landslides. A schematic diagram of a shallow landslide is presented in Figure 2.2.
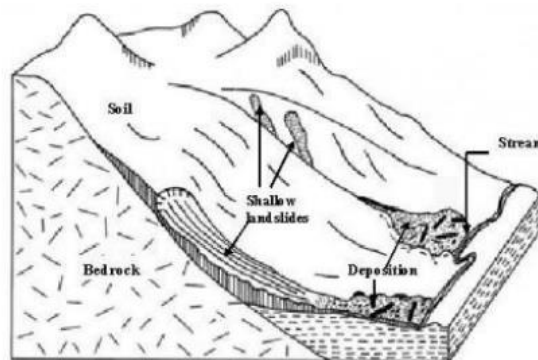
Figure 2.2 Schematic representation of shallow landslide (Sidle et. al,1985)

Shallow landslides are often triggered by rainfall. Rainfall infiltration increases pore-water pressures and therefore reduces the soil-shear strength. Analysis and prediction of stress conditions leading to landslides is largely grounded on Terzaghi's (1950) effective stress principle for saturated materials. This principle states that the controlling variable for the mechanical behavior of earth materials is effective stress, defined as the difference between total stress and positive pore water pressure. However, this definition may not be appropriate for assessing the state of stress in hillslopes nor completely describe shallow failure of hillside materials under partially

saturated conditions since it neglects the effect of unsaturated soil conditions on the soil-shear strength (e.g., Rahardjo et al., 2008; Terlien, 1998; Van Asch et al., 1999). Theoretical and analytical results from a variety of geologic and climatic settings have advanced the hypothesis of shallow slope failure in partially saturated materials (Morgenstern and de Matos, 1975). Godt et al. (2009) reported instrumental observations from a coastal bluff in the Seattle, WA area where a shallow landslide occurred in the apparent absence of positive pore water pressures under partially saturated soil conditions. When rainwater infiltrates through an unsaturated zone, the advancement of the wetted zone near the slope surface may lead to failure during periods of prolonged rainfall. If the effective cohesion of soil is zero (c′=0), and the slope angle(β) greater than or equal to the effective internal friction angle of the soil ($\varphi′$), the unsaturated soil slope fails from a loss of apparent cohesion upon saturation of the soil by the infiltrating wetting front. In this case, failure from a reduction in the shear strength because of a rise in the ground water table or the occurrence of a perched water table is unlikely since the slope can only be stable with the shear strength due to the matric suction that fully disappears before saturation is achieved. However, if the slope angle does not exceed the effective friction angle of the soil, slopes are not susceptible to failure from the loss of matric suction since the slopes remain stable without the additional shear strength due to the matric suction; yet the slopes will fail from a reduction in the effective stress in the saturated condition that results in the reduction in the shear strength of soil. When a slope possess an effective cohesion component (c′), and the effective cohesion of the soil is adequate, even a partially saturated slope with a slope angle that is greater than the effective friction angle can remain stable in spite of a complete loss of apparent cohesion. However,even these types of slopes would fail in the saturated condition if an increase in pore pressure reduces the effective stress (Sudhakar, 1996).

Water plays a major role not only in the initiation of failure but also in the way that the earth then flows or slides and the distance that it travels. In many cases shallow landslides are fast-moving and are extremely destructive. Figure 2.2 illustrates many of the important factors culminating in the exposure of society to safety and economic consequence (road, urban area, landscape).
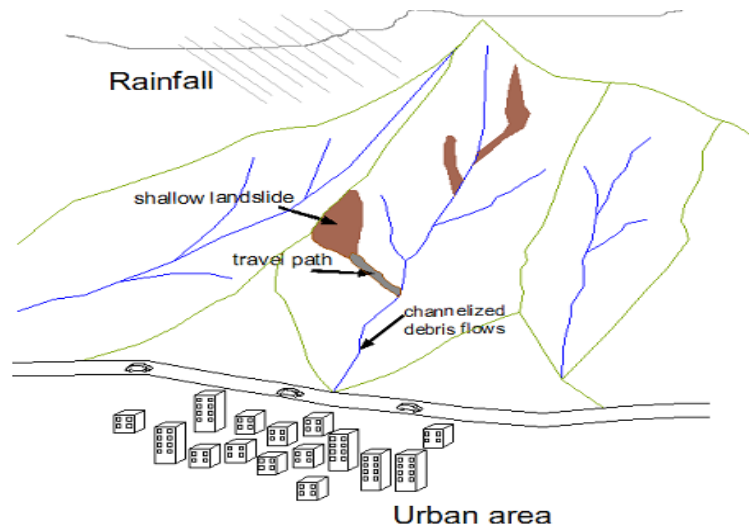
Figure 2.3 Shallow landslides within the context of landslide risk (Lanni, 2012)

2.3 Impact Assesssment:

There are three types of landslide maps useful to planners and general public.

- **Landslide inventory maps** depict areas where landslides have occurred.The maps can simply denote areas of past landslides or include detailed information such as components of individual landslides (scarp and accumulation zones), type of movement, activity, geological age, rate of movement, and other characteristics. Inventory maps help identifying areas for detailed studies, and are fundamental for producing other potential impact maps (Highland and Bobrowsky, 2008).

- **Landslide susceptibility maps** denote areas ranked according to the tendency to the occurrence of landslides; based on local conditions (geology, topography, groundwater, vegetation). The temporal probability of occurrence of landslides, which depends on triggering events (rainfall, earthquakes), is not considered (Soeters and van Westen, 1996). Susceptibility maps only expresses the spatial probability of occurrence of landslides, however, they provide information on areas where landslides have not occurred yet.

- **Landslide hazard maps** delineate areas of past, and recent landslides and the probability of occurrence of potential landslides. For a given area, hazard maps contain detailed information on type of landslides, extent of failure, and maximum extent of ground movement (Highland and Bobrowsky,2008).

  Terms related to the effects of landslides on human activity and the environment according to the definitions by Committee on the Review of the National Landslide Hazards Mitigation Strategy (2004) (Source: Pimiento E.,2010) are-

- **Landslide hazard** is the potential for occurrence of a damaging landslide within a given area. Damage refers to loss of life or injury, damage of property, social and economic disruption, or environmental degradation.

- **Landslide vulnerability** is the extent of potential loss of a given element within the area affected by landslide hazard, expressed on a scale from 0(no loss) to 1 (total loss). It depends on physical, social, economical and environmental conditions.

- **Landslide risk** is the probability of damaging consequences within a landslideprone area. It is the product of hazard and vulnerability.

- **Landslide risk evaluation** is the application of analysis and assessments to determine risk management alternatives, which may include the decision that the risk is acceptable or tolerable.

- **Landslide hazard zonation** is the division of the terrain in homogeneous areas and ranking them according to their degree of actual or potential hazard or susceptibility to landslides.

2.4 Susceptibility Analysis Approaches

Glade and Crozier (2005) reviewed the techniques to produce landslide susceptibility and hazard maps, and recommended approaches based on analysis scale(Table 2.4). Techniques are classified in qualitative and quantitative methods. Shallow landslide modeling is based on a variety of approaches and models.

Available online at http://www.ijart.info/

2.4.1 Qualitative methods:

Qualitative methods are based on expert knowledge and experience. They are subjective and difficult to apply to different areas. However, they can be accurate if the person or group who make the analysis know well the processes and the area (Glade and Crozier, 2005).

Landslide inventories and heuristic methods are qualitative methods. Landslide inventories are spatial databases, often used for modeling and for validation.

Heuristic approaches can be geomorphic analysis or qualitative map combination (Soeters and van Westen, 1996). Geomorphic analysis consists in mapping hazard in the field. Qualitative map combination consists in selecting parameters related to the occurrence of landslides, assigning weights to parameters classes, combining maps and classifying results to express qualitative degrees of hazard. Topographic, geological, ,hydrological, geomorphic or geotechnical parameters are often used to estimate susceptibility or hazard (Soeters and van Westen, 1996).

Table 2.4 Recommended approaches for landslide susceptibility analysis (Pimiento,2010)

Scale	Qualitative methods		Quantitative methods		
	Inventory	Heuristic analysis	Statistical analysis	Probabilistic prediction analysis	Deterministic analysis
>1:10,000	Yes	Yes	Yes	Yes	Yes
1:25,000-1:50,000	Yes	Yes	Yes	Yes	Probable
1:100,000-1:500,000	Yes	Yes	Probable	Probable	No
<1:1,000,000	Yes	Yes	No	No	No

2.4.2 Quantitative methods:

Quantitative approaches are based on objective criteria, producing the same results for similar data sets, and it is possible to reproduce them in other areas. Statistical, probabilistic, and deterministic approaches are quantitative methods (Glade and Crozier, 2005).

Statistical approach:

The statistical methods are based on conceptual models. These models first require identification and mapping of a set of landslide causing (geological and geo-morphological) factors that are directly or indirectly related to slope failures. Then, it involves an estimate of the relative contribution of these factors in generating slope failures, and classification of land surfaces into zones of different hazard or susceptibility degree (Aleotti and Chowdhury, 1999). Bivariate and multivariate statistical methods are the most commonly used for these predictions. The bivariate statistical analysis is a method that describes the relationship between two variables. In landslide modeling, the bivariate method links each landslide causing factor to the landslide distribution map.

On the other hand, in multivariate statistical analysis, the weighted factors controlling the landslide occurrence indicate a relative contribution of each of these factors to the degree of landslide hazard within a defined land unit. The common property of these analyses is their nature of being based on the presence or absence of stability phenomena within these previously defined land units (Van Westen, 2000). Probabilistic methods for hazard assessments are based on Bayesian probability and fuzzy logic. Results are probabilistic prediction models (Glade and Crozier, 2005).
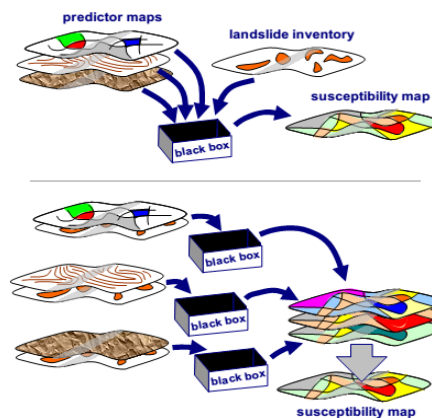
Figure 2.4 Multivariate(top) and bivariate(bottom) statistical approach (Mergili,2008)

Physically-based models

Physically-based models attempt to extend spatially the slope stability models (e.g., the "infinite slope stability method") widely adopted (Wu and Sidle, 1995). To link

rainfall pattern and its history to slope stability/instability conditions, physically-based models incorporate infiltration models. Various approaches have been proposed to predict the accumulation of the infiltrated water into the ground from relatively simple "pipe and pot" models to parsimonious topographic-index based models to complex, 3D variably saturated flow models based on Richards equation.

Topographically-based modeling has become very popular due to availability and quality of digital elevation models (DEMs). Elevation data are used in algorithms to calculate surface derivatives such as slope, aspect, flow direction, upslope contributing area, and topographic index. These topographic attributes are used in distributed hydrological modeling (Beven and Moore, 1993) and catchment scale shallow landslide modeling (Tarboton, 1997;).

Deterministic Models are widely used nowadays especially after the evolution of fast processing computers and the GIS technology. Only the use of deterministic models will result the real hazard map. Deterministic Model captures the input data such as the thickness of soil layer, strength properties of soil, depth below the terrain surface to the potential sliding surface,slope angle and pore pressure conditions to be expected on the slip surfaces. The use of infinite slope model calculates the safety factor for each grid in GIS based deterministic model. All the inputs parameters are in the Raster GIS forms which are used for evaluation of safety factor for each grid in different soil-water conditions. The output map layer calculated(Factor of Safety Map) is then classified into different categories according to their numerical factor of safety.

2.5 Deterministic Models for landslides assessment:

SHALSTAB:

 SHALSTAB model was developed by Montgomery and Dietrich (1994) . The model performs an infinite-slope stability analysis assuming equilibrium (steady-state) conditions and flow parallel to the surface and uses Darcy's law to estimate the spatial distribution of pore pressures .This model combines a hydrological model with a slope stability model to identify susceptible landslide areas.

Available online at http://www.ijart.info/

The hydrological model considers the model developed by O'Loughlin to estimate soil saturation levels. This model calculates the saturation level based on upstream flows from a given point, slope angle, and soil transmissivity. Hydrological model can be solved based on the saturated proportion of the soil (h/z), assuming that saturated conductivity does not vary with depth, as follows:

$$\frac{h}{z} = \left(\frac{Q.a}{T.b.\sin\theta} \right)$$

where, h is the water-table height, z is the soil thickness, a is the upslope contributing area (m^2), b is the grid cell size (m), θ is the local ground slope (degrees), T is the soil transmissivity (m^2/day), and Q is the steady-state rainfall intensity. Infinite-slope theory can be solved based on the h/z ratio, which has the following equation:

$$\frac{h}{z} = \left(\frac{C'}{\rho_w \cdot g \cdot z \cdot \cos^2\theta \cdot \tan\varphi} \right) + \left(\frac{\rho_s}{\rho_w} \right)\left(1 - \frac{\tan\theta}{\tan\varphi} \right)$$

The combination of hydrological and slope stability model uses the h/z ratio resulting from the following equation:

$$\frac{Q}{T} = \frac{\sin\theta}{(a/b)}\left(\left(\frac{C'}{\rho_w \cdot g \cdot z \cdot \cos^2\theta \cdot \tan\varphi} \right) + \left(\frac{\rho_s}{\rho_w} \right)\left(1 - \frac{\tan\theta}{\tan\varphi} \right) \right)$$

TRIGRS Model:

The Transient Rainfall Infiltration and *G*rid Based Regional *S*lope-Stability Model (TRIGRS) is a FORTRAN program designed for modeling the timing and distribution of shallow, rainfall-induced landslides. The program computes transient pore-pressure changes, and attendant changes in the factor of safety, due to rainfall infiltration. The program models rainfall infiltration, resulting from storms that have durations ranging from hours to a few days, using analytical solutions for partial differential equations that represent one-dimensional, vertical flow in isotropic, homogeneous materials for either saturated or unsaturated conditions. Use of step-function series allows the program to represent variable rainfall input, and a simple runoff routing model allows the user to divert excess water from impervious areas onto more permeable downslope areas. The TRIGRS program uses a simple infinite-slope model to compute factor of safety on a

cell-by-cell basis. An approximate formula for effective stress in unsaturated materials aids computation of the factor of safety in unsaturated soils. Horizontal heterogeneity is accounted for by allowing material properties, rainfall, and other input values to vary from cell to cell. This command-line program is used in conjunction with geographic information system (GIS) software to prepare input grids and visualize model results.

Level I Stability Analysis (LISA):

LISA is a tool for risk assessment developed by the USDA Forest Service for areas (defined as polygons on a map) with similar topography and geology. A factor of safety map (comprised of polygons) may be generated for a study area where details of the geology are known.For this study, we assume the geology and soil to be uniform throughout the study area and therefore we assess the effects of slope, location of the water table, soil thickness distribution and soil strength on the factor of safety. LISA performs a probabilistic analysis based on the factor of safety, FS, calculated by Eqn. below. Values for each parameter in the equation are defined by probability distribution functions (PDF's). Results are presented in a histogram showing the distribution of the factor of safety calculated for up to 1000 different combinations of parameters using a Monte Carlo simulation (Hammond et al., 1992*)*. A probability for failure is also calculated from the different combinations of parameters .

Iverson's Transient Response Model:

The final stability analysis involves the mathematical model developed by *Iverson* (*2000*) based on the Richards equation for unsaturated shallow groundwater flow. This model assesses the effects of transient rainfall infiltration on the timing and locations of landslides by approximating the pore pressure response in shallow soils to individual (short term) rainstorms. In this model, the pore pressure is calculated for vertical flow not slope parallel flow as in SINMAP, in the unsaturated zone above the water table as well as in the saturated zone (water table). The transient response model assumes that slopes are initially wet and the catchment area (*A*) is much greater than the thickness (*H*) of the landslide (dimensionless length scale, $\varepsilon = H/\sqrt{A} \ll 1$).

The pore pressure water head (P) in the soil for short-term rainstorms ($t<<A/D_o$; where D_o is the hydraulic diffusivity) is approximated by a simplified version of the Richards equation with the following assumptions: $\varepsilon = H/\sqrt{A} <<1$, such that when the Richards equation is non-dimensional , terms of order e and e^2 can be neglected. This assumption reduces the equation to a one-dimensional equation l equation in the vertical direction (Z).

$$P(Z, t \leq T) = Z * \left[\beta(1 - d/Z) + \frac{I}{k} * R(t^*) \right]$$

$$P(Z, t > T) = Z * \left[\beta(1 - d/Z) + \frac{I}{k} * R(t^* - T^*) \right]$$

Where t is time, T is the rainfall duration, d is the initial steady state water table depth, I is the infiltration rate equal to rainfall rate, k is the hydraulic conductivity and $R(t^*)$ is the pressure head response function.

$$R(t^*) = \sqrt{t^*/\pi} \; \exp(-1/t^*) - \text{erfc}\,(1/\sqrt{t^*})$$

Where $t^* = t/(Z^2/4D_o)$ is dimensionless time and D_o is the hydraulic diffusivity (assumed to equal k/soil moisture content). Dimensionless rainfall duration is expressed as $T^* = T/(Z^2/4D_o)$.

Slope failure on an infinite slope is described by the factor of safety calculation, FS, that balances the downslope component of gravitational stress against basal frictional shear stress and pore pressure (pressure head): $FS = F_f + F_w + F_c < 1$. The components of FS are defined as:

$$F_f = \frac{\tan \phi}{\tan \alpha}$$

$$F_w = \frac{- P(Z, t)\, \gamma_w \, \tan \phi}{\gamma_s \, Z \, \sin \alpha \, \cos \alpha}$$

$$F_c = \frac{c}{\gamma \, Z \, \sin \alpha \, \cos \alpha}$$

Where α and φ are the slope and soil friction angle, c is soil cohesion, γ_s is depth average soil unit weight, γ_w is the unit weight of water. During a rainstorm, the factor of safety will vary as a function of depth and time reflecting the pore pressure response.

Nakagawa Two Layer Model:

The method proposed by Nakagawa (2001) divides the upper soil layer in three different layers. First the very top soil about 30 cm, second composed of deposited materials about 70 cm and the third layer of watershed rocks at bottom. The factor of safety is computed for each layer considering vegetation, cohesion, porosity of soil infiltration capacity and the two dimensional flow of the water in subsurface. The method also considers the temporal variation of subsurface flow in each layer. The lateral flow is computed using the differential equation of the conservation of mass and continuity equations. The method requires the complicated mathematical modeling in two dimensions with huge set of data to calibrate.

Similarly some other models are-

CHASM-It is a 2D combined hydrological and slope stability model. It is a commercial model.

LAPSUS-LS-It is an extension to the landscape evolution model LAPSUS based on critical rainfall and distribution maps,partly GIS based.

GISLIP- It is an extension to the SHETRAN sediment transport model

SHESLIP-LIP computes hydrology and factor of safety (based on GIS),SHESLIP executes the failure pattern at coarser resolution.

JUST-SLOPE-It is a slope stability model for rotational failures,including ordinary method on slices and Bishop Method.

2.6 Selection of SINMAP Model

The most widely used approach for slope stability and landslide hazard assessment include (Montgomery and Dietrich, 1994): Many of the approaches do not take full advantage of the fact that debris flow source areas are, in general, strongly controlled by surface topography through shallow subsurface flow convergence, increased soil

saturation, increased pore pressures and shear strength reduction (Montgomery and Dietrich,1994). Recently, the availability DEM data has prompted the development of methods that take advantage of geographic information system (GIS) technology to quantify topographic attributes related to slope instability and landsliding. GIS technology permits patterns of instability to be resolved and mapped at the scale of the DEM. This relatively fine scale mapping which can pinpoint hazard areas has particular value for land management. Montgomery and Dietrich (1994) combine a contour based steady state hydrologic model with the infinite slope stability model (simplified for cohesionless soils) to define slope stability classes based upon slope and specific catchment area. Wu and Sidle (1995) present a more elaborate model that couples dynamic modeling of the hydrology with the infinite slope stability model, in a more complex form, accounting for cohesion and varying root strength.

The theoretical background of SINAMP is similar to that of Montgomery and Dietrich (1994) in that it combines steady state hydrologic concepts with the infinite slope stability model. There are a few differences:

 (1) Grid-based rather than contour based DEM methodology is used following the work of Tarboton (1997). This choice is primarily a matter of convenience. Grid-based DEMs are more common and their analysis is easier.

 (2) Cohesion is retained in the infinite slope stability model. This can be used to account for soil cohesion or root strength as modeled by Wu and Sidle (1995), or it may be set to 0 by a user who wants to consider cohesionless situations.

(3) Parameter uncertainty is incorporated through the use of uniform probability distributions and lower and upper bounds on uncertain parameters. This is akin to the probabilistic approach of Hammond et al. (1992), and reflects the real uncertainty associated with estimating parameters in terrain stability mapping.

These are the important capabilities of the model. The results reduce to the deterministic case (equivalent to Montgomery and Dietrich, 1994) when upper and lower uncertainty bounds of the parameters are specified as equal and cohesion is set to zero. The range of uncertainty of the hydrologic wetness parameter may, in an approximate sense, substitute

for the dynamic modeling over a range of storm events used by Wu and Sidle (1995), without requiring analysis and input of weather data. From this the complexity and additional computational burden of analyzing sequences of weather data is unwarranted.

For all these reasons, SINMAP Model has been selected for shallow landslides susceptibility assessment along the Narayanghat-Mugling Highway and the detailed methodological description of SINMAP Model is explained in the next chapter.

2.7 Introduction To Deris Flows

According to Iverson (1997) debris flow is a geological phenomenon in which water laden masses of soils and rocks

- rush down mountainsides,
- funnel into stream channels,
- entrain objects in their path,
- form lobate deposit when they spill onto valley.

Debris flows are a type of mass wasting processes. Mass movement processes can be categorized following some parameters such as the release mechanism, the sort of material, the sediment composition, the proportion of the solid phase, the velocity, the time of the event, the slope of the movement plane, the material behavior, and the physical processes during the mass movement.

Lots of classification of the mass wasting processes can be found in the literature.

Jakob and Hungr. (2001) explained the following terms "earth", "debris" and "mud".

Earth refers to unsorted clayey colluviums, from clay or weathered clay-rich rocks. Earth consistency is closer to plastic limit than the liquid limit.

Debris represents loose unsorted material of low plasticity such as that produced by mass wasting processes, weathering, glacier transport, explosive volcanism, human activity (for instance mine debris). It is a mixture of sand, gravel, cobbles, and boulders and can contain organic material (logs, tree stump and tree trunk). Its consistency is non-plastic or weakly plastic.

Mud is defined as a soft, remoulded clayey soil whose matrix (sand and finer) is significantly plastic and whose liquidity index during motion is greater than 0.5.

Debris flows are composed of water and debris (solid particles). The solid phase occupies a larger volume than the liquid phase. The solid particles can be classified in two groups: fine particles (clay, silt and sand) and coarse particles (gravel, cobbles, boulders and organic particles too). Debris flows and mudflows have more or less the same water concentration but they differ in the solid particle size. Indeed solid particles of a debris flow are coarser than those of mudflow or lahars. Debris flows and mudflows are mixture of water and fine and coarse particles . Boulder diameters go up to a few meters. Generally boulders look suspended in the mass.

• Some authors rather consider Debris flow as landslide with a fluid-like runout behaviour (Corominas et al. 2008)

• Others consider it as runoff with very high sediment concentration, with sediment predominantly originating from the stream bed (O'Brien,2003;Rickenmann,1999).

As stated by Rickenamnn (1999), debris flows are phenomena intermediate between landslides and runoff. Many debris flow events in the real world share features of both types of processes, but many of them have a clear tendency to the one or the other. Some authors distinguish between debris flows on slopes (from landslides) and debris flows in channels (from erosion in and around the stream bed; e.g. Wichmann,2006).

Different processes are often tightly coupled, for example when a landslide rushes into a stream bed and the deposit is transported further downwards by the influence of stream flow either immediately or after a certain delay (e.g. during the next heavy rainfall event). Debris flow movement shows properties different from the flow of clear water, requiring specialized and complex methods to be modeled in a fully deterministic way (Savage& Hutter1989; Hungr1995; Iverson1997).

2.8   Mechanics of Debris Flows

Debris flows occur when masses of poorly sorted sediment, agitated and saturated with water, surge down slopes in response to gravitational attraction. Both solid and fluid

forces vitally influence the motion, distinguishing debris flows from related phenomena such as rock avalanches and sediment-laden water floods. Whereas solid grain forces dominate the physics of avalanches, and fluid forces dominate the physics of floods, solid and fluid forces must act in concert to produce a debris flow. Other criteria for defining debris flows emphasize sediment concentrations, grain size distributions, flow front speeds, shear strengths, and shear rates [e.g., Varnes, 1978;], but the necessity of interacting solid and fluid forces makes a broader, more mechanistic distinction. Generally the debris flow have a very high volumetric concentration. The maximum velocity can even exceed 10ms^{-1}.
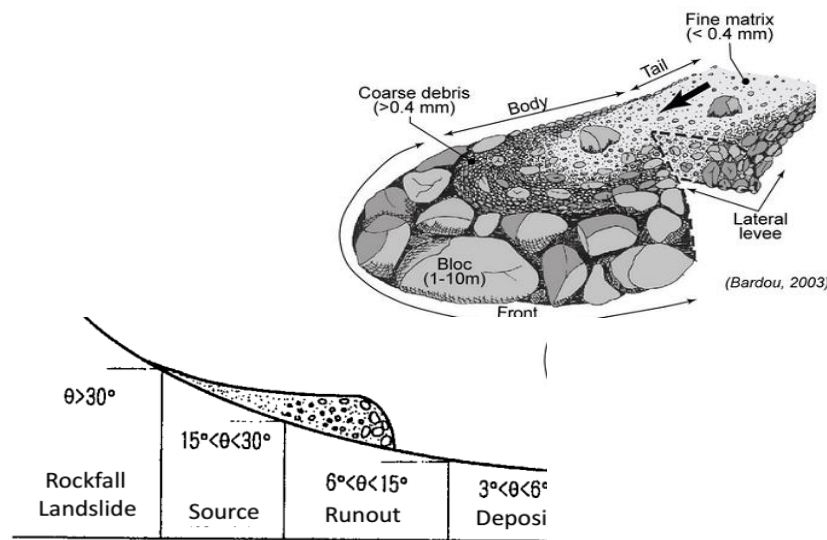
Figure 2.5 Illustration of mechanism of debris flows (Source: Wu, 2014)

According to Takahasi (2007), the triggering conditions for debris flows are-

• Mass source for debris flow

–Loose, unpacked sediment deposition, or mass from landslide

• Input enough water

–Rainfall from typhoon, storm

• Appropriate slope angle (15~30˚)

–Too steep (>30˚), only landslide

–Too mild (<15˚), only flood

    In the due process, soil/rocks & water separates .

Velocity is a key variable that determines the destructiveness and catastrophic influence of debris flows around the world .They can reach extreme velocities and increase their sediment discharge, picking up more sediments and larger objects down the run out path.

Table 2.5 Debris flow rates of movement (Source: WP/WLI, 1995)

Movement Rate	Velocity Class	Velocity Limits	Rate (mm/sec)	Debris Flow Range
Extremely rapid	7			
Very rapid	6	5m/sec	5×10^3	
Rapid	5	3m/min	50	
Moderate	4	1.8m/hour	0.5	
Slow	3	13m/month	5×10^{-3}	
Very slow	2	1.6m/year	50×10^{-6}	
Extremely slow	1	16mm/year	0.5×10^{-6}	

Two main forms of debris flow can be distinguished-

Hillslope (open source) debris flows- Hill slope debris flows create their own path down the valley slope as tracks or sheets depositing their materials on lower slope gradients(Varnes,1978)

Channelized debris flows-These follow existing channels like valleys, gullies and other types of topographic depressions. According to Cruden (1991), channelized flows are of high density with 80%solids by weight. These further seem to have a consistency similar to that of wet concrete in many cases (Hutchinson,1988).

a) Hillslope Debris Flow   b) Channelised Debris Flow
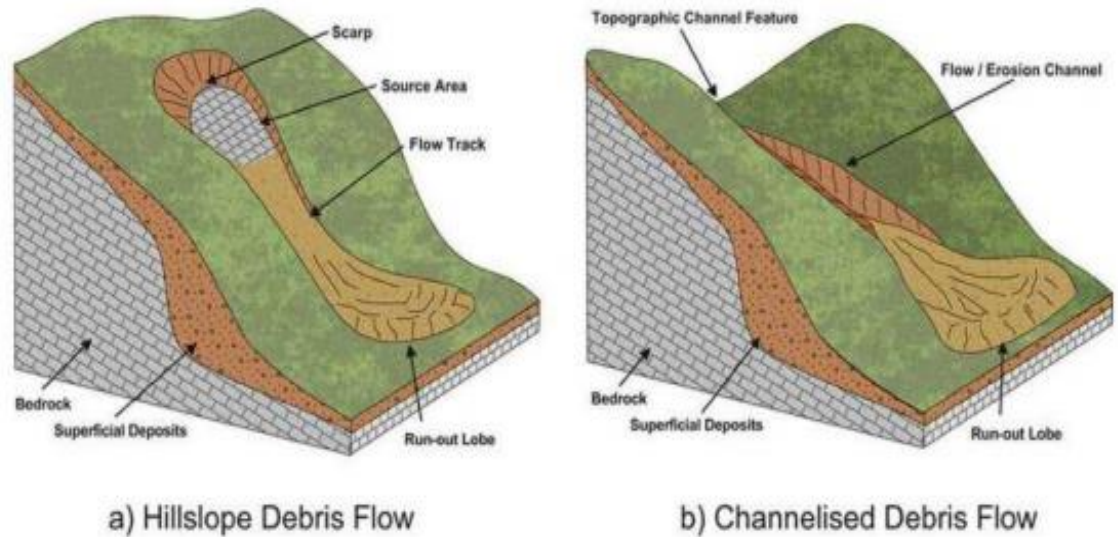
Figure 2.6 Hillslope and Channelised debris flow (Nettleton et.al,2005)

The formation mechanism of the rainfall-induced slope flow can be explained as follows. Because of rainwater infiltration, the pore water pressure of the rock increases, and soil shear strength reduces; a part of soil mass exhibits shear failure, and there are shear fissures and tension fissures in the slope soil, which leads to the expansion of some existed fissures and holes. The rainwater infiltration saturated these fissures; the pore water pressure of the damaged soil continually increases and begins to form an excess pore water pressure; soil shear-failure zone extends and connects to form a shear surface, and along the shear surface, there is percolating force caused by seepage, resulting in further reduction of soil strength. When the shear strength is below the shear stress in the failure surface, the slope rock-soil masses start to slide down; in the course of sliding, soil mass collides and disintegrates accompanied with mud-making, then leading to a debris flow.

2.8.1 Formulation and evolution process of slope flow
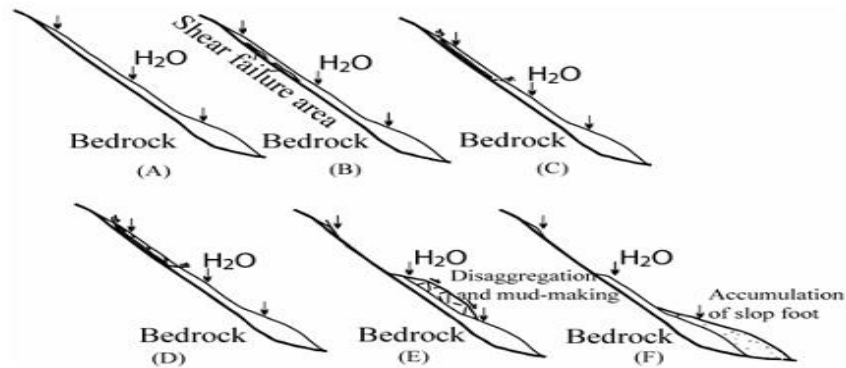
Figure 2.7 Formulation evaluation sketch map of debris flow on slope induced by rainfall

(Weimin et.al.,2007)

A-Rainwater infiltration and saturation stage. Because of the rainstorm or continued rainfall infiltration, the pore of the non-saturated soil mass fills with water, matrix suction will gradually decrease or loss, and the pore water pressure of potential failure surface will increase.

B- Local shear failure phase. With the pore water pressure increasing, the residual soil and the soil mass near the rock interface exhibits shear deformation owing to the effective stress decreasing, which results in the pore water pressure of soil masses in the shear deformation zones decreasing, and this causes the water in pores and fissures to infiltrate into the shear failure soils.

C- The throughout extending stage of the slide.The intensity of local slope soil decreases with shear failure, and at the same time, the pore water pressure restored and increased in the shear soil, which leads to further decrease of the soil intensity. With the intensity of the damaged soil decreasing, the shear stress shifts to the adjacent soil, and this may cause higher shear stress than its shear strength and leads to the shear failure of the adjacent territory soil. With the shear failure region extending, it finally expands throughout and forms a continuous shear failure surface.

Available online at http://www.ijart.info/

D- The initiation of landslide on slope After the shear failure surface of the slope soil is formed, there are tensile cracks in the back edge of the slope. The surface flow on the slope infiltrates along the tensile cracks, and produces downward infiltration stress along the shear failure surface. Once the shear stress and the infiltration stress are greater than the shear strength of the soil mass, the slope soil start to rush down as a whole.

E- Disintegration and mud making stage of the slide. After the slope soil started to rush down, they are subjected to collision, separation and disintegration owing to the tension fissure and shear fissure in the slip masses and different slip rates amongst blocks, and the debris mud forms by the effect of slope current and pore pressure.

F- Slope flow movement and accumulation . Debris mud masses are accelerated downward along the steep slope surface by gravity; they meet the surface water and rainwater in the course of movement and their content of slurry water and mobility increase. Because the slurry mud masses have higher viscosity, they cut and erode the slope in the course of their movement, which increases the content of solid debris in the mudflow. Finally, the debris flow may stop and pile up at a gentle slope (often at the foot of a slope), or stop at a place on their path owing to the depletion of their kinetic energy and pile up on either side of the ditches

Debris flow, as other gravitational mass movement, can be divided in three phases:

Initiation phase, in which the initial mass is released .It consists of a   steep open source or may contain depressions like gullies and existing stream channels. In this zone, slope failure or increase in discharge in a channel triggers materials to loosen and descends down the slope. Debris flow at this zone can first start off like other type of landslides like translational/rotational, scree/rock falls, rock slides or debris avalanches and eventually form into a debris flow further down the flow path. Heavy rainfall forms an important triggering factor which contributes to the disintegration of sediments and combines it with surface water to further mobilize the flow downstream.

Transition phase, also called transport zone, in which the initial mass propagates along the travel path. It can often be a steep mountain channel where debris is incorporated by erosion(entrainment). Coarse granular avalanches can shift into a flow like motion,where

volume and saturation of the debris flow is most likely to increase within the transport zone. In this zone of flow path the decrease in slope angle once reaching below a specific value starts triggering the deposition of debris(Jackob and Hungr ,2005).Deposition within the transportation zone, when observed in the field can have the form of levees or cone shaped lobes.

Deposition phase, when the mass stops and is deposited on a colluvial fan. It is in most cases a debris fan and starts at the fan apex, where the debris flow starts depositing materials as the slope decreases. Possible reasons for deposition of debris onto the fan are obstructions within the channel, momentum loss on bends or decrease in channel height, causing the flow to be less confined and avulsions to take place. This zone is most likely to have elements at risk, being hit by the debris flow deposits like bridges, roads ,houses and electrical lines.
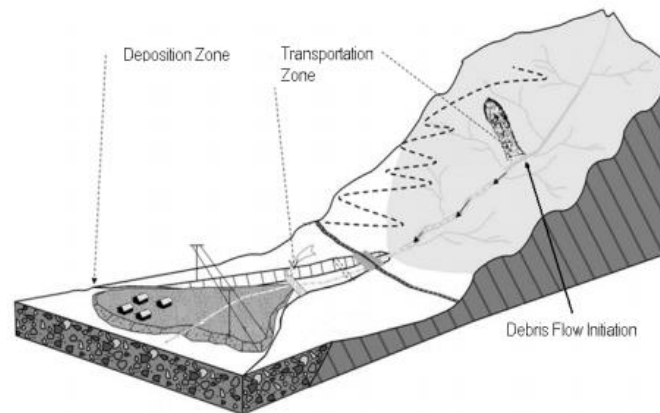
Figure 2.8 Schematic diagram of a debris flow path (Hussin, 2011)

The debris flow can be initiated by one of the following ways-

2.8.2 Landslide-induced debris flow

Debris flows, mobilized from numerous small landslides or from a large and individual landslide, are the most common type. They occur when a debris slide or landslide changes into a debris flow. The process of forming debris flows from a static mass of water-laden soil, sediment or rock is called mobilization. Mobilization occurs under three conditions which are:

- the failure of the mass,
- a sufficient amount of water to saturate the mass,
- a sufficient conversion of the gravitational potential energy to the internal kinetic energy. The conversion of the energy changes the type of mass movement from a slide on a failure surface to a flow.

In addition to the water content in the soil, torrents can contribute to increase the water content. But in general, the required amount of water is already contained in the soil mass when the failure occurs. In this case, the water comes from rainfall infiltration or snow melt.

When the initial landslide mass rides on the torrent bed deposits , an undrained loading process may generate a high pore-water pressure within the torrent deposits and this helps incorporate those deposit into moving mass. This phenomenon is called the liquefaction failure of the torrent deposits which results in the entrainment of the bed material. Thus the volume of the debris flow increases significantly.
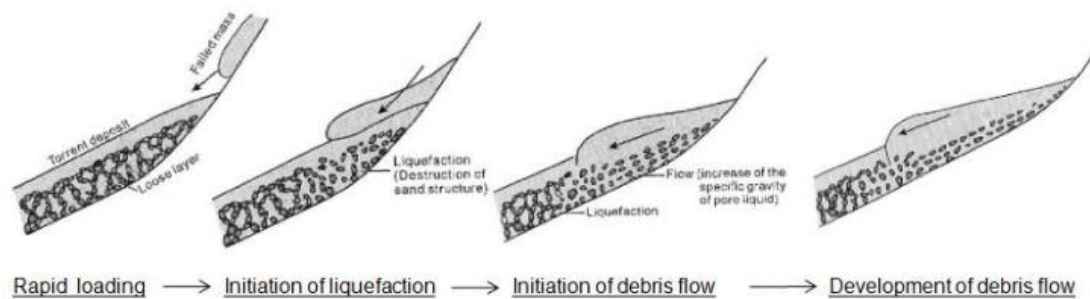
Figure 2.9 Illustration of the initiation of debris flow (Sassa,1985)

Flow Variation in time:

Debris flows are unsteady and non-uniform flows because they move downslope as waves or series of waves. They are pulsating flows. Surges are separated by watery inter surge flow. Surges grow extempore due to flow instability, or due to the occurrence of consecutive landslides releasing material, or due to a slowdown of the flow followed by a boulder dam break. The volume of each surge may vary. The time separating surges is seconds to hours. Debris flow events can be composed of one to many tens waves.

Geomorphologic characteristics:

The solid concentration varies in the surge and thus debris flow surges have a typical longitudinal cross section. (Figure 2.10). Surges are composed of three parts. The tail, also called "after flow", is a flow of sediment-laden water. This part has the same characteristics as a debris flood, i.e. dilute and turbulent. This part continues until the next debris flow surge comes or until the debris flow event stops. The body of the surge is the middle part where there is a finer mass of liquefied debris. The last part of the surge is the head, which has an abrupt front. It carries the greatest concentration of large boulders and other debris. The head is free of matrix. The large sediment class can be incorporated and retained in the head if the flow takes them during the motion. Otherwise they come from the tail and migrate to the head by preferentially transport. The depth of the flow and the concentration of solid decrease progressively from the head to the end of the tail . The body of the surge is a water-saturated and liquefied fluid whereas the snout is unsaturated. The interactions between both parts give the debris flow motion and deposition characteristics, for instance the lateral levees.(Blanc,2008)
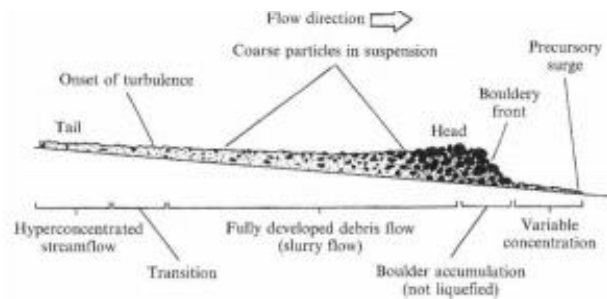
Figure 2.10 Sketch of debris flow surge (Pierson,1987)

2.9 Research On Debris Flow Modelling

2.9.1 1D Debris flow Models:

1D Analytical Models:

1D analytical models are approaches that reduces the debris flow to one point and calculate its dynamics along a previously selected flow path. All forces acting on the

moving mass can be described at any position using Newton's second law and applying a simple flow resistance law.

Analytical models were used to calculate dynamics of different types of mass movements including rock avalanches (Körner, 1976),flow slides (Hutchinson, 1988); snow avalanches (Voellmy,1955) and also debris flows (Rickenmann, 1990). The frictional-turbulent Voellmy fluid flow rheology has been applied to granular debris flows both in continuum models (Hungr, 1995) and in the mass point model (Rickenmann,1990). For the latter, it can be expressed by

$$\frac{1}{2}\frac{dv^2}{ds} = g(\sin\theta - \mu_m \cos\theta) - \frac{v^2}{k}$$

where s is the curvilinear distance;gthe gravity, andθthe slope angle.The twoflow resistance parameters are the sliding friction coefficient, μ_m, and the "turbulence"coefficient,k, which is called "Mass to Drag ratio"by Perla et al. (1980). Both parameters should be determined by back analysing of historic events.

Another analytical model considers only the depositional part of debris flows. Applying the momentum principle and assuming both constant discharge and bed slope on the fan (Hungr et al., 1984; Takahashi, 1991), this model allows a more exact calculation of the runout distance and flow velocity on the fan, but it requires additional input data, such as the velocity and flow depth at the fan apex. Similarly as for the previous mass point model, an appropriate friction slope has to be calibrated based on observed runout distances on the fan (Rickenmann et. al., 2006).

 1D Numerical Models:

In the last decades, many 1D numerical codes have been developed to simulate debris flows (e.g.Savage and Hutter, 1989; Hungr, 1995;Iverson, 1997). For most models it is assumed that the solid–fluid mixture behaves as a quasi-homogeneous fluid. A number of models are based on a rheological formulation for a Bingham or viscoplastic fluid (e.g.Laigle and Coussot, 1997; Fraccarollo and Papa, 2000; Imran et al.,2001), some of them including a friction term accounting for channel roughness and turbulence (Han and

Wang, 1996; Jin and Fread, 1999). Only in some model applications, the exact values of the rheological parameters were known. Often, appropriate values for the rheological parameters were assumed or back-estimated from field observations. In several model applications, the Voellmy fluid flow rheology was successfully used for back-calculating velocity and runout distance of debris flows (e.g.Jakob et al., 2000; Hürlimann et. al., 2003b; Revellinoo et al., 2004; Naef et al., 2006). The application of Voellmy fluid rheology to numerical modeling can be expressed by the total friction slope S_f.

$$S_f = \mu \cos\theta + v^2/(C^2 R)$$

where μ is the dry friction coefficient; C the turbulent friction term (a pseudo Chezy coefficient for debris flows) and R the hydraulic radius.

The required input data for 1D modeling normally consists in a topographic profile, cross-section shape, initial volume or input hydrograph and rheological or friction parameters. The selection of both the appropriate rheological flow law and the suitable parameter values are of great importance. The calibration of model parameters can be best developed through the back analysis of historic events. Contrary to the previous runout methods, numerical models can simulate the total runout distance, as well as the velocity and flow depth at each point along the flow path

2.9.2 2D Debris Flow Models

In the case of debris-flow hazard assessment, the two-dimensional models are widely used now. Necessary input data are the DEM, position and magnitude of initial volume or input hydrograph and rheological parameters. The main advantages of 2D models are the simplified description of the flow properties (e.g. the friction relations used as an approximation of the flow "rheology"), and the ability to describe the flow routing in case of irregular ground topography. Frequently the models assume a fixed set of friction coefficients for an event which are difficult to accurately calibrate (Stolz and Huggel, 2008; Hurlimann et al., 2008)

FLO2D:

FLO-2D model developed by O'Brien and Julien,1985, simulates debris-flow using finite-difference routines in two dimensions. The modeling of a debris-flow is controlled by topography and is performed using numerical integration of movement and continuity equations and flow-resistance parameters. Sediment flows are simulated using hyper-concentrated sediment-flow routines with continuous flows, which enable to predict the behavior of fluid flow from a fluid matrix governed by sediment concentration. FLO-2D uses a quadratic rheological model, developed from field and laboratory mudflow data, and enables appropriate simulations of flooding conditions ranging from clear water to hyper concentrated sediment flows . O'Brien and Julien define the FLO-2D rheological model with the following approximation:

$$S_f = S_y + S_v + S_{td}$$

where, S_f is the total friction slope, S_y is the sum of the yield slope, S_v is the viscous slope, and S_{td} is the turbulent-dispersive slope. The total friction slope can be written as follows:

$$S_f = \frac{\tau_y}{\gamma_m\, h} + \frac{K\, \eta\, V}{8\, \gamma_m\, h^2} + \frac{n_{td}^2\, V^2}{h^{4/3}}$$

The first term is the yield stress where, τ_y is yield stress, γ_m is the specific weight of the slurry(debris flow), h is flow depth; The second term describes a viscous stress where K is an empirical resistance parameter growing with roughness, η is the fluid viscosity(Bingham dynamic viscosity), V is flow velocity ; and the third and fourth terms are turbulent and dispersive stress, respectively, merged into one variable n_{td} that is described as a turbulent dispersive roughness connected with fluid concentration and n_{td} is Manning's roughness coefficient.

The yield stress and fluid viscosity are defined from :

$\tau_y = \alpha_1 \exp(\beta_1 C_v)$

$$\eta = \alpha_2 e(\beta_2 C_v)$$

where, α_1 and β_1 are empirical coefficients defined by laboratory experiments . Simulation of debris-flow with the FLO-2D model requires measurement of the flow tension and viscosity.

RAMMS Model :

The RAMMS model was initially developed as a tool to assist practitioners for solving snow avalanche runout problems which could not be solved with existing 1D runout models. The Voellmy friction relation used to describe the motion of flowing snow has also been used to describe the motion of debris flows (Rickenmann et. al, 2006), the main difference being the density of the materials and the typical values of the friction coefficients. The initial application of RAMMS to debris flows was tested largely in the framework of research theses written by students (Scheuner, 2007). The RAMMS: DEBRIS FLOW module was developed to simulate the runout of muddy and debris-laden flows in complex terrain. The module is used in Switzerland and worldwide for debris flow hazard analysis and to aid in the design mitigation measures. It combines state-of-the-art numerical solution methods with helpful input features and user-friendly visualization tools. Many of the input and output features have been optimized to allow engineers and geoscientists to define event scenarios, evaluate simulation results, and predict the influence of proposed structural mitigation measures on the runout of debris flows.

The model is based on a finite-volume solution to the depth-averaged equations of motion for granular flows:

$$\partial_t H + \partial_x (HU_x) + \partial_y (HU_y) = 0$$

$$\partial_t (HU_y) + \partial_x (HU_x^2 + g_z \frac{H^2}{2}) + \partial_y (HU_x U_y) = S_{gx} - S_{fx}$$

$$\partial_t (HU_y) + \partial_x (HU_x U_y) + \partial_y (HU_y^2 + g_z \frac{H^2}{2}) = S_{gy} - S_{fy}$$

where, H is the flow depth, U is the velocity, g is the gravitational acceleration; Sg is the driving gravitational; and Sf denotes the frictional resistance, with subscripts x and y indicating the quantities in the x and y directions. RAMMS uses the Voellmy friction approach, which splits the total friction into a velocity-independent dry Coulomb term which is proportional to the normal stress at the base of the flow (friction coefficient μ) and velocity-dependent so-called turbulent or viscous friction (coefficient ξ). The Voellmy relation can be written (analogously in both the x and y directions):

$$S_f = g_z H \mu + \frac{g_z U^2}{\xi}$$

In an optimal case, μ (–) and ξ (m s-2) are selected to best match data from historical events. When data are not of sufficient quality to permit calibration, μ is typically initially selected to be the same as the local slope on the area where debris flows have stopped in the past, and then ξ is selected to provide plausible velocities which may be based on existing observations, back-calculated flow velocities estimated by geomorphic methods (such as super-elevation around channel bends).

KANAKO-2D:

The GUI-equipped debris flow simulator is called "Kanako", (Ver.2.00), which can simulate 1-D debris flow in gullies and two-dimensional (2-D) debrisflow in alluvial fans. For gullies, it uses a 1-D numerical simulation model to reproduce variations in a mountainous riverbed caused by debris flow and to simulate the effects of closed, slit, and grid types of Sabo dams [Satofuka and Mizuyama, 2005]. For alluvial fans, it uses a 2-D numerical simulation model to reproduce changes in flow depth and sedimentation to simulate the passing area of debris flow.

Many models simulate the boundary areas between gullies and alluvial fans using the 1-D downstream end result as the 2-D upstream boundary condition. In contrast, our integration model simulates 1-D results for gullies and 2-D results for alluvial fans at each time step, incorporating mutual influences in both models. This enables the system to produce more accurate results, especially when marked sedimentation occurs in a boundary area.

The basic 2-D debris flow equations are shown below. The system applies the same equations used in 1-D debris flow simulations, but includes y-axis direction terms. The equations for momentum, continuation, riverbed deformation, erosion/deposition, and riverbed shearing stress are based on previous research [Takahashi and Nakagawa, 1991], as are the staggered scheme and arrangement of variables [Takahashi and Kuang, 1987](Source: Nakatani et. al.,2008)

The continuation equation for the total volume of debris flow is-

$$\frac{\partial h}{\partial t} + \frac{\partial uh}{\partial x} + \frac{\partial vh}{\partial y} = i$$

The continuation equation for determining the debris flow of the k-th grade of particle i is –

$$\frac{\partial C_k h}{\partial t} + \frac{\partial C_k hu}{\partial x} + \frac{\partial C_k hv}{\partial y} = i_k C_*$$

Here, two groups of grain-size classes are considered for sediment material: the larger grain size group, which affects grid-type sabo dam blockage; and the smaller grain size group, which does not affect blockage. When considering riverbed deformation (except when setting the upper point of a grid-type sabo dam), the average grain-size of all sediment materials is used, including both larger and smaller grain-size groups.

The phenomenon of x-axis direction (flow-) flow is given by a momentum equation, as follows:

$$\frac{\partial u}{\partial t} + u\frac{\partial u}{\partial x} + v\frac{\partial u}{\partial y} = g\sin\theta_{wx} - \frac{\tau_x}{\rho h}$$

The phenomenon of y-axis direction (cross-direction) flow uses a momentum equation, as follows:

$$\frac{\partial v}{\partial t} + u\frac{\partial v}{\partial x} + v\frac{\partial v}{\partial y} = g\sin\theta_{wy} - \frac{\tau_y}{\rho h}$$

The equation for determining change in bed surface elevation is as follows:

$$\frac{\partial z}{\partial t} + i = 0$$

IJART

SPH-Depth integrated Model:

The depth integrated, coupled with the SPH model, is able to simulate the propagation of debris flows (and also landslides). It is based on a mathematical model, on rheological models and on a numerical model. The mathematical model, which is the coupled depth integrated model, comes from a velocity-pressure version of Biot-Zienkiewicz equations. Next, rheological models relate stress and strain tensor. The third part is dedicated to the description of basic concept regarding the SPH method, which constitutes the numerical model. Then the next describes both the Egashira and Hungr erosion laws.

Assuming a fixed volume, which corresponds to a column integrated along depth and moving with an averaged velocity, the equations of the depth integrated model are:

$$\frac{Dh}{Dt} + h\,\mathrm{div}(\bar{v}) = e_r$$

$$\rho \frac{D(h\bar{v})}{Dt} + \mathrm{grad}\left(\frac{1}{2}\rho g h^2\right) = -\frac{1}{\rho}e_r\bar{v} + \rho b h + \mathrm{div}(h\bar{s}) - \rho g h\,\mathrm{grad}\,Z - \tau_b - \rho\,h\,\bar{v}\,\mathrm{div}(\bar{v})$$

$$\frac{\partial}{\partial t}\left(P_{w_i}h\right) + \frac{\partial}{\partial x_k}\left(\bar{v}_k P_{w_i}h\right) = -\frac{\pi^2}{4h^2}c_v P_{w_i}$$

Smoothed particle hydrodynamics is a meshless method based on discretized forms of integral approximations of functions and derivatives. The method was introduced independently by Lucy (1977) and Gingold and Monaghan (1977) and applied to astrophysical modeling, a domain where SPH presents important advantages over other methods (Monaghan and Latanzio,1985).(Source: Blanc, 2008)

2.10 SELECTION OF DEBRIS-2D MODEL

Debris flows are frequent phenomena in Nepal. To minimize the possible hazards caused by debris flows, the common countermeasures include the construction of dams, the limitation of land use, and habitant evacuation. Two of the common uncertainties during the planning of countermeasures are the hazard zone area and the path of debris flows.

Several empirical formulas may be used to obtain part of the information required in the designing processes. However, empirical formulas may be inaccurate in complicated

geographic regions, even for the order of magnitude. A superior method to obtain the required information is to use numerical simulation.

Non-Newtonian fluid models were often used in previous studies of debris flow. Early analytical or numerical studies of Bingham-like fluids were limited mainly to one- or two-dimensional spreading on an inclined plane. Liu and Mei (1989) presented a two-dimensional theory for the unidirectional slow flow of Bingham fluid on a slope. Huang and Garcia (1998) worked on the same problem for Herschel–Bulkley fluid. For three-dimensional flows, the slow and steady spreading of mud released from a point source on a plane was investigated by Hulme (1974) with a Bingham model, and by Coussot and Proust (1996) and Wilson and Burgess (1998) with a Herschel–Bulkley model. The static problem of the final deposit on an inclined plane was studied experimentally by Coussot et al. (1996) and by Osmond and Griffiths (2001). For a horizontal plane bottom, Coussot (1997), Griffiths (2000) and Mei, Liu and Yuhi (2001) derived analytical and numerical solutions for the radically symmetric evolution. For high-speed flows, Liu and Mei (1994) and Ng and Mei (1994) examined the nonlinear formation of roll waves for a Bingham fluid and a power-law fluid, respectively. Most debris-flow models focused on laboratory scale experiments or slow debris flow motion in a regular channel. However, debris flows occurring in the field markedly differ from those in a controlled environment. It is difficult to simulate debris flow both numerically and experimentally. Major and Iverson (1999) used a two-phase flow model to simulate debris flow moving from a large flume(2 m wide by 95 m long) to a wide deposition basin. O'Brien and Julien (1997) used a quadratic constitute to simulate high concentration flows. The DEBRIS-2D program was developed by Liu and Huang (2006) for field debris flow simulation. This model was verified by a 1-D analysis solution, laboratory testing and a field case. In addition, this model was used in numerous practical applications in Taiwan.

VERIFICATION OF DEBRIS-2D MODEL:

   The verification of DEBRIS-2D Model can be done by comparing, in the following ways: (Huang, 2003; Liu & Huang, 2006)

–Analytical solution (Error < 0.2 %)

–Flume tests in the laboratory (Error < 2 %)

–Field case study (Error ≈10 %)

$\Delta x = 0.01$

$\Delta t = 0.001$

Error ≤ 0.2%

Front Position
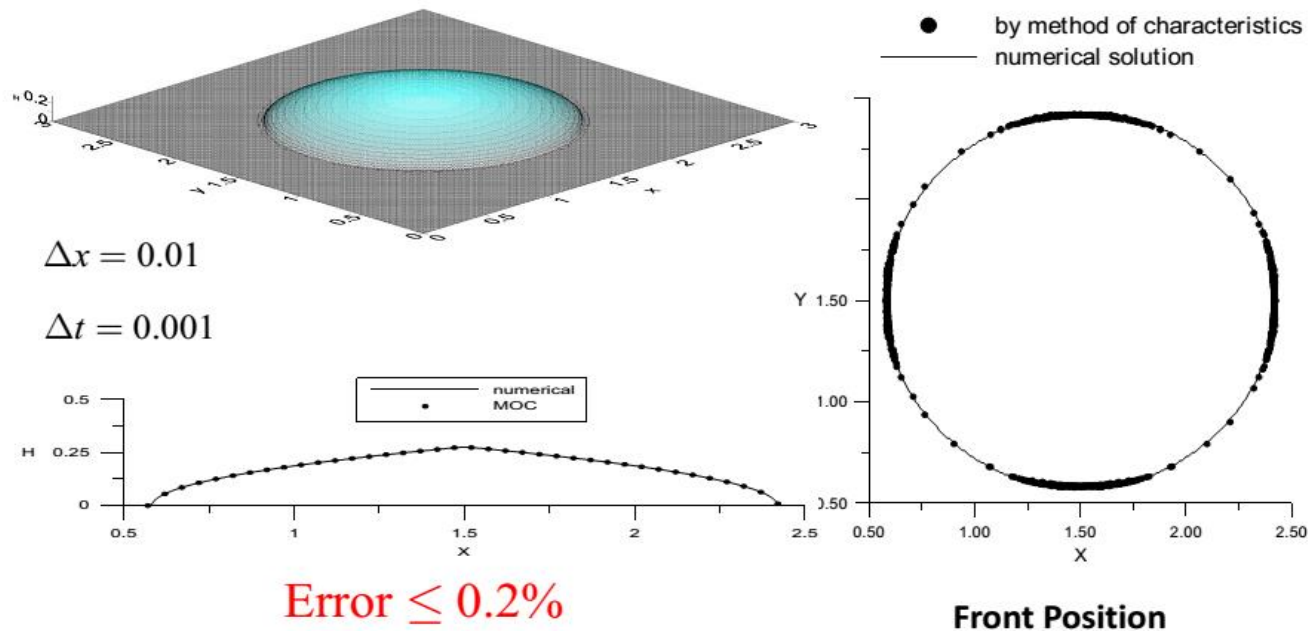
Figure 2.11 Analytical and numerical solution of DEBRIS-2DVerification (Huang,2003)

Error ≤ 2%

Comparison Result
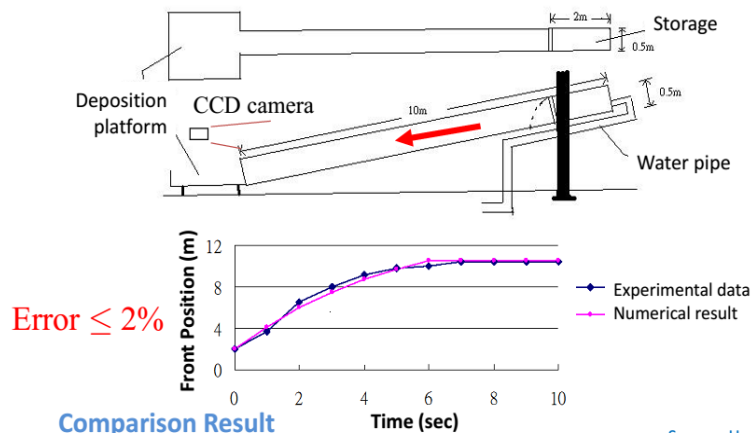
Figure 2.12 Experimental Setup of Flume Test for verification of DEBRIS-2D

(Huang,2003)
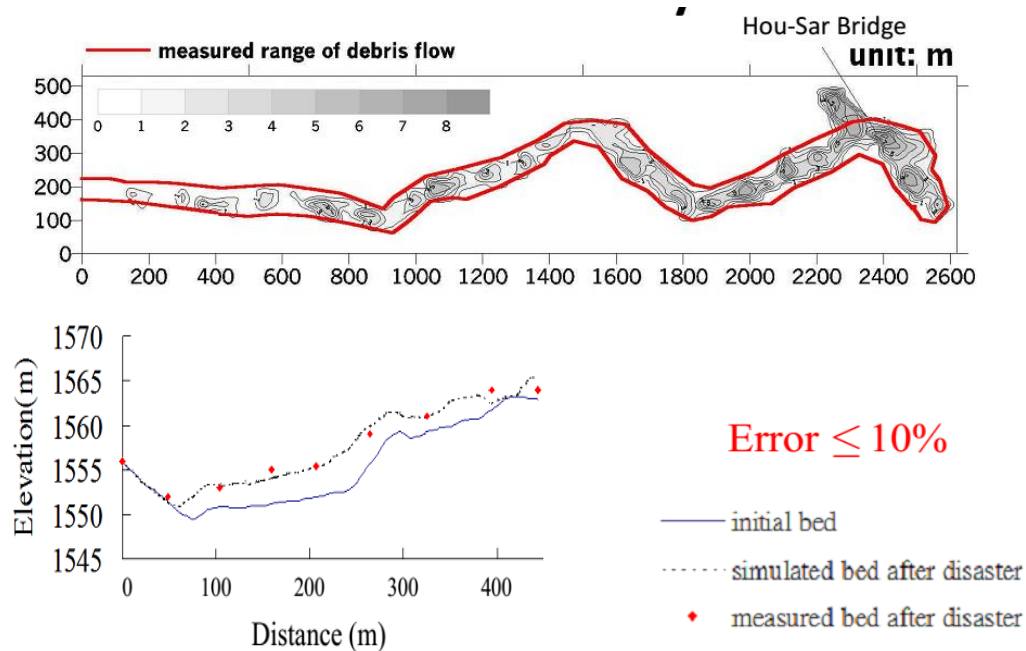
Figure 2.13 Field Case Study for DEBRIS-2D Verification (Huang, 2003)

Although numerical simulation is considered a superior approach, the challenges for real engineering projects is in the uncertainties of numerous input data. The geographical data is available, but is rarely in high precision. Two main problems are the total amount of available soil that can be eroded or mobilized during heavy rainfall and the rheological properties that can correctly represent the field material. If these parameters are not precisely resolved, any modeling would be incorrect. However, for engineering purposes, a 20 % error in these data may be common; therefore, we must determine the errors that will be induced in the final result. If the parameters are sensitive, efforts to precisely locate the parameter must be emphasized. Conversely, for insensitive parameters, an approximate estimate may satisfy engineering purposes.

This model have been widely used for hazard map preparation for local governments in Taiwan for over 10 years. It has been used as Design Reference for control engineering or countermeasure and also as an official teaching tool for ICL & UNESCO. It has been verified to be practical and reliable on debris flow simulation. For all these reasons,DEBRIS-2D model was used to simulate the debris flow in Kamere Khola watershed along Mugling Narayanghat Highway. The results obtained would be useful for engineering designs and estimates to mitigate effectiveness.

Available online at http://www.ijart.info/

3. METHODOLOGY

The two models have been used to assess the landslides and debris flow phenomenon. In order to assess the susceptibility approach to terrain stability mapping along the N-M Highway deterministic process-based computer-modeling program have been chosen, i.e., SINMAP (Stability INdex MAPping) (Pack et al., 2005).Moreover,to quantify the debris flow potential and to apply the simulation technique on debris flow hazard zone delineation in Kamere Khola Watershed along the same Highway(24+740),DEBRIS-2D have been chosen. More detailed methodological description of these two models are described below:

3.1 Inroduction to SINMAP Model

SINMAP is an objective terrain stability mapping tool that compliments other types of terrain stability mapping methods. It is applied to shallow translational landsliding phenomena controlled by shallow groundwater flow convergence. The SINMAP (Stability INdex MAPping) methodology is based upon the infinite slope stability model (e.g. Hammond et al.,1992; Montgomery and Dietrich, 1994) that balances the destabilizing components of gravity and the restoring components of friction and cohesion on a failure plane parallel to the ground surface with edge effects neglected. The pore pressure due to soil moisture reduces the effective normal stress, which through the friction angle is related to the shear strength. Pore water pressure is computed assuming a hydrologic steady state with depth of saturated soil computed sufficient to sustain a lateral discharge proportional to the specific catchment area (the upslope area per unit contour length). SINMAP derives its terrain stability classification from inputs of topographic slope and specific catchment area and from parameters quantifying material properties (such as strength) and climate (primarily a hydrologic wetness parameter). Each of these parameters is delineated on a numerical grid over the study area. The primary output of this modeling approach is a stability index, the numerical value of which is used to classify or categorize the terrain stability at each grid location in the study area. The topographic variables are automatically computed from digital elevation model (DEM) data. The other input parameters are recognized to be uncertain so are

IJART

specified to SINMAP in terms of upper and lower bounds on the ranges they may take. The stability index (SI) is defined as the probability that a location is stable assuming uniform distributions of the parameters over these uncertainty ranges. This value ranges between 0 (most unstable) and 1 (least unstable). Where the most conservative (destabilizing) set of parameters in the model still results in stability, the stability index isdefined as the factor of safety (ratio of stabilizing to destabilizing forces) at this location under the most conservative set of parameters. This yields a value greater than1.(Pack et.al.,2005)

3.1.1 Infinite Slope Stability Model In SINMAP

SINMAP methodology is based upon the infinite-slope stability model (Hammond et al., 1992; Montgomery and Dietrich, 1994) that balances (with edge effects neglected) destabilizing components of gravity against stabilizing components of friction and cohesion on a failure plane parallel to the ground surface. Based on the infinite-slope form of the Mohr–Coulomb failure law as expressed by the ratio of stabilizing forces (shear strength) to destabilizing forces (shear stress) on a failure plane parallel to the surface, the safety factor (SF) calculation in SINMAP is(simplified for wet and dry density the same, from Hammond et al., 1992):

$$SF = \frac{C_r + C_s + \cos^2\theta[\rho_s g(D - D_w) + (\rho_s g - \rho_w g)D_w]\tan\phi}{D\rho_s g \sin\theta \cos\theta}$$

(1)

 where,

 C_r is root cohesion (N m^{-2}),

$C_s$is soil cohesion (N m^{-2}),

θ is slope angle (°),

ρ_s is wet soil density (kg m^{-3}), ρ_w is the density of water (kg m^{-3}),

 g is gravitational acceleration (9.81 m s^{-2}),

D is the vertical soil depth (m),

D_w is the vertical height of the water table within the soil layer (m), and

ϕ is the internal friction angle of the soil (°),

θ is the arc tangent of the slope S, expressed as a decimal drop per unit horizontal distance.

Fig. 3.1 illustrates the geometry assumed in Eq. (1).
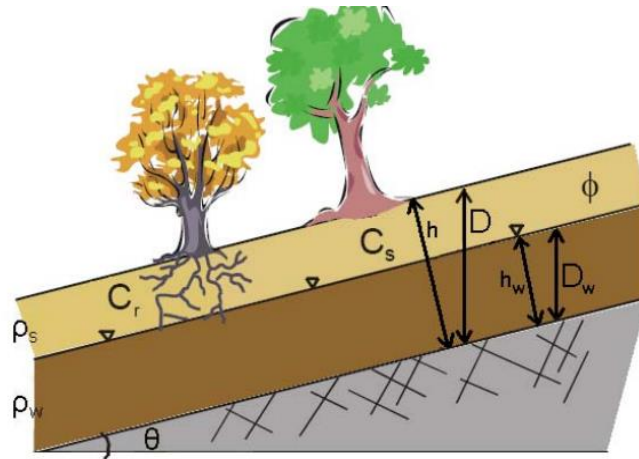
Figure 3.1 Diagram illustrating the geometry of assumed infinite slope stability model including parameters

Soil thickness, h(m), and depth D are related as h=Dcosθ, which produces the dimensionless form of the infinite-slope stability model:

$$SF = \frac{C + \cos\theta(1 - wr)\tan\phi}{\sin\theta}$$
(2)

where,

w= D_w/D = h_w/h   (3)

is the relative wetness,

C=(C_r+C_s)/(hp$_s$g)   (4)

is the combined cohesion (root and soil) made dimensionless relative to the perpendicular soil thickness, and

$r=p_w/p_s$ (5)

is the water-to-soil density ratio

Equation (2) is the dimensionless form of the infinite slope stability model that we use. This is convenient because cohesion (due to soil and root properties) is combined with the soil density and thickness into a dimensionless cohesion factor, C. This is the ratio of the cohesive strength relative to the weight of the soil, or the relative contribution to slope stability of the cohesive forces. Figure 3.2 illustrates this concept. The second term in the numerator of equation (2) quantifies the contribution to stability due to the internal friction of the soil (as quantified by friction angle, φ, or friction coefficient, tanφ).This is reduced as wetness increases due to increasing pore pressures and consequent reductions in the normal force carried by the soil matrix. The sensitivity to this effect is controlled by the density ratio r (equation 5).

Practically, the model works by computing slope and wetness at each grid point, but assuming other parameters are constant (or have constant probability distributions) over larger areas. With the form of equation (2) this amounts to implicitly assuming that the soil thickness (perpendicular to the slope) is constant. An alternative definition of C as

$C' = (Cr+ Cs)/(D\rho_s\ g)$ (4a)

would lead to instead of (2)

$$FS = \frac{C'+\cos^2\theta\,[1-wr]\tan\phi}{\sin\theta\cos\theta}$$

(2a)

which implicitly assumes the soil depth D (measured vertically) is constant, implying that soils on steeper slopes are thinner. In SINMAP we chose (2) and (4) over (2a) and (4a), in part for compatibility with the hydrology where constant soil thickness is consistent with constant transmissivity (hydraulic conductivity times thickness), and in part because it is probably more realistic.(Pack et.al.,2005)
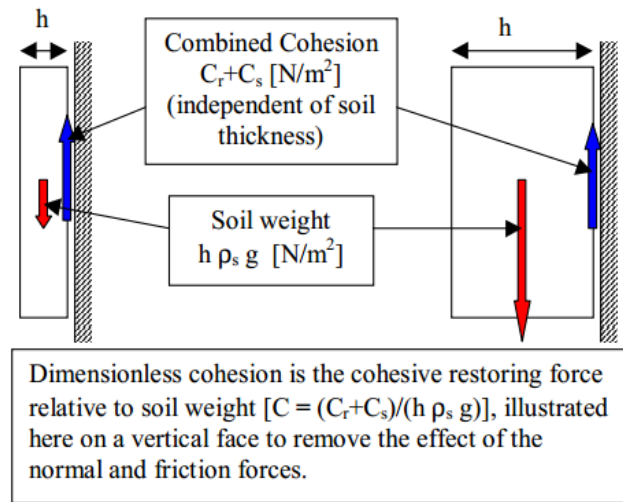
Figure 3.2 Illustration of Dimensionless Cohesion(Source: Pack et.al.,2005)

3.1.2 Topographic wetness index (TWI)

The areas in which the soil cover has higher water content (and degree of saturation) tend to occur in convergent hollow areas of the hill slopes, and landslides usually originate in such areas (Montgomery and Dietrich, 1994). The parameter a (specific catchment area), which is defined as the upslope contributing area of catchment per unit contour length $(m^2 m^{-1})$(Fig. 3.4), has been incorporated into SINMAP. This parameter is closely tied to hydrologic models that represent runoff generation by saturation from below (Beven and Kirkby, 1979)According to TOPMODEL and other similiar topographically-based wetness index models, the following assumptions are adopted in SINMAP:

 (1) shallow-lateral subsurface flow (through flow) advances along topographic gradients, implying that the contributing area to flow at any point is given by the specific catchment area defined from the surface topography (Fig. 3.4);

(2) lateral discharge at each point is in equilibrium with a steady-state recharge R(m day−1); and

 (3) the capacity for lateral flux at each point is Tsinθ, where T is the soil transmissivity (the vertical integral of the hydraulic conductivity of soil and is determined by $T=(Ks)\times h[m^2 day^{-1}]$, where K_s is the uniform hydraulic conductivity [m day^{-1}]of a soil

mantle overlying relatively impermeable bedrock, and h is the thickness of the soil [m] above the failure surface.

Assumptions 1 and 2 together imply that lateral discharge q, depth integrated per unit contour length, is estimated by

$$q = R \times a \ (m^2 day^{-1}) \tag{6}$$

With assumption 3 the relative wetness is expressed as:

$$w = min(Ra/Tsin\theta, 1) \tag{7}$$

The relative wetness has an upper boundary of 1 with any excess assumed to form overland flow. As illustrated in Fig. 3.1, the relative wetness defines the depth of the perched water table within the soil layer. The ratio R/Tin Eq. (6) quantifies the relative wetness in terms of assumed steady-state recharge proportional to the soil's capacity for lateral drainage of water.

In the physically based models, the three often used algorithms for specifying flow directions are:

• D8 (O'Callaghan & Mark, 1984); it assigns flows from each grid cell to one between its eight neighbors (cardinal or diagonal) with the lowest elevation; it is a very simple approach but it may depend strongly on the orientation of the grid system (Montgomery & Dietrich, 1994); The D8 approach has disadvantages arising from the discretization of flow into only one of eight possible directions, separated by 45° (Fairfield and Leymarie, 1991; Quinn et al., 1991; Tarboton, 1997).

• FD8 (Quinn et al.,1991); these approaches allocate water flow, fractionally, to each lower neighbor in proportion to the slope; as Tarboton (1997) pointed out, they have the disadvantage that flow from a pixel is dispersed to all neighboring pixels with lower elevation.

• *D∞* (Tarboton, 1997); this approach defines eight planar triangular facets between each grid point and its neighbors; only the two neighboring cells defining the steepest facet receive upslope flow; the fractional flow is divide according the rule referred in Figure 3.3;

In this *D∞* method, the flow direction angle measured counter clockwise from east is represented as a continuous quantity between 0 and 2π. This angle is determined as the direction of the steepest downward slope on the eight triangular facets formed in a 3 x 3 grid cell window centered on the grid cell of interest as illustrated in Figure 3.3. A block-centered representation is used with each elevation value taken to represent the elevation of the center of the corresponding grid cell. Eight planar triangular facets are formed between each grid cell and its eight neighbors. Each of these has a downslope vector which when drawn outwards from the center may be at an angle that lies within or outside the 45⁰ (π/4 radian) angle range of the facet at the center point. If the slope vector angle is within the facet angle, it represents the steepest flow direction on that facet. If the slope vector angle is outside a facet, the steepest flow direction associated with that facet is taken along the steepest edge. The slope and flow direction associated with the grid cell is taken as the magnitude and direction of the steepest downslope vector from all eight facets (Tarboton ,1997).
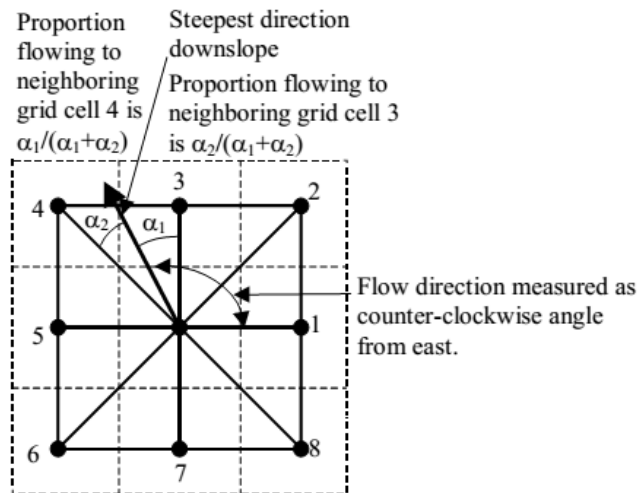
Figure 3.3 Flow direction defined as steepest downward slope on planar triangular faces on a block centered grid (Source: Pack et.al, 2005)

In the case where no slope vectors are positive (downslope), the flow direction is set using the method of Garbrecht and Martz (1997) for the determination of flow across flat areas. This makes flat areas drain away from high ground and towards low ground. These procedures have minimal impact when used in SINMAP because flat areas are always

unconditionally stable, but are included for completeness and compatibility with other hydrologic uses, and to avoid data gaps in the maps produced (Pack et.al,2005).
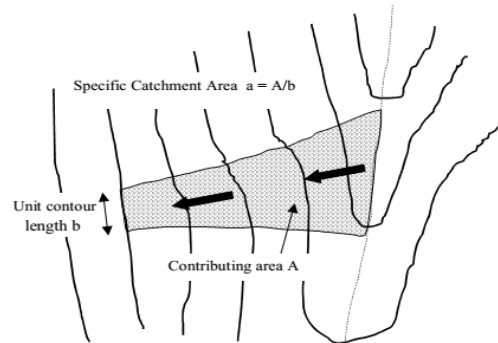
Figure 3.4 Illustration of definition of specific catchment area (Source: Pack et.al., 2005)

Specific catchment area, a, is the upslope area per unit contour length, taken as the number of cells times grid cell size (cell area divided by cell size). This assumes that grid cell size is the effective contour length, b, in the definition of specific catchment area (Fig 3.4) and does not distinguish any difference in contour length dependent upon the flow direction(Pack et. al,2005).

Upslope area (counted in terms of the number of grid cells) is calculated using a recursive procedure that is an extension of the very efficient recursive algorithm for single directions (Mark, 1988). The upslope area of each grid cell is taken as its own area (one) plus the area from upslope neighbors that have some fraction draining to it. The flow from each cell either all drains to one neighbor, if the angle falls along a cardinal (0, $\pi/2$, π, $3\pi/2$) or diagonal ($\pi/4$, $3\pi/4$, $5\pi/4$, $7\pi/4$) direction, or is on an angle falling between the direct angle to two adjacent neighbors. In the latter case the flow is proportioned between these two neighbor pixels according to how close the flow direction angle is to the direct angle to those pixels, as illustrated in Figure 3.3.(Pack et. al,2005)

3.1.3 Stability Index

The first step of defining the stability index (SI) is to incorporate the wetness index from Eq. (7) into the dimensionless SF of Eq. (2):

$$SF = \frac{C + \cos\theta\left[1 - \min\left(\frac{R}{T}\frac{a}{\sin\theta}, \ 1\right)r\right]\tan\phi}{\sin\theta}$$

(8)

The variables a and θ are derived from the DEM topography whereas the values of C, $\tan\varphi$, r and R/T are user input. The density ratio r is essentially treated a constant (with a value of 0.5) but uncertainty is allowed in the other three quantities through the specification of lower and upper bounds. Formally these bounds define the limits of uniform probability distributions over which these quantities are assumed to vary at random.

Denoting R/T = x, $\tan\varphi$= t, and the uniform probability distributions with lower and upper bounds as

C ~ U(C1, C2)

x ~ U(x1, x2)   (9)

t ~ U(t1, t2)

SINMAP incorporates the probabilistic approach described by Hammond et al.(1992), while combining the infinite slope stability model with the steady state hydrology approach suggested by Montgomery and Dietrich (1994). The smallest C and t, (i.e. C1and t1) together with the largest x (i.e. x2) define the worst case (most conservative) scenario under this assumed uncertainty (variability) in the parameters. Areas where under this worst case scenario FS is greater than 1 are, in terms of this model, unconditionally stable and for which we define stability index as

$$SI = FS_{min} = \frac{C_1 + \cos\theta\left[1 - \min\left(x_2\frac{a}{\sin\theta}, 1\right)r\right]t_1}{\sin\theta}$$

(10)

For areas where the minimum factor of safety is less than 1, there is a possibility (probability) of failure. This is a spatial probability due to the uncertainty (spatial variability) in C, $\tan\varphi$ and T. This probability does have a temporal element in that R characterizes a wetness that may vary with time. Therefore, the uncertainty in x combines both spatial and temporal probabilities. In these regions (with $FS_{min} < 1$) it is defined as-

$$SI = Prob(FS > 1) \tag{11}$$

over the distributions of C, x, and t (equations 9). The best case scenario is when C=C2, x=x1, and t=t2,which leads to

$$FS_{max} = \frac{C_2 + \cos\theta\, [1 - \min\left(x_1\dfrac{a}{\sin\theta}, 1\right)r]t_2}{\sin\theta} \tag{12}$$

In the case that $FS_{max} < 1$, then

$$SI = Prob(FS > 1) = 0 \tag{13}$$

Regions with SI > 1 ($FS_{min} > 1$), 0 < SI < 1 and SI = 0 ($FS_{max} < 1$) are illustrated in Figure 3.4 in a space defined in terms of slope (tanθ) and specific catchment area. This provides a useful visualization medium for understanding this approach.
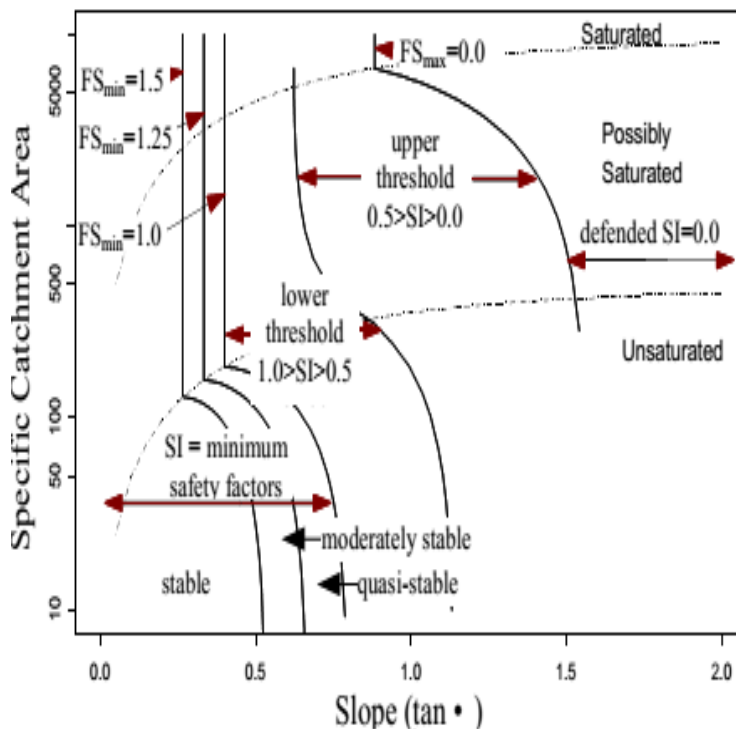
Figure 3.5 Stability index defined in slope-area space (Source: Pack et.al, 2005)

Available online at http://www.ijart.info/

Table 3.1 Classes of slope stability based on value of the Stability Index (SI), as set by

the deterministic slope-instability model SINMAP(Source: Deb ,2009)

Condition	Class	Predicted state	Parameter range	Possible influence of factors not modeled	Reclassified predicted state
$SI>1.5$	1	Stable slope zone	Range cannot model instability	Significant destabilizing factors are required for instability	Safe area
$1.5>SI>1.25$	2	Moderately stable slope zone	Range cannot model instability	Moderate destabilizing factors are required for instability	Low-to-medium susceptibility
$1.25>SI>1.0$	3	Quasi-stable slope zone	Range cannot model instability	Minor destabilizing factors are required for instability	
$1.0>SI>0.5$	4	Lower threshold slope zone	Pessimistic half of range required for instability	Destabilizing factors are not required for instability	High susceptibility
$0.5>SI>0.0$	5	Upper threshold slope zone	Optimistic half of range required for instability	Stabilizing factors may be responsible for stability	Very high susceptibility
$0.0>SI$	6	Defended slope zone	Range cannot model stability	Stabilizing factors are required for stability	

IJART
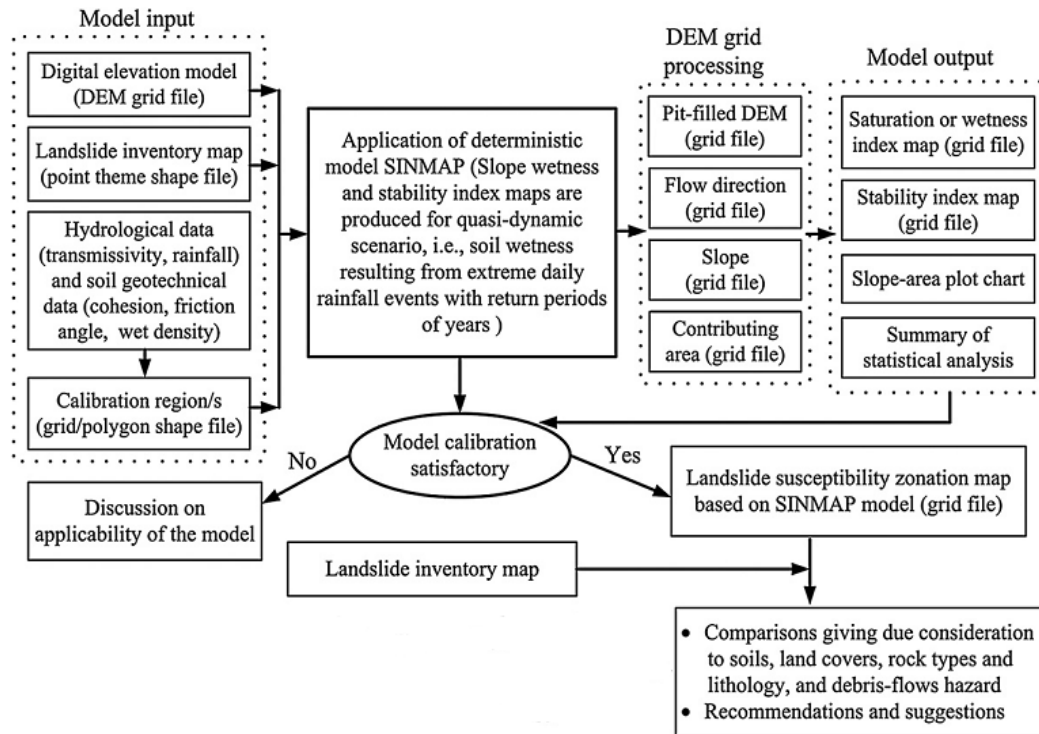
Figure 3.6 Schematic diagram of the methodology used to apply SINMAP to the study under maximum rainfall events (Source: Deb, 2009)

Hence, it is clear that the SINMAP model is a slope stability predictive tool, within which is a hydrologic flow modeling component. It uses the surface topography to route flow downslope, assuming that the subsurface hydrologic boundary parallels the surface, and soil thickness and hydraulic conductivity are uniform. The flow model predicts relative levels of groundwater across a watershed area. This prediction is then used to assess slope stability.

The model requires three groups of input data

1. terrain topography in a DEM grid format;
2. soil mechanical and hydraulic properties in a grid or polygon vector format;
3. landslide source areas inventory in a point vector format.

Topographic data in DEM format are preprocessed by a built-in pit-filling module. The next step is to compute the required topographic parameters, such as slope and specific catchment area.

The model requires the following soil properties data:
• range of cohesion values;
• soil density value;
• range of internal friction angle values;
• range of R/T ratio.

For calibration purposes the landslides inventory map is needed, obtained from aerial or satellite orthophotos.

The output data are presented in a form of the following maps:
• stability probability expressed as stability index divided into six classes;
• topographic wetness index divided into five classes;
• graph of landslide occurrence in fields of slope and specific catchment area;
• summary table.

By adopting suitable ranges for variables it is possible to calibrate and group the majority of observed landslides into the smallest SI classes (Table 3.1)

   The Graphical User Interface(GUI) of SINMAP Model can be illustrated as-
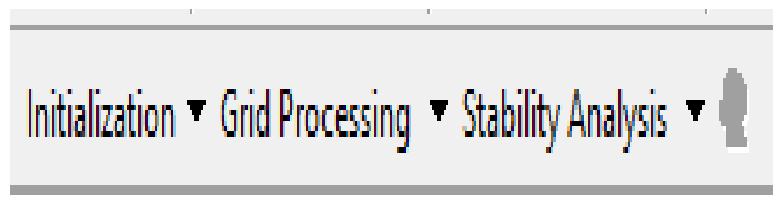
Figure 3.7 Windows GUI of SINMAP Model
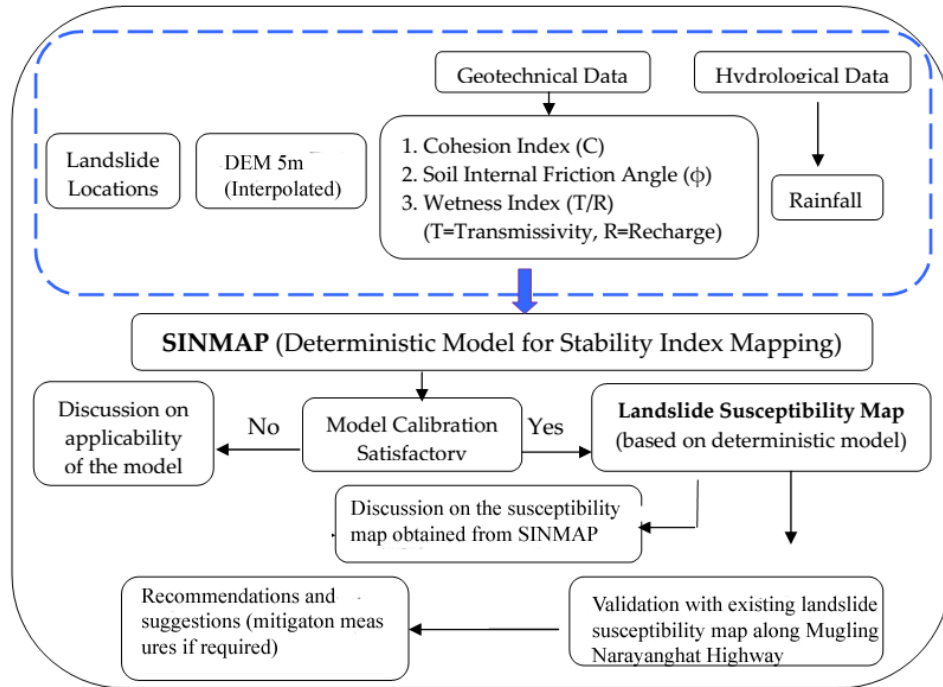
Figure 3.8 Methodology including required input datas in SINMAP

3.2 Introduction To DEBRIS-2D Model

DEBRIS-2D is a two-dimensional debris flow simulation program (Liu,K.F & Huang,M.C, 2006; Wu Y.H, 2014). It treats debris flow as a yield stress fluid (non-Newtonian fluid mechanics).It can simulate   flow depth, velocity, impact force and affected area of debris flow. Simulation of water-soil mixture flow motion can be done by this model. Variables that can be obtained are:

–Depth-average x, y-direction velocities

–Flow depth and affected area

–Impact force from debris flow on solid

   The viscoplastic objects are nonNewtonian fluids, i.e. their flow behavior is viscous when weak forces are applied. However,when under significant forces, the material starts to flow like a liquid (toothpaste effect): it changes phase from non-Newtonian viscous but almost solid behavior to Newtonian liquid. Unlike viscoelastic objects, viscoplastic

materials have no memory: a rupture does not induce a "spring effect" of any part. This work is based on the recent advances of Mendes et al. in formulating a viscosity function for viscoplastic objects that encompasses both viscous and liquid phases. The conciseness and generality of this formulation provides an efficient control of the viscosity, since it mainly depends on one physical parameter, named the jump number, which replaces multiple parameters, such as stiffness, compressibility, plasticity, viscosity, cohesion. The visco-plastic-collision model which is one of the basis for DEBRIS-2D Model is-

$$\tau = \tau_0 + \mu_d \frac{du}{dz} + \mu_c \left(\frac{du}{dz}\right)^2$$

$$\tau \geq \tau_0$$

Strong Shear

$$\frac{du}{dz} = 0$$

$$\tau < \tau_0 \quad \text{Weak Shear}$$

(Plug Flow)

τ_0 is the yield stress.

For engineering purposes, all the rheological parameters are assumed to be constants.
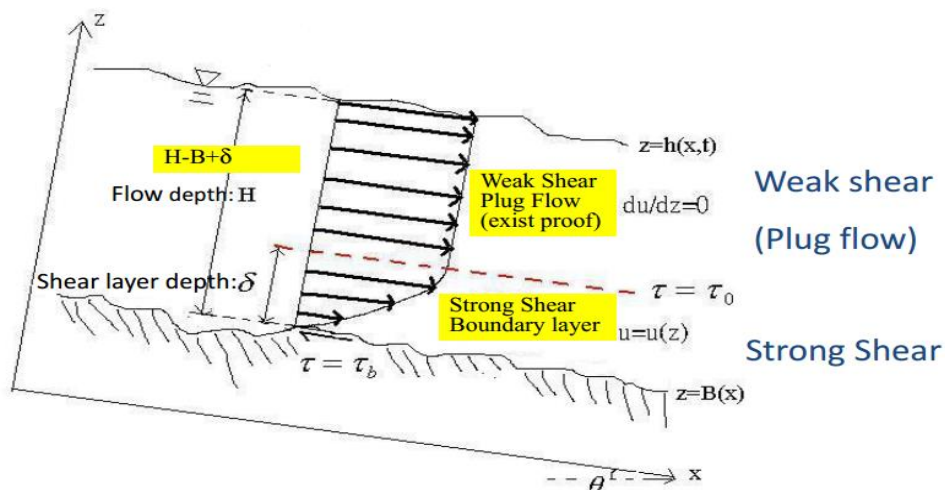
Figure 3.9 Illustration of vertical velocity profile of flowing debris flow (Source: Wu,2014)

Analysis by field data shows δ<10% of H. δ can be ignored (Liu K.F   and Huang,M.C,2006)

3.2.1 Governing Equations Of DEBRIS-2D Model

The governing equations for Debris2D are conservation of mass and momentum. The constitutive law was proposed by Julien and Lan (1991) which added the quadratic term of strain rate to modify the Bingham model to interpret the effects of particle collisions in the motion of solid-liquid mixture. The original O'Brien and Julien (1985) rheological relationship from a one-dimensional version was extended to a three dimensional version, as follows:

$$\tau_{ij} = \left(\frac{\tau_0}{|\dot{\gamma}_{ij}|} + \mu_d + \mu_c |\dot{\gamma}_{ij}| \right) \dot{\gamma}_{ij}, \qquad |\tau_{ij}| \geq \tau_0 \qquad\qquad 14a$$

$$|\gamma_{ij}| = 0 \ , \qquad\qquad\qquad |\tau_{ij}| < \tau_0 \qquad\qquad 14b$$

where, τ_{ij} is the shear stress tensor and γ_{ij} is the strain rate tensor. τ_0 is the yield stress, μ_d is the dynamic viscosity and μ_c is the turbulent-dispersive coefficient. τ_{ij} and γ_{ij} represent the second invariant of the shear stress and strain rate tensor, respectively. Liu,K.F and Lai,K.W (2000) defined the portion of debris flow with stress greater than the yield stress as the boundary layer. The depth ratio between the boundary layer and the main debris flow was verified as small. This implied that most of the flow region was in a weak stress condition, that is, the plug region. The corresponding constitutive law is shown in Eq. (14b), which can be expressed as follows:

$$|\dot{\gamma}_{ij}| = \sqrt{2\frac{\partial u}{\partial x}^2 + 2\frac{\partial v}{\partial y}^2 + 2\frac{\partial w}{\partial z}^2 + (\frac{\partial u}{\partial y} + \frac{\partial v}{\partial x})^2 + (\frac{\partial u}{\partial z} + \frac{\partial w}{\partial x})^2 + (\frac{\partial v}{\partial z} + \frac{\partial w}{\partial y})^2}$$

$$= 0 \ , \qquad\qquad\qquad |\tau_{ij}| < \tau_0 \qquad\qquad (15)$$

where the x -axis coincides with the averaged bottom of the channel and is inclined at angle θ with regard to the horizon. The y -axis is in the transverse direction and the z-axis is perpendicular to both the x - and y - axes. u, v, w are the velocity components in the x , y , z directions, respectively. Because debris flow in a lab or in the field is usually

considered long waves, that is, the depth scale is substantially smaller than the horizontal length scales; it can be obtained from Eq. (16) by neglecting the small terms, as follows:-

$$\frac{\partial u}{\partial z} = 0, \quad \frac{\partial v}{\partial z} = 0$$

(16)

This implies that the portion of debris flow near the free surface at which the stress free condition applies is a two-dimensional plug flow [that is, $u \neq u(z)$ and $v \neq v(z)$].

 Substituting Eq. (16) into the momentum equations obtained the following-

$$\frac{\partial u}{\partial t} + u\frac{\partial u}{\partial x} + v\frac{\partial u}{\partial y} = -\frac{1}{\rho}\frac{\partial p}{\partial x} + g\sin\theta + \frac{1}{\rho}\frac{\partial \tau_{zx}}{\partial z}$$

$$\frac{\partial v}{\partial t} + v\frac{\partial v}{\partial x} + v\frac{\partial v}{\partial y} = -\frac{1}{\rho}\frac{\partial p}{\partial y} + \frac{1}{\rho}\frac{\partial \tau_{zy}}{\partial z}$$

$$0 = -\frac{1}{\rho}\frac{\partial p}{\partial z} - g\cos\theta$$

(17 a, b, c)

where ρ is density of debris flow, and p is pressure. The stress free condition is applied at the free surface z =h(x,y,t). The upper boundary of the thin boundary layer near the bottom is defined as z = B(x,y,t)+δ(x,y,t) , where the natural bottom of the debris flow is z = B(x,y,t). Because the thickness of the boundary layer is small compared to the flow depth, the natural bottom can be used as the boundary for the plug flow. Equation (17) leads to static pressure in z.

$$p = \rho g \cos\theta (h - z)$$

(18)

Integrating Eqs. 17 a and b in z from the bottom to the free surface obtains the results in conservative form as follows:

$$\frac{\partial u H}{\partial t} + \frac{\partial u^2 H}{\partial x} + \frac{\partial uv H}{\partial y} = -g\cos\theta H\frac{\partial(B+H)}{\partial x} + g\sin\theta H - \frac{1}{\rho}\frac{\tau_0 u}{\sqrt{u^2+v^2}}$$

$$\frac{\partial v H}{\partial t} + \frac{\partial uv H}{\partial x} + \frac{\partial v^2 H}{\partial y} = -g\cos\theta H\frac{\partial(B+H)}{\partial y} - \frac{1}{\rho}\frac{\tau_0 v}{\sqrt{u^2+v^2}}$$

(19)

The depth integration of continuity equation gives-

$$\frac{\partial H}{\partial t} + \frac{\partial uH}{\partial x} + \frac{\partial vH}{\partial y} = 0 \tag{20}$$

where H=h(x,y,t)–B(x,y,t) is the flow depth. Equations (19) and (20) may be used to solve the three unknowns, H, u and v.

$$\frac{\partial(uH)}{\partial t} + \frac{\partial(u^2H)}{\partial x} + \frac{\partial(uvH)}{\partial y} = -gH\cos\theta\left(\frac{\partial B}{\partial x} + \frac{\partial H}{\partial x}\right) - gH\sin\theta - \frac{\tau_0 u}{\rho\sqrt{u^2+v^2}} \tag{21}$$

$$\frac{\partial(vH)}{\partial t} + \frac{\partial(uvH)}{\partial x} + \frac{\partial(v^2H)}{\partial y} = -gH\cos\theta\left(\frac{\partial B}{\partial y} + \frac{\partial H}{\partial y}\right) + \frac{\tau_0 v}{\rho\sqrt{u^2+v^2}} \tag{22}$$

where, θ is the slope angle of topography, ρ is density of debris-flow, g is gravitational acceleration, H is flow thickness, B is the elevation of river bed, u and v are depth averaged x and y velocity respectively. Eq.20 is the mass conservation equation in the conservative form. Eq.21and Eq.22 are x and y momentum conservation equations, and there are convective terms in LHS, and pressure, gravitational and shear stress terms in RHS. Due to the existence of yield stress in the constitutive law, motion can only start if the bottom stress exceeds the yield stress(Tsai,M.P et. al., 2007).

$$\left(\frac{\partial B}{\partial x} + \frac{\partial H}{\partial x} - \tan\theta\right)^2 + \left(\frac{\partial B}{\partial y} + \frac{\partial H}{\partial y}\right)^2 > \left(\frac{\tau_0}{\rho g\cos\theta H}\right)^2 \tag{23}$$

In Eq.23, the first derivatives of B and H of x and y represent the pressure effects, and $\tan\theta$ is the gravitational effect. If the pressure and gravitational effects are greater than yield stress, the debris-flow would start to move. So far, the bottom erosion from river bed is not considered.

The concept of erosion or deposition during flowing can be assessed through the following:-

$S = k_e(\tau-\tau_b)$ for erosion

$S = k_d(\tau-\tau_b)$ for deposition

These are adopted from ocean and river sedimentation. But k_e and k_d are practically unavailable.For engineering purposes-

a.   It is assumed for the worst cases

b.   It is assumed that everything moves.

The impact force of flowing debris could be calculated by:-

$$F = \rho g h \cos \theta + (\rho/2)u^2 + \rho c_s u$$

1st term-   Static pressure

2nd term - Dynamic pressure

3rd term - Shock wave

No viscous effect is considered(Liu and Lee,1997)

The Numerical Method of DEBRIS-2D can be explained as-

• Explicit finite difference method

–For space:

-   2nd   order- Central difference method

-   1st order- Upwind method: convective term

–For time:

3rd order Adams-Bashforth method

• Time step holds Courant-Friedrichs-Lewy (CFL) condition for stable computation

Mathematically, one condition each for H,u and v is required in the physical boundary. For debris flow simulations in the field, it is usually necessary to obtain computational domain, which contains the whole reach of the debris flows. In real applications, a large computation domain may be selected to prevent debris flows from reaching the domain boundary. Thus, the boundary conditions are as follows:

H (x,y,t) = 0,u = 0,v = 0 on all boundaries   (24)

If debris flows are restrained in a fixed domain, such as flume, a normal flux condition would not be used on all physical boundaries. However, Eq. (24) applies to the front and tail of the debris flow. The tracking of the points with a velocity near zero is crucial. Corrections of overshooting the physical quantities were performed during every time step.

The initial condition is the depth contour in the computation domain with all possible debris flow sources. The value of the rheological properties is also required, which must be obtained from field sample measurements.

3.2.2 Data Processing In DEBRIS-2D Model

Including datum and parameters, there are a lot of data pre-processing needed in order to run Debris2D.A graphic user interface (GUI) is needed for user to follow the steps to input all required data and parameters to make the pre-process of simulation more easily and efficiently.

Table 3.2 All inputs for DEBRIS-2D MODEL

	Steps	Inputs
1	Topography	Input DEM file for interpolation to get grids, two or more DEM files are also available
2	Simulation range	Typing or circling by mouse from the screen to set the simulation range.
3	Mass information	• Select the types of deposition • Input mass locations and volumes.
4	Material parameter	Input the yield stress of mass
5	Ouput setup	• Set the time interval of output • Set the locations information of specified output point • Set if output the final deposition and velocity or flow thickness distribution or not after the end of simulation

All inputs are categorized into five categories. Basic info are topography and simulation range. Mass source information such as location, volume and types of deposition are also needed. Rheological parameter such as yield stress is essential.

Simulation parameters such as output time interval, specified output points setups are required for the sake of output. All the inputs mentioned above are listed in Table 3.2.

Once data is provided by user, the GUI program will start to process all the inputs, and connect them with simulation program.
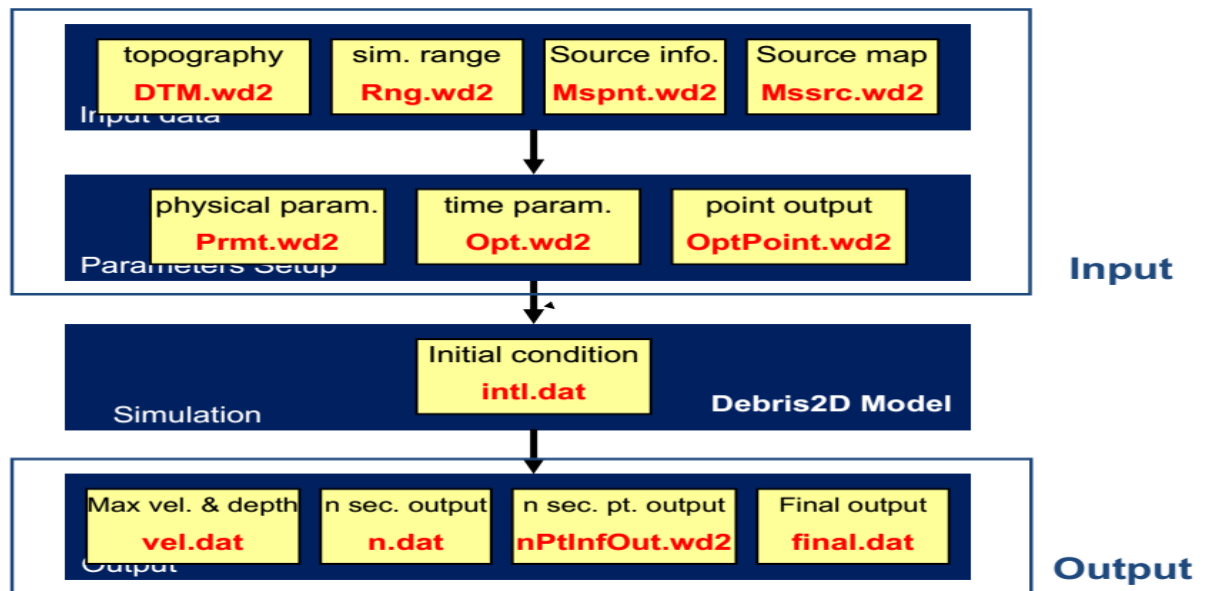
Figure 3.10 Schematic diagram for overview of files for simulation of DEBRIS-2D Model (Source: Wu, 2014)

The determination of input volume of debris flow is a difficult task to perform for simulating DEBRIS-2D Model.

Figure 3.11 Illustration of designed volume of debris flow(Source: Wu,2014)

Solid Volume + Liquid Volume $\longrightarrow$ Concentration Concept

is the main concept behind design volume of debris flow.

An equilibrium concentration conceptual of Takahashi (2007) can be applied to estimate the debris flow volume. Takahashi (2007) derived the equilibrium concentration, as follows:

$$C_v = \frac{\rho_w \tan\theta}{(\rho_s - \rho_w)(\tan\emptyset - \tan\theta)} = \frac{Total\ Volume\ of\ solid}{Total\ volume\ of\ debris\ flow}$$

where, C_v is the equilibrium concentration, ρ_s is the solid density of debris, ρ_w is the liquid density of debris, φ is the rest angle of solids or angle of internal friction of soil, and θ is the slope. In general, ρ_w is the water density, ρ_s and φ may be measured from field samples ,and θ may be calculated from the Digital Topographic Model(DTM).

There are two conditions regarding designed volume for initiation mass input. The two conditions are:-

  • Water is sufficient case in which all mass becomes debris flow and is calculated as-

$$V = \frac{V_d}{C_v} = \frac{Total\ volume\ of\ dry\ debris\ mass}{C_v}$$

• Water is NOT sufficient case in which only a part of mass becomes debris flow.

$$V = V = \frac{V_w}{1 - C_v} = \frac{Total\ volume\ of\ water}{1 - C_v}$$

Among these two cases, the volume of dry debris mass can be calculated either by field survey or estimation. Similarly, the volume of water can be determined by rational method or rainfall-runoff model.

With the input of datas to the model, the model simulates giving the flow depth and velocity at specified location and time interval.
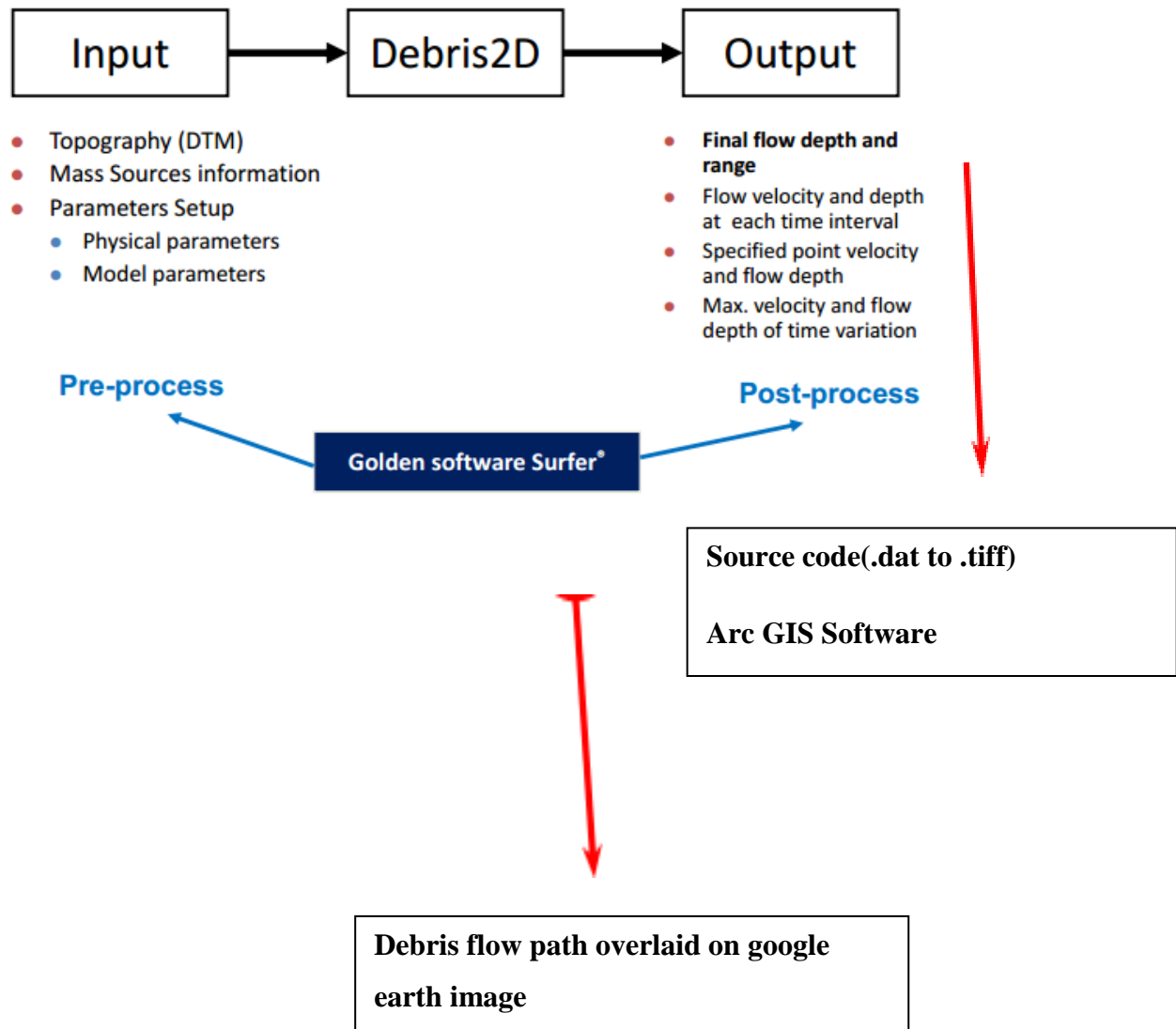
Figure 3.12 Flowchart for Simulation of DEBRIS-2D Model

Practical Application for Input (Initial Condition)

• Designed Volume for event scenario

–initial mass distribution, i.e., H(x,y,t = 0)

Available online at http://www.ijart.info/

• Yield Stress

–Only One material parameter for input

–physically-based rheological measurement
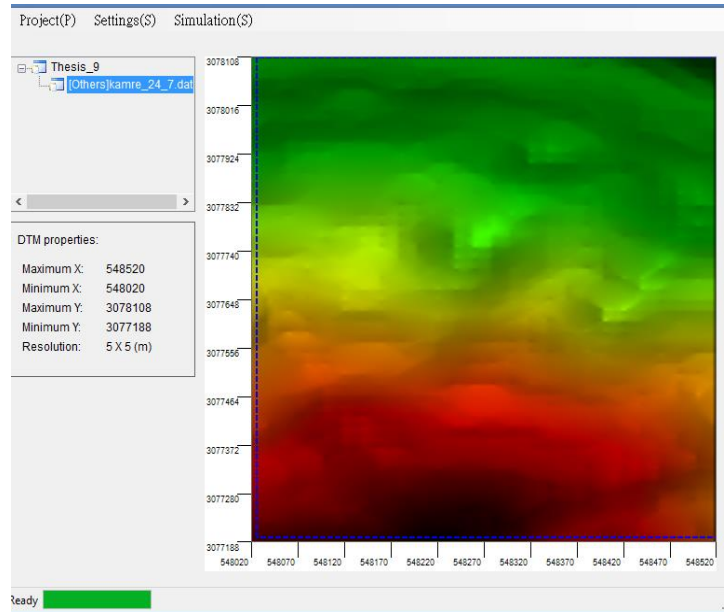
Figure 3.13 Windows GUI of DEBRIS2D Model

Under Settings- DTM Management; Analysis Range; Mass Distribution; Mass Parameters; Output Setup; are the parameters included.

The complete methodological assessment of DEBRIS-2D Model has been described above. Moreover, the detailed description of the input datas and the calibration procedure is explained in the next chapter.

Available online at http://www.ijart.info/

4.   STUDY AREA

4.1 Background

The accomplishment of study was done in a series of different phases. The methods were used in a way that it would best describe the physical processes of landslide and debris flow in the simplified form. Availability of data,internationally accepted researches,time and computer software are the major considered factors in the selection of method. The study has tried to focus on more systematic,efficient,low cost and reliable methods that would be applicable further in similar type of studies.

Since the thesis work is based on susceptibility assessment of landslides and debris flow simulation,hence for the shallow landslides terrain susceptibility mapping Mugling-Narayanghat Highway has been chosen for the study area and for debris flow simulation Kamere Khola watershed falling across the same highway has been chosen based on volumetric equilibrium concentration. Kamere Khola watershed(CH-24+740)has been chosen for debris flow simulation considering that water is sufficient to cause debris flow and all mass becomes debris flow. The detailed description is described below:

4.2 Introduction to Narayanghat-Mugling Highway

   Upto the 1970's, the only link between Kathmandu and Birgunj was the Tribhuvan Rajpath (H-02). This road is narrow and involves steep gradients. In the 70's, the Chinese constructed the Prithvi Rajpath (H-04) linking Kathmandu to Mugling and Pokhara. Thereafter, they also constructed the Narayanghat to Mugling highway (H-05), as an alternative to the Tribhuvan Rajpath. The road was constructed initially as a single lane road. Later it was widened to intermediate lane with additional structures. The Narayanghat-Mugling road follows the leftbank of the Trishuli river and does not involve steep gradients. For this reason, the road has been the preferred route to and from Kathmandu, specifically for trade traffic moving from/towards Biratnagar, Birgunj and Siddhrathnagar.The road lies in Chitwan district of Central Development region of Nepal.

Salient Features of Mugling Narayanghat Highway:-

➤ Important Link (designated as H-05) of Strategic Highway Network of Nepal

> Connects Narayanghat located at east-west Mahendra Highway (H-01) to Mugling located at east-west Prithvi Highway (H-04)

> Part of Asian Highway AH-42 (297 in Nepal from Kodari to Birgunj) as categorized by UN ESCAP (IGA Nov 18, 2003). AH42 is a route of the Asian Highway Network, running 3,754 km from AH5 in Lanzhou, China to AH1 in Barhi, India. It passes along Kodari, Kathmandu, Narayangarh, Pathlayia and Birganj.

> Aligned along river valley along left bank of Trishuli river.

> Lesser Himalaya and Siwalik geological belts encountered.

> Crosses a number of cross drains: number of tributaries at the eastern bank
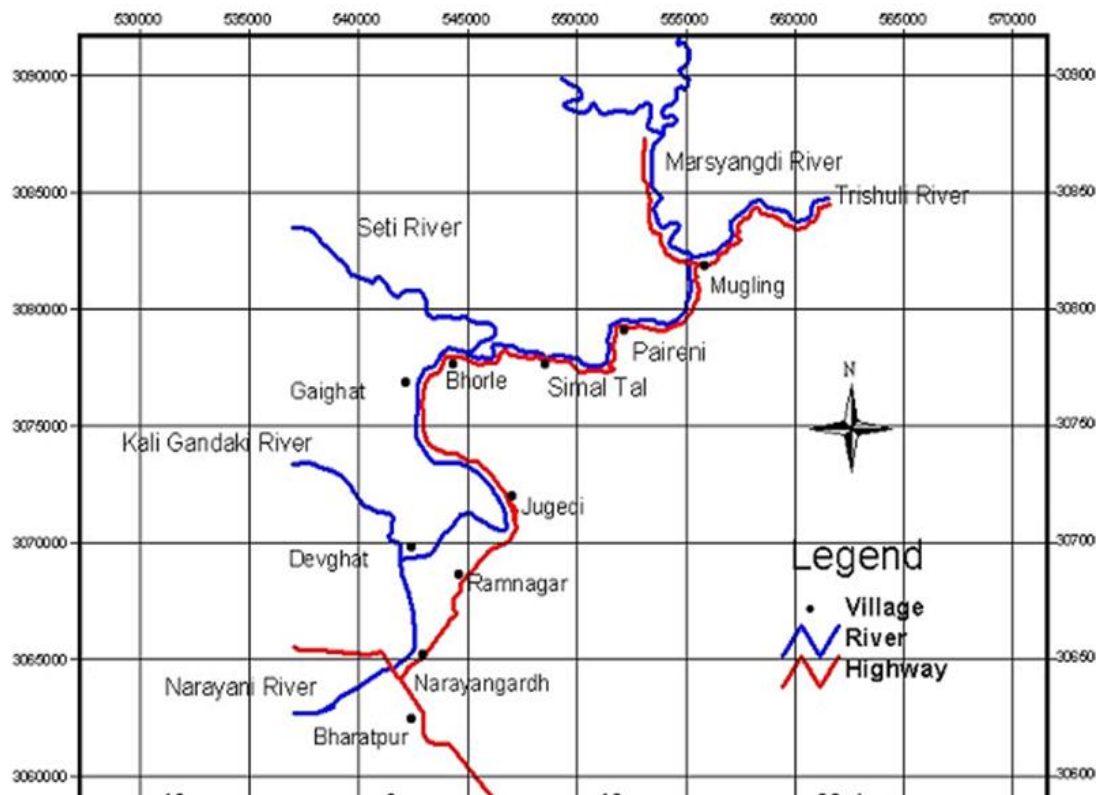
Figure 4.1 Location Map of Mugling-Narayanghat Highway

4.2.1 Topography

The topographical setting of the road alignment area is characterized by hill and river basin. It is largely a rugged terrain consisting of north-west to south-east and north to south trending ridges. The road starts at an elevation of 200m at Narayanghat and ends at

1,800m at Mugling.   The Narayanghat-Mugling road gradually ascends from Narayanghat (chainage 0+000; 200m above msl) to Ramnagar (chainage 5+500; 250m above msl) along northern face of the hilly terrain. From Narayanghat, the road alignment runs nearly in flat terrain formed by the old river deposits. After Ramnagar (km 5+500) the road runs along the Trishuli River and the alignment gradually ascends towards Bhateri (km 8+00; 300m above msl). After crossing Bhateri, the road alignment toward Mugling becomes steeper (chainage 35+677; 1250m above msl). The road follows the left bank of the Trishuli River from Ramnagar (km 5+500) up to Mugling (km 35+677).The project road has bridge crossings over 18 tributaries of Trishuli River. Presently, the width of road is 6m to 10 m. The pavement of the road is bituminous and the riding quality varies across the various sections. Traffic movement is around 6000 vehicles per day. The road passes through forest area, settlement and cultivated land. Major settlements along the road alignment are Aptari, Ramnagar, Jugedi, Dasdhunga, Ghumaune, Simaltar, Khahare, Syauli Bazar and Mugling. Initially, the road alignment follows the flat land of the Chitwan Dun valley and then runs in northern face of the hill just below the ridge and just above the Trisuli River valley.

4.2.2 Geology

The tectonic structure of Nepal Himalaya can be subdivided into the five major belts: Fore Himalaya, Higher Himalaya, Lesser Himalaya, Sub Hiamalya (Siwaliks) and the Indo-gangatic plane. These five belts are separated by major thrust faults, namely South Tibetian Detachment System (STDS), Main Central Thrust (MCT), Main Boundary Thrust (MBT) and Himalayan Frontal Thrust(HFT). These tectonic features have created large amount of deformation in the rocks and soil, thus making them susceptible to landsliding.(Regmiet.al.,2013). Mugling–Narayanghat road section and its surrounding region consists of rocks belonging to the Lesser Himalayan Precambrian rocks of Nawakot Complex (Stocklin and Bhattarai 1978), Miocene Siwaliks and Holocene terrace deposits. The Lesser Himalayan rocks in this area are part of the Lower Nuwakot Group of the Nuwakot Complex, which include the Kunchha Formation, Fagfog

Quartzite, Dandagaun Phyllite, Nourpul Fommation and Dhading Dolomite and Benighat Slate Formation belonging toUpper Nawakot Group (Fig. 1a). Stratigraphically, the Lower Nawakot Group isconsidered as an overturned sequence with the Kunchha Formation at the bottom and the Dhading Dolomite on the top. The Dandagaun Phyllites, Nourpul Formation and Dhading Dolomite appear repeatedly in some parts, due to folding and faulting. Benighat (Fig. 4b). The Siwalik Group in the study area consists of Lower Siwalik and Middle Siwalik (Ganser 1964). The Holocene deposits consist of river terraces of different ages. The main rock types are mudstones, sandstones, limestones, dolomites, slates, phyllites, quartzites and amphibolites (Table 1). The majority of instabilities are observed within the rocks of Nourpul Formation and Puribesi Quartzite. The main geological structure that demarcates the study area is the MBT (Main Boundary Thrust) that separates the Lesser Himalaya from the overlying Siwaliks (Fig. 4b). It crosses the Mugling–Narayanghat road section near around 14 km, south of the Phwatar and runs east–west. The area has three other thrust in the north of the MBT and one in the south of it. Kamalpur Thrust, Simaltal Thrust and Virkuna Thrust lie to the north of MBT, while Jugadi Thrust lies to the south of it. In addition, there are a large number of normal faults demarcating the study area. Simaltal Thrust and Virkuna Thrust have a common root zone. The area has also undergone local folding of different scales at places. Another major geological structure in the road section is the western closure of the Mahabharat Synclinorium. It isa huge syncline in the Mahabharat Range of the central Nepal and is locally known by the Jalbire Syncline .Geologically, the road alignment runs through the sediments of the Chitwan Dun valley and Siwaliks comprised of inter-bedded sandstone and mudstone. Road alignment traverses through rocks of the Lower Nuwakot Group and upper Nuwakot Group. The lower Nuwakot Group is composed of KunchaFormation, Fagfog Quartzite, Dandagaon Phyllite, Nourpul Formation and Dhading Dolomite. The Upper Nuwakot Group contains Benighat Slate, Malekhu Limestone and Robang Formation. The Kuncha Formation consists of alteration of phyllite, phyllitic quartzite. The Fagfog Quartzite contains thick-bedded white, coarse-grained quartzite with frequently developed rippled marks and the Dandagoan Phyllite consists of phyllite. The Nourpul Formation has metasandstone and phyllite and Dolomite. The Dhading Dolomite is represented by the presence of bluish grey dolomite.

The Benighat Slate is composed of dark slate. Along the road alignment only slate, metasandstone, quartzite, dolomite, phyllite, sandstone and mudstone are exposed. In general, the sediments of the Dun valley are composed of boulders, cobbles and pebbles, which are loose recent sediment and deposited by river. After crossing Dun valley, the road alignment passes through rocks of the Siwaliks (mainly the sedimentary rocks) and finally it crosses through low-grade metamorphic rocks of the Lesser Himalaya of the Central Nepal. The road runs on the flat land of the Dun valley, foothill of the Siwaliks and through the mountains of the Lesser Himalaya and crosses the Das dung Khola, Jugedi Khola, Khahare Khola, Rowan Khola, Seti Khola and other tributaries which are not dry even during the dry season and drain out in Trishuli River. Along the road, sandstone, mudstone of the Siwaliks; slate, meta-sandstone of the Nourpul formation; dolomite, quartzite and schist of the Kuncha formation are exposed.(DOR,MOPPW,2012).

Table 4.1 Distribution of the Common Rock Types along the Road (DOR,2012)

S.No.	Common Rock Type	Coverage(%of road length)	Length(metre)	Remarks
1	Hard rock	15.28%	6300	Dolomite, Quartzite
2	Soft Rock	17.5%	5500	Slate, Phyllite

Table 4.2 Distribution of the Soils along the Road Alignment (DOR,2012)

S.No.	Common Soil Type	Coverage(% of road length)	Length(metre)	Remarks
1	Boulder mixed soils	67.22%	24,200	Alluvium and colluvium soils

IJART
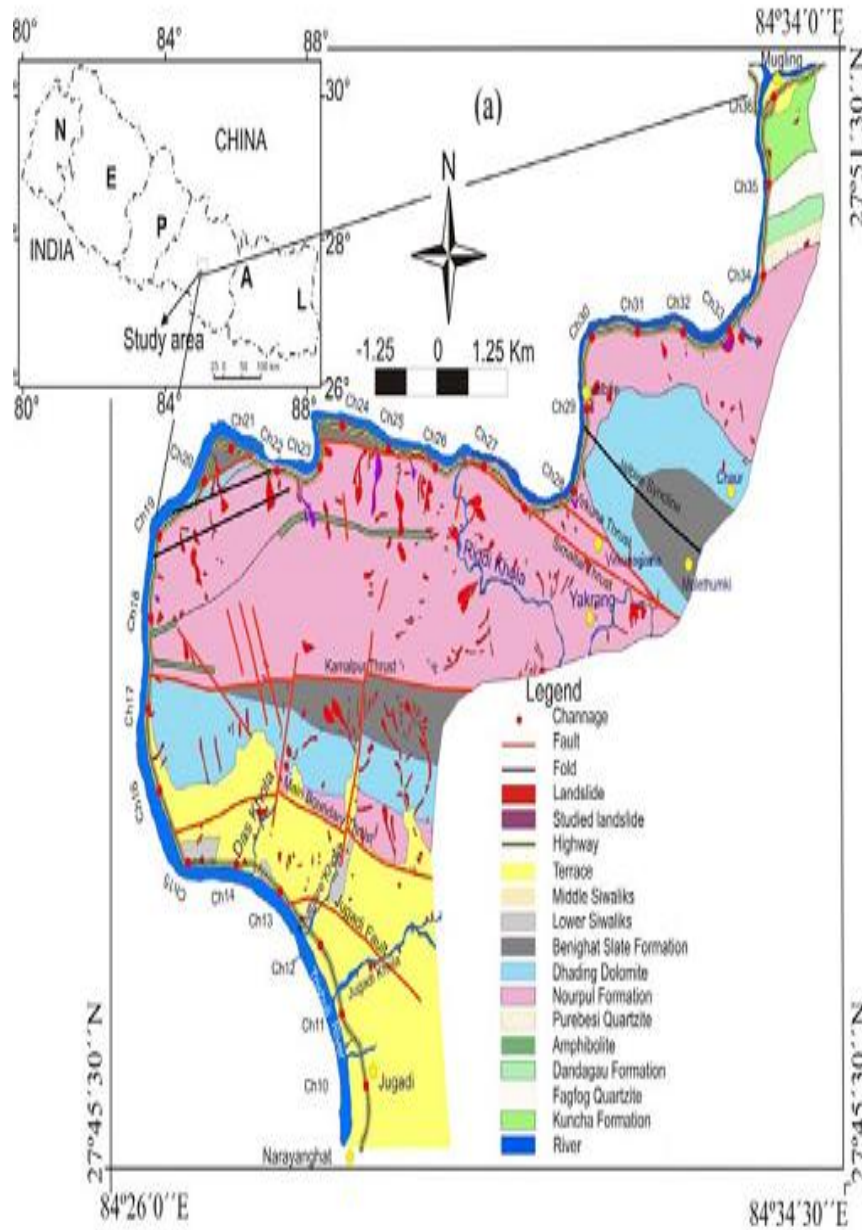
Figure 4.2 Geological Map of Mugling-Narayanghat Highway(Source: Regmi et.al,2013)

Available online at http://www.ijart.info/

Figure 4.3 Landslides across Narayanghat-Mugling Highway(Picture taken 27th Sep,2014)

The first four pictures shows the potential of shallow landslides across Nar-Mug corridor and the last two pictures depict the risk of existing bulidings

Available online at http://www.ijart.info/

4.3 Watershed for debris flow Simulation: Kamere Khola Watershed(CH-24+740)

Kamere Khola watershed is a small watershed occupying an area of about 0.119sq.km. but is a heavily debris flow laden watershed. It is prone to debris flow disaster as a result of which it caused a lot of destruction during 2003 and 2006 disaster along N-M Highway. Especially in this watershed debris flows have frequently occurred and disturbed the highway transportation. In this thesis work it has been tried to simulate the debris flow of this Kamere Khola watershed. It is located on north facing and dip slip slopes.

Figure 4.4 Debris fan formation and deposition in Kamere Khola watershed (Picture taken 27thSep,2014)
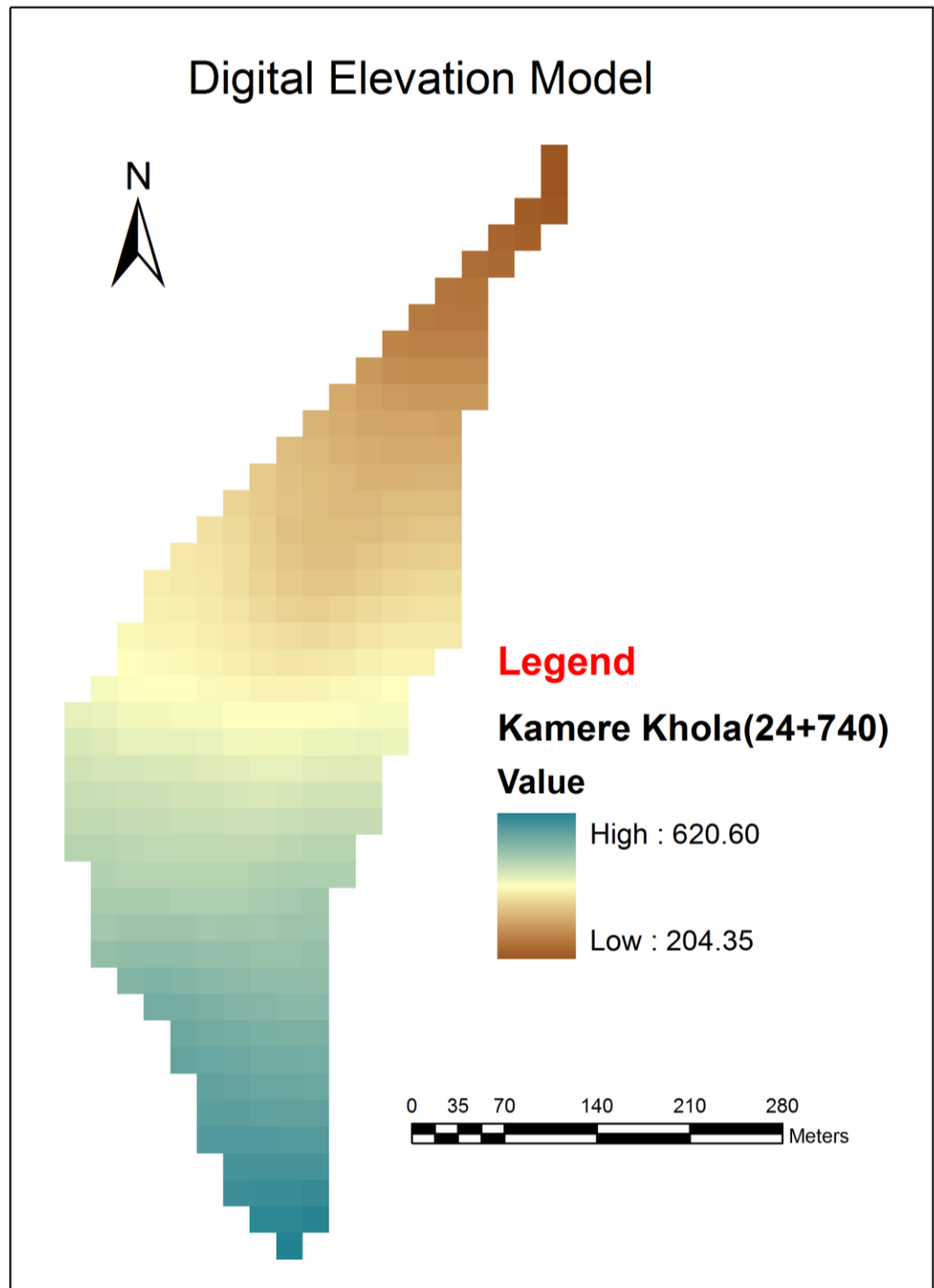
Figure 4.5 Digital Elevation Model of Kamere Khola Watershed (CH-24+740)
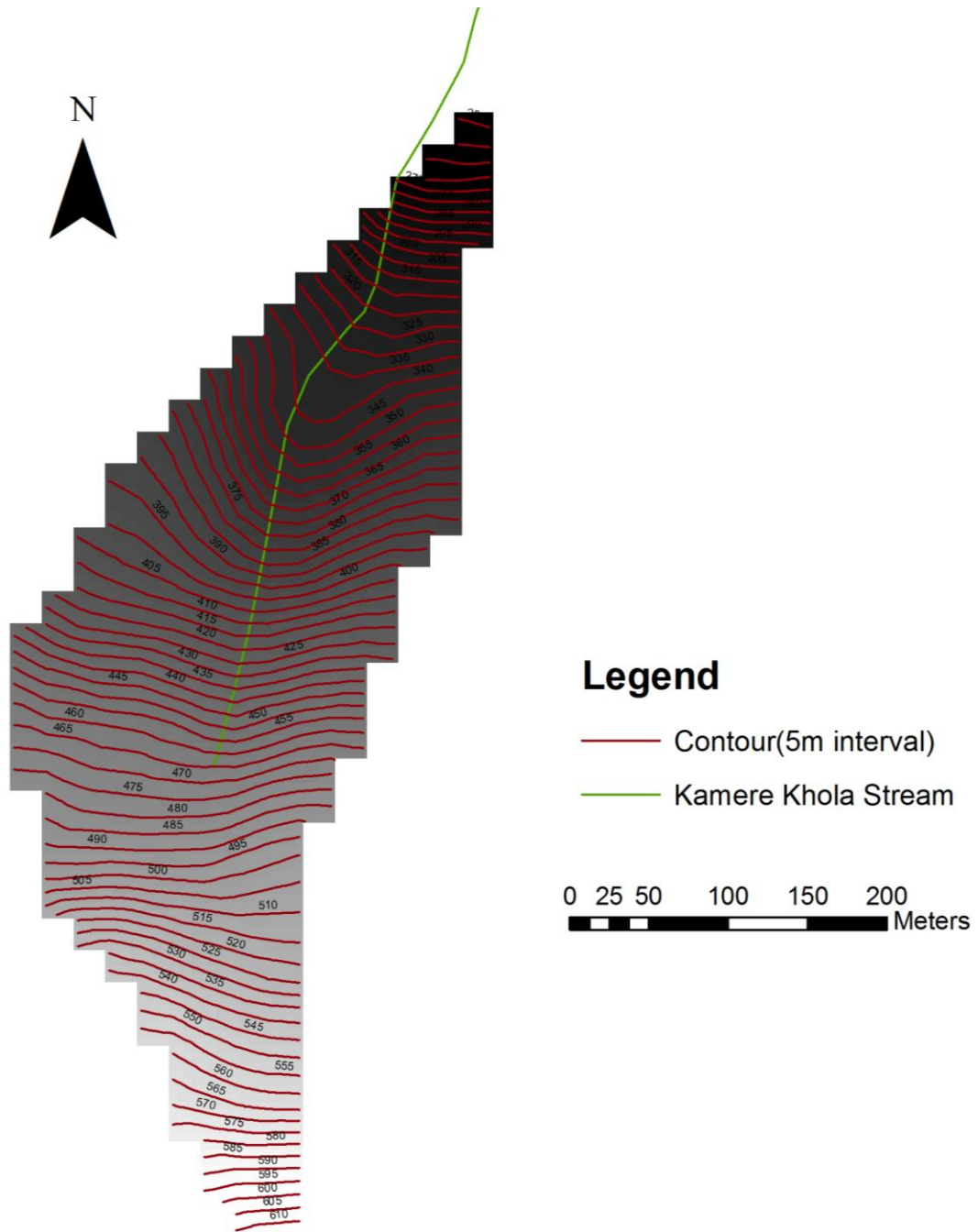
Figure 4.6 Contour Map of Kamere Khola Watershed (24+740)

Available online at http://www.ijart.info/

4.4 Hydrology

Rainfall is primarily dominated by the monsoons characterized by heavy rainfall during the summer monsoon from June to September. The remaining period is known as extra-monsoon period receives only 20% of the annual rainfall.

4.4.1 Types Of Rainfall

 In Nepal, mainly convectional, orographical, and monsoon rainfalls are prevailed, they are briefly discussed below.

Convectional rain: This rain occurs heavily but briefly with thunder and lightning. When warm air rises and reaches upper layer of the atmosphere, it cools and condenses. The condensed air forms cumulous clouds and cause rainfall. This type of rain is common during summer and in the hotter part of the day (noon).

Orographical rain: The high mountain forces the saturated air mass laden cloud to rise up and cool, and causes greater rainfall on the windward slope and rain shadow occurs on the leeward slope. For instance, the strong windward and leeward effects are observed in the Annapurna mountain area. Pokhara located at windward side of the Annapurna receives more than 3000 mm annual rainfall whereas the Mustang area leeward side receives less than 500 mm annual rainfall.

Monsoons rain: The summer monsoon developed over the Bay of Bengal and Indian Ocean is transported to Nepal by seasonal wind, and cause heavy rainfall in the whole country during summer monsoon season (June to September). Similarly, northeast monsoon makes small rainfall in the remaining period of the year.

4.4.2 Rainfall Stations

The rainfall stations along the Narayanghat-Mugling Highway were visited to know about operational conditions of the stations, data availability, and types of rain gauges installed.

4.4.2.1 Spatial Distribution

The spatial distribution of rainfall stations along Mugling-Narayanghat Highway were observed. There is one station at Khahare Khola (at 11 km from Narayangharh on the highway) and other nearby stations from the highway are Devghat (at downstream of confluence of Kali Gandaki) and Bharatpur (at Bharatpur Municipality compound). All these 3 stations lie on the southern part of the highway. There are no rainfall stations along the highway on the northern part. The stations which are near from the northern part of the highway are Shakher and Majhimtar stations.
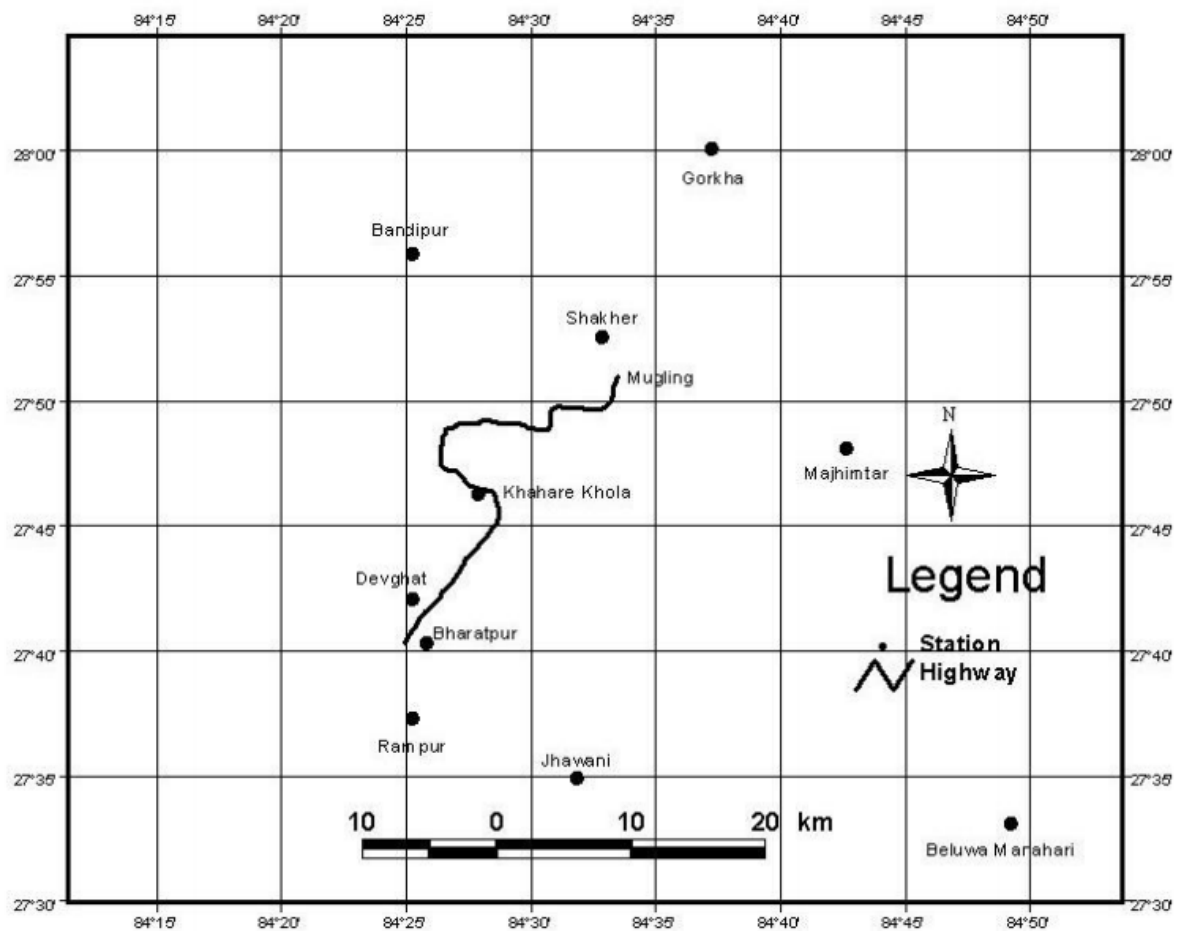
Figure 4.7 Rainfall Stations in and around Narayanghat-Mugling Highway

Khahare Khola Station: This station was established after 2003 disaster by the Divisional

Road Office, Bharatpur at 11 km on Narayangharh-Mugling highway. Non-recording rain gauge

was installed. Present operational condition of the station seems satisfactory.

Devghat Station: This station is located at downstream of confluence of Kali Gandaki River. At this station, both non-recording and recording types of rain gauges are installed by the Department of Hydrology and Meteorology (DHM). The daily rainfalls are being recorded at this station since 1998. Operational condition of the station at present is satisfactory.

Bharatpur Station: The station has non-recording rain gauge and is located in Bharatpur Municipality compound. This station is managed by Department of Hydrology and Meteorology (DHM). Operational condition of the station seems satisfactory. Station in-charge reports daily rainfall and other meteorological data to Narayani Sub-Basin Office of DHM, Pokhara.

4.4.2.2 Rainfall Intensity Analysis

The intensity of rain during 2003 disastrous rainfall was analyzed, and found that intensity of rain was extremely high. The maximum 1-hour, 6-hour and 12-hour rainfall intensities were 94.5 mm, 294.0 mm and 382.5 mm, respectively (Fig. 6.5). The extremely high intensity rain (i.e. 94.5 mm/hr) after 13 hours of continuous moderate intensity rainfall led the devastating debris flows on streams crossing the highway. The rainfall with this pattern is considered most disastrous.

Similarly, rainfall intensity curve of 2003 disastrous rainfall is developed to use as a reference for getting ideas on devastating intensity of rain and thereby develop the warning system for the possibility of the highway disasters (Fig. 6.6). The 1-hour, 3-hour, 6-hour, 9-hour and 12-hour intensities of rain were 94.5 mm/hr, 67.4 mm/hr, 48.1

mm/hr, 38.1 mm/hr and 31.9 mm/hr, respectively. The total amount of rainfall at specified time duration can be determined readily using this rainfall intensity curve. The relation used for developing rainfall intensity curve is given below

$$I = C/(t+a)^b$$

Where,

I   = Rainfall intensity (mm/hr)

t   = Time duration (min)

a ,b ,C   =   Constants
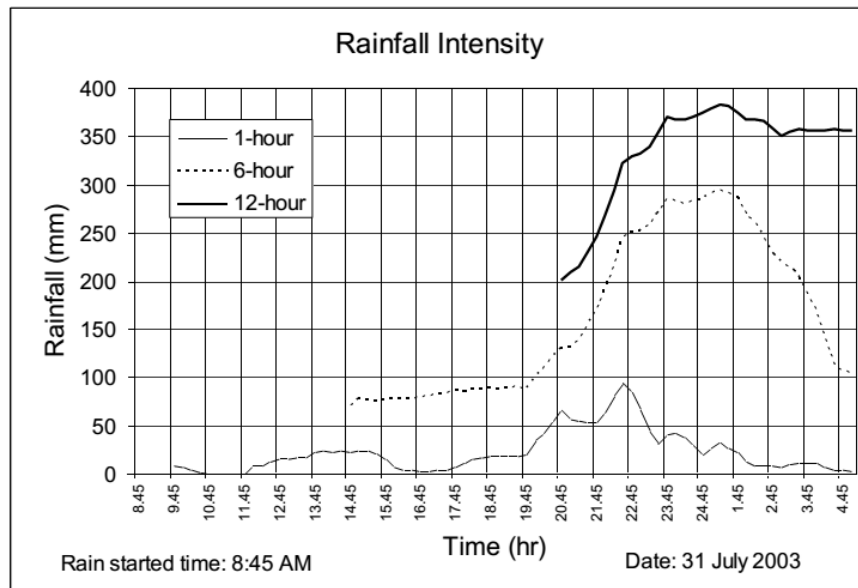
Figure 4.8 Rainfall Intensity on 31 July 2003 at Devghat Station

From the above analysis, it can be concluded that occurrence of very high intensity rain (i.e. more than 80 mm/hr) after almost 12 hours of continuous rainfall with considerable amount can cause devastating debris flow along the streams crossing the highway.
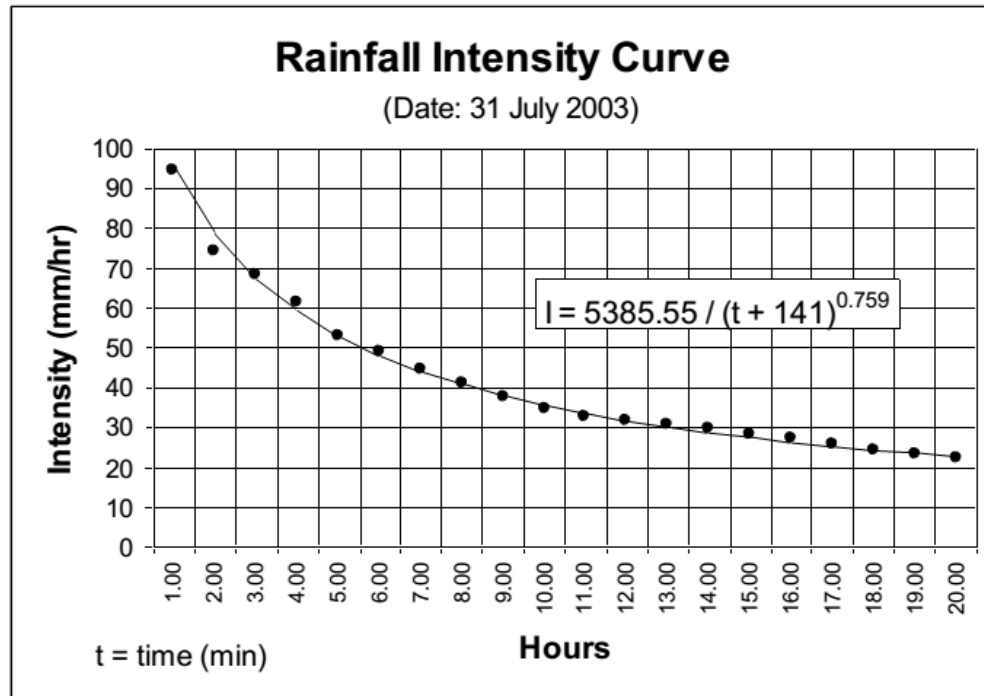
Figure 4.9 Rainfall Intensity Curve for 31 July 2003 (Devghat Station)

Estimation of Time of Concentration:

It is the time required for water to flow from the most remote (in time of flow) point of the area to the outlet once the soil has become saturated and minor depressions filled. There are several methods for computing time of concentration.The most popular method is the Kirpich equation.

$$T_c = 0.0078\ L^{0.77}S^{-0.385}$$

L = maximum length of flow(=868.48m in this case)

S   = the watershed gradient or the difference in elevation between the outlet and the most remote point divided by the length L(=0.364 in this case)

T_c = **5.247 minutes**   ,then, **Intensity at Tc = 122.44 mm/hr**

4.5 Key Characteristics of Narayanghat-Mugling Highway

Name of Road	Narayanghat – Mugling Road
Geographical Location	Central Development Region
Zone	Narayani Zone
District	Chitawan
Altitude of the lowest point	200m
Altitude of the highest point	265m(1586m in this study of area of interest)
Climate	Sub-tropical
Total Road Length	36 km
Class Of Road	National Highway - H05

4.6 Key Characteristics of Kamere Khola Watershed(24+740)

Watershed Area	sq.km.	0.119
Name of the Watershed		Kamere Khola Watershed
Chainage	km+m	24+740
Average Slope Of Watershed		0.364(20 degrees)
Length of the Catchment	m	868.48
Length from outlet to centroid	m	463.3
Estimated time of Concentration	minutes	5.247
Runoff coefficient		0.5
Elevation	m	620.6-204.35
Percentage of Monsoon Rain	%	80
Major Rock Types		milky white quartzite and light gray phyllite of Nourpul Formation

5.   MODEL PARAMETERIZATION AND CALIBRATION

5.1 Introduction

Callibration is the process by which the values of model parameters are identified for further use in particular application. It consists of the used known system and procedure to identify the model parameter that provides the best agreement between the estimated and the recorded one. In this thesis, two ,models have been used to understand the terrain stability mapping as a result of geophysical movement of earth mass moving downwards. SINMAP model is used to assess the susceptibility assessment of shallow landslides along the N-M Highway and DEBRIS2D Model is used to simulate the debris flow in Kamere Khola Watershed(24+740). The complete Model parameterization and calibration of these two models are described below:

5.2 Parameterizaton and Calibration: SINMAP Model

SINMAP version 2.0 is an ArcGIS extension of the Environmental Systems Research Institute (ESRI) that implements the computation and mapping of a slope-stability index based on the mathematical scheme. This model uses the surface topography to route flow downslope, assuming that the subsurface hydrologic boundary (or bedrock-drift boundary) parallels the surface and the hydraulic conductivity of a soil mantle overlying impermeable bedrock is uniform. The flow model predicts relative levels of the perched water table across the area characterizing subsurface flow through the colluvium or regolith. This prediction is then used to assess slope stability. SINMAP calculations require a DEM, a map of observed landslides, and the values of calibration parameters. Data needed for model development and calibration include the range of cohesion values, soil-density values, range of internal friction-angle values, and range of T/R ratios. By adopting suitable ranges for variables it is possible to calibrate and group the majority of observed landslides into the smallest SI classes.

The calculations are expressed by SI based on values of SF ranging from 0to>1.5 (Pack et al., 1998b, 2005This procedure included an interactive calibration based on visual qualitative assessment, adjusting parameters using observed landslides as

references. As suggested by Pack et al. (2005),the adjustment of parameters was performed such that the stability map captured a high proportion of observed landslides in regions with low stability index values, while minimizing the extent of low stability regions and subsequent alienation of terrain to regions where landslides have not been observed. Model outputs include stability probabilities expressed as stability indices, topographic wetness indices, graphs of landslide occurrences within slope-specific catchment area spaces, and summary tables of statistical analyses. The parameterization and calibration of the parameters of SINMAP Model are discussed below:

5.2.1 Inventory of past landslides

Accurate positioning of the initiation locations of known shallow landslides is an essential element for a successful SINMAP calibration. Data were compiled through interpretation of aerial photographs(satellite images) obtained from google earth. Analysis was aided by recognizing topographic features indicative of landslides on aerial photographs and topographic maps and by field verification of landslide data;

Although great care was taken in compiling and analyzing available data, information used for preparing the landslide-inventory map is subject to a high degree of uncertainty because of a number of factors. The information was compiled from sources having few explanatory notes concerning the exact initiation location of the landslides. Although shallow landslides and the resulting debris flows occurs both on natural and manmade hillslopes, distinctions could not be made between the two hillslope types because of uncertainty regarding their exact locations (Torikai and Wilson,1992).

In landslide hazard assessment, database partitions are based on time, space and random techniques. Time partition is using databases from different time periods; the older one for modelling and the later for validation. Space partition is dividing the study area in two sub areas, and using one for prediction and the other for validation. Random partition consists in dividing randomly the landslides in two groups, one for

prediction and the other for validation. It is pretended that the landslides from the validation dataset have not occurred yet (Chung and Fabbri, 2003).Partition approach depends on the data available. When databases from different time periods are available, time partition is the best approach (Fabbri and Chung, 2008). Otherwise it is better to use random partition. Space partition is not appropriate, because sub areas usually present different conditions regarding geology, geomorphology, and hydrology.

Random partition is the most common approach (Chung and Fabbri, 2003; Fabbri and Chung, 2008; Remondo et al., 2003). On the other hand, the partition dataset size affects the results; larger prediction datasets produce better results, and some authors recommend a half and half partition (Brenning,2005; Fabbri and Chung, 2008).

 A total of 339 landslide inventory points were identified. In this thesis, random partition approach was followed by dividing the landslides into two groups . Random partition consists in dividing randomly the landslides in two groups, one for prediction and the other for validation. 197 "debris slides" (through aerial interpretation and from the hazard map prepared by Nippon Koei,2008 in collaboration with DWIDP, Nepal as well) was used for modeling calibration and 142 polygon themes which were classified as "landslide zones" was used for validation.

The inventory map of a total of 197 shallow landslides, as shown in Fig. 5.1 , was prepared as an ArcGIS point theme. All 197 inventoried landslides were classified as "debris slides", meaning that they are shallow, translational, and composed of a mixture of coarse- and fine-grained soils.
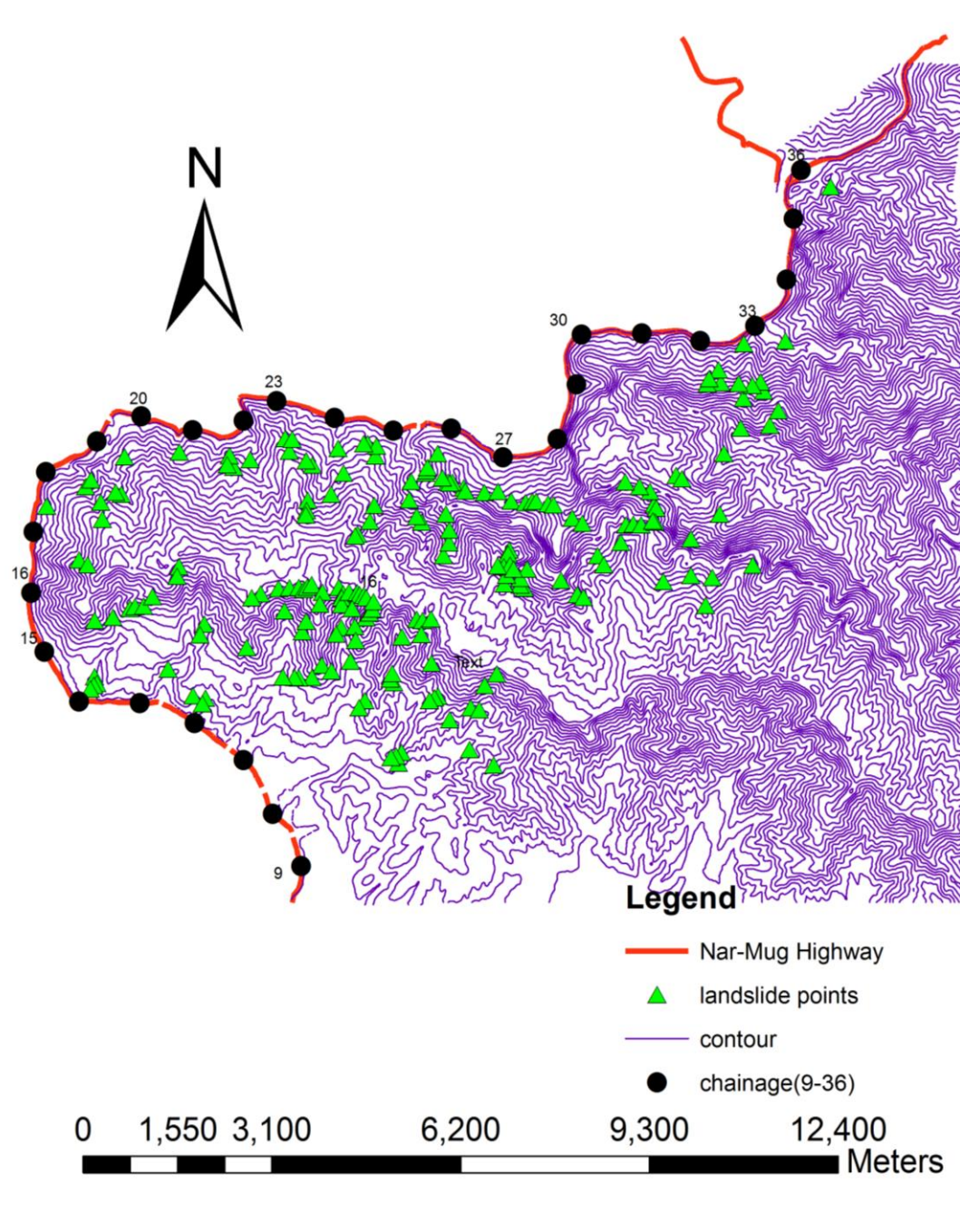
Figure 5.1 Map showing the landslide points along Narayanghat-Mugling Highway used for SINMAP calibration

5.2.2 Topographic data

A topographic map(contours) of the study area is shown in Fig. 2. Data used in the SINMAP were derived from a 20-m DEM of digitized topo map produced by the Department of Survey(DOS),Nepal and interpolated into a 5m DEM in ArcGIS and used as a input for the SINMAP Model. The topo maps used were of that of MUGLING(278403C)and JUGEDI BAJAR(278402D). The DEM has a coordinate system as follows:

 Spheroid- Everest 1830

Projection- MUTM (Modified Universal Transverse Mercator)

Origin- Longitude 84^0 East, Latitude 0^0 North

False coordinate - 500000m Easting, 0 m Northing

Scale factor at CM (Central Meridian)-   0.9999

 All raster data have a spatial resolution of 5 m(interpolated from 20m) and are in the ESRI grid format.

5.2.3 Hydrological data

Hydrological data needed for the model includes a wetness index defined as the ratio of transmissivity over steady-state recharge (T/R). The depth of a shallow landslide is generally not more than 1–2m. As also observed in several field studies (Baum et al., 1990, 1991; Baum and Reid, 1992; Ellen et al., 1995), the thickness of the soil above the failure surface varies within the study area. According toPack et al. (1998b, 2005), the T/Rratio multiplied with the sine of the slope angle can be interpreted as the length of hillslope required to develop saturation in a critical wet period. Although the term'steady state'is used with lateral flux, the parameter R does not refer to a long-term (e.g., annual) average of recharge in SINMAP. Instead it represents the effective recharge for a critical period or event of wet weather that is likely to trigger landslides. TheT/Rratio, which is treated as a single parameter, combines both climate and hydrogeological factors. The effective R value can be defined as rainfall minus evapotranspiration and infiltration. Evapotranspiration and

infiltration are assumed as negligible in this study. Such an assumption represents a worst-case scenario by overestimating the value of R. However it is generally acceptable for heavy storms of short duration. As mentioned earlier, previous studies of landslides and associated debris flows on several landslide sites along Mugling-Narayanghat Highway reveal that shallow landslides are activated by extreme and intense rainfall events. During the monsoon of 2003 and 2006,heavy and intense rainfall occurred and it brought a lot of devastating effects along that highway. Hence,the maximum daily rainfall event during the monsoon of 2003 and 2006 disastrous moments are used for SINMAP calibration.

Rainfall Isohyets:

The rainfall isohyets of 20 mm intervals were prepared for the day of 2003 disaster (Fig.5.2). The rainfall isohyets were prepared using daily rainfall of 11 stations in and around the study area. The rainfall isohyets showed 446.2 mm of rainfall was occurred at Devghat and its surrounding areas which caused the disaster on the Narayangharh-Mugling highway. The isohyets could be developed more precisely if there were other rainfall stations along the highway. The isohyets provide ideas on rainfall distribution patterns on the day of disaster. The isohyets show 280 - 446 mm rainfall occurred on the stretch of the highway where landslides and debris flows found most severe(NipponKoei,2008).
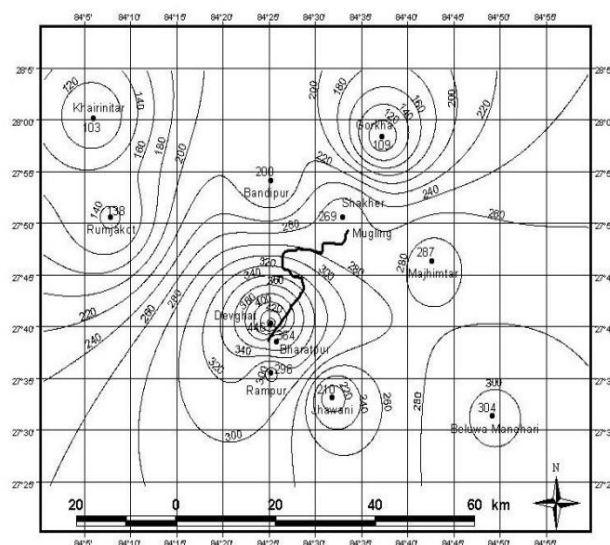
Figure 5.2 Daily Rainfall Isohyets (31 July 2003) (Source: Nippon Koei,2008)

Rainfall Distribution Analysis

The rainfall distribution pattern of 31 July 2003 was studied. The rainfall chart of recording rain gauge of Devghat station showed rain started at 8:45 AM of 30 July and continued until 5:00 AM of 31 July, and the total rainfall amount was 446.2 mm in 20.25 hours (Fig. 6.4). It showed about 25% of total rainfall (i.e. 114.5 mm) had occurred in the first 10 hours (between 8:45 AM and 18:45 PM), about 50% of total rainfall (i.e. 221.5 mm) had occurred in 12.5 hours (between 8:45 AM and 21:15 PM), and about 75% of total rainfall (i.e. 339.5 mm) had occurred in 14 hours (between 8:45 AM and 22:45 PM). It indicates that in 4 hours period (between 18.45 PM and 22.45 PM) 225.5 mm of rainfall occurred, and it devastated the highway with landslides and debris flows(Nippon Koei,2008).
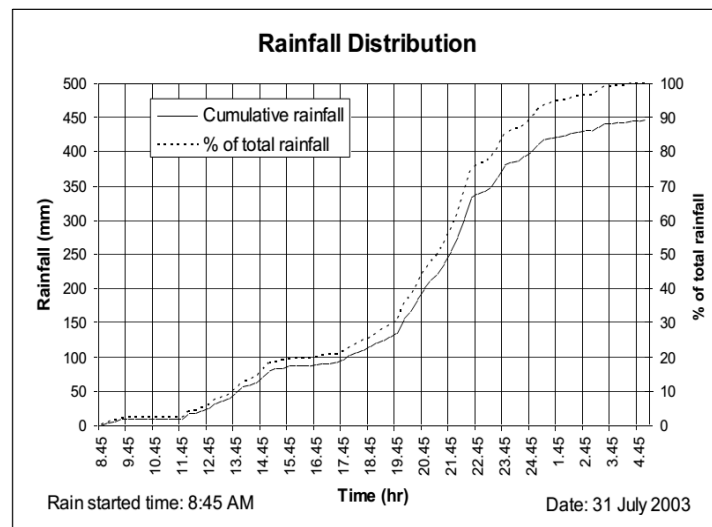
Figure 5.3 Rainfall Distribution on 31 July 2003 at Devghat station (Source: Nippon Koei,2008)

Maximum 1-day Rainfall:

The daily rainfall records of nine years (1998-2006) of Devghat station were analyzed on the basis of disastrous event of 2003 and 2006. Based on those daily rainfall records of the station, the maximum annual daily rainfalls of the station were sorted out . The records show the highest value of the maximum annual daily rainfalls

of 446.2 mm on 31 July 2003 and which is followed by 376.4 mm on 9 September 2006. Moreover, the lowest value of the maximum annual daily rainfall of 100.3 mm is found on 7 August 2005.
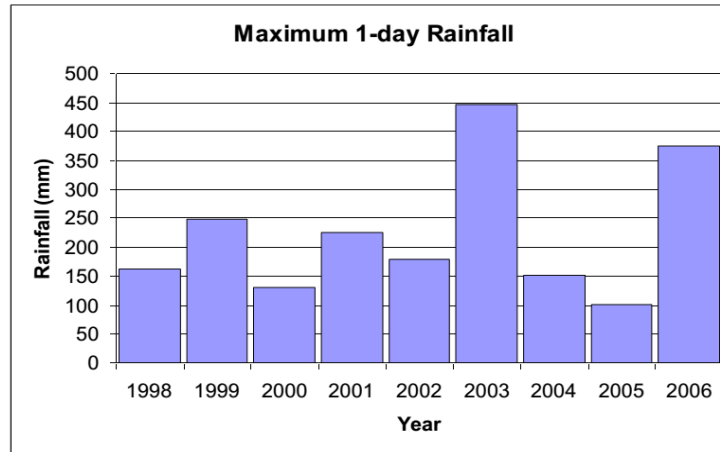
Figure 5.4 Maximum 1-day Rainfall (Devghat Station)

Return Period of 1-day Rainfall:

The maximum annual daily rainfalls of past nine years (1998-2006) were analyzed using various distribution functions to know non-exceedance probability of certain levels of daily rainfalls. The probability plotting positions of observed maximum daily rainfalls were determined using Weibull method. Among the distribution functions, three parameters Lognormal distribution was found to be the best fitted for the maximum annual daily rainfalls data of the station.

The domain, probability density function [f(x)], cumulative distribution function [F(x)] of Lognormal (3P) distribution are presented below.

Domain:

$\varepsilon < x < +\infty$

The   functions   are:

$$F(x) = \emptyset \left[\frac{\ln(x - \varepsilon) - \mu}{\sigma} \right]$$

$$f(x) = \frac{exp\left[-\frac{1}{2}\left\{ \frac{\ln(x-\varepsilon)-\mu}{\sigma} \right\}^2 \right]}{(x - \varepsilon)\sigma\sqrt{2\pi}}$$

Where,

f(x)   =   Probability density function (pdf)

F(x)   =   Cumulative distribution function (cdf)

Φ   =   cdf of standard normal distribution

x   =   Variable (daily rainfall)

ε   =   Lower bound parameter or location parameter

μ, σ |=| Normal parameters

Kolmogorov Smirnov goodness of fit test was carried out to see the maximum deviation of the fitted curve. The maximum deviation (D) is determined as shown below.

D   = $\max|F_o(x) - S_n(x)|$

$S_n(x) = k/n$

   Where, Fo(x) = the proportion of cases expected to have scores less than or equal to x, k = no. of observations less than or equal to x, and n = total no. of observations.

Available online at http://www.ijart.info/
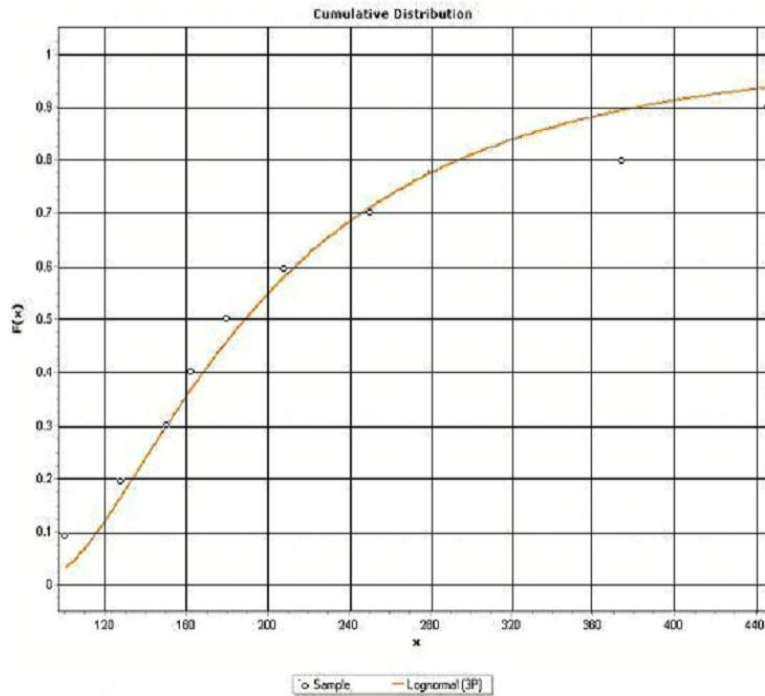
Figure 5.5 Lognormal (3P) Distribution Fitting for Maximum 1-day Rainfalls

The values of the parameters in the distribution fitting are $\sigma = 0.766$, $\mu = 4.754$ and $\varepsilon = 72.616$. Kolmogorov Smirnov goodness of fit value is 0.095.   Further, cumulative distribution function of Lognormal (3P) distribution was applied to compute return periods of certain levels of daily rainfalls. It is found that 200, 300 and 400 mm daily rainfalls have return periods of 2, 5 and 10 years, respectively (Table below).

Table 5.1 Return Period of 1-day Rainfall

S.N.	Daily Rainfall(mm)	Return Period(years)
1	200	2
2	250	3
3	300	5
4	350	7

5	400	10
6	450	16

446.2mm is the maximum daily rainfall event observed on 31 July,2003 disaster and it is satisfied in 16 years return period and hence we used this value of rainfall for the calibration of SINMAP Model.
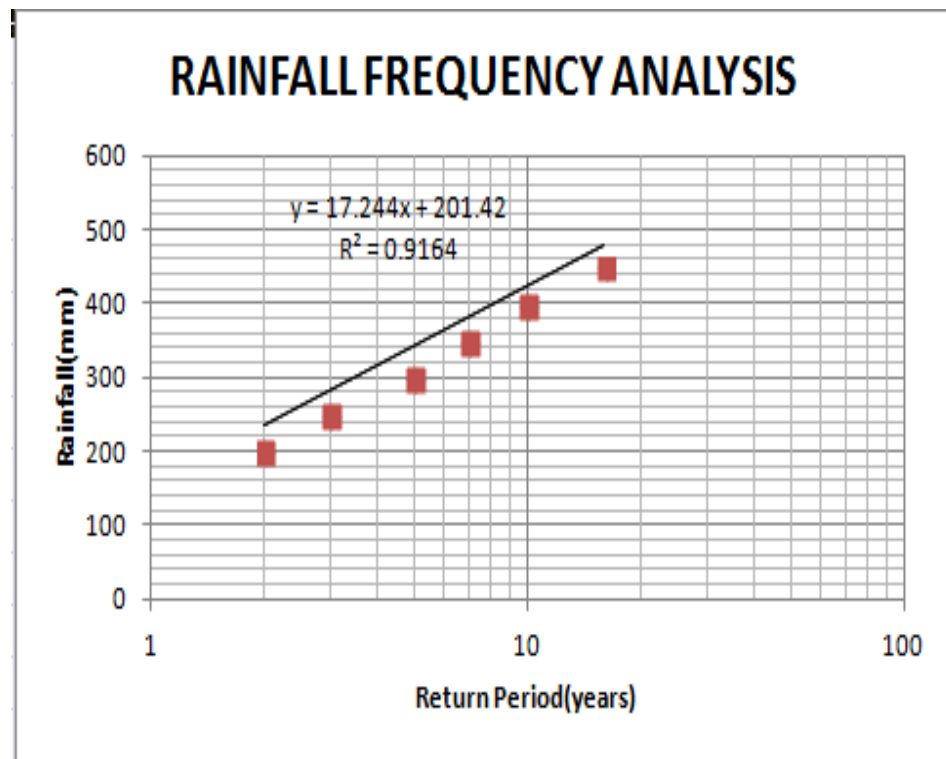
Figure 5.6 Daily Rainfall Frequency Analysis using LogNormal(3P) distribution fitting

Plotting the above values we get the required equation as y= 17.24x+201.42 with R^2=0.0.9164,where,y=rainfall; x=return period(yrs).

For 25 years return period, rainfall= 632.5 mm and for 50 years return period, rainfall= 1063.42mm

Hydraulic conductivity, symbolically represented as k, is a property of vascular plants, soils and rocks, that describes the ease with which a fluid (usually water) can

move through pore spaces or fractures. It depends on the intrinsic permeability of the material and on the degree of saturation, and on the density and viscosity of the fluid. Saturated hydraulic conductivity, K_{sat}, describes water movement through saturated media. The value of saturated hydraulic conductivity has been observed in the field itself by digging a pit, pouring it with water and calculating the distance the water percolates observing the time taken .Similarly, different literature well describes the value of saturated hydraulic conductivity as shown in the table below:

Table 5.2 Values of Ksat for different soils (Source: Ferguson and Debo, 1990)

Material	Hydraulic Conductivity	
	in/hr	ft/day
ASTM Crushed Stone No. 3	50,000	100,000
ASTM Crushed Stone No. 4	40,000	80,000
ASTM Crushed Stone No. 5	25,000	50,000
ASTM Crushed Stone No. 6	15,000	30,000
Sand	8.27	16.54
Loamy sand	2.41	4.82
Sandy loam	1.02	2.04
Loam	0.52	1.04
Silt loam	0.27	0.54
Sandy clay loam	0.17	0.34
Clay loam	0.09	0.18
Silty clay loam	0.06	0.12
Sandy clay	0.05	0.1
Silty clay	0.04	0.08
Clay	0.02	0.04

Hence, the value of saturated hydraulic conductivity ranges from 0.012m/day(clay) to 5.04 m/day(sand).The depth of soil ranges from 1to 2 m in case of shallow landslides. Deb S.K ,2009,while doing his research in Oahu, has taken the maximum value of k_{sat} as 12.192.

K_{max} = 12m/day

k_{min}= 0.012 m/day

 The saturated transmissivity is a measure of how much water can be transmitted horizontally in an aquifer. Transmissivity is defined as hydraulic conductivity multiplied with the saturated thickness:

$$T = K * h$$
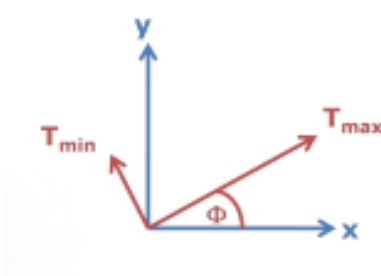
Figure 5.7 Illustration of max and min values of transmissivity (Wikpedia; Assesed: 28th Sep, 2014)

Maximum value of transmissivity=12*2=24m^{2}day^{-1}

Minimum value of transmissivity = 0.012*2=0.024 m^{2}day^{-1}

Sharma,R.H,2002,while doing his thesis along Dharan Dhankuta highway took the value of transmissivity as 65 m^{2}day^{-1} .Hence,for better accuracy and being in the conservative side ,the upper and lower bound values of transmissivity are taken as-

Transmissivity(max or upper bound)=45 m^{2}day^{-1}

Transmissivity(min or lower bound)=0.024 m^{2}day^{-1}

Hence,the value of T/R is calibrated as,

For normal max rainfall (446.2 mm on 31 july,2003 at Devghat station),

T/R(max or upper bound)=(45 m^{2}day^{-1} /446.2 mm)=100mday^{-1}

T/R(min nor lower bound)=(0.024 m^{2}day^{-1} /446.2mm)=0.05mday^{-1}

For 25 yrs return period (632.5 mm max daily rainfall),

T/R(max or upper bound)=(45 m^{2}day^{-1} /632.5mm)=71.14

T/R(min nor lower bound)=(0.024 m^{2}day^{-1} /632.5mm)=0.04mday^{-1}

For 50 yrs return period(1063.42mm max daily rainfall) ,

T/R(max or upper bound)=(45 m^{2}day^{-1} /1063.42mm)=42.31 mday^{-1}

T/R(min nor lower bound)=(0.024 m^{2}day^{-1} /1063.42mm)=0.02mday^{-1}

5.2.4 Geotechnical data

The geotechnical data is one of the important parameter for input to SINMAP Model .Different geotechnical input can be described as:

The cohesion index (dimensionless cohesion factor C) and the soils internal friction angle (ϕ) represent the geotechnical data input into the model. C is the relative contribution of soil and root cohesive forces in preventing the development of a failure plane. To avoid the complication of variable landslide parameters in a regional analysis and to isolate the topographic control on landslide initiation, we used uniform parameter values of friction angle and cohesion of the soil in the study area.

In addition to the geology, rainfall, land use changes, and some other human activities, the landslide activity in Mugling-Narayanghat section is also controlled by the presence of high swelling clay mineral illite along with the low swelling clay minerals chlorite and kaolinite(Neupane Bhupati,2011)

.Field observations of soil exposed at the head scarp of landslides demonstrate that tree roots do not penetrate into the weathered rock, and consequently the root zone is situated above the failure plane. Based on the soil-root morphology nomenclature suggested byTsukamoto and Kusakabe(1984), these conditions are referred to as Type A, which have the root strength (C_r) probability distributions defined by a mean value of 3 kNm^{-2} and standard deviation of 2 kNm^{-2}i.e.

Mean value of C_r (μ)= 3 kNm^{-2}

Standard deviation(σ) = 2 kNm^{-2}

We considered values for the root cohesive force (Cr)of 0–3kNm^{-2} and for soil cohesive force(Cs)of 0–25 kN m^{-2} (testing of field sample soil in lab).

Dimensionless Cohesion(C)=(C$_r$+C$_s$)/(h ρ_sg)

Such values provided lower and upper boundary values of the cohesion index (C)of approximately 0 to 0.7.

Available online at http://www.ijart.info/

A series of SINMAP calculations in which the values of C varied and all other parameters remained unchanged showed the significant influence of such a parameter on slope-stability calculations in all regions.

The moist bulk density of soil was calibrated at 1800kg/m^3.

Values for the soil friction angle for certain soil types can be estimated from tables provided by Hammond et al., (1992). These tables require that the soil be classified according to the Unified Soil Classification (USC) system. The value of internal friction of soil was tested in the laboratory of the soil sample from the field.given that this study requires that parameters be generalized over large areas, a wide variation encompassing the properties of several different soil types,from clayey to sandy and gravelly soils, is more realistic than a small range of values. It was found to be in the range of 35° to 40°. Finally we selected calibrated lower and upper boundary values of 30° and 45°, and 0 and 0.65 for friction angle of soils and dimensionless cohesion, respectively. These calibrated values were used in the SINMAP application for stability index mapping along N-M Highway

5.3 Summary of Model Parameters for Callibration of SINMAP Model

Combined Cohesion(C)	lower bound	0(Dimensionless)
Combined Cohesion(C)	upper bound	0.65 (Dimensionless)
Transmissivity(T)	lower bound	45 m2day^{-1}
Transmissivity(T)	upper bound	0.024 m2day^{-1}
Effective Recharge(Rainfall)	Normal Max	446.2 mm
Effective Recharge(Rainfall)	25 yrs return period	632.5 mm
Effective Recharge(Rainfall)	50 yrs return period	1063.42 mm

Transmissivity to Recharge(T/R)	upper bound(Normal)	0.05 m day^{-1}
Transmissivity to Recharge(T/R)	lower bound(Normal)	100 m day^{-1}
Transmissivity to Recharge(T/R)	upper bound(25 yrs return)	0.04 m day^{-1}
Transmissivity to Recharge(T/R)	lower bound(25 yrs return)	71.14 m day-1
Transmissivity to Recharge(T/R)	upper bound(50 yrs return)	0.02 m day^{-1}
Transmissivity to Recharge(T/R)	lower bound(50 yrs return)	42.31 m day^{-1}
Internal Friction($_\varphi$max)	upper bound	30^0
Internal Friction($_\varphi$min)	lower bound	45^0
Moist Bulk Density(ɣ)		1800kgm^{-3}

In this manner, by using the above calibrated values of the parameters, SINMAP Model was successfully simulated and the results obtained reached a much more satisfactory values while fitting the landslide points to the callibraton curve within the SA-plot. These parameters along the Mugling-Narayanghat Highway can be well used for further applicaton as well.

5.4 Parameterization and Calibration: DEBRIS-2D Model

Debris-2D is a two-dimensional debris flow simulation program and treats debris flow as a yield stress fluid(non-Newtonian fluid mechanics)(Liu & Huang, 2006; Liu et al., 2009; Wu et al., 2013).It can simulate flow depth, velocity, impact force and affected area of debris flow. This model can simulate the water soil mixture flow

motion. The different input data that have been used for the model calibration are as follows:

5.4.1 Topographical Data

The Digital Elevation Model(DEM) is the topographical data required for the calibration of DEBRIS-2D Model. DEM of 20m*20m prepared from 20m contour interval digitized Topo map obtained from Department Of Survey ,Nepal was interpolated into 5m*5m in ArcGIS and then used as a topographical input data to DEBRIS-2D Model.

5.4.2 Mass parameter(Rheological Parameter)

Yield Stress(Pascal) is the only one material input to DEBRIS-2D Model.It is the physically based rheological measurement (Liu and Hang,2006).It can reasonably be determined by soil composition and for this thesis work it was experimentally determined in the field itself.

$$H^2 = \frac{2\tau_0}{\rho g} X$$
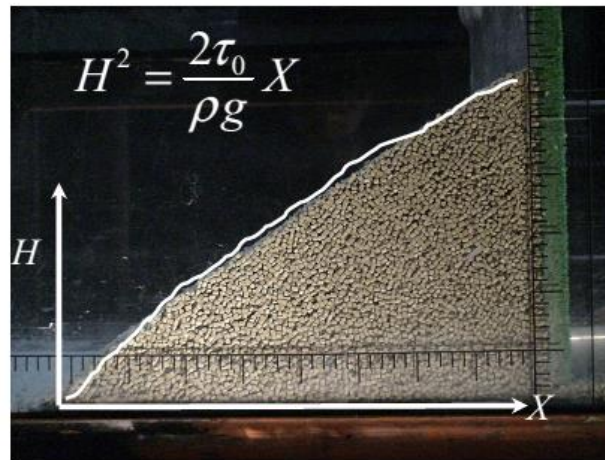
Figure 5.8 Physical Measurement of Yield Stress

The field measurement converged to the average value of yield stress as 700Pa

5.4.3 Mass Source and Distribution

For the mass source and distribution as input to DEBRIS-2D Model,it is important to know the location,distribution,type and volume of debris flow.Designed volume of debris flow can be determined based on equilibrium volumetric concentration.

Solid Volume + Liquid Volume $\longrightarrow$ Concentration Concept

An equilibrium concentration conceptual of Takahashi (2007) was applied to estimate the debris flow volume. Takahashi (2007) derived the equilibrium concentration, as follows:

$$C_v = \frac{\rho_w \tan \theta}{(\rho_s - \rho_w)(\tan \varnothing - \tan \theta)} = \frac{Total\ Volume\ of\ solid}{Total\ volume\ of\ debris\ flow}$$

where, C_v is the equilibrium concentration, ρ_s is the solid density of debris, ρ_w is the liquid density of debris, φ is the rest angle of solids or angle of internal friction of soil, and θ is the slope. In general, ρ_w is the water density, ρ_s and φ may be measured from field samples ,and θ may be calculated from the DEM. From the field samples, the solid density was

ρ_s =2.6 g cm^{-3},

$\varphi \approx 35°$

With the liquid density of ρ_w =1gcm^{-3}, the average slope is calculated from Slope Map
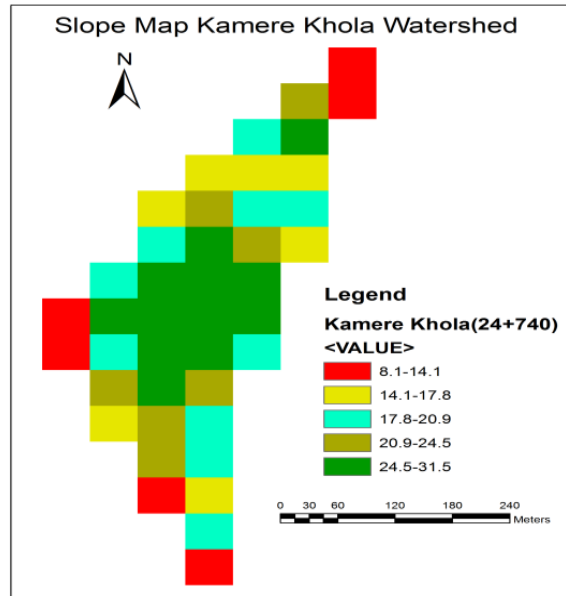
Figure 5.9 Slope Map of Kamere Khola Watershed

Average slope of Kamere Watershed = $(8.1+31.5)/2 \sim\sim 20^0$

The equilibrium concentration was calculated as;

$$C_v = \frac{1*(\tan 20)}{(2.6-1.0)*(\tan 35 - \tan 20)} = 67.65\% = 0.676$$

Maximum value of C_v can't exceed 0.603(Huang,M.C, 2003).Hence ,

Take value of $C_v = 0.603$

There are two conditions regarding designed volume for initiation mass input. The two conditions are:-

• Water is sufficient case in which all mass becomes debris flow and is calculated as-

$$V = \frac{V_d}{C_v} = \frac{Total\ volume\ of\ dry\ debris\ mass}{C_v}$$

• Water is NOT sufficient case in which only a part of mass becomes debris flow.

$$V = \frac{V_w}{1-C_v} = \frac{Total\ volume\ of\ water}{1-C_v}$$

The hydrologic analysis of Kamere Khola watershed (24+740) was performed. The water (rainfall)accumulation in the required time before initiation of debris flow was calculated. The amount of water required to induce debris flow in this watershed could be estimated with rainfall data and empirical equations. If the amount of water was insufficient to mobilize all the source material to form a debris flow, the volume of the debris flows would be smaller.Conversely, if the amount of water was sufficient to mobilize all the source material to form debris flow volume of debris would be more.

5.4.4 Hydrologic Analysis

Daily Rainfall Pattern during 2003 Disaster:

The daily rainfall patterns of Devghat and Bharatpur stations were analyzed (Fig.5.10). During 2003 disaster on the highway, at Devghat station daily rainfall pattern were 39.8 mm, 446.2 mm and 71.6 mm on 30^{th}July, 31^{st}July and 1st August, respectively. Further, at Bharatpur station during the disaster, daily rainfall pattern were 11.5 mm, 364.5 mm and 23.8 mm on 30^{th}July, 31^{st}July and 1st August, respectively. The rainfall pattern shows, at Devghat station, during 2003 disaster the maximum 2-day and 3-day rainfall were 517.8 mm and 557.6 mm, respectively. Similarly, during that disaster, the maximum 2-day and 3-day rainfall at Bharatpur station were 388.3 mm and 399.8 mm, respectively. With analyzing daily rainfall pattern of Devghat station during 2003 disaster, it can be concluded that landslides and debris flow occur on the highway if rainfall continued for 2 days with considerable amount of rainfall on the first day and heavy rainfall of more than 300 mm on the second day.
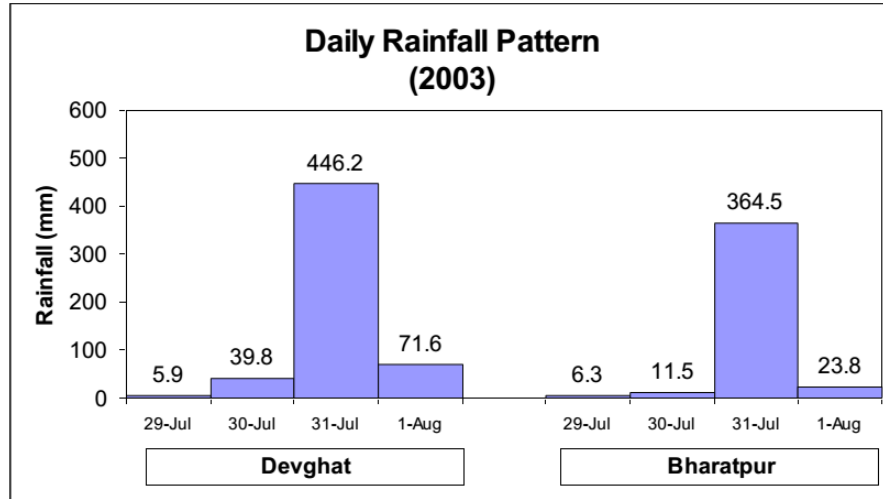
Figure 5.10 Daily rainfall pattern during 2003 Disaster

Analysis of rainfall accumulation before initiaton of debris during 2003 disaster:

The rainfall chart of recording rain gauge of Devghat station showed rain started at 8:45 AM of 30 July and continued until 5:00 AM of 31 July, and the total rainfall amount was 446.2 mm that day. It was found that in 4 hours period (between 18.45 PM and 22.45 PM) 225.5 mm of rainfall occurred, and it devastated the highway with landslides and debris flows.

The event rainfalls of certain duration other than diurnal,which couldn't be estimated from the available daily rainfall data,were estimated by the relationship developed by Shakya(2002),who related hourly rainfall and 24-hr rainfall data for the same events,taking into account the data from few automatic sations of Nepal.The relation between 24 hour and lower duration rainfall depths of some specified storm periods can be estimated by the following equation:-

$$\frac{P_t}{P_{24}} = \sin\left(\frac{\pi * t}{48}\right)^{0.4727}$$

Where,

t is the specified time(in hours)for which rainfall amount needs to be estimated;

P_t is the rainfall in t hours and P_{24} is the total rainfall in 24 hours;$Sin((\pi t)/48)$is in radians.

For 2003 disaster, it is clear that 446mm rainfall was observed on 31st July,2003 and debris flow triggered between 18.45 PM and 22.45 PM i.e. at around 20:45 PM, so the total rainfall accumulation on that day can be calculated by the above equation:-

P_{24}=446.2 mm

t = (8:45AM-20:45PM)=12hrs

Using the above equation ,P_t=380mm

So, the total rainfall accumulation before the initiation of debris flow during 2003

= 5.9(on 29 July)+39.8(30 July)+380(31 July before initiation of debris)

=425.7 mm

Hence,425.7 mm rainfall was accumulated in 60 hours during 2003 disaster before initiation of debris flow.

Daily Rainfall Pattern during 2006 Disaster:

The daily rainfall patterns of Devghat, Bhratpur and Khahare Khola stations were analyzed. During 2006 disaster, at Devghat station daily rainfall pattern were 0.0 mm, 376.4 mm and 289.6 mm on 8th, 9th and 10th September, respectively. At Bharatpur station, daily rainfall pattern were 0.0 mm, 236.0 mm and 99.0 mm on 8th, 9thand 10thSeptember, respectively. Further, at Khahare Khola station, daily rainfall pattern were 0.0 mm, 256.0 mm and 346.0 mm on 8th, 9thand 10thSeptember, respectively. The rainfall pattern shows, during 2006 disaster, the 2-day rainfall were 660.0 mm, 335.0 mm and 602.0 mm at Devghat, Bharatpur and Khahare Khola stations, respectively. It shows that 2-day rainfall during 2006 disaster was more than 2003 disaster at Devghat station but slightly less at Bharatpur station.

With analyzing daily rainfall pattern of Devghat and Khahare Khola stations during 2006 disaster, it can be concluded that landslides and debris flow occur on the highway if rainfall continued for 2 days with considerable amount of rainfall on the

first day and heavy rainfall of more than 300 mm on the second day as concluded earlier.
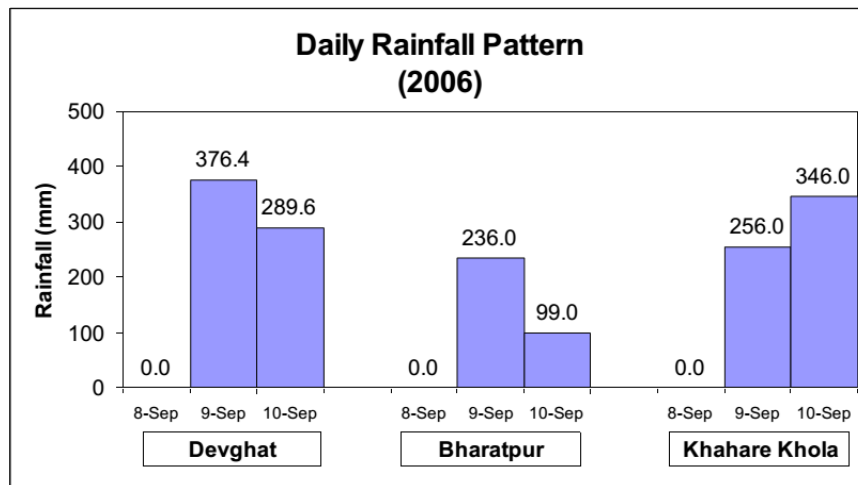
Figure 5.11 Daily Rainfall pattern during 2006 Disaster

Since the maximum precipitation is observed at Devghat station,hence considering the worst case,Devghat station is analyzed.

The relation between 24 hour and lower duration rainfall depths of some specified storm periods can be estimated by the following equation(Shakya,2002):-

$$\frac{P_t}{P_{24}} = \sin\left(\frac{\pi * t}{48}\right)^{0.4727}$$

t is the specified time(in hours)for which rainfall amount needs to be estimated;

P_t is the rainfall in t hours and P_{24} is the total rainfall in 24 hours; $\sin((\pi t)/48)$is in radians

From the daily rainfall graph it is seen that 376.4 mm rainfall was observed on 9 Sep 2006 and 289.6 mm was observed on 10 Sep. Assuming the initiation of debris occurred at around mid of 10 Septemmber and Using the above equation,we have,

P_{24} = 289.6mm

t   = 12 hours

P_t = 245.83mm

Hence, the total rainfall accumulation before the initiation of debris flow during 2006

= 0(8 Sep)+376.4(9Sep)+245.83(10 Sep before initiation of debris)

= 622.2 mm

≈   650mm

Hence, 650 mm rainfall was accumulated in 36 hours during 2006 disaster before initiation of debris flow.

Analysis of 2 day rainfall:

Maximum 2-day rainfalls in each year at Devghat station were sorted out for 1998-2006 . The highest value of maximum 2-day rainfall was 666.0 mm (during 9 & 10 September 2006) which is followed by 517.8 mm (during 31 July & 1 August 2003). The lowest value of maximum 2-day rainfall was 154.6 mm (during 6 & 7 August 2005). The maximum 2-day rainfall in each year of Devghat station is presented.
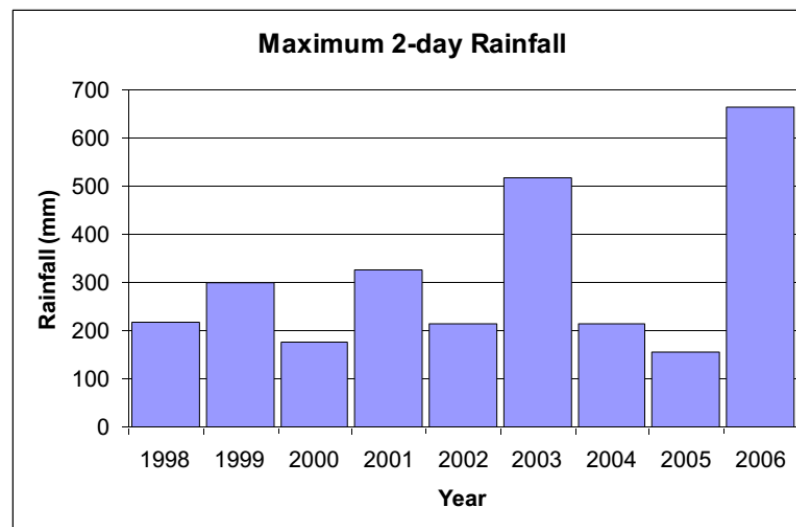
Figure 5.12 Maximum 2day rainfall at Devghat station

Similarly, maximum 3-day rainfalls in each year of Devghat station were sorted out for the duration of 1998-2006. The highest value of maximum 3 -day rainfall was 690.5 mm (during 9-11 September 2006) which is followed by 557.6 mm (during 30 July to 1 August 2003). The lowest value of maximum 3-day rainfall was 186.3 mm (during 6-8 August 2005). The maximum 3-day rainfall in each year of Devghat station is presented in graphical form (Fig:5.13)
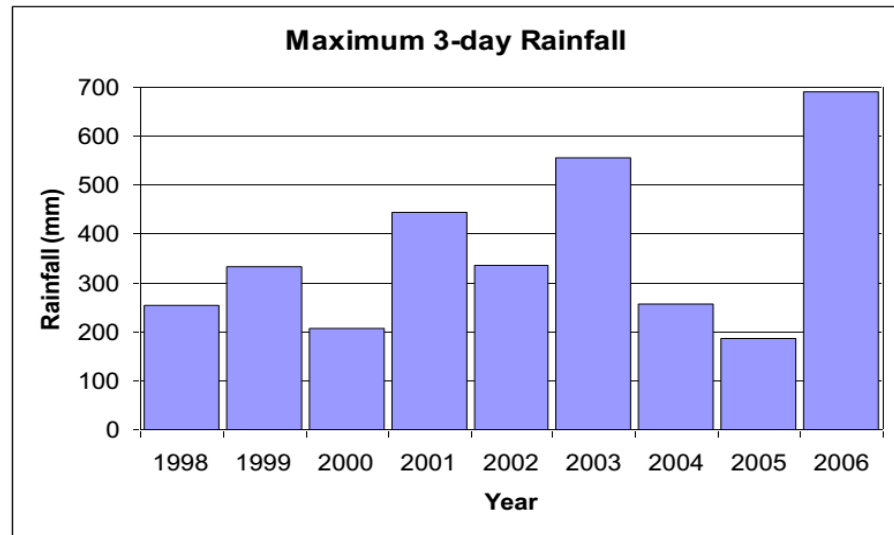
Figure 5.13 Maximum 3-Day Rainfall (Devghat Station)

It was observed that 650 mm of rainfall was accumulated in 36 hours during 2006 disaster before the initiation of debris flow.

Rational Method:

The most widely used uncalibrated equation is the Rational Method. Mathematically, the rational method relates the peak discharge (q, m^3/sec) to the drainage area (A, ha), the rainfall intensity (i, mm/hr), and the runoff coefficient (C).

 SI Units   **q = 0.0028CiA**

Where q = design peak runoff rate in m^3/s

C = the runoff coefficient

i = rainfall intensity in mm/h for the design return period and for a duration equal to the "time of concentration" of the watershed

English Units   **q = CiA**

Where q – ft^3/sec

i = rainfall intensity (in/hr)

A = watershed area in acres

C = runoff coefficient, ratio of the peak runoff rate to the rainfall intensity, dimensionless

Taking, C = 0.5; i=122.44 mm/hr for T$_c$=5.247 minutes (as mentioned in the previous chapter);A=0.119sq.km(i.e.11.9ha),we have,

q = 2.02m^3/s(Peak Discharge available at the outlet)

In this case, for the calibration of DEBRI2D Model, we have calculated that 650mm of rainfall was accumulated in 36 hours before the initiation of debris flows.

Average rainfall intensity before initiation of debris flow = 650mm/36 hr

= 18.05mm/hr

This value of rainfall intensity is available at the upstream end of Kamere Khola Watershed(24+740) before the initiation of debris flows and this debris starts to move downwards.

Assuming based on real scenario that this much amount of water is sufficient to cause debris flow and based on equilibrium volumetric concentration and field observation as well,DEBRIS2D is calibrated for designed volume event scenario considering the first case above(i.e.considering water is sufficient to cause debris flow).

According to Neupane,B. (2011),from the research, the landslide at Kamere Khola (CH 24+740) was 60 m long, 30 m wide and 5 m deep. Furthermore ,he added the X-ray analysis of the soil sample taken from the Kamere Khola landslide showed the presence of chlorite peak at 2theta = 6.3, illite peak at 2theta = 8.8, kaolinite peak at 2theta = 12.4,and again chlorite at 2theta = 18.9.

With this consideration,

Taking volume of dry debris = 60*30*5 = 9000 m^3

Total Volume of Debris Flow = Volume of dry debris/C_v

$$= 9000/(0.603)$$

$$= 14925.373 \text{ m}^3$$

$$\approx 15000 \text{ m}^3$$

Location of Initial Mass Distribution(Datum Everest 1830)

X   - 548210

Y   - 3077507

Volume - 15000 m^3

5.4.5 Output Setup(Analysis Range and Time Interval)

The analysis range of DEBRIS2D Model was calibrated with the following information(Everest 1830)-

The coordinates of up left corner are setup as:

Xmin : 548020

Ymax : 3078108

The coordinates of right bottom corner are setup as:

Xmax : 548520

Ymin : 3077188

The output time interval was setup at 10s.

5.5 Summary of Model Parameters for Inputs to DEBRIS2D Model

S.N.	Parameters	Inputs
1	Topography	Input the 5m×5m DEM file (after interpolation) which is stored in .dat format

2	Simulation Range	Manual Input (Everest 1830) Rectangular input The coordinates of up left corner are setup as: Xmin : 548020 Ymax : 3078108 The coordinates of right bottom corner are setup as: Xmax : 548520 Ymin : 3077188
3	Mass Information	• the type of mass distribution is surface deposition • Total Volume of Debris Flow = Volume of dry debris/C_v $\qquad = 9000/0.603$ $\qquad = 15000 \ m^3$ X - 548210 Y - 3077507 Volume - 15000 m^3
4	Material Parameter	Yield stress set at 700 Pa
5	Output Setup	The output time interval set up at 10 seconds.

6.   RESULTS AND DISCUSSION

6.1 Background

The model results for SINMAP and DEBRIS-2D has been obtained for a variety of parameter ranges, to describe the effectuality of each model, and to identify the most sensitive model parameters. SINMAP and DEBRIS2D results are compared herein to identify the pros and cons inherent to each model.

A number of slope movements are generated by an excessive amount of water, usually due to heavy precipitation or a moderate rainfall lasting several days. Slope movements in soil and weathered rock are usually produced on steep slopes during the most intense part of a storm (Wieczorek, 1996). Intense rainfall results in a higher groundwater table, saturation of the soil, a temporary increase in soil pore-water pressure, and a decrease in internal cohesion between soil particles (Easterbrook, 1999). These factors decrease the frictional resistance along a slope and may induce failure within the material or along an existing plane of weakness. Thin, loose soils on hillslopes with sparse vegetation are particularly prone to failure during an intense rainfall.

Soils with a high rate of hydraulic conductivity (the amount of water that will move through a porous medium in unit time) have the ability to transmit water more quickly downslope. This decreases soil pore pressureand may help to increase shear strength. Typically, an unconsolidated, coarse grained, well- rounded,and well-sorted soil will have a higher value of hydraulic conductivity (Fetter, 1994).

Debris flows may be triggered in a variety of ways. The most common trigger is an abundant amount of moisture, either from intense rainfall or rapid snowmelt, or a combination of heavy precipitation and antecedent soil moisture. Topography also influences debris-flow initiation by concentrating subsurface flow and determining slope. Soil thickness, conductivity, soil strength, bedrock-fracture flow, and root strength also influence the spatial distribution of debris flows and other types of shallow landslides (Montgomery and Dietrich, 1994). During a heavy rain event, piezometric head in the stratum increases while shear strength and cohesion decrease to the point where failure may occur (Neary et al., 1986). A debris flow typically begin as a debris and sediment

laden slurry that gains material as it travels downslope or as a shallow-slope movement that is mobilized into a flow (Ritter et al., 1995).

Since, excessive rainfall is one of the most important triggering factors leading to hazardous landslides and debris flows, it is to be considered most carefully. In this thesis, SINMAP model has been calibrated for normal maximum annual daily rainfall(occurred on 31st July,2003 disaster) and Stability Index maps has been developed for 25 and 50 years return period as well along Narayanghat-Mugling Highway.

Similarly, for DEBRIS2D model accumulation of rainfall leading to initiation of debris flows was considered and max rainfall accumulation was calculated. It was seen that maximum accumulated rainfall before the initiation of debris flow was found during 2006 disaster (8th ,9th and 10th September,2006).

As shown in fig:5.2 of the previous chapter, the rainfall isohyets of 20 mm intervals were prepared for the day of 2003 disaster .Isohyet method is used to illustrate the condition of rainfall in the study area. Isohyet method is a good method which can be used to depict the study area, because topography can be accommodated. Isohyets method is a line in the map which connects places having same amount of rainfall during a certain period. The rainfall isohyets were prepared using daily rainfall of 11 stations in and around the study area. The rainfall isohyets showed 446.2 mm of rainfall was occurred at Devghat and its surrounding areas which caused the disaster on the Narayanghat-Mugling highway. The isohyets could be developed more precisely if there were other rainfall stations along the highway. The isohyets provide ideas on rainfall distribution patterns on the day of disaster. The isohyets show 280 - 446 mm rainfall occurred on the stretch of the highway where landslides and debris flows found most severe (Nippon Koei,2008).

The rainfall variation during the monsoon days of 2003 and 2006 disaster can be shown as-
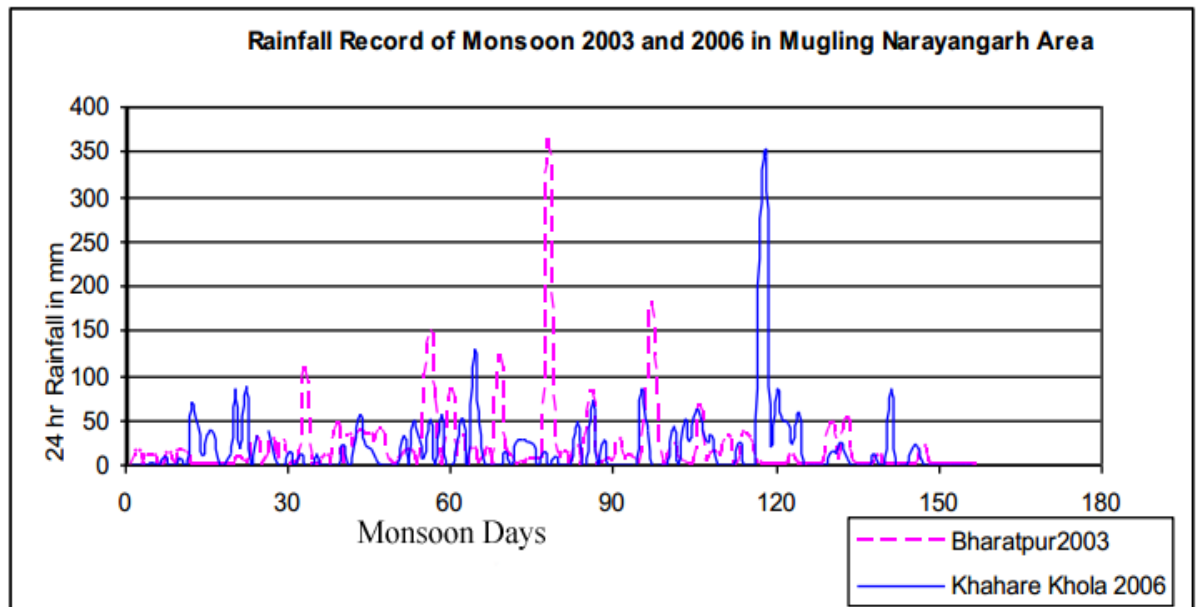
Figure 6.1 Variation of Rainfall during the monsoon of 2003 and 2006 along

Narayanghat-Mugling

The rainfall variation clearly depicts that the peak rainfall during a certain day has led to landslides and debris flow.The intense rainfall is one of the triggering factors for landslides and debris flows along Naraanghat-Mugling Highway.

6.2 Results: SINMAP Model

SINMAP was calibrated by comparing simulation results against inventoried landslide initiation points. Parameter uncertainty was simplified with the use of uniform probability distributions with upper and lower boundaries of parameters and the following results were obtained-

Available online at http://www.ijart.info/
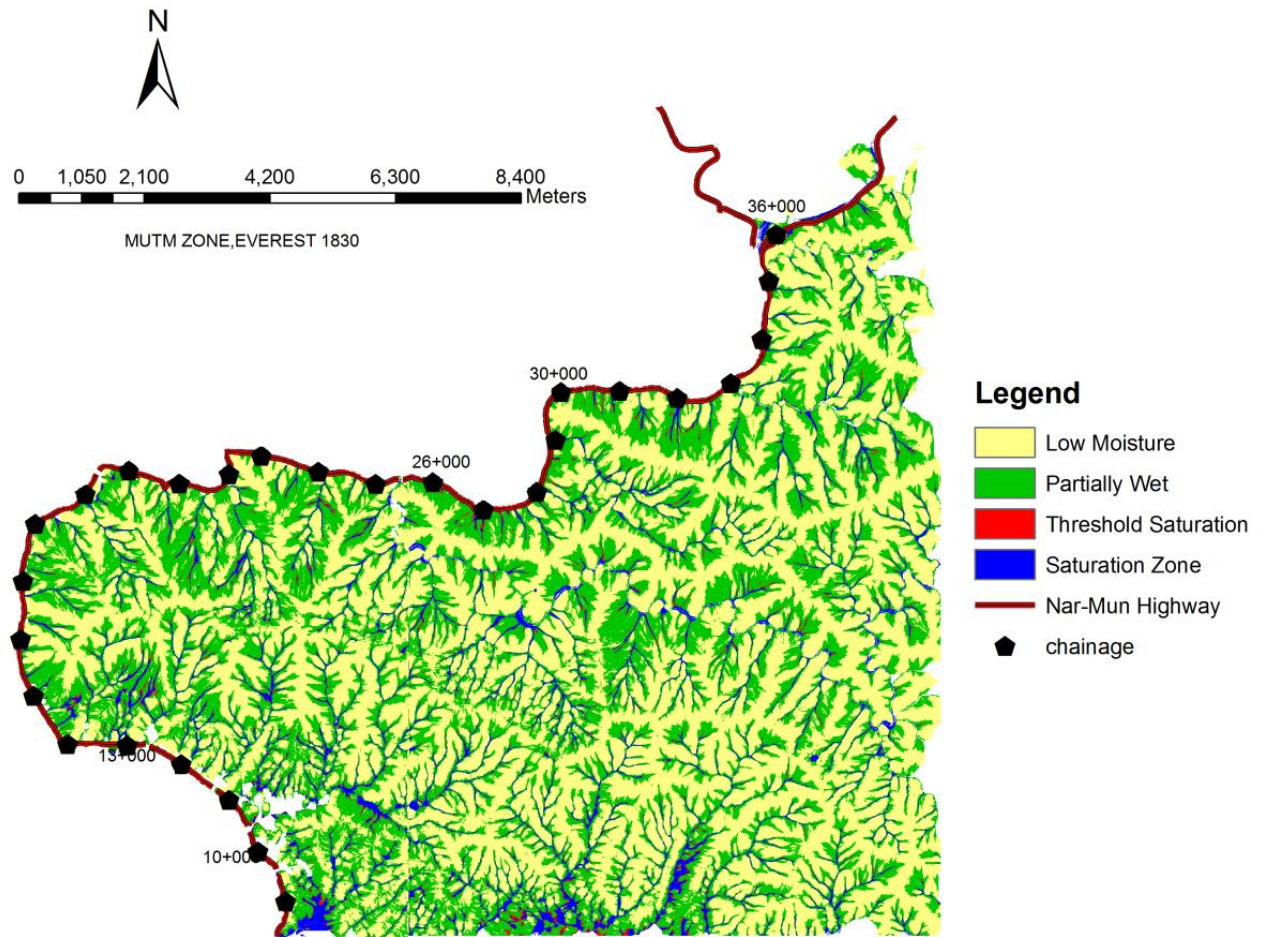
Figure 6.2 Saturation index map(Wetness Map) derived by SINMAP analysis along

Narayanghat-Mugling Highway

Available online at http://www.ijart.info/
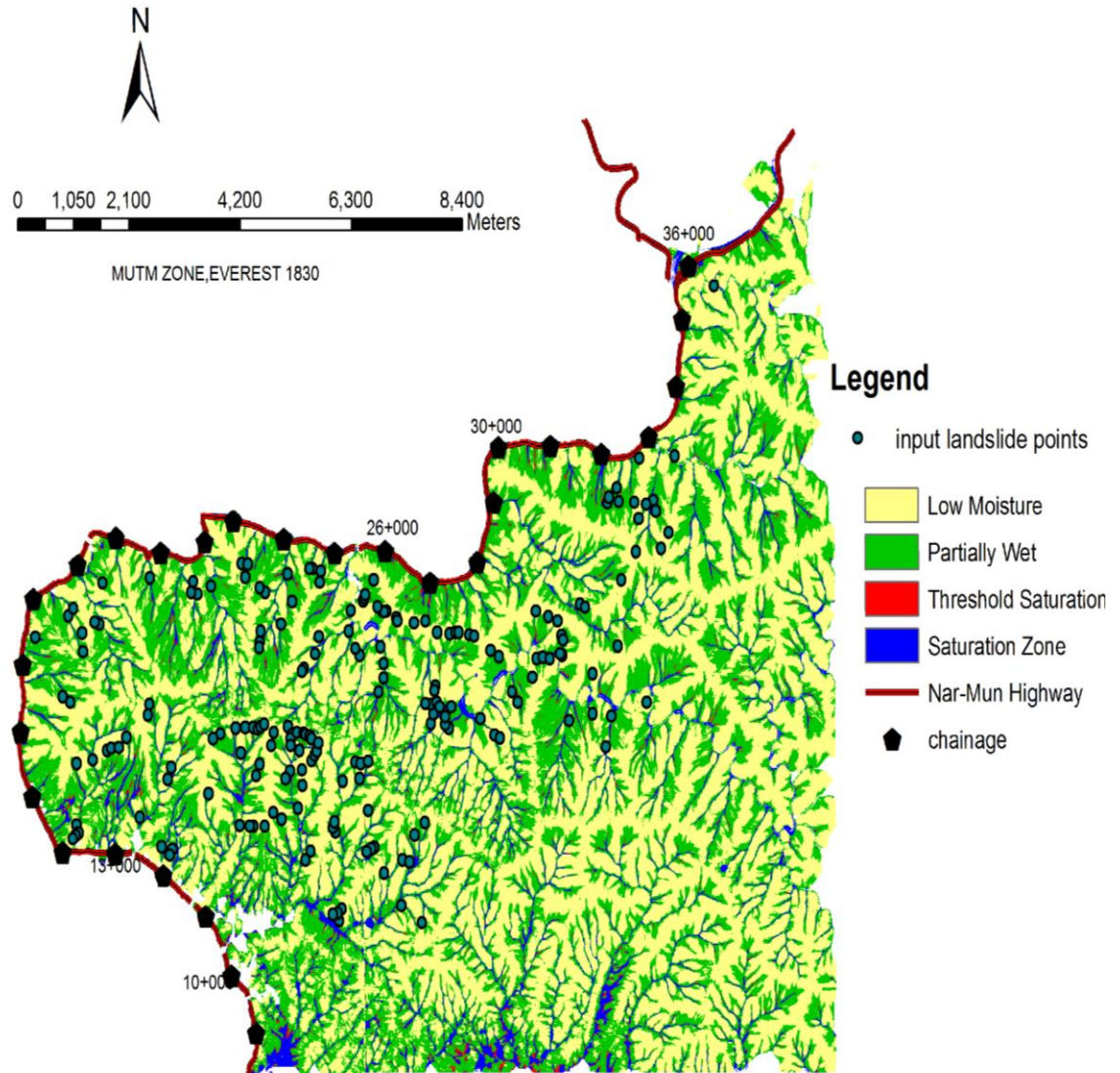
Figure 6.3 Overlaying input landslide initiation points in saturation index map derived
from SINMAP analysis

Available online at http://www.ijart.info/
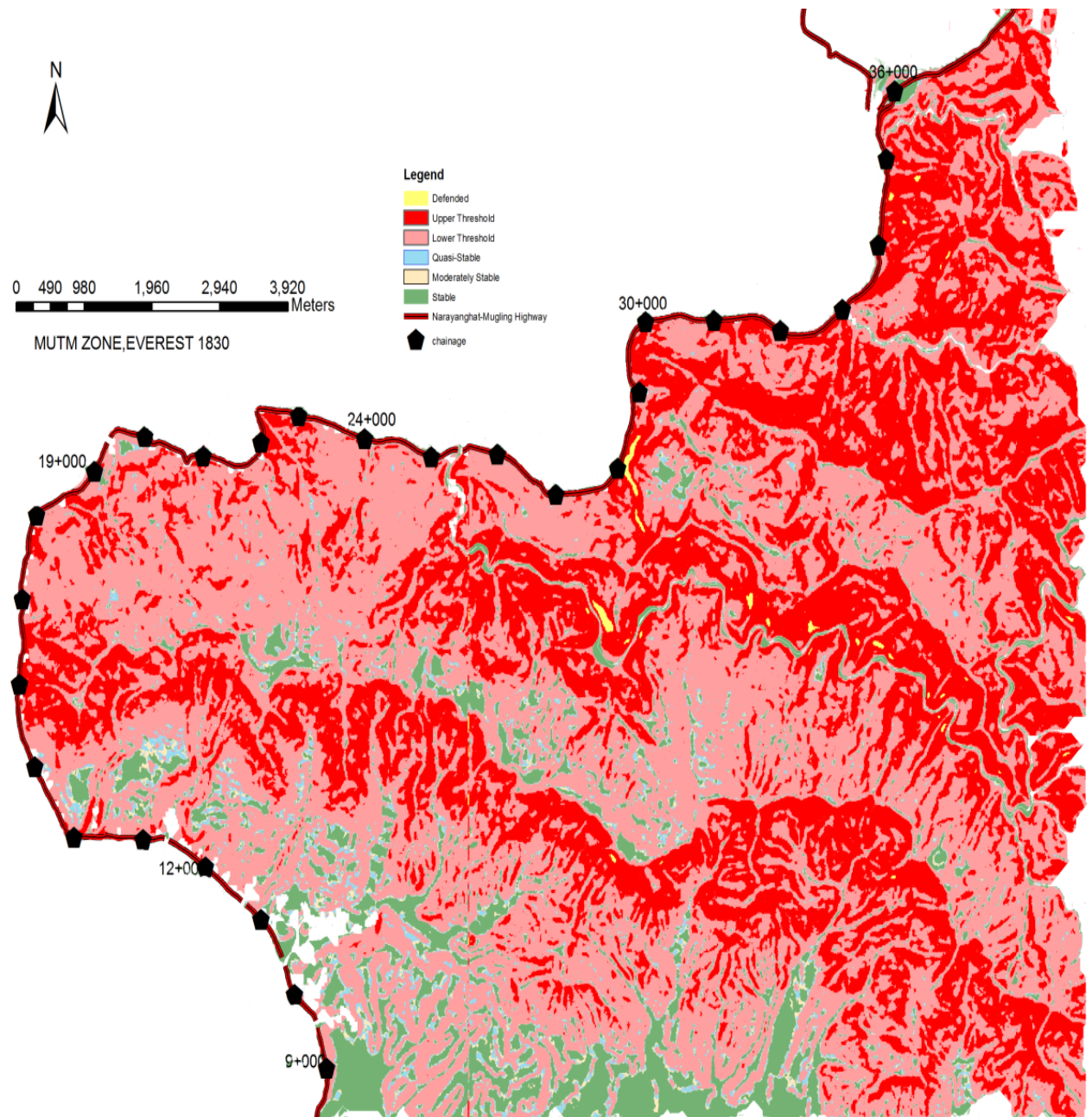
Figure 6.4 Slope Stability Index Distribution Map along Narayanghat Mugling Highway
derived by SINMAP analysis

Available online at http://www.ijart.info/
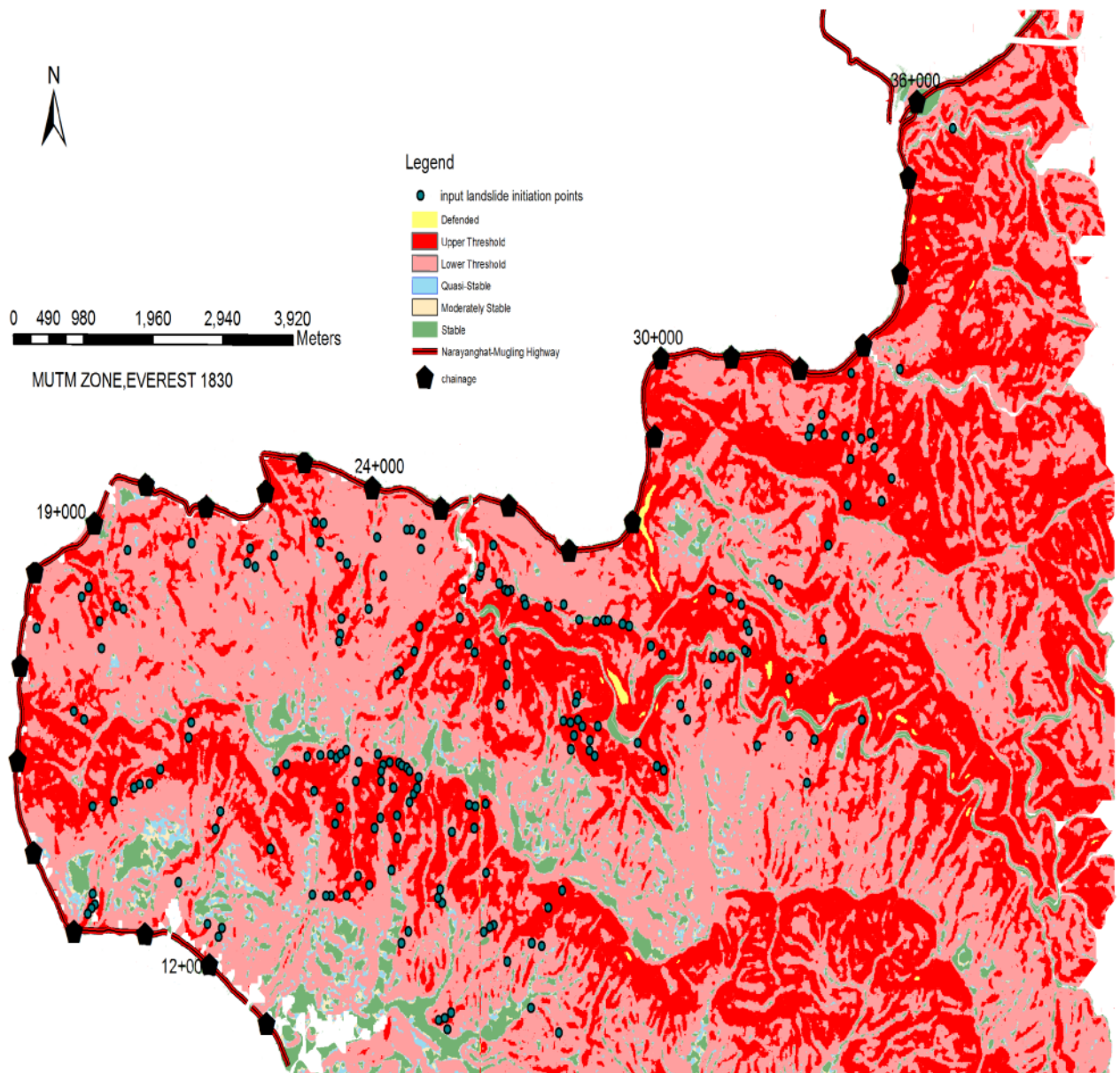
Figure 6.5 Overlaying input landslide initiation points in Slope-Stability Index

distribution map derived from SINMAP analysis

Figure 6.6 Plot showing the relationship between catchment area and the ground-surface slope calculated at grid cell points and inventoried landslides along N-M Highway

Stability index region lines (vertical lines) define boundaries for regions within slope-specific catchment area space that have similar potential for stability or instability.Saturation region lines (near-horizontal curved lines) provide boundaries for regions within slope-specific area space that have similar wetness potential.

Table 6.1 Summary of the analytical data (Statistics) resulted from SINMAP analysis along Narayanghat Mugling Highway

Stability Class	Stable	Moderately Stable	Quasi-stable	Lower Threshold	Upper Threshold	Defended	Total
Region 1							
Area(km^2)	10.45	2.315	3.975	63.876	43.891	0.121	124.631
Percent of region	8.388	1.858	3.189	51.252	35.216	0.097	100
Number of landslides	3	0	2	100	90	2	195
Percent of slides	1.523	0	1.015	50.761	45.685	1.015	100
Density(number/km^2)	0.287	0	0.504	1.566	2.051	16.529	1.564
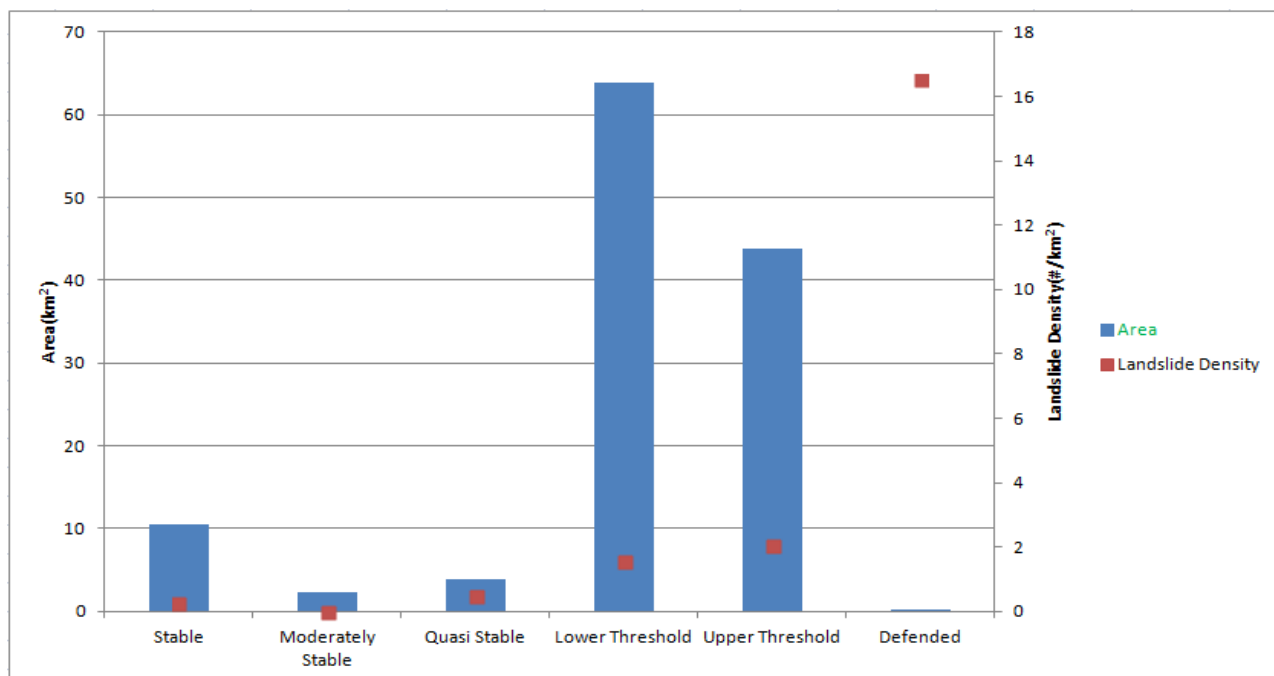
Figure 6.7 Summary of the SINMAP Model(Prediction accuracy of SINMAP)(square= landslide density, bars= area of the stability class)
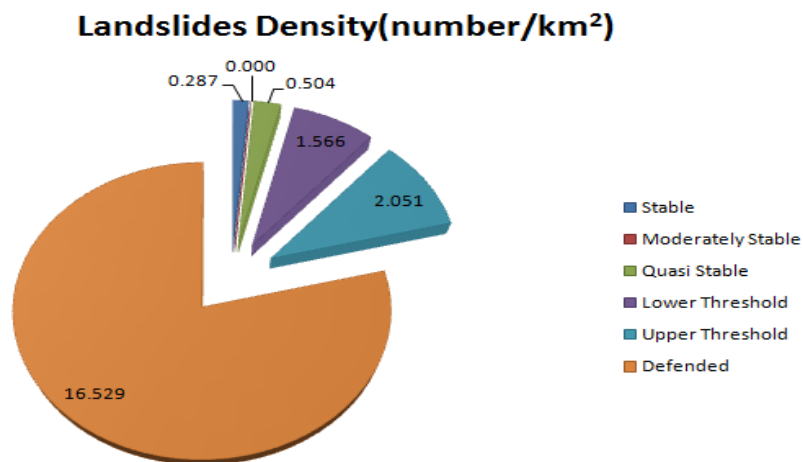
Figure 6.8 Pie chart demonstrating the landslide density in different classes of slope stability resulted from SINMAP analysis along Narayanghat-Mugling Highway
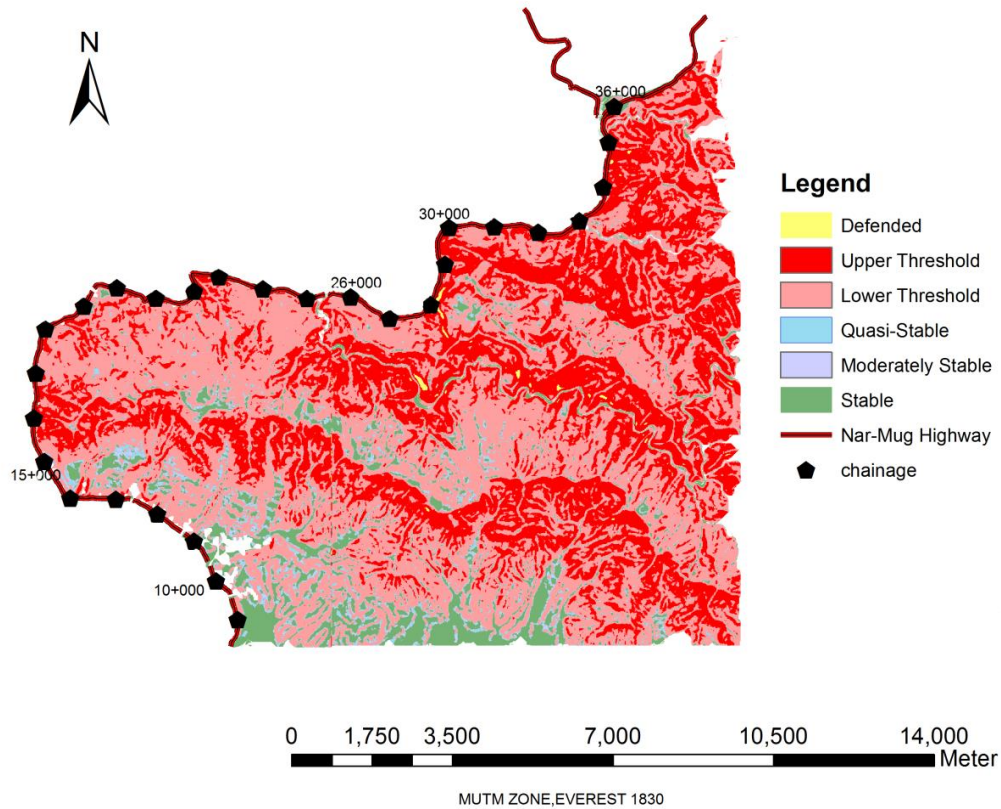
Figure 6.9 Slope-Stablity Index Distribution map along Narayanghat-Mugling Highway
derived from SINMAP analysis for 25 years return period
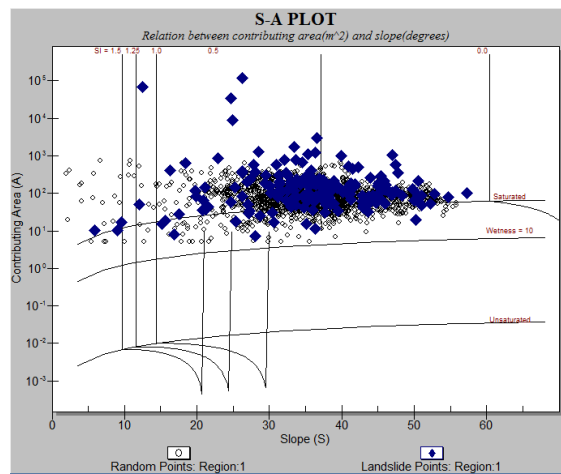
Figure 6.10 Slope Area Plot showing the relationship between catchment area and the
ground-surface slope calculated at grid cell points and inventoried landslides along N-M
Highway for 25 years return period
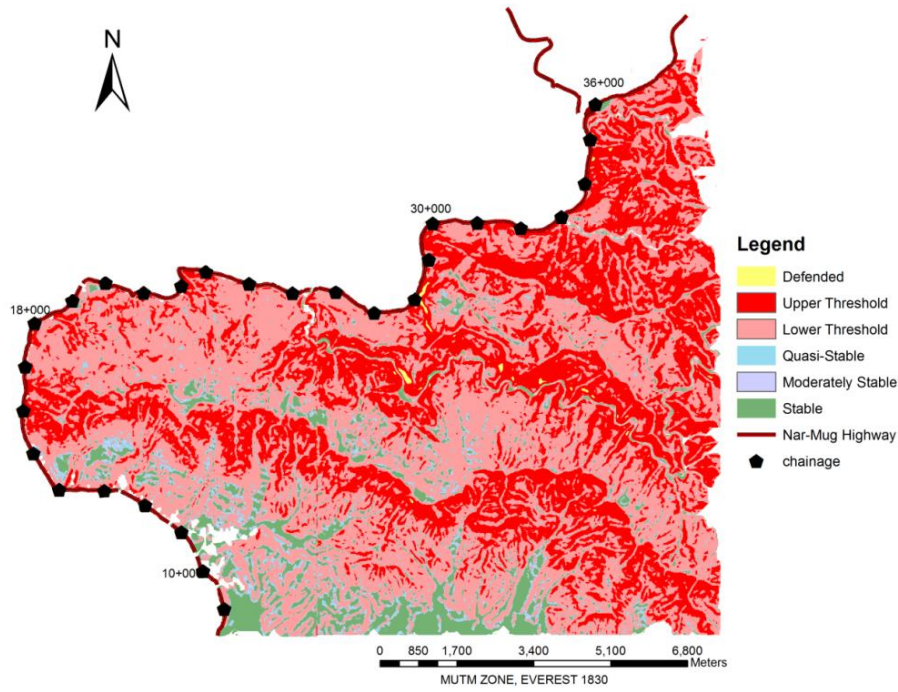
Figure 6.11 Slope-Stablity Index Distribution map along N-M Highway derived from
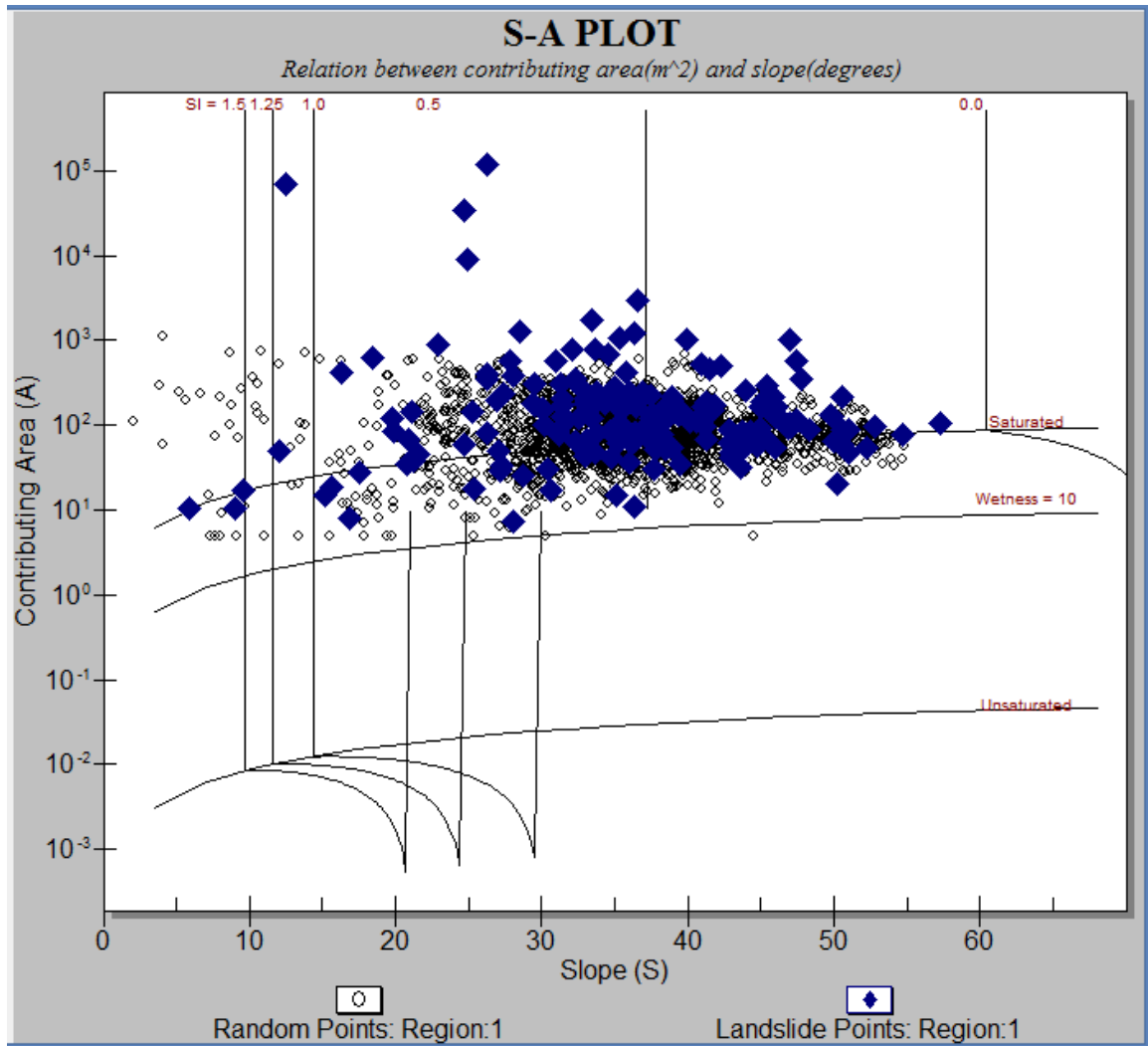
SINMAP analysis for 50 years return period
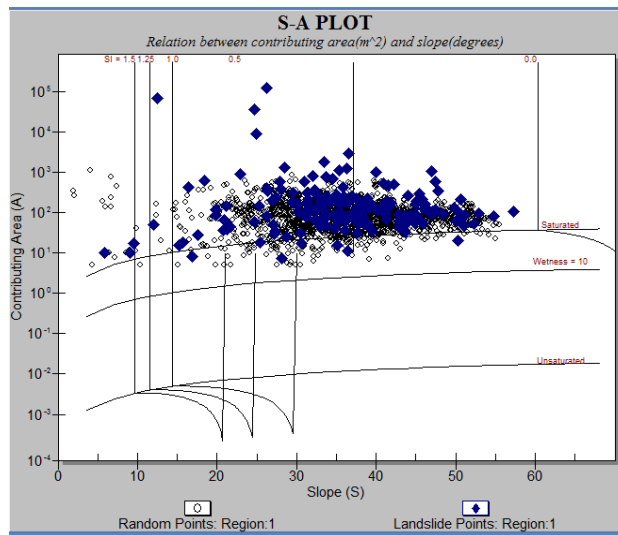
Figure 6.12 Slope Area Plot showing the relationship between catchment area and the ground-surface slope calculated at grid cell points and inventoried landslides along N-M Highway for 50 years return period

6.3 Discussion And Interpretation: SINMAP Model

The discussion and interpretation can be done as per the output themes obtained as results from SINMAP analysis.

OUTPUT THEMES

Saturation theme:

SINMAP model uses the following equation to calculate the relative wetness (w) (Pack et al.1998):

$$w = Min\left(\frac{Ra}{T\sin\theta},1\right)$$

Where: R: is the recharge ;a: specific catchement area T: is soil transmissivity;The values of R and T are used to assign values to each grid cell in the saturation theme.

Fig: 6.2 shows the wetness map derived from SINMAP analysis. It is divided into four zones via saturation zone, threshold saturation, partially wet and low moisture. Fig: 6.3 illustrates the spatial patterns of wetness on the map and input landslide points located within it. It can be clearly seen that many of the input landslide initiation points are falling within saturation zone and partially wet zone.

Stability Index Theme:

Stability index values are 0.0 or greater, with values greater than 1.0 indicating some level of stability. The Stability Index theme is grouped into six classifications. Each grid cell contains the actual calculated SI value, which may be determined by clicking on the cell with the Identify tool.

Fig: 6.4 shows the stability index grid theme classified into six different zones.

Among the six classes, Stable, moderately stable, and quasi-stable are used to classify regions that should not fail with the most conservative values of the specified parameter

ranges. SI for these cases is the factor of safety that gives a measure of the magnitude of destabilizing factors (e.g. increased wetness due to road drainage, local loading, or local enhancement of pore pressures due to soil pipe effects) required for instability. Lower threshold and Upper threshold are used to characterize regions where, according to the parameter uncertainty ranges quantified by the model, the probability of instability is less than or greater than 50% respectively. Instability may arise simply due to a combination of parameter values within the bounds with which uncertainty and variability can be quantified. The defended-slope classification is used to characterize regions where the slope should be unstable for any values within parameter ranges, i.e., the probability of failure with the specified range of parameters is the greatest. Where such slopes occur in the field they are held in place by forces not represented in the model, or the model is inappropriate, as in the case of bedrock outcrops.

Slope-Area Plot Chart (SA):

The SA Plot provides a view of study data in slope -area space-not in geographic space. The data in the plot are derived from a feature table, which points to a dbase file created by SINMAP (Pack et. al, 1998). The file is created by extracting data from the slope theme, contributing area theme, and the landslides theme.

Fig: 6.6 shows the SA-plot for the calibrated parameters using SINMAP analysis along Narayanghat-Mugling Highway.

The slope area (SA) plot shows the relationship between contributing areas and groundslope (Tarboton 1997). The geometric points (little squares) represent landslide locations. The single points represent a random selection of points within the calibration region. The slope and contributing areas are generated from the DEM. The vertically oriented curves are the breaks between stability index areas.

• Points to the left of the SI line of 1.5 are in the stable region.

• Points between 1.5 and 1.25 SI lines fall into the moderately stable region.

• Points between the 1.25 line and the 1.0 line fall in the quasi-stable region.

• Points between the 1.0 and the 0.5 line fall into the lower threshold region.

• Points between the 0.5 and the 0.0 line fall into the upper threshold region.

• Points to the right of the 0.0 line fall into the defended region.

The location of the 1.0 SI line is controlled by the lower bounds of the C and φ parameters. The location of the 0.0 SI line is controlled by the upper bounds of the C and φ parameters. The area between the 0.0 SI line and the 1.0 SI line represents the uncertainty associated with the parameters.

The horizontally oriented lines represent the wetness that is controlled by the T/R calibration parameter. All points above the upper line are saturated.The position of the upper line is controlled by the upper bounds of the T/R ratio. The position of the middle line is controlled by the lower bounds of the T/R ratio. Points between the upper and middle lines fall into the possible saturated area that represents the uncertainty associated with the T/R ratio. Points that fall below the middle line are unsaturated. The bottom line represents 10 percent wetness.

Calibrating the input parameters to the landslide points involves shifting the lines of the SA plot to fit the landslide occurrence by changing the upper and lower boundaries of the input parameters. A stability index of 1.0 may be thought of as a factor of safety. Very few landslides should occur to the left of the 1.0 line since the factor of safety is >1.0 and the same occurred in this case as well. These landslides can be identified on the stability index map from the SA plot using the (REX) tool in the SINMAP program. The REX tool is a Golden Retriever icon on the tool bar that enables the user to click on a landslide on the SA plot and find the same landslide point spatially on the stability index map.

Statistical Summary:

The statistical summary is the analytical description of the results obtained from SINMAP Model.

 The statistical summary of the results of the analysis shown in Table 2 indicates that the'defended' stability index includes 2 landslides or 1.015% of the total landslide inventory. At the same time, this class includes 0.121km^2 or 0.097% of the study area. This class has an average landslide density of 16.529 landslides per square kilometer. The

'upper threshold' class has an average landslide density of 2.051 landslides per square kilometer and includes a total of 90 landslides. This class includes 35.216% of total study area and 45.685% of total landslide inventory. The 'lower threshold' class includes 100 landslides with 50.761% of the total landslide inventory and has an average landslide density of 1.566 landslides per square kilometer. The remaining stability index classes represent 16.74km^2 or 13.427% of the total area. These classes include 5 landslides and 2.538% of total landslide inventory.

These data depicts that Narayanghat-Mugling Highway is a highly vulnerable corridor for landslides.

Fig: 6.7 shows the summary of SINMAP Model in bars .This can also be used as a basis for SINMAP prediction accuracy which shows a good model performance in this case. Fig: 6.8 illustrates the landslide density in pie chart which again shows a good performance of the model and as well as clearly defines the susceptibility of this area as the lower threshold, upper threshold and defended area covers a large area with high landslide density.

Fig:6.9 shows the slope-stability index distribution map for 25 years return period and fig: 6.10 shows the SA-plot for 25 years return period. Fig:6.10 shows the slope-stability index distribution map for 50 years return period and fig: 6.10 shows the SA-plot for 50 years return period. The data depicts that with greater return period the percentage of defended area i.e. hazardness is increased.

6.4 Results: DEBRIS2D Model

DEBRIS2D model can simulate debris flow in 2 directional mode. The flow depth, velocity and affected area of debris flow has been found out from this model across Kamere Khola Watershed(24+740) along Narayanghat-Mugling Highway.

The following variables has been obtained:

–depth-averaged x, y-direction velocities

–flow depth and affected area

–impact force from debris flow on solid boundary

The results obtained would be very much useful for real engineering detailed designs and for many other purposes. The proper mitigating measures could also be applied proportionately.

6.4.1 Diagrammatic Representation of Debris Path During Initial Distribution , Highway Coverage And Final Deposition

The path followed by debris flow (depth and velocity) during the initial mass distribution, during the coverage of section of Narayanghat- Mugling Highway and during the final deposition has been illustrated in detail in the following diagrams. It is anticipated to be useful in the proper design of mitigating structures and also in proper land resources management not only for engineers but for planners as well.
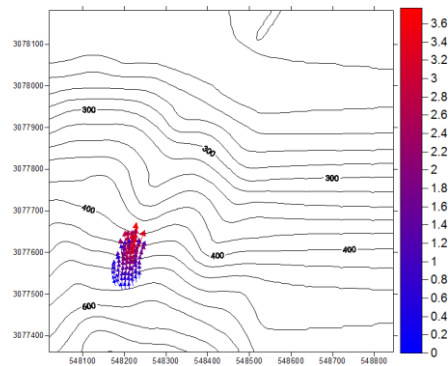
Figure 6.13 Debris flow depth contour map during initial mass distribution at 10 seconds
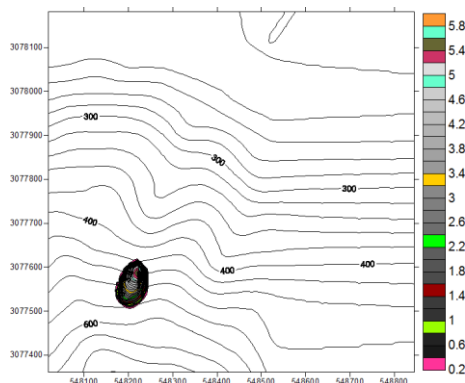
Figure 6.14 Debris flow velocity vector map during initial mass distribution at 10 seconds
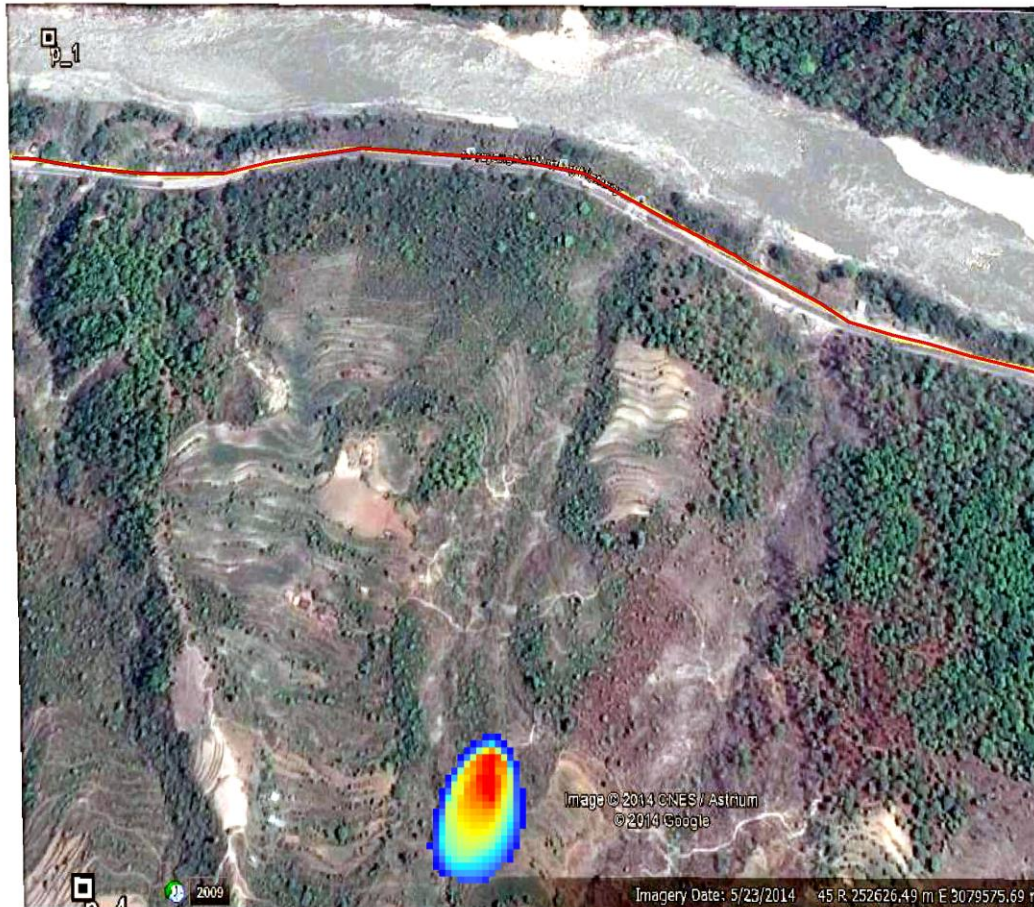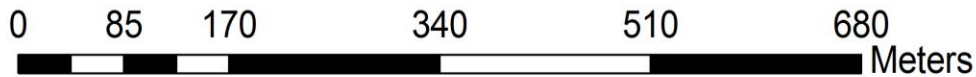
Figure 6.15 Debris flow depth path overlaid on google earth image (imagery date 5-23-2014) during initial mass distribution at about 10s

     Available online at http://www.ijart.info/
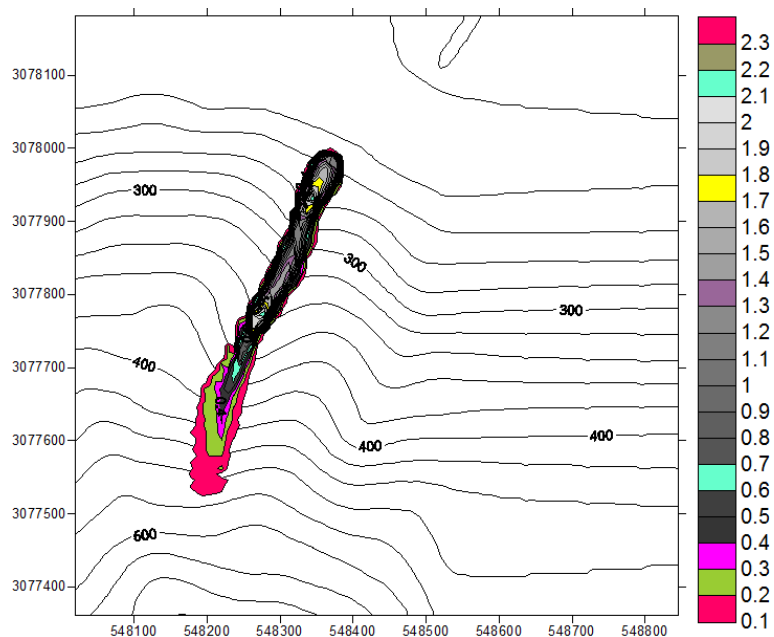
Figure 6.16 Debris flow depth contour map just covering N-M Highway at about 7.6
minutes
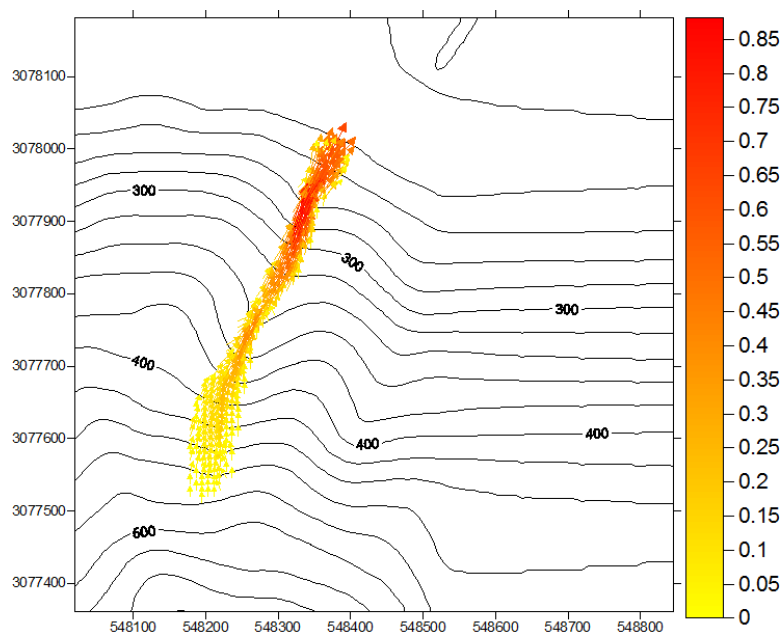
Figure 6.17 Debris flow velocity vector map just covering N-M Highway at about 7.6
minutes
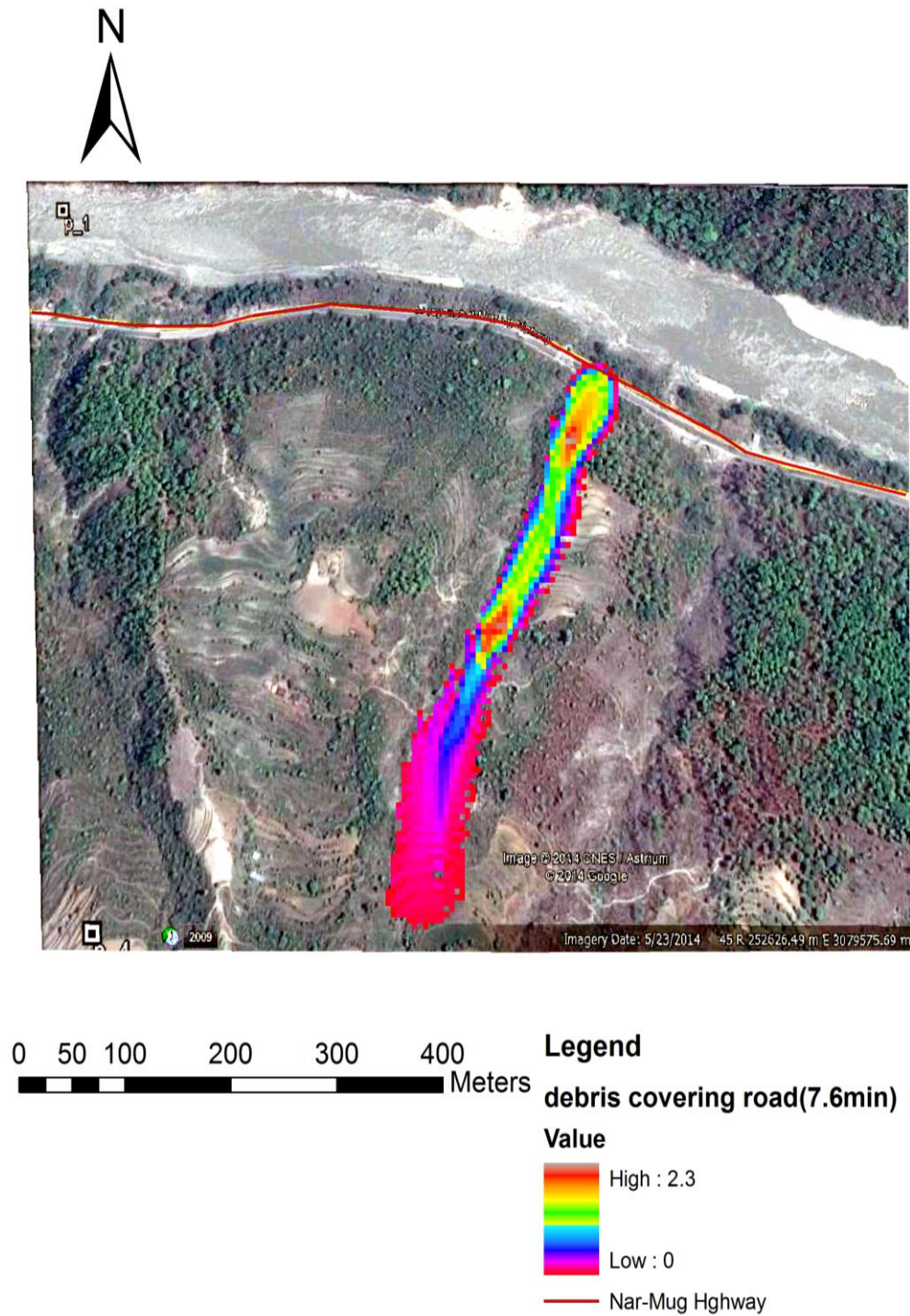
Figure 6.18 Debris flow depth path just covering the N-M Highway at about 7.6 min overlaid on google earth image(imagery date 5-23-2014)
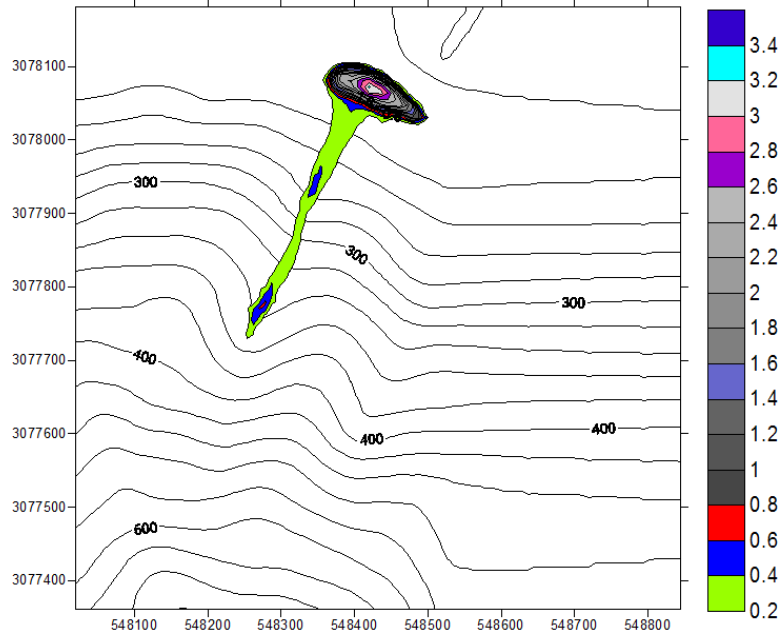
Figure 6.19 Debris flow depth contour map during final deposition at about 1 hour
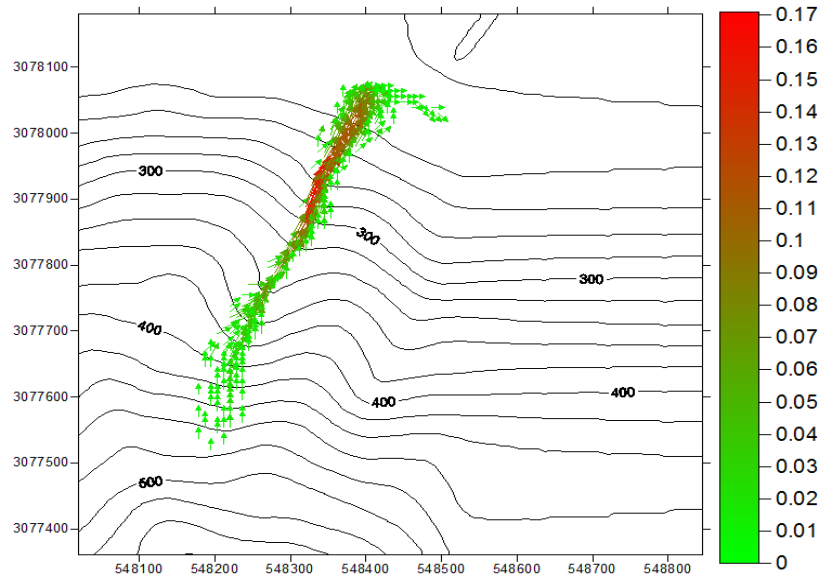
Figure 6.20 Debris flow velocity vector map during final deposition at about 1 hour

Available online at http://www.ijart.info/
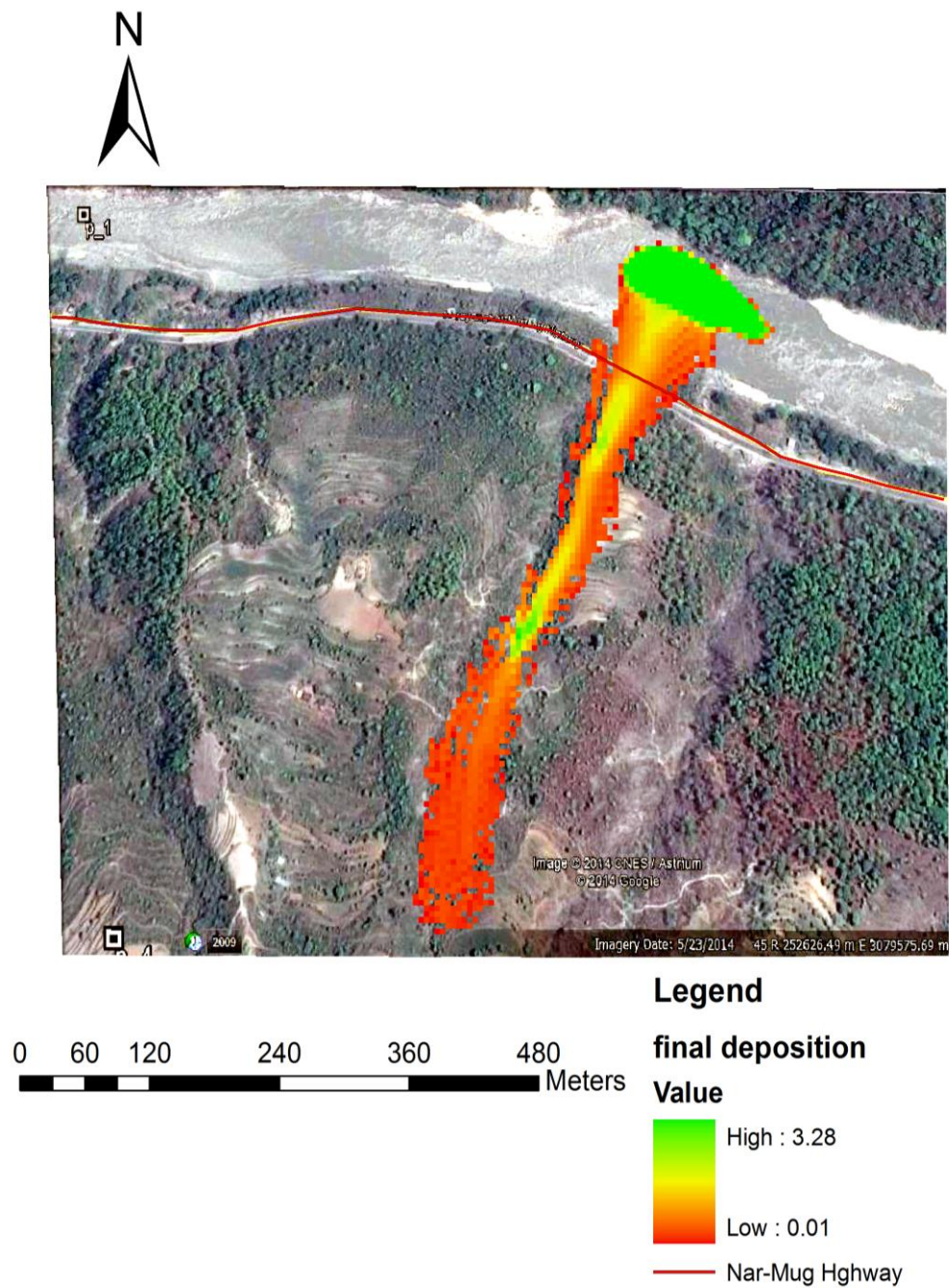
Figure 6.21 Debris flow depth path during final deposition at about 1hour overlaid on google earth image(imagery date 5-23-2014)

6.4.2 Diagrammatic Representation of Temporal Variation Of Debris Flow
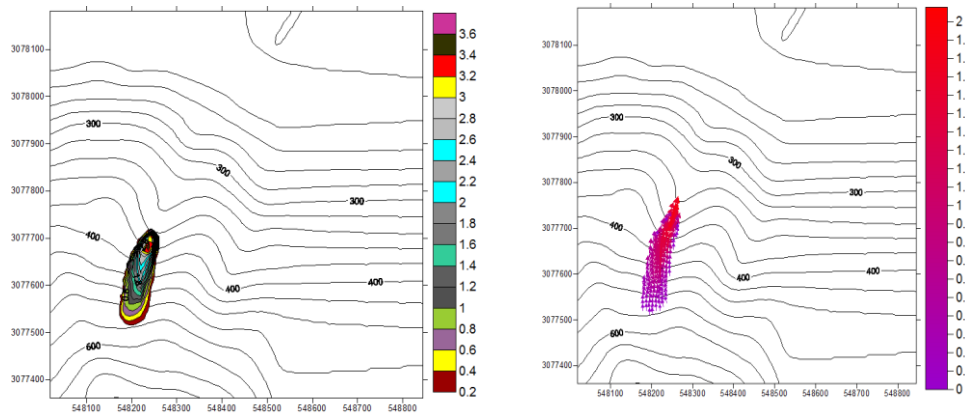
Figure 6.22 Debris flow depth contour map and velocity vector map at about 1 min
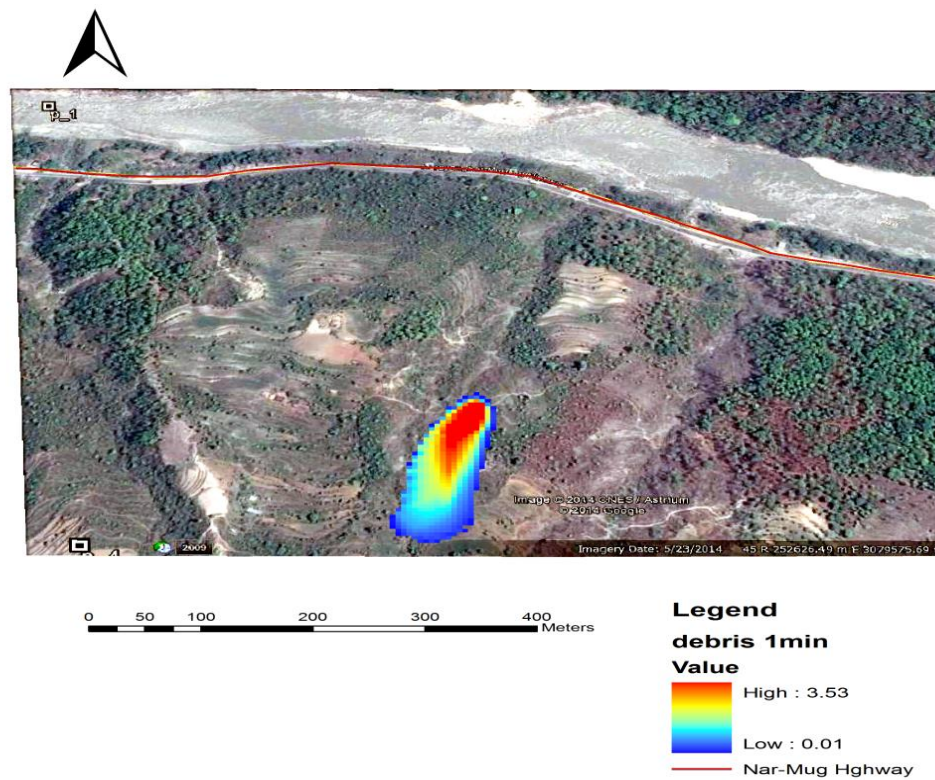
Figure 6.23 Debris flow depth path at about 1min overlaid on google earth

image(imagery date 5-23-2014)
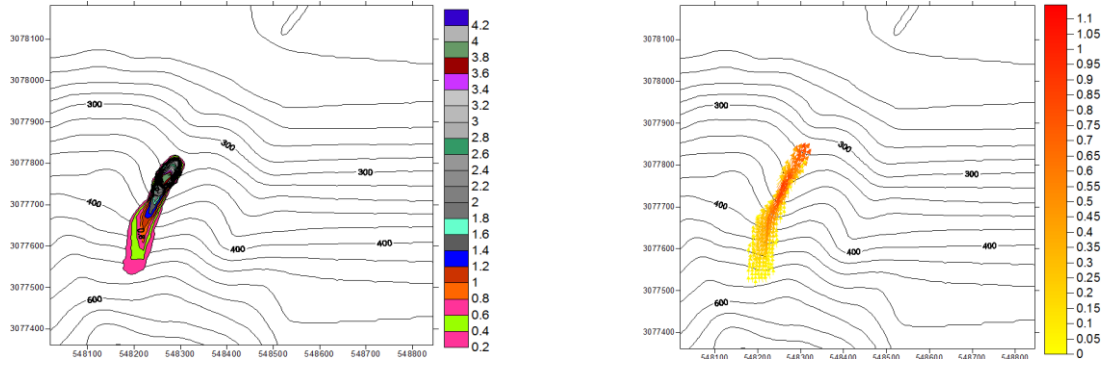
Figure 6.24 Debris flow depth contour map and velocity vector map at about 3 min
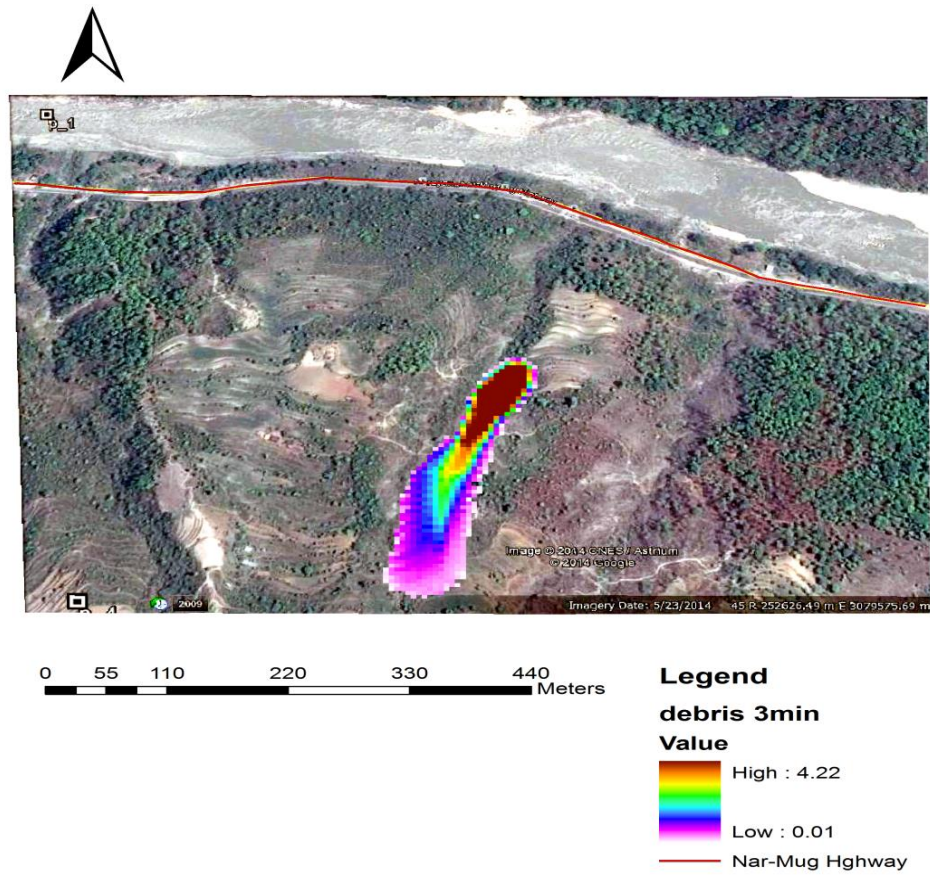
Figure 6.25 Debris flow depth path at about 3min overlaid on google earth

image(imagery date 5-23-2014)

Available online at http://www.ijart.info/
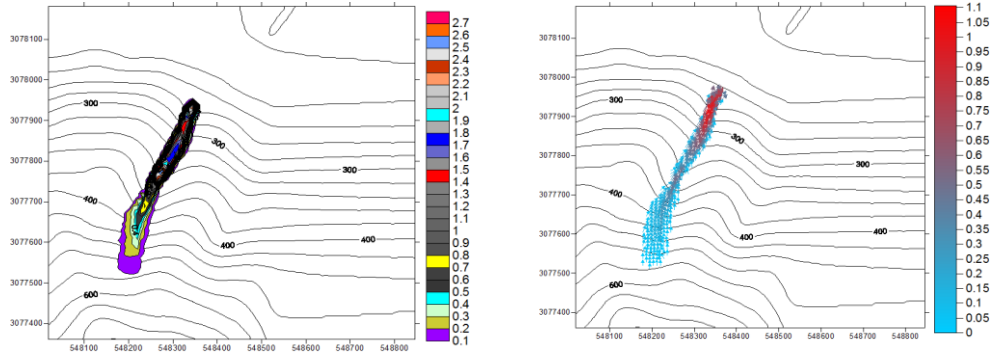
Figure 6.26 Debris flow depth contour map and velocity vector map at about 6 min
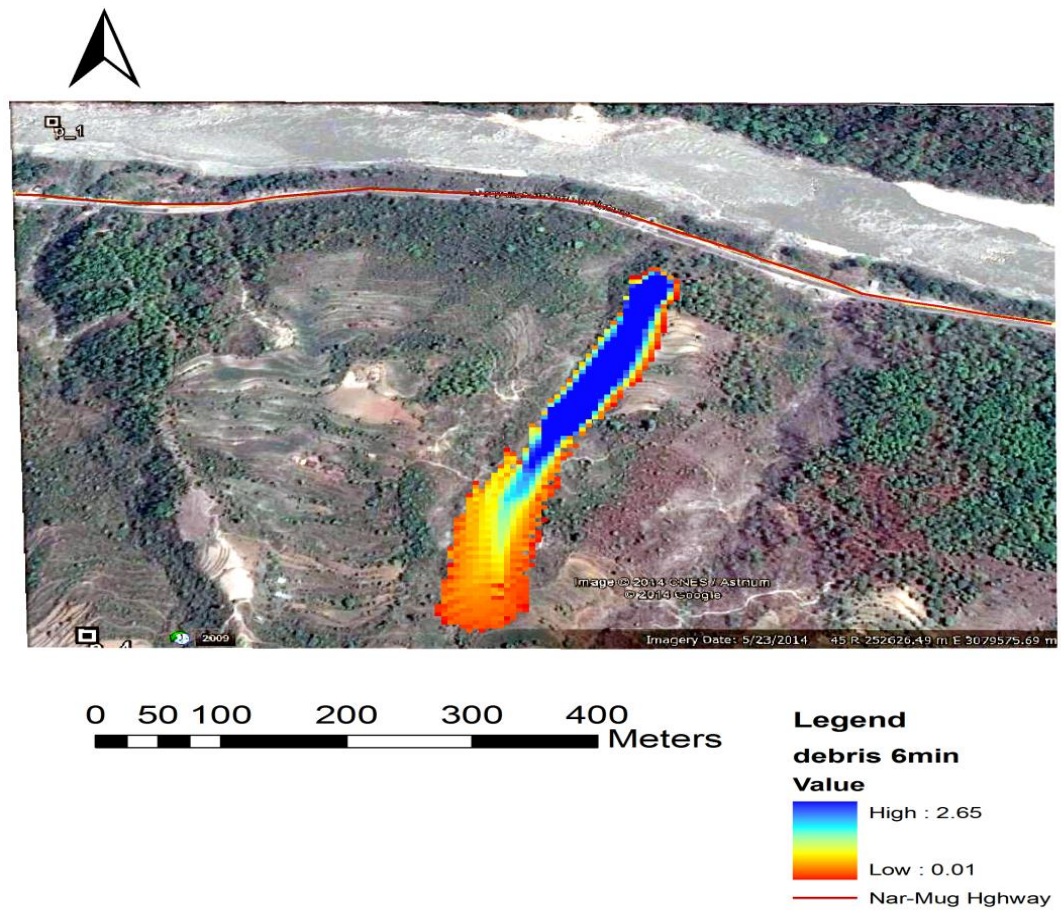
Figure 6.27 Debris flow depth path at about 6min overlaid on google earth

image(imagery date 5-23-2014)

Available online at http://www.ijart.info/
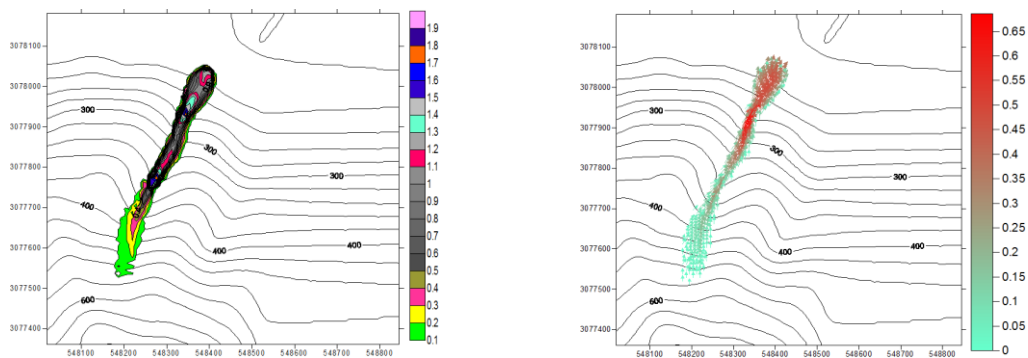
Figure 6.28 Debris flow depth contour map and velocity vector map at about 10 min
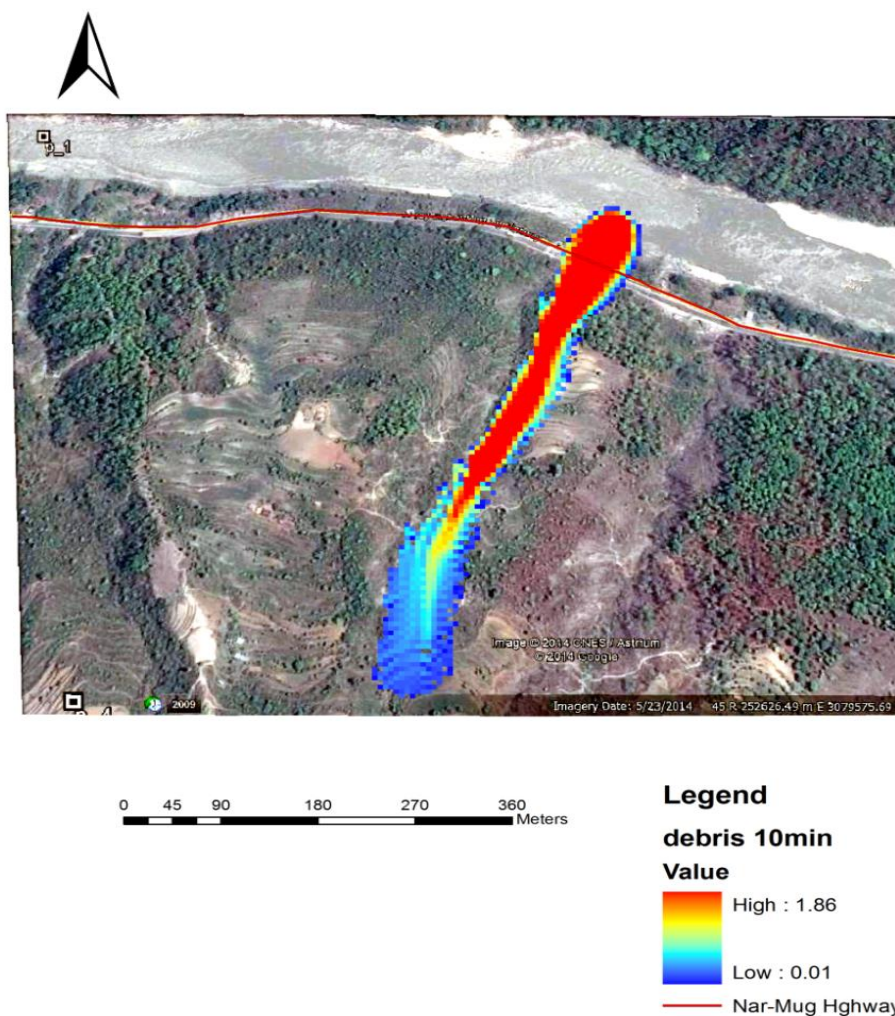
Figure 6.29 Debris flow depth path at about 10min overlaid on google earth image

(imagery date 5-23-2014)
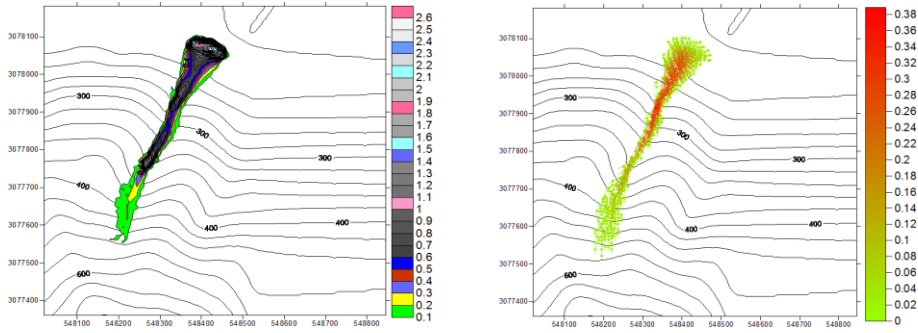
Figure 6.30 Debris flow depth contour map and velocity vector map at about 20 min
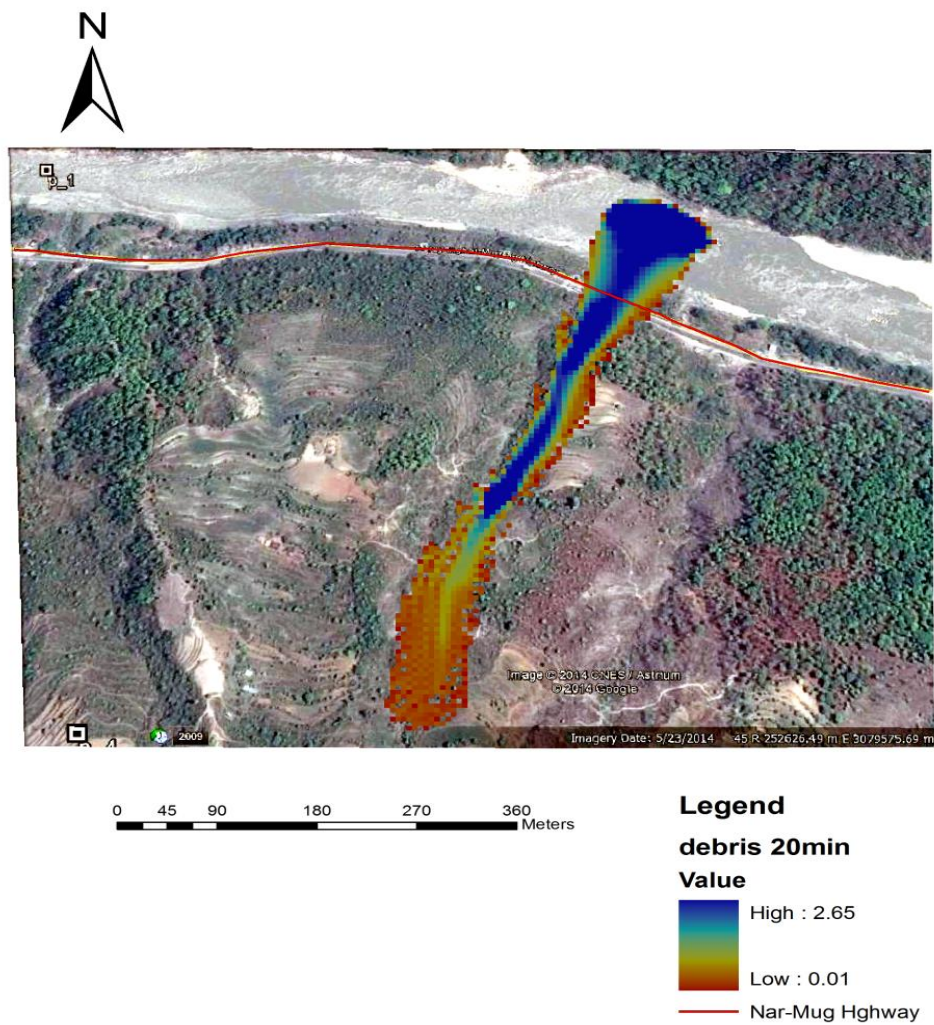
Figure 6.31 Debris flow depth path at about 20min overlaid on google earth

image(imagery date 5-23-2014)
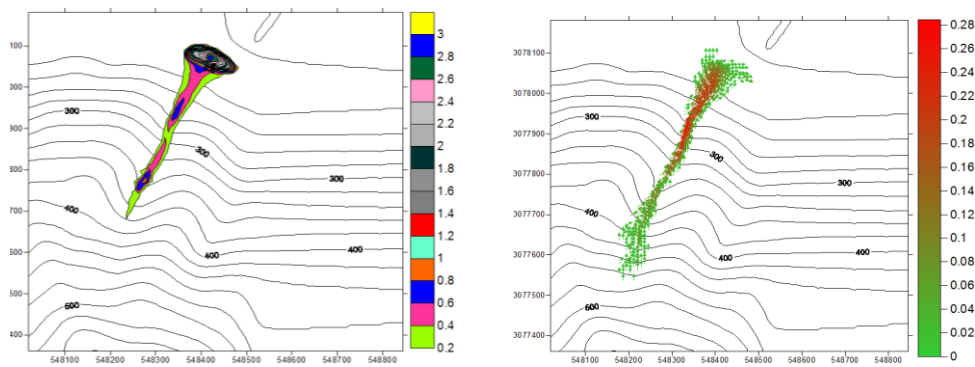
Figure 6.32 Debris flow depth contour map and velocity vector map at about 30 min
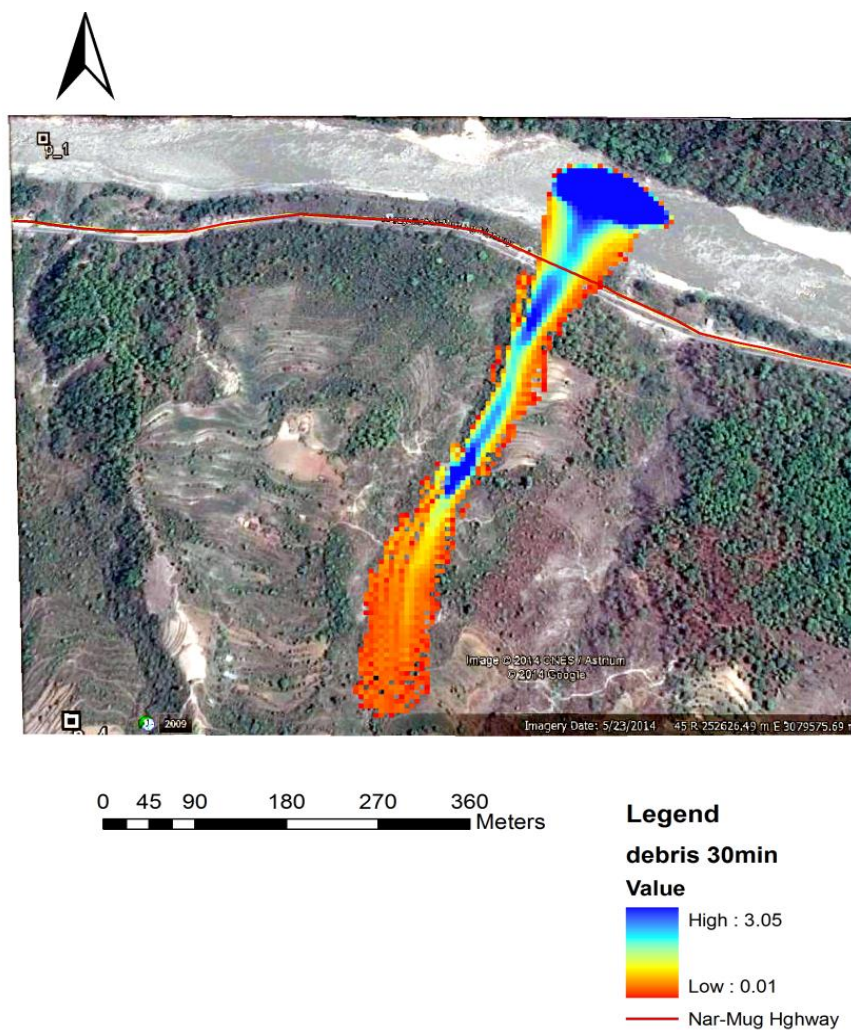
Figure 6.33 Debris flow depth path at about 30min overlaid on google earth

image(imagery date 5-23-2014)

Available online at http://www.ijart.info/
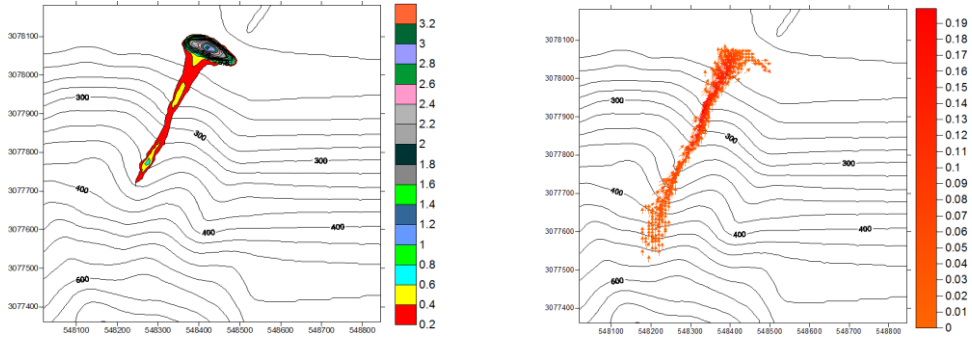
Figure 6.34 Debris flow depth contour map and velocity vector map at about 45 min
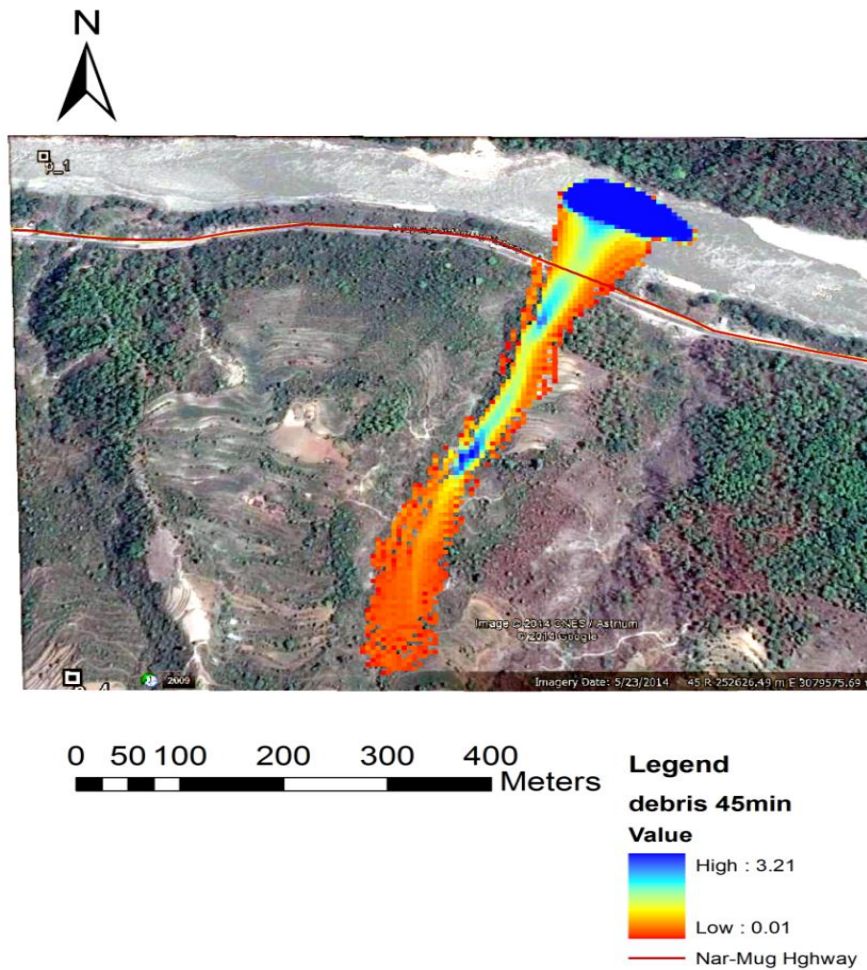
Figure 6.35 Debris flow depth path at about 45min overlaid on google earth

image(imagery date 5-23-2014)

Available online at http://www.ijart.info/

6.4.3 Graphical Representation of Maximum Velocity And Maximum Depth With Time
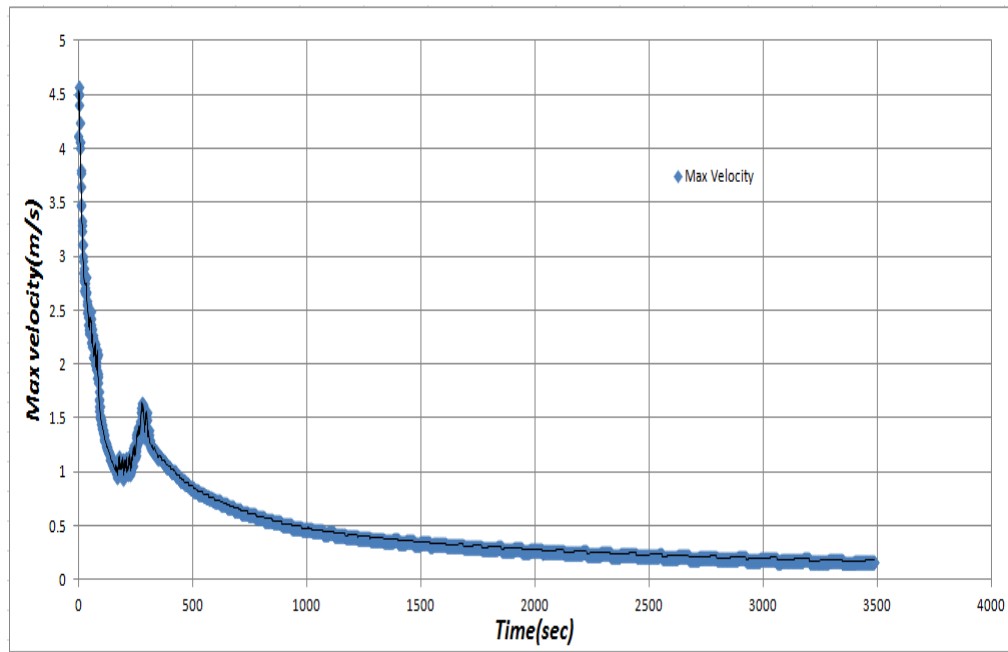
Figure 6.36 Graphical Representation of maximum velocity with time
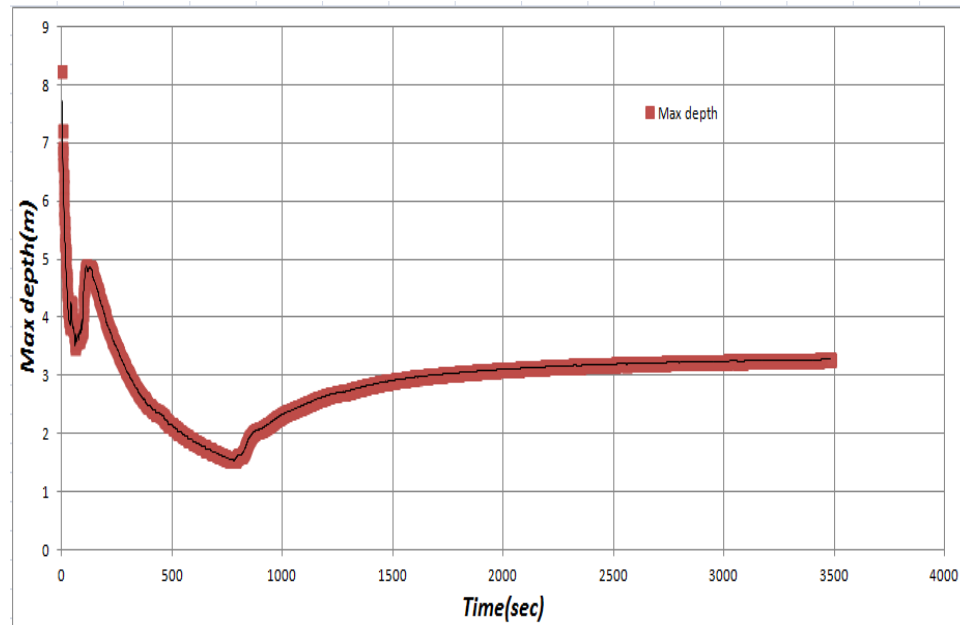
Figure 6.37 Graphical Representation of maximum depth with time
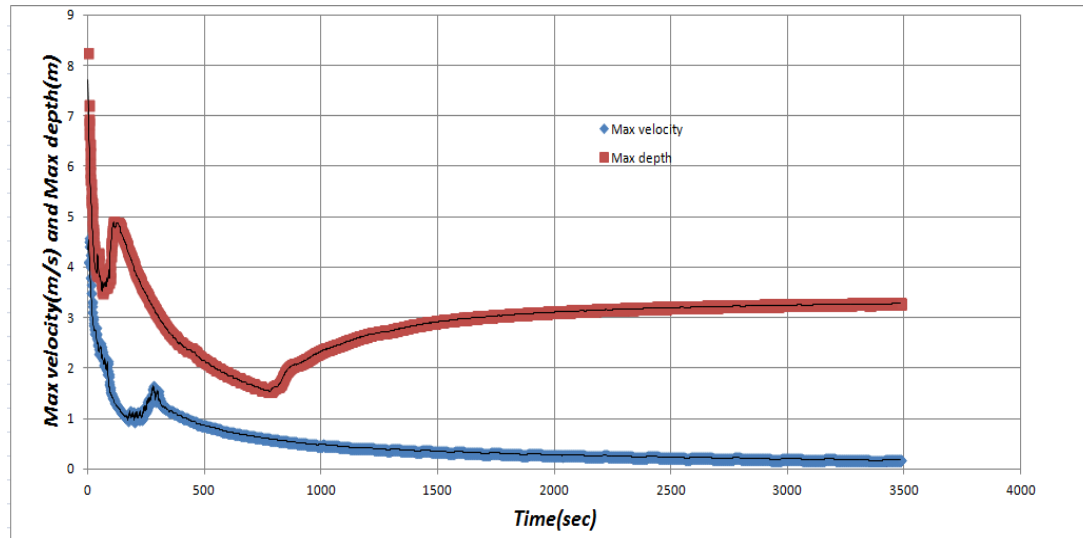
Figure 6.38 Graphical Representation of maximum depth and maximum velocity with time

6.5 Discussion and Interpretation : DEBRIS2D Model

From the debris flow simulation as shown in the figures above (Fig: 6.13 to Fig: 6.35) ,the total process of the transport of debris flow is about 1 hour. The distance is about 640.226 m from the landslide trigger site to the deposition site in the downstream. The maximum velocity nearby the trigger site is about 4.1 m/s. Illustration of debris flow simulation during initial mass distribution (at about 10s), debris covering N-M highway (at about 7.6 min) and final deposition (at about 1 hour) are shown in the figure above. It is seen that the debris covers the section of N-M highway at about 7.6 min from it's initiation.The width of the debris flow when it nvades the section of highway is about 2.3 m and the maximum velocity is about 0.9 m/s. After then it passes away the section of highway and deposition occurs along the certain width of Trishuli river downstream. The affected area along the section of N-M Highway can be shown in the fig: 6.18 above.

Similarly, the temporal variation of debris flow (debris flow at different time interval) with depth and depth averaged X and Y direction velocities are shown in the(figures 6.22 to 6.35) above. The debris path followed by the debris flow at different time

intervals (temporal variation) are shown overlaying in the goggle earth image. The modeling clearly gives an idea of two dimensional debris flow simulation.

The variation of maximum velocity and maximum depth with time is as shown in the figures 6.36 and 6.37 above. The combined graph of maximum velocity and maximum depth with time is shown in fig: 6.38 above. It is seen that the maximum velocity goes on decreasing with time, slightly attains an increase and again gradually decreases to zero just before final deposition. Similarly, if the variation of maximum depth is seen ,it also goes on decreasing with time and gradually attains a constant maximum depth just before the final deposition.

From the figure it is clear that the fan starts to form after the debris flow crosses the main highway. From the figure the different parameters of debris flow are analyzed as below. The different parameters that has been obtained from the simulation of debris flow using DEBRIS2D Model are as follows-

Horizontal projection of maximum runout distance from initiation to final deposition = 237.54m

Horizontal projection of maximum runout distance from initiation to the point just before fan formation = 180m

Elevation difference between initial point and final deposition point = 266.64m

Elevation difference between initial point and the point just before fan formation = 256m

Total Runout distance = 640.22 m

Runout distance of fan (L_{fan}) = 60 m

Lateral spread at fan(B) = 200m

Width of channel at outlet(B_c) = 80.2 m

7.   VALIDATON AND SENSITIVITY ANALYSIS

7.1 General Introduction

In the context of simulation modeling, validation of a model is the process of confirming if it is correctly implemented with respect to the conceptual model (it matches specifications and assumptions deemed acceptable for the given purpose of application). During validation the model is tested to find and fix errors in the implementation of the model. Various processes and techniques are used to assure the model matches specifications and assumptions with respect to the model concept. The objective of model verification is to ensures that the implementation of the model is correct.

There are many techniques that can be utilized to validate a model. Including, but not limited to, have the model checked by an expert, making logic flow diagrams that include each logically possible action, examining the model output for reasonableness under a variety of settings of the input parameters, and using an interactive debugging algorithm. Validation of Computer Simulation Models is conducted to check the efficiency of the model so that it can reflect the actual real scenario. Simulation models are increasingly being used to solve problems and to aid in decision-making. The developers and users of these models, the decision makers using information obtained from the results of these models, and the individuals affected by decisions based on such models are all rightly concerned with whether a model and its results are correct. This concern is addressed through validation of the simulation model.

Simulation models are approximate imitations of real-world systems and they never exactly imitate the real-world system. Due to that, a model should be verified and validated to the degree needed for the models intended purpose or application. Model validation is comparing the results with real world data to assess the model accuracy. Validation checks the accuracy of the model's representation of the real system. Model validation is defined to mean "substantiation that a computerized model within its domain of applicability possesses a satisfactory range of accuracy consistent with the intended application of the model"(Sargent,Robert,2011). A model is built for a specific purpose

or set of objectives and its validity determined for that purpose. There are many approaches that can be used to validate a computer model. The approaches range from subjective reviews to objective statistical tests. One approach that is commonly used is to have the model builders determine validity of the model through a series of tests.

Sensitivity analysis is the study of how the uncertainty in the output of a mathematical model or system (numerical or otherwise) can be apportioned to different sources of uncertainty in its inputs(Saltelli,2008). A related practice is uncertainty analysis, which has a greater focus on uncertainty quantification and propagation of uncertainty. Ideally, uncertainty and sensitivity analysis should be run in tandem .

Sensitivity analysis can be useful for a range of purposes, including:

- Testing the robustness of the results of a model or system in the presence of uncertainty.

- Increased understanding of the relationships between input and output variables in a system or model.

- Uncertainty reduction: identifying model inputs that cause significant uncertainty in the output and should therefore be the focus of attention if the robustness is to be increased (perhaps by further research).

- Searching for errors in the model (by encountering unexpected relationships between inputs and outputs).

- Model simplification – fixing model inputs that have no effect on the output, or identifying and removing redundant parts of the model structure.

- Enhancing communication from modelers to decision makers (e.g. by making recommendations more credible, understandable, compelling or persuasive).

- Finding regions in the space of input factors for which the model output is either maximum or minimum or meets some optimum criterion
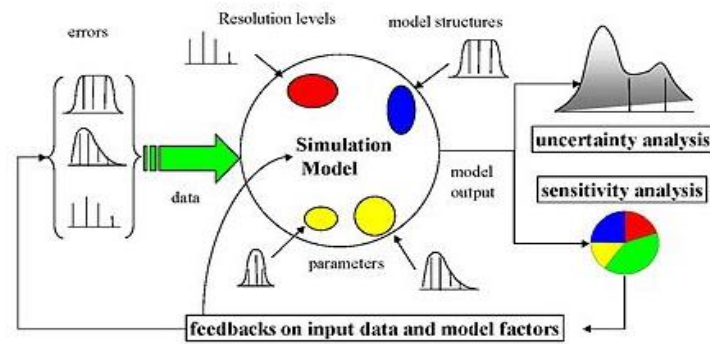
Figure 7.1 Ideal scheme of a possibly sampling-based sensitivity analysis(Wikipedia,2014)

Fig: 7.1 depicts that uncertainty arising from different sources—errors in the data, parameter estimation procedure, alternative model structures—are propagated through the model for uncertainty analysis and their relative importance is quantified via sensitivity analysis.

7.2 Validation : SINMAP Model

In quantitative landslide susceptibility prediction modelling, it is not possible to compare the model with future landslides. Therefore, it is necessary to divide the landslide database in a modelling dataset and a validation dataset (Chung and Fabbri, 2003).

In this thesis, random partition approach was followed by dividing the landslides into two groups .197 "debris slides" (through aerial interpretation and from the hazard map prepared by Nippon Koei,2008 in collaboration with DWIDP, Nepal as well) was used for modeling calibration and 142 polygon themes which were classified as "landslide zones" was used for validation.

Validation of landslide susceptibility models give information about the confidence of the model to the user. Validation also permits to compare different models or model parameter variables (Begueria,2006). In landslide susceptibility assessment, accuracy is the capacity of the map to differentiate landslide-free from landslide-prone areas. Accuracy and objectivity depend on model accuracy, input data, experience of the concerned experts and size of the study area (Soeters and van Westen, 1996). On the

other hand, model evaluation is the assessment of its adequacy to the needs of the final user. In landslide susceptibility modeling, it is mainly used to define hazard classes for practical purposes, such as to prioritize areas with the highest susceptibility for further investigations (Begueria, 2006).

Accuracy statistics require the splitting of the classified objects into a few classes by defining specific values of the susceptibility index that are called cut off values. For statistical models, a statistically significant probability cut off (p cut off) exists, equal to 0.5. In different conditions or for other typologies of landslide susceptibility models, such as physically-based, heuristic, artificial neural networks, and fuzzy logic, the choice of cut off values to define susceptibility classes is not scientifically sound. A solution to this limitation consists in evaluating the performance of the models over a large range of cut off values by using cut off independent performance criteria such as success-rate curves, ROC curves and Cost curves. Here, in this study, ROC curve is used for evaluating the performance of SINMAP Model. (Safeland, 2011).

Validation is performed by analyzing the agreement between the model results and the observed data. Since the observed data consist in the present/absence of a landslide within a certain terrain unit, the simpler method to assess the accuracy is to compare these data with a binary classification of susceptibility in stable and unstable units. This classification requires a cut off value of susceptibility that divides stable terrains (susceptibility lower than cut off) and unstable terrain (susceptibility higher than cut off). The comparison of observed data and model results reclassified into two classes is represented through contingency tables (Table 7.1).

Table 7.1 Contingency table used for landslide model evaluation (NO and PO: number of stable and unstable observation, NP and PP: number of stable and unstable predictions; T: total number of observations(Source:Safeland,7th framework programme,2011)

Observed		Predicted	
	Class 0 (-) stable	Class 1 (+) unstable	
Class 0 (-) stable	(-|-) true negative, tn	(+|-) false positive, fp	N_O
Class 1 (+) unstable	(-|+) false negative, fn	(+|+), true positive, tp	P_O
	N_P	P_P	T

IJART

Available online at http://www.ijart.info/

For heuristic and physically-based models it is necessary to follow the following procedures: (Source: Safeland, 7th framework programme,2011)

1. the susceptibility index (derived from objective or subjective ranking or based on stability measures) is reclassified into two classes (stable and unstable) using a cut off value;

2. the resulting classified susceptibility map needs to be overlaid with landslides, in order to calculate either the percentage of landslides (as number or area) correctly laying within the area classified as unstable; or to calculate the number of terrain units with or without landslides;

3. the contingency table can be derived for the specific cut off by intersecting the susceptibility classes and the presence/absence of landslides.

Assuming a cut-of value , the susceptibility statistics table was reclassified. The susceptibility map prepared from SINMAP Model was overlaid with the landslide potential zone hazard map (polygon) prepared by Nippon Koei,2011 in collaboration with DWIDP, Nepal and the landslide density(number/km^2) was calculated.The contingency table was derived for the specific cut off value by intersecting the susceptibility classes and the presence/absence of landslides.

Table 7.2 Illustration of percent of slides and landslides density of calibration and validation dataset

	FS>1.5	FS=1.5to1.	FS=1.25to1.	FS=1.0to0.5	FS=0.5to0	FS<0
		CALIBRATION(MODELLING) DATASET				
% of slides	1.523	0.000	1.015	50.761	45.685	1.015
Density(number/km^2)	0.287	0.000	0.504	1.566	2.051	16.529
		VALIDATION DATASET				
% of slides	2.143	1.429	1.429	60.714	32.143	2.143
Density(number/km^2)	0.287	0.866	0.504	1.331	1.025	24.793

The validation of simulated result from SINMAP Model was done in the following three ways-

7.2.1 Overlaying the validating landslide polygon theme with the obtained result
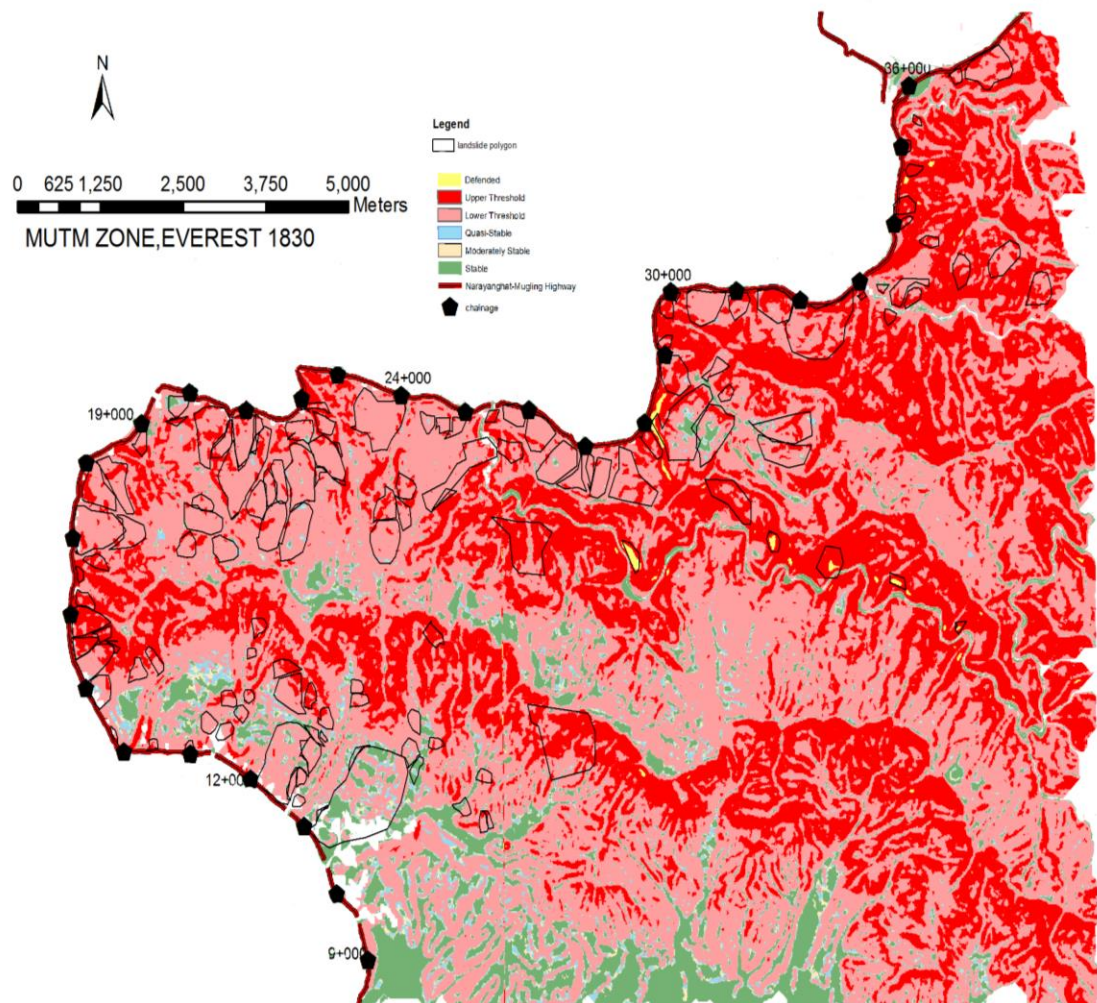
Figure 7.2 Overlaying landslide polygons(validation landslide inventory) with the stability index map prepared from SINMAP calibration

Overlaying of landslide polygons in the stability index map showed a very good result as many of the landslide polygons(validation) are falling under the defended, upper threshold and lower threshold zone(unstable zones). Further, evaluation was done by calculating the efficiency.

7.2.2 Preparation of Receiver Operating Characteristics(ROC)Curve and Calculation of Area Under Curve(AUCROC)

The datas from Table 7.2 are used as a basis for plotting of ROC Curve.

However, Begueria (2006) noted that the model efficiency greatly depends on prevalence, the relation between false positives (type I errors) and false negatives (II errors). Begueria recommends using statistics not affected by prevalence, proportion of positive and negative cases. They are

- sensitivity, the proportion of positives observations correctly identified;
- specificity, the proportion of negatives observations correctly identified;
- false negative rate,
- false positive rate, and
- likelihood ratio.

Validation of landslide susceptibility maps is commonly based on statistics from cross-area tabulation, also known as the confusion matrix or contingency table (Bonham-Carter, 1994). Based on a threshold, continuous susceptibility values are categorized in a binary map (susceptible and not susceptible classes) and then compared with a binary landslide distribution map (presence or absence of landslides).

Cross-tabulation consists in the calculation of overlap areas between the two binary maps. The possible combinations are as follows: landslide areas are classified as susceptible areas (true positive observations); landslide-free areas are classified as no susceptible areas (true negative observations); landslide areas are classified as no

susceptible areas (false negative observations); and landslide-free areas are classified as susceptible areas (false positive observations) as shown in Table 7.2.

Table 7.3 Confusion matrix. (Source Begueria 2006).

a, true positives;

 b, false positives (error type I);

 c, false negatives (error type II);

 d, true negatives

In landslide susceptibility assessment there are two types of prediction errors;

 1) landslides may occur in areas that are predicted to be stable, and

 2) landslides may actually not occur in areas that are predicted to be unstable (Soeters and van Westen, 1996).

 The first type of errors is a false positive (type I error) and the second type is a false negative (type II error).

ROC CURVE:

ROC plot is a graph of sensitivity versus specificity, statistics not affected by prevalence. It is calculated by estimating the parameters for many thresholds. The area under the ROC plot (AUC) is a statistic accuracy of the model and it is independent of the prediction threshold. AUC is 0.5 when there is no variation with threshold definition and 1 when the model makes a perfect prediction. AUC below 0.5 indicates that performance

is lower than classification by chance. The higher the AUC, the higher the model accuracy (Fawcett, 2006).

Assuming landslide density(number/km^2)as the basis of analysis as of Table 7.3,

Table 7.4 Demonstration of data for drawing ROC Curve and illustration of other parameters

	Cutoff points		
	0.5	1	1.25
a(True Positives,TP)	18.58	20.146	20.65
b(FP,TypeI error)	7.238	7.003	9.073
c(FN,TypeII error)	0.631	0.866	0.866
d(TrueNegatives,TN)	2.357	0.791	0.287
Sensitivity(= a/ (a + c))	0.967	0.959	0.960
Specificity(= d/(b+d))	0.246	0.101	0.031
False positive rate(=b/(b+d))	0.754	0.899	0.969
False negative rate c/ (a + c	0.033	0.041	0.040
Likelihood ratio+ =sensitivity/ (1-specificity)	1.282	1.067	0.990
Likelihood ratio- =(1-sensitivity) / specificity	0.134	0.406	1.313
Youden's Index J = sensitivity + specificity - 1	0.213	0.060	-0.010

IJART

The graph of ROC Curve can be shown as-
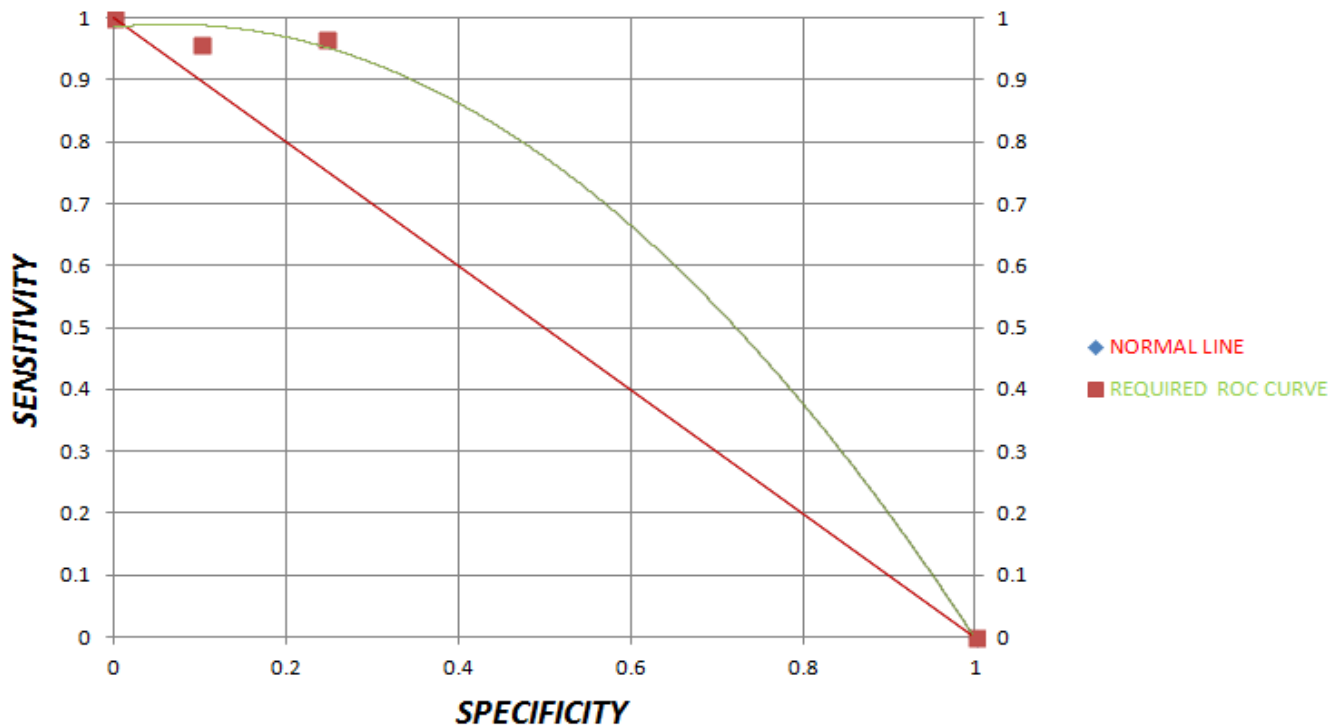
Figure 7.3 Graph showing the Receiver Operating Characeristics (ROC) Curve

Line A is line of no discrimination (AUC is 0.5). Line B represents the accuracy of model B with the values of specificity and sensitivity calculated for different thresholds, and the Area Under Curve(AUC)can be calculated as(by adding the areas of the polygons between the thresholds (Begueria, 2006))-

$$AUC = \sum_{i=1}^{n+1} \frac{1}{2} \sqrt{(x_i - x_{i+1})^2} \; (y_i + y_{i+1})$$

where, x_i is specificity and y_i is sensitivity at threshold i and $x_{n+1} = 0$, $y_{n+1} = 1$

AUC = 0.03+0.067 + 0.139 + 0.364

= 0.601

The AUC of the model was 0.601. The result means that for the target area, the efficiency or prediction power of the model is higher than classification by chance.

IJART

This indicates that it is more than an average good model to predict the occurrence of shallow landslides along Narayanghat-Mugling Highway.

7.2.3 Calculation of Efficiency considering cutoff(threshold) point

The Youden's index (J), is the difference between the true positive rate and the false positive rate. Maximizing this index allows to find, from the ROC curve, an optimal cut-off point independently from the prevalence. According to its definition and as illustrated on Fig.1, J is the vertical distance between the ROC curve and the first bisector (or chance line). If F(x) is the function describing the ROC curve, with x = 1-specificity, we may write

$$J(x) = F(x)\text{-}x$$

When J is maximal, J'(x) = 0, where J' is the derivative of J.

From Eq. 1:   J'(x)= F'(x) -1,

where F' is the derivative of F.

Hence, when J is maximal, F'(x) = 1, meaning that the tangent to the ROC curve is parallel to the first bisector (slope = 1). It implies that, around this point, a gain (or a loss) in specificity results in a loss (or a gain) of the same amplitude in sensitivity.
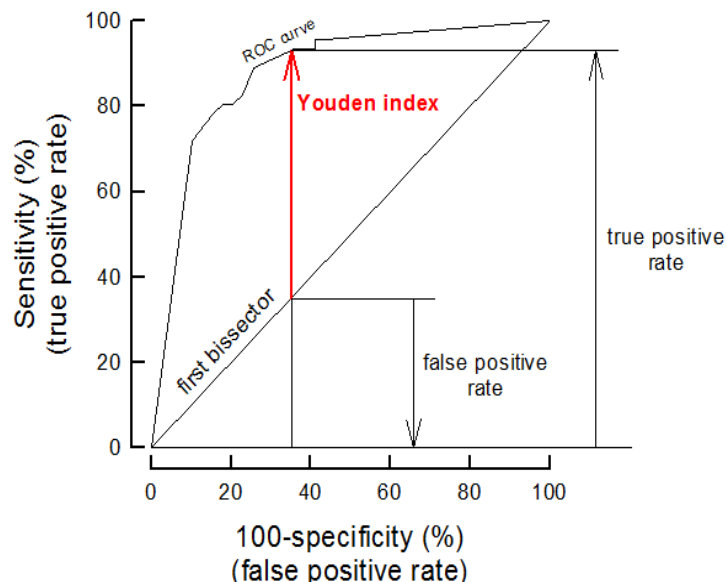
Figure 7.4 Graph demonstrating Youden's Index

Red Vertical line is maximum value of Youden's index for the ROC curve.

Since,Youden's Index(J) is maximum for cutoff point 0.5(as in Table:7.4 above),taking 0.5 as cutoff point for classifying as high susceptibility and low susceptibility i.e

Safety factor <0.5 are unstable (high susceptibility)

Safety factor >0.5 are stable (low susceptibility)

Taking data from Table 7.3(the values obtained below are also shown in Table 7.4)

a = landslide areas classified as susceptible areas (true positive observations, TP)

= 16.529+2.051= 18.58

d = landslide-free areas classified as no susceptible areas (true negative observations)

= 0.287+0+0.504+1.566= 2.357

c = landslide areas classified as no susceptible areas (false negative observations, Type II error)

= (0.287+0.866+0.504+1.331)-2.357 = 0.631

b = landslide-free areas classified as susceptible areas (false positive observations, FP, Type I error)

= (1.025+24.793)-18.58 = 7.238

Success and prediction and rates are the most common approaches (Brenning,2005; It is calculated comparing the model to the modeling dataset. The prediction rate is calculated comparing the model to a dataset different from the modeling dataset, a validation dataset.

$$Efficiency = \frac{(a+d)}{(a+b+c+d)}$$

Efficiency = (18.58+2.357)/(18.58+2.357+0.631+7.238)

= 0.7268(72.68%) which is the proportion of correctly classified observations

Misclassification rate = (b + c) / N

$$=(7.238+0.631)/(18.58+2.357+0.631+7.238)$$

=0.2731(27.31%) which is proportion of incorrectly classified observation

Odds ratio = (a + d) / (b + c)

= 2.66 which is the ratio between correctly and incorrectly classified cases

Positive predictive power = a /(a + b)

= 0.7196(71.96%) which is p(X1|X1'), or the proportion of true positives in the total of positive predictions

Negative predictive power = d/ (c + d)

= 0.788(78.8%) which is p(X0|X0'), or the proportion of true negatives in the total of negative predictions

7.3 Sensitivity analysis: SINMAP Parameters

The uncertainties in the use of the model have led to increase reliance on sensitivity analysis, the process by which a model is tested to establish a measure of the relative change in model results caused by the corresponding change in model parameters. This type of analysis is necessary to complement to the modeling exercise, especially since it provides information on the level of certainty(uncertainty) to be placed on the result of the modeling. The issue of model sensitivity of parameter variations is particularly important in the case of deterministic models having some conceptual components. Because of the conceptual components, calibration are strictly valid only in narrow variable ranges. Therefore, errors in parameters need to be ascertained in a qualitative way.Sensitivity is usually analyzed by isolating the effects of certain parameters.If a model is highly sensitive to certain parameters, small change in this value of parameter may cause correspondingly large change in the model output. It is therefore,necessary to concentrate on these sensitive parameters and the insensitive secondary parameters are used for fine tuning.

For the purpose of the sensitivity analysis the following model parameters are taken-

Rainfall:

For annual maximum rainfall of 450mm,650mm and 1000mm the percentage of defended(most unstable) area was found to be 0.097,0.127 and 0.142 respectively which showed that with the increase of rainfall the hazard risk was increased.
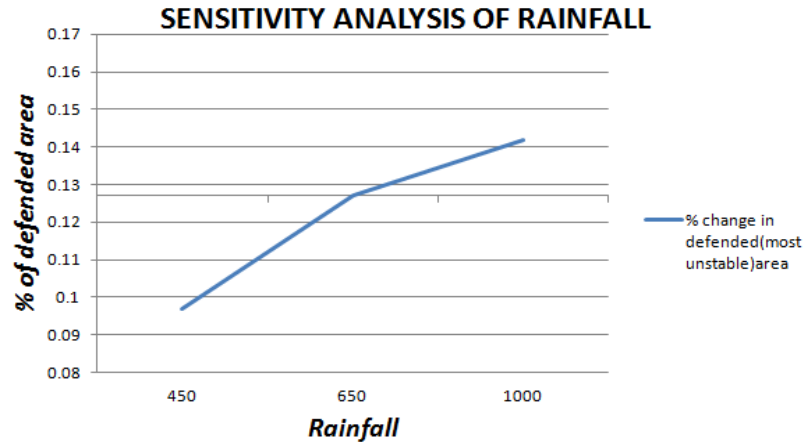
Figure 7.5 Sensitivity analysis graph of Rainfall (Parameters C,φ,ɣ,T remaining constant)

It is clearly seen that with the increase in rainfall the most unstable(defended)zone increases and with the decrease in rainfall the defended zone decreases.When the value of rainfall was increased by30%,the hazard potential increased by about 15%.Similarly,when the value of rainfall was dereased by 30%,the hazard potential was decreased by about 20%.

Angle of internal Friction (φ):

It is the measure of soil slope retention capacity by the frictional action. When the range of values of this parameter was decreased and increased by 15% a slight change occurred in the SA-plot graph which is shown below-
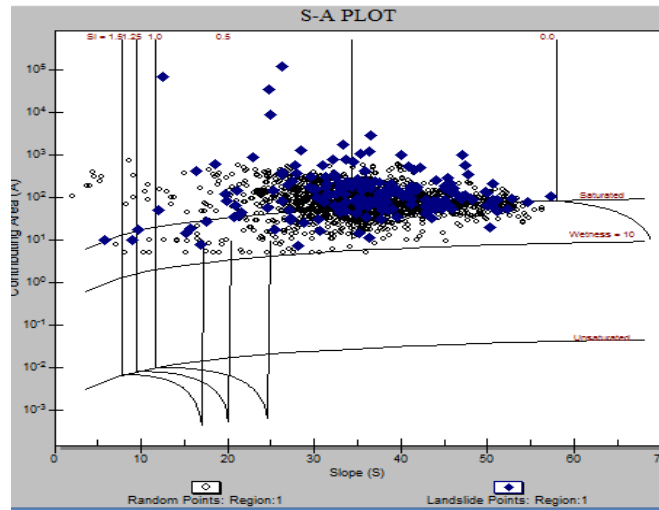
Figure 7.6 SA-plot diagram for φmin=25^0 and φmax=40^0,decreased by 15% from calibrated value (C,ɣ,T remaining constant)
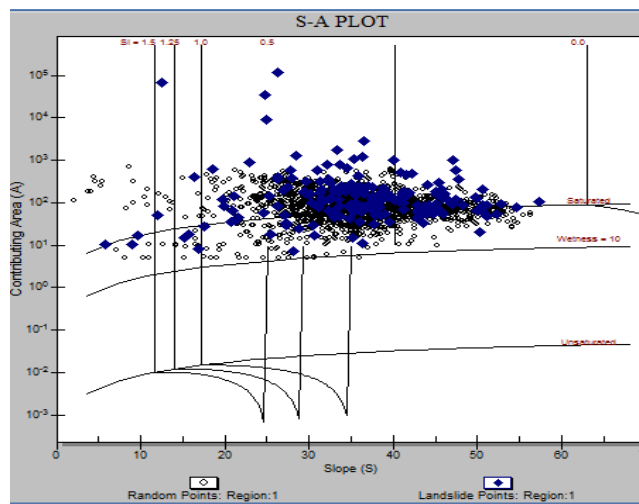
Figure 7.7 SA-plot diagram for for φmin=35^0 and φmax=50^0,increased by 15% from calibrated value(C,ɣ,T remaining constant)

\

If we compare the two graphs above ,there is not much variation only the difference lies in the distribution of landslide points. In fig:7.4 above, few landslide points are closer to SI=0 line whereas in fig:7.5 landslide points are farther from SI=0 line. In fig:7.5 few landslide points are within SI=1 and SI=1.25 line whereas in Fig:7.4 no landslide points

are within SI=1 and SI=1.25 line. This illustration clearly depicts that decrease in φ increases the landslide susceptibility whereas increase in φ decreases the landslide susceptibility.

Dimensionless Cohesion(C):

Dimensionless cohesion is the cohesive restoring force relative to soil weight , [C = (Cr+Cs)/(h ρ_sg)],whose sensitivity test is shown below-
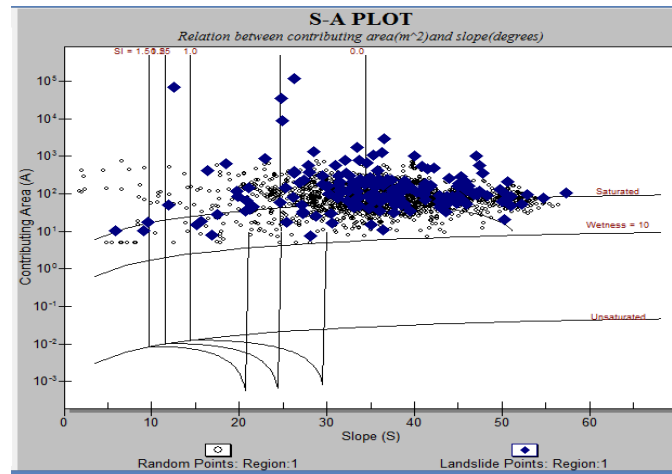
Figure 7.8 SA-plot for Cmin=0 and Cmax=0.2,decreased by 50% from the calibrated value (φ,ɣ,T remaining constant)
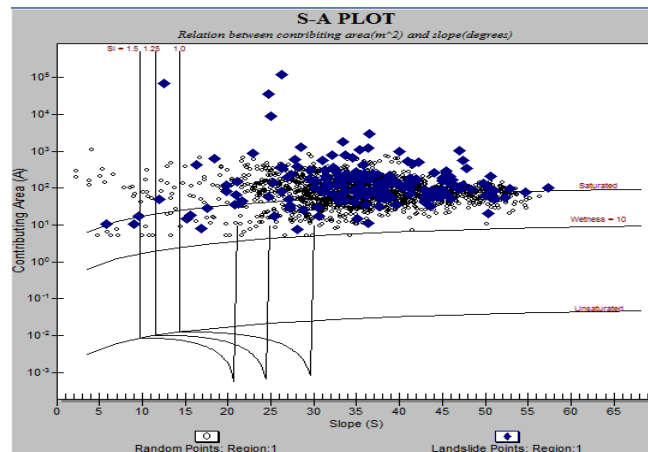
Figure 7.9 SA-plot for Cmin=0 and Cmax=1.1,increased by 50% from the calibrated value (φ,ɣ,T remaining constant)

From the Fig: 7.6, it is clear that many of the landslide points are falling beyond the SI=0 line whereas in fig:7.7 SI=0 and SI=0.5 line has disappeared and landslides are distributed within that region. It is because of the fact that, according to the definition of dimensionless cohesion if C>1, the cohesion is sufficient to hold the soil on a vertical slope so Factor of Safety and Stability Index can never be greater than 1 but it is physically possible for C to be greater than 1 if the soil is thin and highly cohesive. Moreover, sensitivity analysis of the role of the parameter C was carried out assuming that plant roots can be influential. It can be understood from the sensitivity analysis that with the increase in value of C (i.e. with the increase in root shear strength C_r),the strength increases and the plant root has an influential role in making the hill slope stable. It is clear from the figure that if the value of C is decreased or increased, then the landslide susceptibility is increased or decreased respectively.

7.4 Validation : DEBRIS-2D Model

The validation of DEBRIS2D model was done by the following 3 ways-

7.4.1 Comparing with actual event of 2003 Disaster

From the DEBRIS2D model result, the debris flow covered Narayanghat-Mugling Highway at approximately about 7.6 minutes from it's initiation.

Max depth at 7.6 minutes = 2.3 metre

Max velocity at 7.6 minutes = 0.932 m/s

Area of debris fan at 7.6 min. = 2350.7m (from Arc GIS)

Total volume of debris flow = 2350.7*2.3

$$= 5406.61m^3$$

According to DWIDP Bulletin 2005-6, at 24+740,

 Contractor's E/W Work Volume = 3671 m^3

Machinery work Loader = 16.75 hr

Total no of disturbed days= 8

Extra volume = 1089 m^3

Total Volume = 3671+1089 m^3

$$= 4760 \text{ m}^3$$

The obtained volume might be overestimated because maximum depth has been used.

Variation = (5406.61-4760)/5406.61

$$= 0.119(11.9\%) \text{ which is acceptable}$$

7.4.2 Comparing with Empirical Equations

Empirical relationships are one of the most widely-used techniques to estimate the maximum runout distance of landslides and debris flows. There are many different publications dealing with this topic and analysing overall data sets (Hsü, 1975; Corominas, 1996; Legros, 2002), while others present correlations for debris flows (Cannon, 1993; Rickenmann, 1999; Fannin and Wise, 2001; Bathurst et al., 2003; Crosta et al., 2003). The most common empirical relationships estimate the maximum runout distance making use of the reach angle, α, also called "Fahrböschung"(Heim, 1932). The reach angle is expressed as the ratio between the vertical drop,H, and the horizontal projection of the maximum runout distance Lmax, and is mostly linked to the debris-flow volume,V. A worldwide dataset including 154 debrisflow events was analysed byRickenmann (1999), resulting in the following expression:

$$L_{\max} = 1.9V^{0.16}H^{0.83}$$

Other formulae correlate directly volume with the reach angle, which simplifies the graphical determination of the maximum runout. Corominas (1996)compared a dataset of 52 debrisflows, debris slides and debris avalanches that occurred in the Pyrenees to 19 worldwide events and proposed:

$$\tan\alpha = H/L_{\max} = 0.97V^{0.105}$$

Another empirical correlation is the relationship developed by Rickenmann (1999) between the run out distance on the fan, L$_{fan}$, and volume:

$$L_{fan} = 15V^{1/3}$$

Empirical equations (Table 7.5) are widely used for estimating hazard mapping parameters (Rickenmann, 1999), and classification schemes are available to estimate the required parameters (D'Agostino et al., 2010).(Source: Source: Hurlimann et.al,2008)

Table 7.5 Empirical Equations by different authors in debris flow hazard delineation(Source: Bertoldi et.al,2012)

Variable	Empirical relation	Author	Eq. number
Runout (R)	$R = 8,6 \cdot (V \tan \theta_u)^{0,42}$	Ikeya (1989)	(1)
	$R = 25V^{\frac{1}{3}}$	Rickenmann, 1994, in D'Agostino et al. (2010)	(2)
Travel distance (L)	$L = 1,9V^{0,16} H_e^{0,83}$	Rickenmann (1999)	(3)
Lateral spread (B)	$B\,\text{max} = R$ (granular) $B\,\text{max} = 0,55R$ (low cohesion)	Cesca (2008)	(4a) (4b)
	$\frac{B}{B_c} = k_1 + k_2 \left(\frac{R}{B_c} \right),$ $k_1=1,788 \ e \ k_2=0,185$	D'Agostino e Cesca (2009)	(5)

R = runout,

V = volume,

θ_u = source area slope,

L = travel distance,

H_e= elevation difference between the starting point and the lowest point of deposition of the mass movement,

B = lateral spread, B_c= width of channel at the outlet

Table 7.6 Validation of calculated runout distance with empirical equations

REFERENCE(AUTHOR)	VARIABLES	VALUES	VARIATION
DEBRIS2D(CALCULATED)	RUNOUT DISTANCE	640.226m	
Ikeya (1989)	RUNOUT DISTANCE	453.37m	29.10%
Rickenmann, 1994, AND D'Agostino 2010	RUNOUT DISTANCE	616.55m	3.69%

Available online at http://www.ijart.info/

Table 7.7 Validation of calculated travel distance and reach angle with empirical equations

REFERENCE(AUTHOR)	VARIABLES	VALUES	VARIATION
DEBRIS2D(CALCULATED)	TRAVEL DISTANCE(L_{max})	237.54m	
Rickenmann (1999)	TRAVEL DISTANCE(L_{max})	800m	235%
DEBRIS2D(CALCULATED)	Reach angle(H/L_{max})	1.12	
Corominas (1996)	Reach angle(H/L_{max})	2.35	109%

Table 7.8 Validation of calculated runout on fan with empirical equations

REFERENCE(AUTHOR)	VARIABLES	VALUES	VARIATION
DEBRIS2D(CALCULATED)	Runout on fan	60m	
Rickenmann (1999)	Runout on fan	225m	275%

Table 7.9 Validation of calculated lateral spread with empirical equations

REFERENCE(AUTHOR)	VARIABLES	VALUES	VARIATION
DEBRIS2D(CALCULATED)	LATERAL SPREAD(GRANULAR		
DEBRIS2D(CALCULATED)	LATERAL SPREAD(LOW COHESION)	150m	
Cesca (2008)	LATERAL SPREAD(GRANULAR	640.2m	
Cesca (2008)	LATERAL SPREAD(LOW COHESION)	320m	110%

Table 7.10 Validation of calculated ratio of lateral spread and width of channel at outlet with empirical equations

REFERENCE(AUTHOR	VARIABLES	VALUES	VARIATION
DEBRIS2D(CALCULATED)	WIDTH OF CHANNEL AT OUTLET(B_c)	80.2m	
DEBRIS2D(CALCULATED)	RATIO OF B AND B_c	1.87m	
D'Agostino e Cesca (2009)			
	RATIO OF B AND B_c	2.25m	20%

From Table: 7.6, comparing the calculated values with the empirical equations gave approximately good results which shows that the prediction done by DEBRIS2D is good. From Table 7.7, comparing the calculated values with the empirical equations did not match well. It might be because of the fact that across the Kamere Khola Watershed, where the debris flow simulation was done debris crossed the Narayanghat-Mugling Highway and reached the river bank because of which the elevation difference was great.Rickemann(1999) gave the equation relating with elevation difference so the empirical equation might have gave the higher result. Similarly, Corominas (1996) used the relation with elevation difference. Hence, because of similiar reason above, the result of the equation might have been higher. Similarly, From Table 7.8, the empirical equation by Rickemann(1999) predicted the higher result.

From Table: 7.8, the empirical equation with low cohesion case nearly matched with the calculated data. It might be because of the fact that there was presence of some clay particles in the study area during the field visit as well. Generally, granular particles are composed of sediment or unconsolidated particles (gravel, sand, silt) having no clay content. During the field visit and from many researches as well across that section of N-M Highway, there were not completely granular particles but the presence of clayey materials were also significant. Hence, the calculated value is approximately matched with empirical equation with low cohesion case (not granular) proposed by Cesca (2008).

From Table: 7.9, the calculated value was wellmatched with the empirical equation resuting in error of about 20%. Hence, the calculated value can be well justified.

7.4.3 Comparing the simulated debris path with google earth image

Figure 7.10 Google earth image (imagery date 2-7-2009 and 11-2-2010) of the study area Kamere Khola Watershed(24+740)
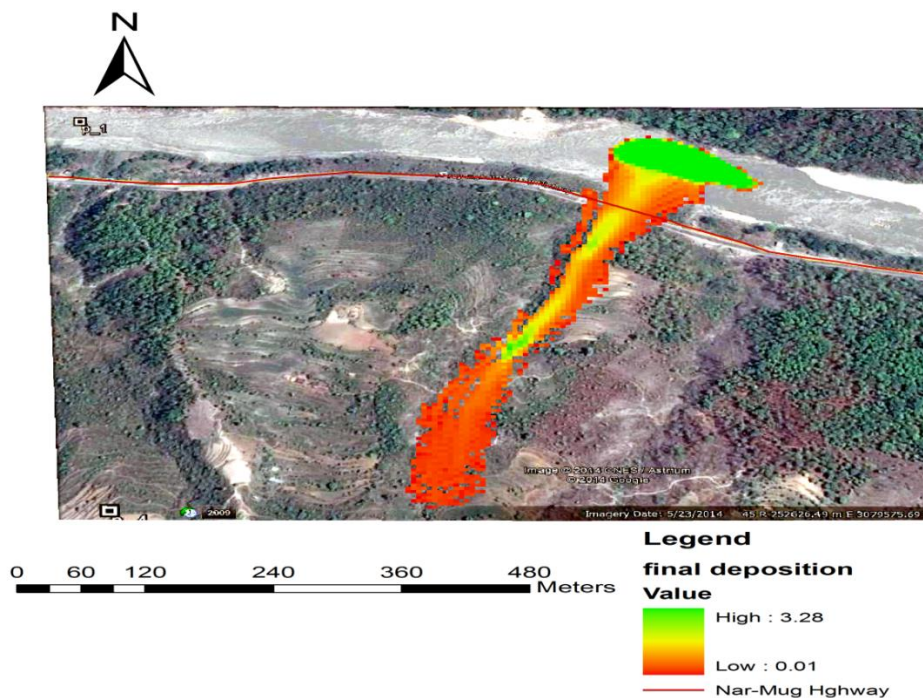
Figure 7.11 Debris flow depth path during final deposition at about 1hour overlaid on google earth image(imagery date 5-23-2014) for validation

It clearly shows the debris path followed by the model is approximately accurate with the actual debris flow path by comparing the figures. The simulated result is consistent with the actual real debris flow path event. Fig:7.9 with figure 7.8

7.5 Sensitivity Analysis : DEBRIS2D Parameter

The sensitivity analysis was performed for the initial debris flow volume. The different variation in frontal position, lateral spread and final maximum depth with the variation in input debris flow initial volume are illustrated below.

For initial volume = 5000 m^3
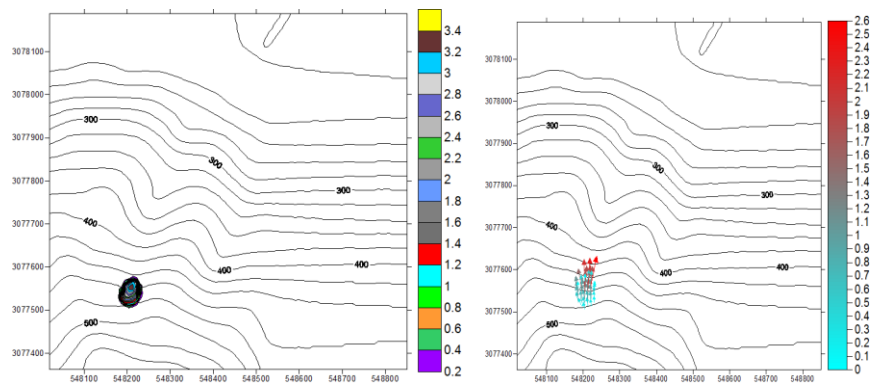
Figure 7.12 Debris flow depth contour map and velocity vector map for initial volume = 5000 m3 during initial mass distribution (at about 10s)
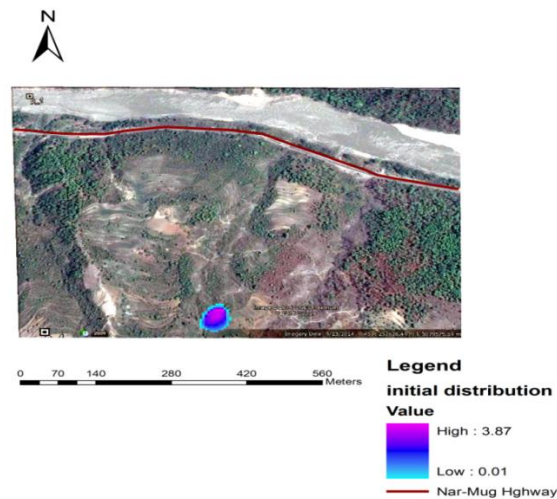
Figure 7.13 Debris flow depth path during initial mass distribution at about 10s for initial volume = 5000 m^3 overlaid on google earth image(imagery date 5-23-2014)
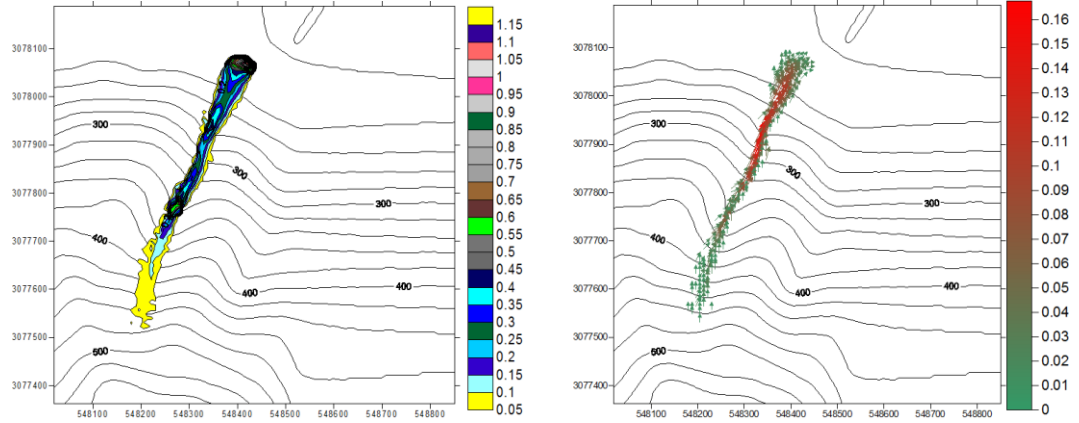
Figure 7.14 Debris flow depth contour map and velocity vector map for initial volume = 5000 m3 during final deposition (at about 51min)
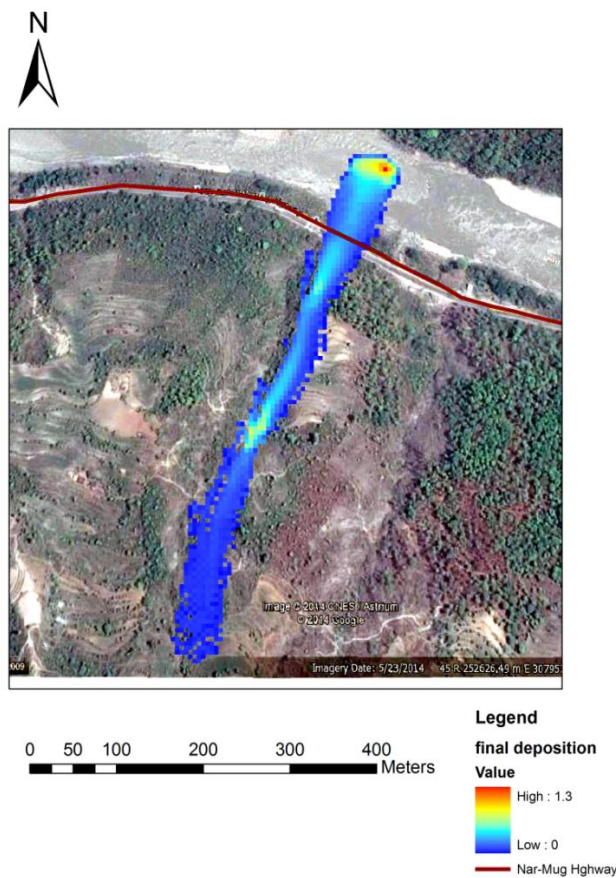
 Figure 7.15 Debris flow depth path during final deposition at about 51minute for initial volume = 5000 m3 overlaid on google earth image(imagery date 5-23-2014)

For initial volume = 10000 m³
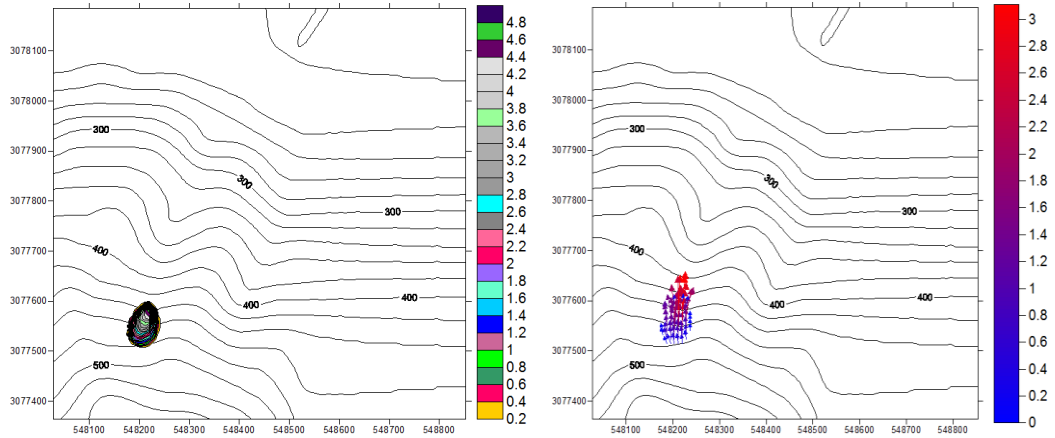
Figure 7.16 Debris flow depth contour map and velocity vector map for initial volume = 10000 m3 during initial mass distribution (at about 10s)
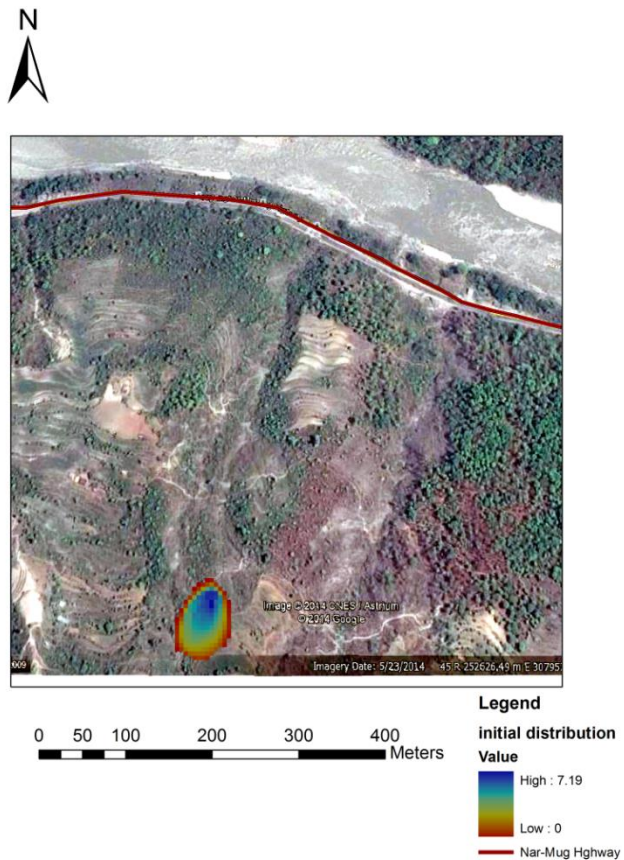
Figure 7.17 Debris flow depth path during initial mass distribution at about 10s for initial volume =10000 m3 overlaid on google earth image(imagery date 5-23-2014)
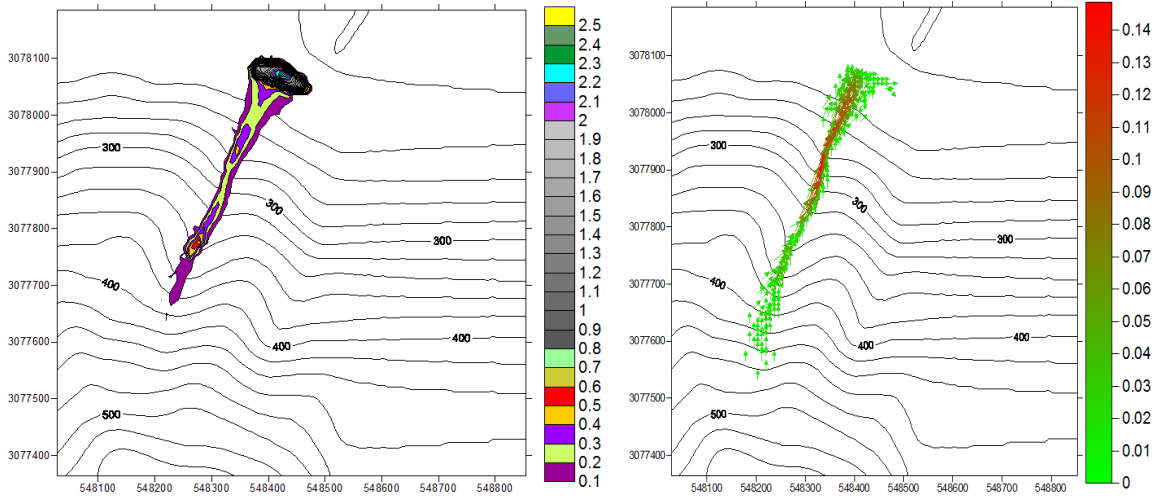
Figure 7.18 Debris flow depth contour map and velocity vector map for initial volume = 10000 m3 during final deposition (at about 58min)
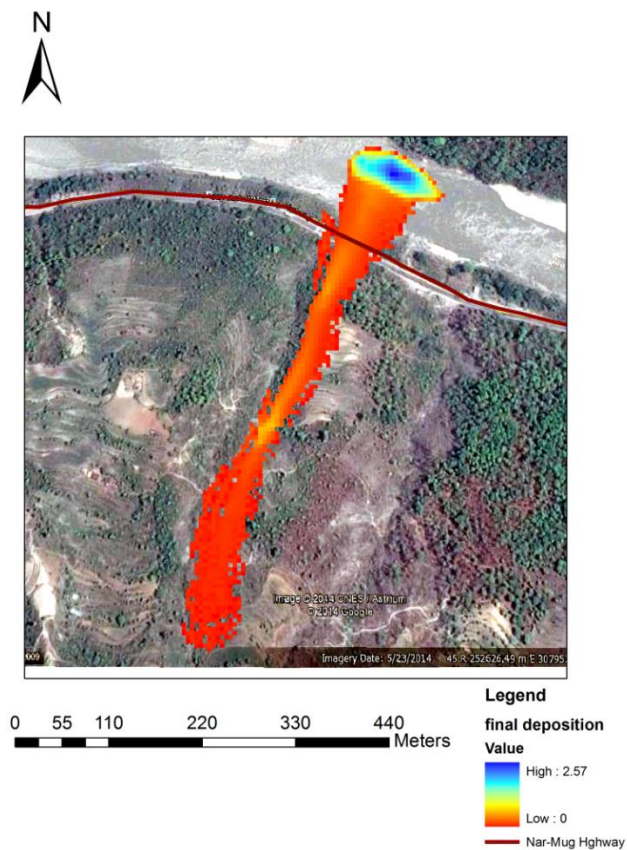
Figure 7.19 Debris flow depth path during final deposition at about 58 minute for initial volume = 10000 m3 overlaid on google earth image(imagery date 5-23-2014

COMPARISION OF HAZARD ZONES IN VARIOUS INITIAL VOLUMES:
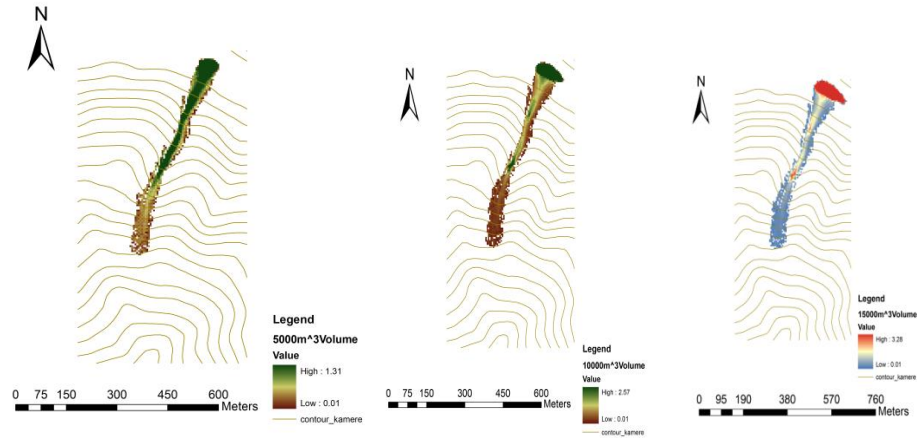
Figure 7.20 Comparison of debris path, frontal position , lateral spread and final depth for various volumes($5000m^3$,$10000m^3$ and $15000m^3$ initial volumes respectively from left)

Variation in frontal position

Table 7.11 Tabular representation of variation in frontal position with respect to various initial volumes

Volume(m^3)	Frontal position(m)	Change in volume from calibrated(m^3)	Change in frontal position from calibrated(m)	Change in volume/ maximum volume(%)	Change in frontal position/ maximum frontal position(%)
5000	46	10000	14	66.67%	23.33%
10000	52	5000	8	33.33%	13.33%
15000	60	-	-	-	-
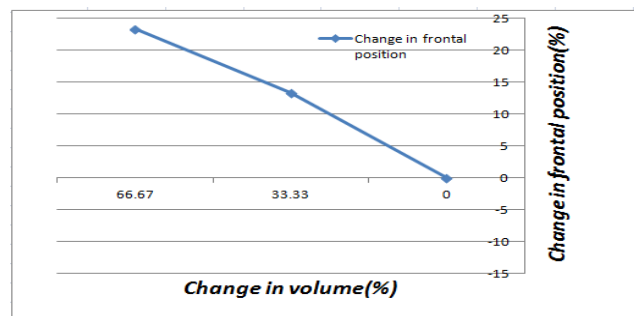
Figure 7.21 Graphical representation of sensitivity analysis of initial debris flow volume with respect to change in frontal position

Variation in lateral spread

Table 7.12 Tabular representation of variation in frontal lateral spread with respect to various initial volumes

Volume(m^3)	Lateral Width(m)	Change in volume from calibrated(m^3)	Change in lateral width from calibrated(m)	Change in volume/ maximum volume(%)	Change in lateral width/ maximum lateral width(%)
5000	68	10000	82	66.67%	54.66%
10000	122.5	5000	27.5	33.33%	18.33%
15000	150	-		-	-
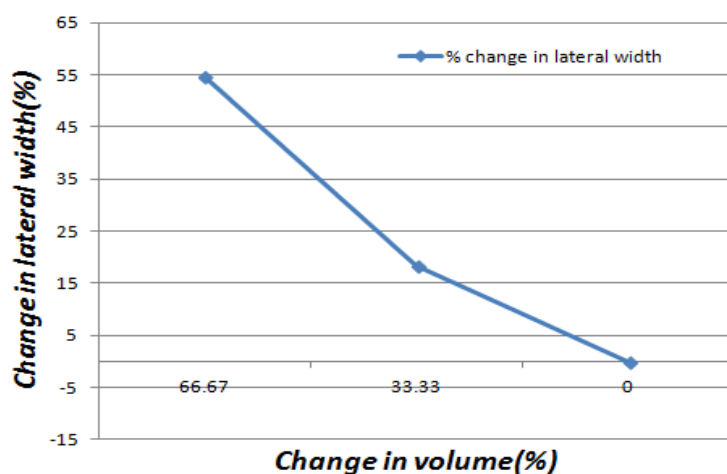
Figure 7.22 Graphical representation of sensitivity analysis of initial debris flow volume with respect to change in lateral width

Variation in final maximum depth

Table 7.13 Tabular representation of variation in final maximum depth with respect to various initial volumes

Volume(m^3)	Final Maximum Depth(m)	Change in volume from calibrated(m^3)	Change in max depth from calibrated(m)	Change in volume/ maximum volume(%)	Change in final depth/ maximum final depth(%)
5000	1.31	10000	1.97	66.67%	60.06%
10000	2.57	5000	0.71	33.33%	21.64%
15000	3.28	-	-	-	-
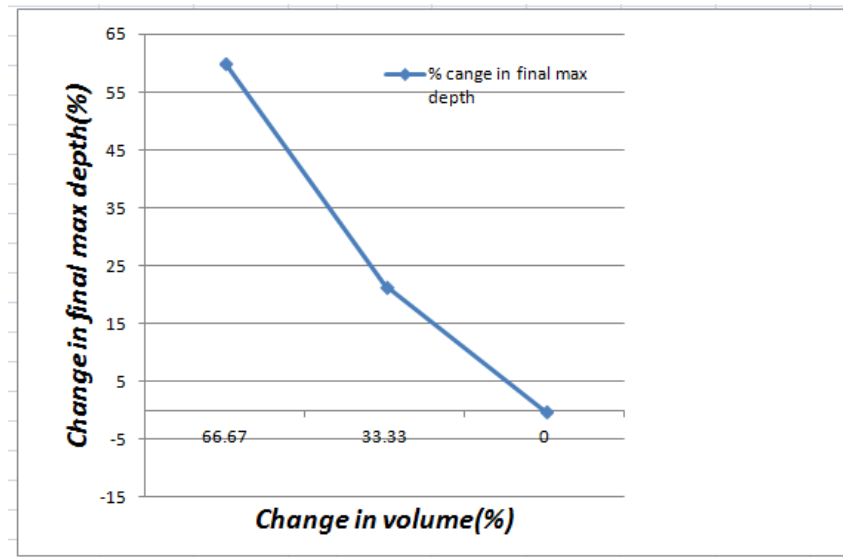
Figure 7.23 Graphical representation of sensitivity analysis of initial debris flow volume with respect to change in final max depth

Hence, the sensitivity analysis of initial debris flow volume clearly demonstrates that the model is very much sensitive to this parameter. Fig: 7.12 to 7.23 shows the final simulated deposited contour maps used for various volumes of debris flow sources. Therefore, the spread of simulation from all three total volumes are equally acceptable. This sensitivity test compared the hazard zones in various volumes as shown in fig: 7.24. The tabular and graphical representation of front position change (Tab: 7.11 and fig: 7.25), lateral width change (Tab: 7.12 and Fig: 7.26) and final maximum depth change (Tab: 7.13 and fig: 7.27) clearly depicts the sensitiveness of initial debris flow volume.

The sensitivity test revealed that a 33.33% variation in estimating the volume results in a 13.33% variation on the final depositional front and a 66.67% variation in estimating the volume results in a 23.33% variation on the final depositional front. Similarly, a 33.33% variation in estimating the volume results in a 18.33% variation on the depositional lateral spread and a 66.67% variation in estimating the volume results in a 54.66% variation on the depositional lateral spread. The sensitivity test also revealed that a 33.33% variation in estimating the volume results in a 21.64% variation on the final depositional maximum depth and a 66.67% variation in estimating the volume results in a 60.06% variation on the final depositional maximum depth. From the test, it is clear that the DEBRIS2D numerical model is very much sensitive to debris flow initial volume.

Available online at http://www.ijart.info/

8.   CONCLUSIONS AND RECOMMENDATIONS

This chapter focuses on the main conclusions from the explanation and discussions in the preceding chapters. The objectives of the thesis are recalled in this chapter in order to put the conclusions in perspective and the main findings from these are stated. From these, the limitations of the study are highlighted leading to recommendations to properly track the future work.

8.1 Conclusions

Conclusions of data analysis in this research are addressed to answer the research objectives. Conclusion for each research objective is presented below preceded by research objective in italic letter-

Objective a: To determine the susceptibility assessment(mapping) of shallow landslides across Narayanghat-Mugling Highway

Concluding Remarks for Objective a-

- The susceptibility assessment predicted by the model was satisfactory. The SINMAP Model predicted that out of the total study area 0.097% was in the defended zone, 35.216% in the upper threshold zone, 51.252% in the lower threshold zone and remaining 13.427% in the quasi stable, moderately stable and stable zones.

- The slope stability class provided by this study would assist in making emergency decisions and ultimately mitigating future landslide risks along Narayanghat- Mugling Highway.

- It was concluded from the study that mitigation measures should be taken and land-use restrictions should be encroached to miniaturize the landslide risk in areas delineated as defended, lower-, and upper-threshold instability. Areas identified as quasi-stable or moderately stable should only be developed after conducting more detailed stability appraisals and applying land-use regulations and well-engineered construction practices. No additional regulations should be required for areas identified as stable.

Objective b: To assess the sensitive parameters for landslide triggering and more specifically determine the sensitivity of SINMAP Model with respect to various input parameters

Concluding Remarks for Objective b-

- The sensitivity analysis of landslide triggering parameters demonstrated some important conclusions. It was concluded that rainfall was the main triggering component for landslides since the increase in 30% of rainfall resulted in about 15% increase in hazardness.

- It was observed that dimensionless cohesion index C also played an important role in landslides susceptibility assessment. With the increase in value of C the slope was more stable. It was because of the fact that increased cohesion can sufficiently hold the soil on a vertical slope and the increase in root shear strength also plays an important role in making the hillslope stable.

- The sensitivity test of angle of internal friction showed only a little change in the final output. The slight change was in the distribution of landslide points in the Slope area plot. Decrease in it's value led to slight increase in provoking landslides and vice versa.

Objective c: To evaluate the accuracy of SINMAP terrain stability mapping proposed by Pack et.al,2005 for its further use in context of Nepal

Concluding Remarks for Objective c

- Overlaying of validating landslide polygon themes in the final result showed a very good matching. The accuracy of the model was concluded to be good.

- Plotting of Receiver Operating Characteristics Curve(ROC) considering 0.5, 1 and 1.25 as cutoff points produced Area Under Curve to be 0.601 which was higher than classification by chance which again indicated that this model was more than an average good model for predicting shallow landslides.

- The efficiency or the proportion of correctly classified observations was found to be 72.68% considering 0.5 as threshold point(i.e. Safety factor< 0.5 as unstable) which again exhibited a good result.
- The SINMAP Model was evaluated to be relatively accurate model and was conclude that it can widely be used in context of Nepal in real engineering detailed designs.

Objective d: To identify the flow depth, X and Y direction velocities and affected area of debris flow, thus evaluating various scenarios and damages, in the Kamere Khola Watershed across N-M Highway

Concluding Remarks for Objective d-

- The model revealed that the total process of transport of debris flow was about 1 hour with the maximum runout distance of 640m. The maximum depth of debris flow when it invades the section of N-M highway was found to be 2.3 m. All these outputs obtained were satisfactory as it well matched the real event scenario during 2003 disaster.
- DEBRIS2D was found to be applicable for the assessment of debris flow deposition and flow condition in Kamere khola watershed(24+740) along N-M highway.
- It was concluded that the results obtained from this study would aid in making any decisions along the watershed for attenuating any type of losses either human or economic.

Objective e : To analyze the sensitivity of initiation volume in the debris flow runout and more specifically, present the sensitivity of debris flow initial volume in case of DEBRIS2D Model regarding the affected area

Concluding Remarks for Objective e-

- The simulated results in various amounts of debris flow initial volume manifested that the maximal depth of debris flow were almost deposited in the same area. It was primarily revealed that a 33.33% and 66.67% variation in estimating the volume resulted in 13.33% and 23.33% variation respectively on the final depositional front, 18.33% and 54.66%

variation respectively on the final depositional lateral spread and 21.64% and 60.06% variation respectively on the final depositional final depth.

- It was concluded that the initial debris flow volume was the fundamental element in causing the final hazard. More the initial volume, more hazard was the final area and hence more was the vulnerability.

Objective f: To assess the applicability of DEBRIS2D Model, in modeling debris flow runouts in the Nepalese environment

Concluding Remarks for Objective f-

- The estimated volume from the model when it invaded the section of N-M highway was compared with the real event scenario of 2003 disaster. It was seen that about 12% variation occurred between the numerical result and the real event which was acceptable.

- Comparing the parameters obtained from the numerical result with the empirical equations again produced a good result besides a few which again proved the applicability of the model.

- The debris flow depth path obtained from the model was overlaid on the google earth image which clearly illustrated that the simulated result was consistent with the actual debris flow path event.

- From all the analyses the applicability of DEBRISD model was highly assessed in modeling debris flow runouts in the real engineering detailed design in the Nepalese context.

8.2 Recommendations

Based on the conclusion of the study, various recommendations have been suggested to expedite a more comprehensive analysis of the objectives in the future for the same type of study. These recommendations have been given below-

a. The landslide susceptibility maps may be further improved by incorporating the heterogeneous and anisotropic soil properties and spatial and temporal variation of rainfall and as well as increasing the accuracy of the mapped locations of landslide initiations.

b. It is recommended to divide the whole N-M highway into different sections for different calibration regions and use separately calibrated values for each region for modeling in order to further improve the result.

c. The model resolution may be enhanced by improving the accuracy of the DEM by using higher-resolution data (e.g., Interferometric Synthetic Aperture Radar [IfSAR/InSAR] DEMs) or a LIDAR DEM can be very useful as input both in case of SINMAP and DEBRIS2D modeling.

d. It is recommended to include the entrainment(channel path and torrent flanks material) processes in the simulation for further research Entrainment, in the recent studies, has been found to be a key feature mechanism that is able to change significantly the mobility of flow, the flow volume and it's rheology.

e. It is recommended to incorporate the bed or lateral bank erosion for further improvement in simulation of debris flow

f. The compiled output data in this thesis can be used to fond relationships between other type of outputs like the total surface extent of the runout, the vertical travel distance and the change in the energy of flow(momentum, kinetic energy etc) versus the input parameters or the initiation volume

REFERENCES

- Alcantara-Ayala,I.,2002, Geomorphology, natural hazards, vulnerability and prevention of natural disasters in developing countries. Geomorphology , 47(2-4):107-124

- Begueria,S.,2006,Validation and evaluation of predictive models in hazard assessment and risk management, Natural Hazards 37(3), 315-329.10.1007/s11069-005-5182-6.

- Bertoldi et.al,2012, " An integrated Method for Debris flow Hazard Mapping using 2D Runout Models"; 12th Congress INTERPRAEVENT 2012 – Grenoble / France Conference Proceedings

- Beven,K.J.,Kirkby,M.J.,1979,A physically based variable contributing area model of basin hydrology. Hydrological Sciences Bulletin 24, 43–69

- Blanc,T.,2008,Master Thesis on "Numerical simulation of debris flows with the 2D - SPH depth integrated model" In The Institute for Mountain Risk Engineering University of Natural Resources and Applied Life Sciences - Vienna

- Cesca,M.,2008,Studio dei meccanismi di deposizione dei Debris Flow: integrazione tra esperienze di laboratorio, analisi di campo e modellazioni numeriche. PhD Thesis, TeSAF Department, University of Padova: 255.

- Chung,C.-J. F. and Fabbri, A. G., 2003, Validation of spatial prediction models for landslide hazard mapping, Natural Hazards 30(3), 451-472. 10.1023/B:NHAZ.0000007172.62651.2b

- Corominas,J.,1996,The angle of reach as a mobility index for small and large landslides.Canadian Geotechnical Journal 33 (2), 260-271

- Corominas,J.,Moya,J.,2008,A review of assessing landslides frequency for hazard zoning purposes Engeneering Geology 102: 193-213.

- Costa-Cabral,M. and Burges,S.J.,1994,"Digital Elevation Model Networks (DEMON): A Model of Flow Over Hillslopes for Computation of Contributing and Dispersal Areas," Water Resources Research, 30(6): 1681-1692.

- Coussot,Ph.,1997,Mudflow Rheology and Dynamics, Publisher, Taylor and Francis Group, 1997.

- Coussot,Ph. and Proust, S.,1996, Slow unconfined spreading of a mudflow, J. Geophys. Res., 101(B11), 25217–25229, 1996.

- Cruden,D.,1991, A simple definition of a landslide, Bulletin of Engineering Geology and the Environment 43(1), 27{29. 10.1007/BF02590167.

- Dai,F.C., Lee, C.F., Ngai,Y.Y.,2002, Landslide risk assessment and management: an overview: Engineering Geology, v. 64, p. 65-87.

- Deb,S.K and El Kadi,A.I.,2009,"Susceptibility Assessment of Shallow Landslides in Oahu,Hawaii under extreme Rainfall Events". Geomorphology 108 (Elesvier) .219-233. DOI: 10.1016/j.geomorph.2009.01.009

- DOR,MOPPW,2012,Draft Report on Environmental Impact Assessment along Narayanghat-Mugling Highway

- DWIDP Annual Bulletin,2005-06

- Easterbrook, D.J.,1999, Surface Processes and Landforms: Macmillan Publishing Company, New York, NY, 546 p.

- Fairfield, J. and Leymarie,P.,1991,"Drainage Networks from Grid Digital Elevation Models," Water Resources Research, 27(5): 709-717.

- Fawcett, T.,2006, An introduction to ROC analysis, Pattern Recognition Letters 27(8), 861{874. doi: DOI: 10.1016/j.patrec.2005.10.010.

- Ferguson,B.K and Debo,T.N.,1990,On site storm water management: applications for landscape and engineering. New York, Van Nostrand Reinhold

- Fetter, C.W., 1994, Applied Hydrogeology: Prentice Hall, Englewood Cliffs, NJ.

- Fraccarollo, L., Papa, M., 2000. Numerical simulation of real debris-flow events. Physics and Chemistry of the Earth 25 (9), 757–763.

- Ganser,A.,1964,Geology of the Himalaya. Inter Science John Wiley, London Gerrard J (1994) The landslide hazard in the Himalayas: geological control and human action. Geomorphology 10:221–230

- Glade, T. and Crozier, M. J.,2005, A review of scale dependency in landslide hazard and risk analysis, in T. Glade, M. Anderson and M. J. Crozier (eds), Landslide Hazard and Risk, Wiley, pp. 75-138.

- Godt,J.,Baum,L.R.,Lu,N.,2009,Landsliding in partially saturated materials. Journal of Geophysical Research Letters Volume 36 Issue 2.

- Griffiths,R.W.,2000,The dynamics of lava flow, Annu. Rev. Fluid Mech., 32, 477–518, 2000.

- Hammond,C.,Hall,D.,Miller,S.,Swetik,P.,1992,"Level I Stability Analysis (LISA) Documentation for Version 2.0," General Technical Report INT-285, USDA Forest Service Intermountain Research Station.

- Han, G., Wang, D.,1996,Numerical modeling of Anhui debris flow. Journal of Hydraulic Engineering 122 (5), 262–265

- Highland, L. M. and Bobrowsky,P.,2008,The landslide handbook. A guide to understanding landslides, Technical Report Circular 1325, U. S. Geological Survey.

- Huang,M.C.,2003,Hazard Assessment of Debris Flow Using Numerical Simulation and Detecting Debris flow With Microwave, Doctoral Dissertation, National Taiwan University, Taipei, Taiwan.

- Hulme,G.,1974,The interpretation of lava flow morphology, Geophys.J. Roy. Astr. S., 39, 361–383, 1974.

- Hungr,O.,Morgan,G.C.,Kellerhals, R.,1984, Quantitative analysis of debris torrent hazards for design of remedial measures. Canadian Geotechnical Journal 21, 663–677.

- Hungr, O.,1995, A model for the runout analysis of rapidflow slides, debrisflows, and avalanches. Canadian Geotechnical Journal 32 (4), 610–623.

- Hürlimann, M.,Rickenmann, D.,Graf, C.,2003b, Field and monitoring data of debrisflow events in the Swiss Alps. Canadian Geotechnical Journal 40 (1), 161–175.

- Hurlimann,M., Rickenmann,D., Medina,V., Bateman,A., 2008, Evaluation of approaches to calculate debris-flow parameters for hazard assessment Engineering Geology 102 (2008) 152–163; (Elesvier)

- Hussin,Y.H.,2011, Probabilistic runout modeling of debris flow in Barcelonnete, France. Thesis ,Enschede , The Netherlands

- Hutchinson,J.N.,1988,A General Report: Morphological and geotechnical parameters of landslides in relation to geology and hydrogeology. In C. Bonnard Ed. Proceedings ,Fifth International Symposium n Landslides (Vol 1 pp 3-35).

- Ikeya,H.,1981,A method of designation for area in danger of debrisflow. Symposium on Erosion and Sediment Transport in Pacific Rim Steeplands. IAHS Publ., vol. 132.Christchurch, N.Z., pp. 576–588.

- Imran,J., Parker,G., Locat,J., Lee,H., 2001, 1D numerical model of muddy subaqueous and sub aerial debris flows. Journal of Hydraulic Engineering 127 (11), 959–968

- Iverson, R.M., 1997, The physics of debrisflows. Review of Geophysics 35 (3), 245–296

- Jakob,M. and Hungr.O.,2005, Debris-flow Hazards and related Phenomena. Chichester. Springer-Praxis.

- Jakob,M.,Anderson,D.,Fuller,T.,Hungr,O.,Ayotte,D.,2000,An unusually large debris flow at Hummingbird Creek, Mara Lake, British Columbia. Canadian Geotechnical Journal 37, 1109–1125.

- Jin, M.,Fread,D.L.,1999,1D modeling of mud/debris unsteady flows. Journal of Hydraulic Engineering 125 (8), 827–834.

- Julien,P.Y. and Lan,Y.,1991, ”Rheology of Hyperconcentrations,” J Hydraul. Eng. ASCE, 117(3), pp.346-353.

- Körner,H.J.,1976,Reichweite und Geschwindigkeit von Bergstürzen und Fliessschneelawinene. Rock Mechanics 8, 225–256.

- Laigle,D.,Coussot,P.,1997,Numerical modeling of mudflows. Journal of Hydraulic Engineering 123 (7), 617–623.

- Lanni,C.,McDonnell,JJ.,Hopp,L.,Rigon,R.,2012,Hydrological controls on shallow landslide triggering: the role of soil depth and bedrock topography. Preliminary accepted for publication in Earth Surface processes and landforms.

- Liu,K.F.,Li,H.C.,Wu,Y.H.,2012,Assessment Social Impact of debris flow disaster by Social Vulnerability Index; KURENAI : Kyoto University Research Information Repository; http://hdl.handle.net/2433/180439

- Liu, K.F., and Lee, F.C., 1997, "Experimental Analysis on Impact Mechanism of Granular Flow," Chin. J. Mech., 13(1), pp.87-100.

- Liu,K.F.,Lee,H.C.,Wu,Y.H.,2012,Assessment Social Impact of debris flow disaster by Social Vulnerability Index, Kyoto Conference Proceedings (The Tenth International Symposium on Mitigation of Geo-disasters in Asia)

- Liu, K.F., and Huang, M.C., 2006, "Numerical Simulation of Debris Flow With Application on Hazard Area Mapping," Computat. Geosci., 10, pp.221-240.

- Liu, K. F. and Lai, K. W,2000, Numerical simulation of two-dimensional debris flows, Proceedings of the 2nd International Conference on Debris Flow Hazards Mitigation, 531–535, 2000.

- Liu, K. F. and Mei, C. C., 1989,Slow spreading of the sheet of Bingham fluid on an incline plane, J. Fluid Mech., 207, 505–529, 1989.

- Liu, K. F. and Mei, C. C.,1994, Roll waves on a layer of a muddy fluid flowing down a gentle slope – A Bingham model, Phys. Fluids,6, 2577–2590, 1994.

- Luna,B.,2012,Thesis for the degree of doctor on "Dyanmic Numerical Runout Modeling For Quantitative Landslide Risk Assessment.

- Major, J. J. and Iverson, R. M.,1999, Debris-flow deposition: Effects of pore-fluid pressure and friction concentrated at flow margins,GSA Bulletin, 111, 1424–1434, 1999.

- McCall,G.J.H.,1992,Geohazards "Natural and Man-Made"London, Chapman and Hall.

- Mei, C. C., Liu, K. F., and Yuhi,M.,2001, Mud flow-slow and fast, Lect. Notes Phys., 582, 548–577, 2001

- Mergili,M.,2008, Thesis for the degree of doctor of science in "Integrated modeling of debris flows with Open Source GIS" Numerical simulations of triggering, mobilization, and runout of debris flows for selected study areas along the Trans-Andean road corridor Mendoza – Valparaíso

- Montgomery,D.R. and Dietrich, W.E.,1994, A physically based model for the topographic control on shallow landsliding: Water Resources Research, v. 30, no. 4, p. 1153-1171.

- Morgenstern,NR., de Matos,MM.,1975,Stability of slopes in residual soils. In Proceedings of the 5th Pan-American Conference on Soil Mechanics and Foundation Engineering, pp. 367–383, A. A. Balkema, Rotterdam, Netherlands.

- Msilimba,G.G.,2002,Landslides Geohazard Assessment of the Vunguvungu /Banga Catchment Area in Rumphi District, MSc. Environmental Science Thesis, Unpublished, Zomba, University of Malawi.

- Naef, D., Rickenmann, D., Rutschmann, P., McArdell, B.W., 2006, Comparison offlow resistance relations for debris flows using a one-dimensional finite element simulation model. Natural Hazards and Earth System Science 6, 155–165

- Nakagawa,H.,Takahasi,T.,1997, Estimation of Debris flow Hydograph and Hazard area: debris flow hazard : Mechanics, Prediction and assessment: ASCE,1997

- Nakatani,K.,Wada,T.,Satofuka,Y.,Mizuyama,T.,2008, Development of "Kanako 2D (Ver.2.00)," a user-friendly one- and two-dimensional debris flow simulator equipped with a graphical user interface. International Journal of Erosion Control Engineering, Vol. 1, No. 2, 2008.

- National Emergency Operation Centre, Ministry of Home Affairs. Assessed: 22nd October, 2014

- Neary,D.G.,Swift,L.W.,Manning,D.M.,Burns,R.G.,1986, Debris avalanching in the Southern Appalachians: An Influence on Forest Soil Formation: Soil Science Society of America Journal, v. 50, p. 465-471.

- Nettleton,I.M., Martin,S., Hencher,S., Moore,R., 2005, Debris flow types and mechanisms . In M.G. Winter ,F. Macgregor and L, Sahckman (Eds) Scottish Road Network Landslides Study pp(45-67). Edinburgh: The Scottish Executive

- Neupane,B.,2011, Role of Clay Minerals in the occurrence of landslides along Narayanghat- Mugling road Section, Central Nepal Journal of Nepal Geological Society ,2011,Vol.43(Special Issue) pp: 301-308.

- Ng, Ch. O. and Mei, C. C., 1994, Roll waves on a shallow layer of mud modelled as a power-law fluid, J. Fluid Mech., 263, 151–184,1994.

- Nippon Koei Co. Ltd, 2008, Final Report on The Study On Disaster Risk Management For Narayanghat- Mugling Highway.

- NV,2011, Understanding Debris Flows

- O'Brien, J. S. and Julien P. Y., 1985, Physical properties and mechanics of hyperconcentrated sediment flows, Proc. ASCE Hyd. Div. Spec.Conf. on Delineation of Landslides, Flash Flood and Debris Flow Hazards, Logan Utah, June 1984, 260–279, 1985.

- O'Brien, J. S. and Julien,P.Y.,1997, On the importance of mud flow routing, Proc., 1st Int. Conf. on Debris-Flow Hazards, Mitigation: Mechanics, Prediction and Assessment, ASCE, Reston,Va., 677–686, 1997.

- O'Callaghan, J.F. and Mark,D.M.,1984,"The Extraction of Drainage Networks From Digital Elevation Data," Computer Vision, Graphics and Image Processing, 28: 328-344.

- O'Loughlin,E.M.,1986,"Prediction of surface saturation zones in natural catchments by topographic analysis," Water Resources Research, 22(5): 794-804.

- Osmond, D. I. and Griffiths, R. W.,2001, The static shape of yield strength fluids slowly emplace on slope, J. Geophys. Res.,106(B8), 16241–16250, 2001.

- Pack,R.T.,Tarboton,D.G.,Goodwin,C.N.,1998a, In: Moore, D.P., Hungr, O. (Eds.), The SINMAP approach to terrain stability mapping. Proceedings of the 8th Congress of International Association of Engineering Geology and the Environment, vol. 2. A. A. Balkema, Rotterdam, pp. 1157–1165.

- Pack, R.T., Tarboton,D.G.,Goodwin,C.N.,1998b, Terrain stability mapping with SINMAP.Technical description and user's guide for version 1.00. Report No. 4114-0. Terratech Consulting Ltd., Salmon Arm, B.C., Canada

- Pack,R.T.,Tarboton,D.G.,Goodwin,C.N.,Prasad,A.,2005, SINMAP 2, a stability index approach to terrain stability hazard mapping. Technical Description and User's Manual for version 2.0. Utah State University, USA.

- Perla,R.,Cheng,T.T.,Clung,D.M.,1980,A two parameter model of snow avalanche motion. Journal of Glaciology 26 (94), 197–208.

- Petley,D.,2012 ,Geology http://dx.doi.org/10.1130/G33217.1

- Pierson,T.C. and Costal, J.E.,1987, A rheological classification of sub aerial sediment water flows: Geological Society of America, Reviews in Engineering Geology, v. 7, p.1-12.

- Pimiento E.,2010, Shallow Landslide Susceptibility Modeling and Validation. A thesis submitted in partial fulfillment for the degree of Master in Geographical Information Science.

- Pouliquen,O. and Forterre,Y.,2002,Friction law for dense granular flows: application to the motion of a mass down a rough inclined plane, J. Fluid Mech., 453, 133–151, 2002.

- Quinn, P., K. Beven, P. Chevallier and O. Planchon,1991, "The Prediction of Hillslope Flow Paths for Distributed Hydrological Modeling Using Digital Terrain Models," Hydrological Processes, 5: 59-80.

- Rahardjo,H., Leong E.C., and Rezaur, R.B.,2008,Effect of Antecedent Rainfall on Pore-water pressure Distribution Characteristics in Residual Soil Slopes Under Tropical Rainfall. (Wiley Interscience)506-523. DOI: 10.1002/hyp.6880

- Regmi,A.D.,Yoshida,K.,Haseda,N.Pradhan,A.M.,Pradhan,B.,Pourghasemi,H.R., 2013,The relationship between geology and rock weathering on the rock instability along Narayanghat-Mugling road corridor, Central Nepal Himalaya.

- Revellino, P., Hungr, O., Guadagno, F.M., Evans, S.G., 2004,Velocity and runout simulation of destructive debrisflows and debris avalanches in pyroclastic deposits, Campania region, Italy. Environmental Geology 45, 295–311.

- Rickenmann,D.,1990,Debris Flows 1987 in Switzerland: modeling and fluvial sediment transport. In: Sinniger, R.O., Monbaron, M. (Eds.), Hydrology in Mountainous Regions; Lausanne Symposium. IAHS, Lausanne, pp. 371–378.

- Rickenmann,D.,1999, Empirical relationships for debris flows. Natural hazards 19 (1) 47–77.

- Rickenmann,D., Laigle D., McArdell B.,Hubl J.,2006, Comparison of 2D debris flow simulation model with field events. Computational Geosciences 10: 241-264.

- Ritter, D.F., Kochel, R.C., and Miller, J.R., 1995, Process geomorphology: Third Edition, Wm. C. Brown Publishers, Dubuque, Iowa, 546 p.

- Safeland, 2011, Living with landslide risk in Europe: Assessment,effects of global change, and risk management strategies; 7thFramework Programme Cooperation Theme 6 Environment (including climate change)Sub-Activity 6.1.3 Natural Hazards

- Sassa,K.,1985, The mechanism of debris flows. Preceedings of XI International Conference on Soil Mechanics and Foundation Engineering San Francisco 3, pp 1173-1176

- Savage,S.B. and Hutter,K.,1989, The motion of a finite mass of granular material down a rough incline . Journal of Fluid Mechanics ,199(1), 177-215

- Scheuner,T.,2007, Modellierung von Murgangereignissen mit RAMMS und Vergleich durch GISbasiertes Fliessmodell. Diplomaarbeti, University of Zurich. Pages: 122.

- Shakya, B.,2002, A New Approach within hydrometereological technique for the estimation of average depth of probable maximum precipitation (PMP) over Nepal In: Eu et. al.(Ed),Flood Defense 2002.Science Press New York Ltd. pp.-599-606

- Sharma, R. H.,2002, Rainstorms Induced Hazards Assessment Using GIS and Numerical Modeling; M.Sc., Thesis, TU

- Sidle, R.C.,Pearce,A.J.,O'Loughlin,C.L.,1985, Hill slope Stability and Land Use, Water Resources Monograph 11 Edition, American Geophysical Union,140p.

- Smith,K.,1996, Environmental Hazards; Assessing Risk and Reducing Disaster, London,Routledge.

- Smith K.,Petley,D.N,2008, Environmental Hazards: Assessing Risk and Reducing Disaster;Fifth Edition;Routledge,London,414p,ISBN 0-203-88480-9

- Soeters, R. and van Westen, C.,1996, Slope stability: recognition, analysis and zonation, in A. Turner and R. Shuster (eds), Landslides: investigation and mitigation, National Academy Press, Washington, D. C., pp. 129-177.

- Stocklin, J., Bhattarai, K. D., 1978,Geology of the Kathmandu area and central Mahabharat range. Report of Department of Mines and Geology/UNDP (unpublished), Nepal Himalaya 86 pp

- Stolz,A.,Huggel,C.,2008,Debris flows in Swiss National Park : the influence of different flow models and varying DEM grid size in modeling results. Landslides 5: 311 – 319.

- Sudhakar,M.R.,1996,Role of apparent cohesion in the stability of Dominican allophone soil slopes. Eng. Geol. 43:265–279.

- Takahashi, T., 1991,Debris Flow. IAHR Monograph. Balkema, Rotterdam. 165 pp.

- Takahashi, T., 2007, Debris flow: mechanics, prediction and countermeasures. Taylor & Francis.

- Takahashi, T., Kuang, S.,1986, Formation of debris flow on varied slope bed, Disaster Prevention Research Institute Annuals, 29(B-2), pp. 345–349.

- Tarboton, D. G.,1997, "A New Method for the Determination of Flow Directions and Contributing Areas in Grid Digital Elevation Models," Water Resources Research, 33(2): 309-319.

- Terlien,M.T.J.,1998, The determination of statistical and deterministic hydrological landslide triggering thresholds. Environmental Geology 35 (2-3);124-130

- Terzaghai,K.,1950, Mechanics of Landslides, Engineering Geology, Berkey, Geology Society of America, 83 - 123.

- Tsai M.P. et.al,2011,Application of simulation technique on debris flow hazard zone delineation: a case study in the Daniao tribe, Eastern Taiwan; Nat. Hazards Earth Syst. Sci., 11, 3053–3062, 2011www.nat-hazards-earth-syst-sci.net/11/3053/2011/ doi:10.5194/nhess-11-3053-2011

- Tsukamoto,Y.,Kusakabe,O.,1984,Vegetation influences on debris slide occurrences on steep slopes in Japan. In: O'Loughlin, C.L., Pearce, A.J. (Eds.), Symposium on Effects of Forest Land Use on Erosion and Slope Stability. University of Hawaii East West Center Environmental and Policy Institute, Honolulu, pp. 63–72

- U S Geological Survey. Online http://pubs.usgs.gov/. Assessed: 2nd Oct.,2014

- Van Asch, T.W.J., and Van Beek, J.B.,L.P.H.,1999,A view on some Hydrological Triggering Systems in Landslides. Geomorphology 30: (Elesvier Science);25-32

- Varnes,D.J.,1978, Slope movement types and processes in Schuster, R., and Krizek, R., eds., Landslides: Analysis and Control: Washington, D.C., National Academy of Science, p. 12-33.

- Voellmy,A.,1955,Uber die Zerstorungskraft von Lawinen. Schweizerische Bauzeitung 73, 212–285.

- Wieczorek, G.F.,1996,Landslide triggering mechanisms, in Turner, A.K. and Schuster, R.J., eds., Landslides: Investigation and Mitigation: Washington, D.C., Transportation Research Board Special Report 247, National Research Council, p. 76-90.

- Wieland, M., Gray, J. M. N. T., and Hutter, K.,1999, Channelized freesurface flow of cohesionless granular avalanches in a chute with shallow lateral curvature, J. Fluid Mech., 392, 73–100, 1999.

- Wiemin,Y.,Shuren,WU.,Yongshuang,Z.,Jusong,S.,Lingzhi,X.,2007,Research on Formation Mechanism of the debris flow on slope induced by rainfall. Earth Science Frontiers, 2007, 14(6): 197–204.

- Wikipedia, Assessed: 28th Sep 2014 and15th October, 2014

- Wilson, S. D. R. and Burgess, S. L.,1998, The steady, spreading flow of a rivulet of mud, J. Non-Newton. Fluid, 79, 77–85, 1998.

- WP/WLI,1995,A suggested method for describing the rate of movement of a landslide. Bulletin of the International Association of Engineering Geology,52,75-78

- Wu, W. and R. C. Sidle,1995,"A Distributed Slope Stability Model for Steep Forested Watersheds," Water Resources Research, 31(8): 2097-2110.

- Wu, Y. H,2014,Debris flow and DEBRIS2D Theory ,Presentation, NTU

- Wu, Y.H., and Liu, K.F., 2014, "The Influence of Countermeasure on Debris Flow Hazards with Numerical SimulationLandslide Science for a Safety Geo-Environment,1, pp.473-478.

Available online at http://www.ijart.info/

ANNEX A: R Code for converting .dat to.tiff

install.packages('raster')

library(raster)

setwd('C:/WD2/Bin/D2D/Kmre_15000')

Converts dat data to raster tiff

Depth is saved in depth folder. So make sure this folder exists 1:100

for (i in c(1,6,18,36,60,120,180,270,348)){ # input range of file name (eg 1:5, or 6:15)

 one_data <- read.table(paste(i,'.dat',sep="), sep="")

 plot_data <- one_data[one_data[,5] >= 0.005,c(1,2,5)];

  r <- rasterFromXYZ(plot_data)

  writeRaster(r,paste('./depth/',i,'.tif',sep="))

}

Velocity

for (i in c(1,6,18,36,60,120,180,270,348)){

  one_data <- read.table(paste(i,'.dat',sep="), sep="")

  xy_data <- one_data[one_data[,5] >= 0.005,c(1,2)];

  v_data <- sqrt(one_data[one_data[,5] >= 0.005,c(3)]^2 + one_data[one_data[,5] >= 0.005,c(4)]^2)

  xyv_data <- cbind(xy_data,v_data)

  r <- rasterFromXYZ(xyv_data)

  writeRaster(r,paste('./velocity/',i,'.tif',sep="))

}

ANNEX B: Field investigation determining yield stress

Figures: Determination of yield stress in the field (27th September, 2014)

ANNEX C: Pictures taken during the field observations of construction of mitigating measures for debris flow

Figures: Different mitigating structures for debris flow across N-M Highway(Picture Taken 27th September, 2014)

Available online at http://www.ijart.info/

ANNEX D: Debris flow and debris deposition across Kamere Khola watershed(24+740)

Figures: Debris flow along Kamere Khola Watershed and Debris deposited by the same watershed just across N-M highway towards Trishuli river(Picture taken 27th Sep,2014)